DISSERTATION

REFRAMING VIRAL INFECTIONS AS ACUTE METABOLIC DISORDERS: DENGUE VIRUSES AND THEIR DEPENDENCY ON HOST METABOLIC PATHWAYS

Submitted by

Laura A. St Clair

Department of Microbiology, Immunology, and Pathology

In partial fulfillment of the requirements

For the Degree of Doctor of Philosophy

Colorado State University

Fort Collins, Colorado

Summer 2022

Doctoral Committee:

Advisor: Rushika Perera

John Belisle
Punya Nachappa
Jeff Wilusz
Mark Zabel

ABSTRACT

REFRAMING VIRAL INFECTIONS AS ACUTE METABOLIC DISORDERS: DENGUE VIRUSES AND THEIR DEPENDENCY ON HOST METABOLIC PATHWAYS

Dengue viruses (DENVs) are the etiological agent of one of the world's most aggressive arthropod-borne disease. At present, there are no available antivirals against DENVs. This fact underscores a dire need to examine host-virus interactions to identify and develop novel therapeutic approaches. As obligate intracellular parasites, DENVs are reliant upon and hijack several host metabolic pathways both to fulfill their replicative needs, and to evade the host immune response. We and others have previously established that infection with DENVs causes significant perturbation to host lipid metabolism, including elevations in sphingolipids in both the human and mosquito host. In addition, we and others previously discovered that the DENV NS1 protein increases sialidase activity in both *in vitro* and *in vivo* models leading to increased endothelial hyperpermeability and vascular leakage which are hallmarks of severe dengue. To further clarify and characterize these previous works, we have performed siRNA-mediated loss of function studies using human hepatoma cells (Huh7 cells) on several metabolic pathways altered during DENV2 infection. First, we examined the role of acyl-CoA thioesterases, enzymes responsible for controlling the intracellular balance of activated fatty acids and free fatty acids, on the DENV2 lifecycle. In these analyses, we determined that the cytosolic ACOT1 enzyme had an inhibitory effect on DENV2 replication and release, while mitochondrial ACOT (ACOTs 2 and 7) functionality was critical for viral replication and release. Moreover, we identified several enzymes within the ACOT family whose expression was dependent on ACOT2 and ACOT7 expression. These results highlighted complex relationships between ACOTs and DENVs, as well as identified yet unknown functional interdependence between ACOT enzymes. Next, we expanded our

previous understanding of the relationship between DENVs and the human sialidase enzymes (NEU1-4). While previously studies linked upregulation of these enzymes with DENV2 pathology, we provide the first evidence showing that NEU1-4 functionality is vital for DENV2 genome replication and viral egress. Moreover, our analyses also revealed previously unknown functionality of NEU4 or its downstream products as transcriptional regulators for NEU1-3. Finally, we provide a profile of the effect of loss of function of enzymes within the entire sphingolipid metabolic pathway (as identified through KEGG pathway database) on the DENV2 life cycle. In this study, we identified that enzymes involved the sphingomyelinase and salvage pathways of ceramide synthesis as opposed to *de novo* ceramide synthesis were critical to DENV2 release from Huh7 cells. In addition, we determined that enzymes involved in the synthesis and degradation of glycosphingolipids were vital for DENV2 release. An especially intriguing result within this arm of sphingolipid metabolism was that the two enzymes which hydrolyze GluCer had differential effects on DENV2 replication and release. GBA1 (lysosomal) had an antiviral effect on DENV2, while GBA2 (non-lysosomal) was required for DENV2 replication and release. This prompted us to profile the changes that occur to glycosphingolipids (GSLs) during infection, and we uncovered several species of GSLs that are elevated during infection. Moreover, we identified that Ambroxol HCl, a pharmaceutical GBA1 chaperone/GBA2 inhibitor, was able to abrogate these elevations in GSLs. Combined, our results allowed us to propose a novel function for GBA2 as a GluCer recycling enzyme during DENV2 infection. In conclusion, together, the work in this dissertation highlights critical metabolic nodes that impact virus replication and provides new directions for investigating viral infections as acute metabolic diseases.

Hypothesis of study: Dengue viruses hijack and manipulate host metabolic pathways for their own replicative advantage. As such, alterations in metabolite levels and metabolic enzyme expression and activity are quantifiable and can be correlated with their roles in the DENV lifecycle. Moreover, these changes in the metabolic landscape can be used to identify novel therapeutics and provide insight into the DENV-induced pathology.

ACKNOWLEDGEMENTS

First and foremost, I would like to express my gratitude to my advisor, Dr. Rushika Perera. There is not enough time or space to list out all the things that I have learned and accomplished because of you during these past three years. You gave me so many opportunities above and beyond my experiences at the bench that will undoubtedly benefit me in the years to come. Thank you for showing me how exciting it can be to push the boundaries of your skillsets and knowledgebase. You have not only taught me how to 'think' like a scientist, but you have provided me with an arsenal of tools, soft-skills, and opportunities to thrive as one. I will be forever grateful.

I would like to also thank the members of my advisory committee: Drs. John Belisle, Punya Nachappa, Jeffrey Wilusz, and Mark Zabel. First, I would like to thank you collectively for keeping Rushika and I grounded. John: thank you immensely for allowing me a seat at the table with you and Rushika as you formed and established the Center for Metabolism of Infectious Diseases. I gained so much by being allowed to participate in and have a voice throughout the process. Punya: I cannot thank you enough for the infusion of positivity, encouragement, and joy you brought to every committee meeting and interaction we had. Jefe: Most of all, I owe you an immense amount of gratitude for being a consummate supporter of 'Team LASC'. Thank you for teaching me everything I know about RNA, for our shared love of terrible puns, and for always keeping a door open for me. Mark: thank you for always being willing to ask questions that challenged us to think outside of our virology and metabolomics expertise, and that challenged me to always think about broader audiences when I presented.

In addition to my 'official' advisory committee, I would like to extend my deepest gratitude to my three 'unofficial' advisors: Drs. Frances Platt, David Priestman, and Michael Spedding. Michael: I am exceedingly grateful that you reached out to Rushika. I do not think either of us could have anticipated how much depth, expertise, and richness it would add to our research efforts. The working group formed between the five of us has been such a joy. I cannot thank

each of you enough for how much your collective expertise in sphingolipid biology/disorders has reshaped my thesis and broadened my thinking. It was never lost on me what a treasure it was to have such access to your expertise as we tried to make sense of our data and decide which questions were the right ones to ask next. It has been and is an absolute honor.

Drs. Ashley McGrew and Rebekah Kading: I am so grateful to have had the opportunity be your graduate teaching assistant as I learned so much about teaching and mentorship from our time together. However, I am more grateful for the incredibly kind friends and lifelong mentors that I gained. I cannot thank each of you enough for the support and love you have shown me over the past few years.

It is impossible to go through graduate school without a deep bench of academic friends, and I have many of you to thank. Elena Lian, Gaby Ramirez, and Carley McAlister: I could write an entire thesis around how much your friendships and partnerships have meant to me during my time as a Ph.D. student. It has been an honor to be your mentor, for you to be mine, and I am profoundly proud to call you all friends. To my Ph.D. cohort, Bekah, Savannah, Lyndsey, Jasmine, and Amy: thank you for being my first friends in graduate school, and for the countless conversations of mutual support, encouragement, and venting. To my Perera lab mates and friends Dr. Rebekah Gullberg, Stephanie Mills, and Oshani Ratnayake: thank you for the collaborations, friendships, and hours of laughter that we have shared. I would also like to thank Anna Fagre, Paula Lado, Corey Rosenberg, Philida Charley, Juliette Lewis, Teca Magalhaes, Ashley Janich, and Michael Young for their friendship and support.

Last, and most certainly not least, I need to thank my three favorite women for all of their love and support. To my mother, EJ Baldridge: Mom, thank you for always encouraging me, picking me up when I was down, making me laugh until I could not breathe, and being a constant cheerleader. To my wife, Amber St. Clair: thank you for supporting and encouraging this dream of mine, even on the worst days. You have been unwavering in your love, care, and support of me through this process, even though it has often made you a ‘graduate school widow’, and I

cannot thank you enough for sticking by me. To my absolute dearest friend, Erin Agee: Pirate, thank you for being that one person who always knows exactly what I need to hear in every moment, who knows me better than I know myself, and for always shouldering every burden and triumph with me. Thank you all for believing in me and supporting me through everything. I could not have done any of this without you. “The truth is, the truth is that I wouldn’t be here without the love I stand on. And every time I get lost in the world, you’ll always be there to care and share in the joy and the pain.”[1] I love you all very much!

[1] Lyrics from “Unbreakable” by Janet Jackson. If you somehow thought I would not work the most influential musician of my life into my thesis acknowledgements, you underestimated me!

DEDICATION

I would like to dedicate this thesis to my late aunt, Patricia Anne Bailey. Words can never adequately express how much I miss you, and I wish you knew that I think of and carry you with me every single day. Thank you for teaching me about compassion and honesty, and for always keeping an open door for me and my never-ending questions. Thank you for always keeping Mom and I on our toes with your quick wit, wicked sense of humor, and constant shenanigans, and for passing all of that onto us. That ability to always find humor in the toughest situations is what keeps me grounded. Above all else, thank you for always believing in me and encouraging me. Your little unicorn did it! My only regret is that you are not here with me now to celebrate. You are my sunshine, forever and always. ~Miss L.A.B.

TABLE OF CONTENTS

Chapter 1: Literature Review

1.1: Introduction

Emerging infectious diseases pose one of the greatest threats to global health. In the past few decades, several pandemics have highlighted how quickly a virus can spread across the globe. At the time of preparing this dissertation, we are currently amid a coronavirus disease outbreak that has caused an estimated 520 million infections and 6.2 million deaths worldwide in the two years since it emerged. While vaccines provide us with the best protection against viral infections, development can be slow and costly. Moreover, as has been witnessed in real-time during the COVID-19 pandemic, viruses can quickly mutate and escape the immunity conferred by vaccines. Likewise, viral mutations also allow many viruses to develop resistance to antivirals that specifically target viral proteins. This underscores a dire need to identify and develop novel antiviral approaches against emerging diseases. Research aimed at investigating virus-host interactions is crucial to these efforts.

As obligate intracellular parasites, viruses are reliant upon and exploit many host metabolic pathways both to fulfill their replicative needs and to evade the host immune response. These changes in cellular metabolism can have dire consequences for the host, contributing to the pathogenesis that accompanies viral infection. While metabolomics is still an emerging field whose full potential is yet unrealized, metabolomics-based approaches have enriched our understanding of the changing cellular landscape upon viral infection. These approaches allow us to characterize what specific molecules are altered, how they contribute to the viral life cycle, and determine how they are altered upon infection (host- or virus-mediated). In turn, metabolomics is a powerful tool that can be exploited to discover metabolic chokepoints that can be targeted both to control viral replication and improve patient outcomes.

Herein, we will discuss various aspects of the relationship between dengue viruses (DENVs), the etiological agents of one of the world's most prevalent and aggressive arthropod-borne disease, and host cellular metabolism. During infection, DENVs cause extensive perturbations to the lipid repertoire within the cell. Thus, we have discussed the knowns and unknowns regarding changes to the lipid landscape upon DENV infection. As well, we have discussed the known roles lipids play in the DENV lifecycle. Additionally, we have discussed the relationship of viruses and sialic acids, which are a predominate sugar residue on glycolipids and glycoproteins, and interactions of DENVs with enzymes involved in regulating sialylation. Finally, we will provide a brief, but detailed biochemical overview of fatty acid metabolism, sphingolipid metabolism, lipid trafficking, and sialic acid biology. These discussions combined are presented as evidence from the literature that informed the investigations and methodologies presented in this dissertation.

1.2: Dengue viruses

Dengue viruses (DENVs), are positive sense, enveloped RNA viruses belonging to the *Flaviviridae* family of viruses [1–3]. There are four known serotypes (DENV1-4), which are endemic and co-circulate in tropical and subtropical regions of the world and are transmitted by *Aedes* spp. mosquitoes [1–3]. Recent modelling by the World Health Organization suggests there are ~390 million dengue infections with ~96 million clinical cases each year [1–3].

Dengue, the disease caused by DENVs, can present as a range of illnesses. Most often, dengue presents as either a subclinical or undifferentiated flu-like disease or as an acute febrile illness (dengue fever or DF) lasting 3-7 days which can be accompanied by severe headache, myalgia, arthralgia, and a maculopapular rash [2,4]. However, some infections are more severe and progress to dengue hemorrhagic fever (DHF) which includes the hallmarks of leukopenia,

thrombocytopenia, and vascular leakage/hemorrhaging and can progress to the fatal dengue shock syndrome (DSS) if fluid loss is unmanaged due to hypovolemic shock [2,4]. Presently, there are no antivirals against DENVs, thus supportive care and fluid restoration remain the only available treatments for hospitalized patients [2,4].

The risk of progression to severe disease is increased in people who have previously been exposed to one DENV serotype, and are subsequently infected by a heterotypic virus [5,6]. This phenomenon is known as antibody-dependent enhancement (ADE), wherein sub-neutralizing antibodies against the primary serotype bind to the secondary, heterotypic virus effectively opsonizing it and thereby facilitating its entry into monocytes, macrophages, and dendritic cells [5,6]. This confers an advantage for DENVs as they display tropism for innate immune cells and tissues, thus ADE increases DENV infiltration and production, but is disadvantageous to the host as by exacerbating the host immune response and increases immunopathology [7].

The ADE phenomenon complicates vaccine development as vaccine-induced immunity in DENV-naïve (seronegative) individuals may predispose them to severe illness when they receive a ‘secondary’ exposure from the bite of a DENV-infected mosquito [8,9]. This was observed and contributed to the controversy surrounding the rollout of Sanofi Pasteur’s Dengvaxia® vaccine, the only currently available vaccine against DENVs [10]. During clinical trials, insufficient data collection of serostatus of trial participants resulted in an undetected risk for seronegative recipients [10]. Nearly 18 months post-vaccine rollout, a safety signal was issued by Sanofi Pasteur [11]. Analysis since showed that the relative risk of hospitalization due to severe illness was 2-4 fold higher in seronegative recipients [10]. Moreover, Dengvaxia® displayed serotype-specific efficacy, providing higher vaccine-induced immunity to DENV3 and DENV4 than DENV1, and lowest efficacy against DENV2 [10]. In the wake of these results, ongoing clinical trials for second-generation live-attenuated vaccines have been extended and stratification of data to include serostatus is required by regulatory agencies [12]. This underscores an urgent need for

the discovery of preventative measures and antivirals to treat patients infected with dengue viruses.

1.2.1 - The dengue virus life cycle

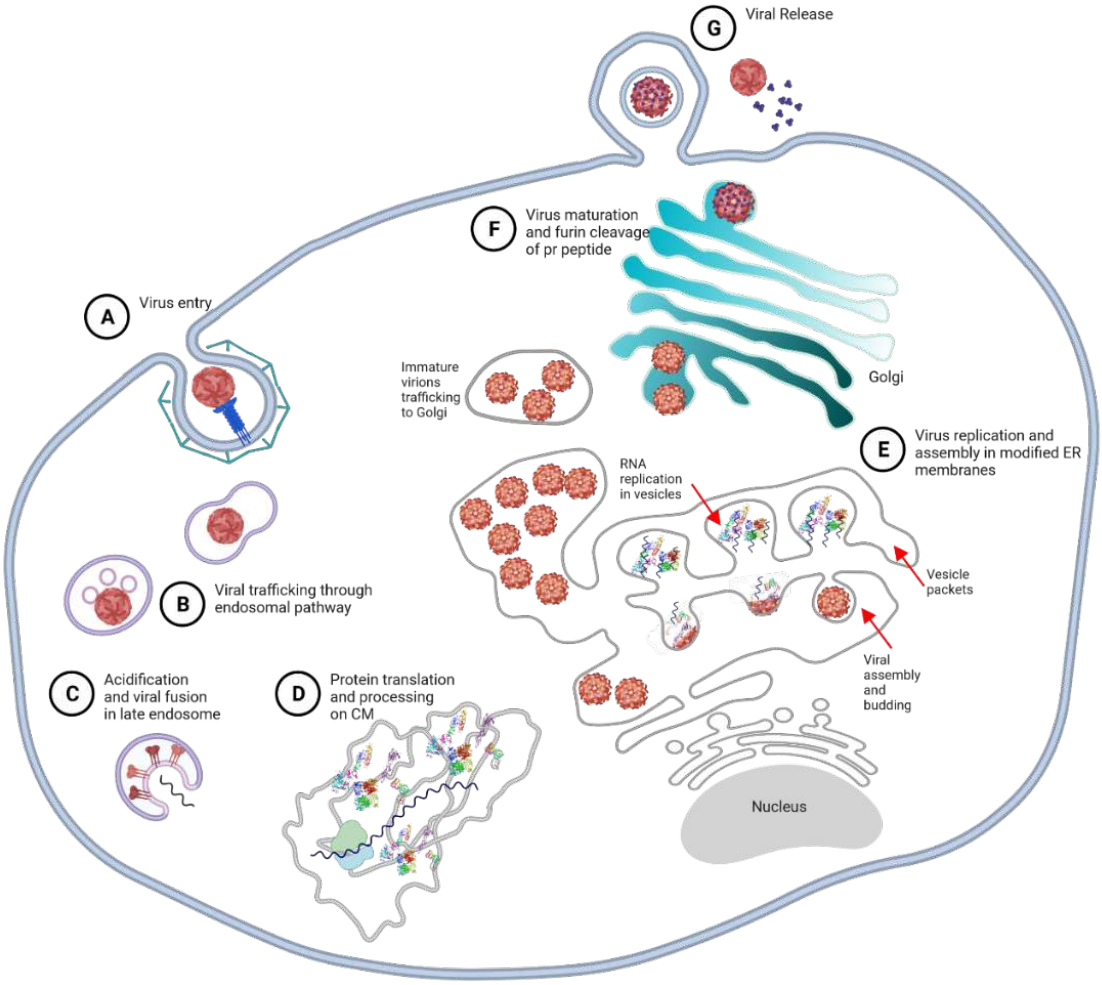

Figure 1.1 – A Schematic of the DENV Life Cycle. (A) DENVs attach to receptor molecules and enter the cell via clathrin-mediated endocytosis. (B) Following endocytosis, virus particles traffic through the endosomal pathway towards the late endosome. (C) Acidification in the late endosome allows for conformation changes in the E glycoprotein, exposing the fusion loop which allows for virus to bind with endosomal membrane and release the viral genome into the cytoplasm. (D) As DENVs are positive sense RNA viruses, protein translation immediately occurs. Translation occurs in ER-derived convoluted membranes. (E) Genome replication and assembly of immature virus particles occur in modified ER membranes. Assembled particles bud from ER cisternae and travel in vesicles to the Golgi for maturation. (F) Acidic pH in the Golgi drives changes in structural conformation of the virus particle, and cleavage of the pr peptide from the M protein. (G) The pr peptide remains associated with the virus particle until the virus is released into the neutral pH environment in the extracellular space to prevent premature fusion within the cell [reviewed in 13,14]. (A-G) Structures are not drawn to scale. Image generated using Biorender.com.

Attachment and entry

Many viruses, such as HIV and influenza, display limited tropism as they can only enter cells bearing specific receptors [15,16]. However, one of the more insidious features of flaviviruses is that they display broad cellular tropism [17]. DENVs have been documented to replicate in peripheral blood, splenic, lymphatic, skin, and hepatic tissues [18–22]. While many putative attachment molecules have been identified, there is no consensus on a specific attachment molecule, a summary of identified molecules are presented in Table 1.1 [14,23–34,reviewed in 35]. It is hypothesized that binding non-specifically may have been an evolutionary mechanism to drive increased cellular tropism [35]. Irrespective of the attachment molecule used, the remaining steps of viral entry are more clearly understood. DENVs will diffuse across a cellular surface, bind to an attachment molecule contained within a clathrin-coated pit, and be internalized via clathrin-mediated endocytosis [36]. Following internalization, virions are delivered to early endosomes where they are sorted for endocytic pathway transport and are delivered to late endosomes [36,37]. As endosomes mature they become increasingly acidic [38], which favors the structural transitions necessary to expose the fusion loop of the viral glycoprotein [39,40]. This allows the viral envelope to fuse with the endosomal membrane and for the viral RNA to be released into the cytoplasm [36,39–41]. Importantly, low pH is not the only determinant of complete fusion and release of viral RNA. It has been demonstrated that complete fusion is dependent upon the presence of the anionic lipid, bis(monoacylglycerol)phosphate (BMP), which is found primarily in late endosomal membranes [42,43]. It is hypothesized that the requirement of BMP for fusion is one mechanism DENVs use to control the intracellular location of genome release [42].

Table 1.1 – Identified Attachment Molecules of dengue viruses – adapted from [14,23–34,reviewed in 35]

Molecule Type	Attachment Molecule	Cell type expressed	Reference
Claudins	Claudin-1	epithelial cells	Gao *et al.*, 2010
C-type lectin	DC-SIGN	dendritic cells	Navarro-Sanchez *et al.*, 2003 Tassaneetrithep *et al.*, 2003
C-type lectin	L-SIGN	endothelial cells in hepatic and lymphatic tissues	Tassaneetrithep *et al.*, 2003 Dejnirattisai *et al.*, 2011
C-type lectin	mannose receptor	macrophages	Miller *et al.*, 2008
Glycosaminoglycan (GAG)	Heperan sulfate	ubiquitously expressed	Chen *et al.*, 1997
Glycoprotein	high affinity laminin receptor	hepatic cells	Thepparit *et al.*, 2004
Glycosphingolipid	neolactotetraosylceramide (nLc4Cer)	ubiquitously expressed	Aoki *et al.*, 2006
Heat-shock protein	HSP70	ubiquitously expressed	Reyes-del Valle *et al.*, 2004
Heat-shock protein	HSP90	ubiquitously expressed	Chen *et al.*, 1999
Heat-shock protein	HSPA5 (aka GRP78)	ubiquitously expressed	Jindadamrongwech *et al.*, 2004
Pattern recognition receptor	CD14	macrophages, dendritic cells, and neutrophils	Chen *et al.*, 1999
Phosphatidylserine receptors (TIM/TAM receptors)	AXL	ubiquitously expressed	Meertens *et al.*, 2012
Phosphatidylserine receptors (TIM/TAM receptors)	TIM-1	ubiquitously expressed	Meertens *et al.*, 2012
Phosphatidylserine receptors (TIM/TAM receptors)	TIM-4	T-cells	Meertens *et al.*, 2012

Viral protein translation and processing

As DENVs are positive-strand RNA viruses, protein translation can be immediately initiated upon contact with a ribosome. The DENV genome is comprised of highly structured 5' and 3' untranslated regions (UTRs) and a single open reading frame (ORF) which is depicted in Figure 1.2 [13]. Importantly, the positive-sense RNA serves as both the template for RNA synthesis and message for viral protein translation. Previously, it was thought that protein translation and viral RNA replication can occur simultaneously from the same RNA template, however recent studies have demonstrated that these events occur exclusively [44–48]. These

events are controlled by the conformational state of the viral RNA, with protein translation dependent upon the linear conformation and genome replication requiring circularization of the RNA [45]. The ORF is translated into a single polyprotein that is then post-translationally cleaved by both host and viral proteases into 10 individual proteins (discussed in Section 1.2.2, illustrated in Figure 3) [49]. Flavivirus proteins are known to cause significant rearrangements of host cellular membranes during infection, including formation of endoplasmic reticulum (ER) derived convoluted membranes (CM) which are implicated as the sites of viral protein translation (depicted in Figure 1.1) [50,51]. Protein translation and processing is presumed to occur on CMs as studies in closely related flaviviruses have revealed that the viral non-structural protein 3 (NS3), and its cofactor, NS2B, which form the viral protease, are found in close association with these membranes [52].

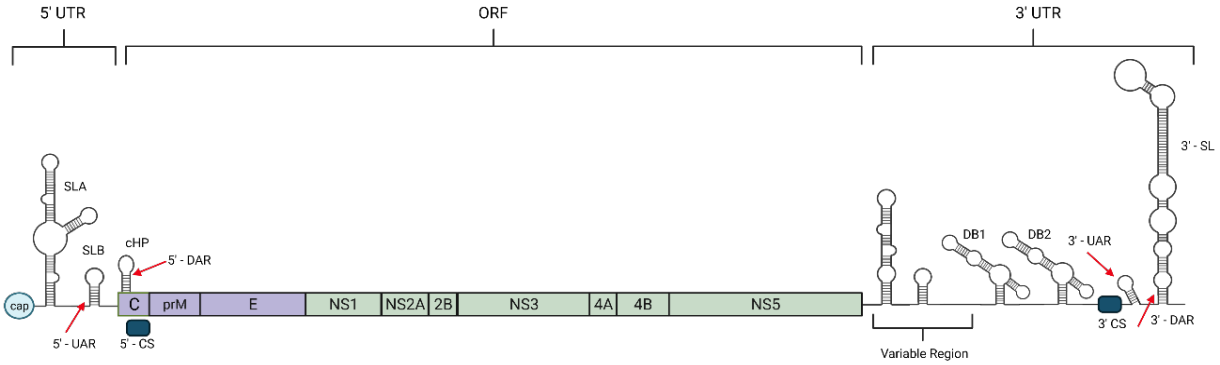

Figure 1.2 – Organization of the DENV Genome. The DENV genome is ~11 kB, is capped at the 5' end, and lacks a poly-A tail at the 3' end. The genome has a single ORF, which encodes 3 structural proteins (indicated in purple) and 7 non-structural proteins (indicated in green.) The 5' and 3' untranslated regions (UTR) of the genome are comprised of highly defined structures that are critical for viral replication, and possibly serve a role in immune evasion. Genome replication is initiated by NS5 binding to a promotor on the 5' stem loop A (SLA). Remodeling of the 5' SLB and 3' SL exposes complementary sequences in the 5' and 3' (5'UAR-3'UAR, 5'DAR-3'DAR, and 5'-CS-3'CS), and triggers circularization of the genome (not depicted). The switch from linear to circular topology promotes the transition of protein translation to viral genome replication [45,46,53,54]. (Abbreviations: cHP: capsid-coding region hairpin element, CS: complementary sequence, DAR: downstream of AUG region, DB: dumbbell, ORF: opening reading frame, SL: stem loop, SLA: stem loop A, SLB: stem loop B, UAR: upstream of AUG region, UTR: untranslated region.) Imaged generated using Biorender.com.

Viral genome replication and assembly

The proposed site of viral replication and assembly is the perinuclear ER where additional viral-protein induced membrane rearrangements lead to the formation of viral replication complexes (RCs) [48,50,51]. These RCs contain both host and viral proteins housed within

vesicles (Ve) that are contained within larger vesicle packets (Vp) and protect replicating viral RNA from host degradative enzymes (depicted in Figure 1.1) [48,50,51]. Viral RNA synthesis is a tightly regulated process, that requires several functional elements contained within the 5' and 3' UTRs of the viral genome (Figure 1.2). First, the viral NS5 protein (the viral RNA dependent RNA polymerase, or RdRp) binds to a promotor region of stem loop A (SLA) in the 5' UTR, displacing translation initiation factors [45,46,53,54]. This is followed by remodeling of the viral RNA through destabilization of the 5' SLB and 3' SL, which exposes complementary sequences in the 5' and 3' regions of the genome, triggering circularization [45,46,53,54]. This restructuring allows for NS5 translocation to the 3' end of the viral genome to produce negative strand RNA which will serve as a template for positive strand (genome) synthesis [45,46,53,54]. In addition to its RdRp activity, the viral NS5 protein also has methyltransferase activity, thus, is also responsible for adding a 5' methylated cap to nascent positive strand RNA [47].

As depicted in Figure 1.1, assembly of immature virus particles occurs in invaginated membranes containing the viral structural proteins (capsid, C; envelope, E; and premembrane, prM) that are physically opposite of the Ve/Vp structures of RCs [51]. Unfortunately, the process of encapsidation of viral RNA is not fully understood but appears to be mediated by the viral NS2A protein (discussed in 1.2.2). RNA-C complexes are formed between newly replicated viral genomes and capsid proteins, and interact with the cytoplasmic face of E-prM complexes embedded in the ER membrane to form immature particles that then bud from the ER lumen [14]. This is also the process by which DENVs obtain their ER-derived lipid membranes [14].

Maturation and release

After budding from ER membranes, immature virus particles have been shown to accumulate in ER cisternae, and are presumably transported to the Golgi via KDEL receptor-mediated vesicular transport [51,55]. KDEL receptors are transmembrane proteins that cycle vesicles between the ER and Golgi whose predominate function is involved in retrieval of ER-resident proteins back to ER from the Golgi [56–58]. In Li *et al.*, 2015, it was demonstrated that

DENVs hijack this transport process via prM/KDELR interactions, and that this interaction is required for transport of immature DENV particles to the Golgi [55]. Interestingly, this mechanism is only observed for DENV1-3, thus transport of DENV4 from the ER to Golgi proceeds via a yet undetermined process [55]. Immature particles will then migrate through the trans-Golgi network to undergo particle maturation. Maturation involves pH-dependent structural transitions in the glycoprotein shell that cause the virus particles to convert from a 'spiky' to 'smooth' outer morphology (discussed further in 1.2.2) [14]. Following maturation, mature virions are released from infected cells. It is important to note that not all virus particles follow to complete maturation, and pleomorphic maturation intermediates are common [14]. While these maturation intermediates arise due to complications in the maturation process, they may confer an advantage for DENVs against host defenses as antibody-mediated responses may be directed towards structures in these particles which are less infectious than mature virus structures [59]. Moreover, immature particles may also contribute to ADE, as sub-neutralizing antibodies may bind these virus particles and facilitate their entry into innate immune cells [60].

1.2.2 - Dengue virus proteins

As discussed above, the DENV RNA consists of a single ORF that is initially translated as a single polyprotein (Figure 1.3.A). This polyprotein is then cleaved by viral and host cell proteases into 7 non-structural proteins, and 3 structural proteins (Figure 1.3.A) [13]. The structures of many of these proteins have been solved (Figure 1.3.B). Each of these viral proteins is involved directly in the propagation of progeny virions, however, many viral proteins also recruit, upregulate, or suppress various host factors. These functions are highlighted below.

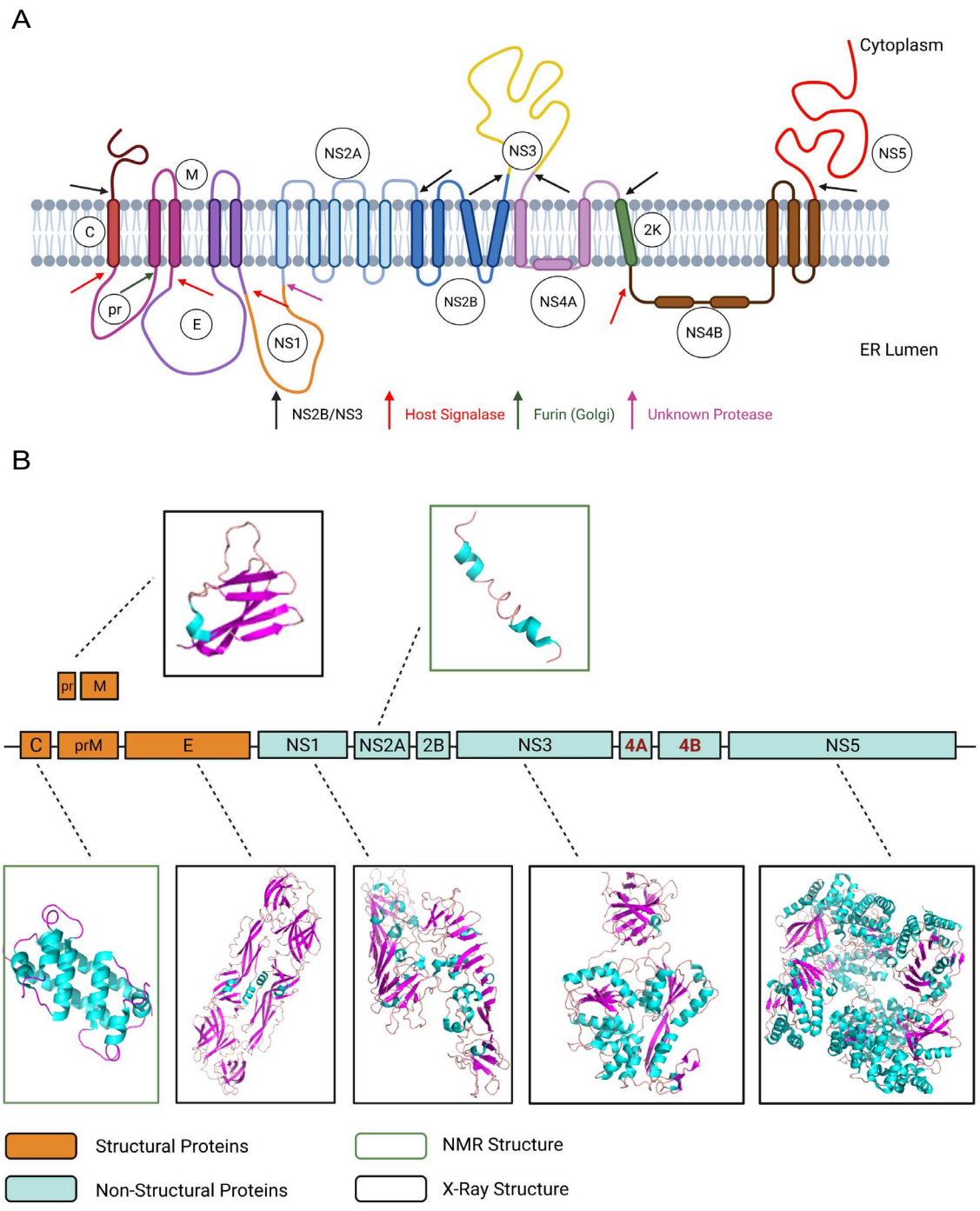

Figure 1.3 – Structural Proteome of DENVs. (A) Membrane topology of the DENV polyprotein. DENVs are translated as a single polyprotein, and then cleaved by host and viral proteases (indicated by arrows) to form 3 structural proteins, C, prM, and E and 7 non-structural proteins, NS1, NS2A, NS2B, NS3, NS4A, NS4B, and NS5 [reviewed in 61]. (B) Solved protein structures of DENV. NMR (outlined in green) and X-ray crystallography structures (outlined in black) are shown for C, pr, E, NS1, NS2A, NS3, and NS5. Structures for NS2B, NS4A and NS4B have yet to be solved (denoted in red). Protein Data Bank Identifiers: 1R6R, 3C5X, 1OKE, 4O1G, 2M0S, 2VBC, and 5ZQK, respectively [62–68]. Protein structures were generated utilizing PyMOL Molecular Graphics System, Version 2.5.2, Schrödinger, LLC. Composite image generated using Biorender.com.

Structural proteins

The capsid (C) protein is a 12 kDa, highly basic protein that functions primarily to package the RNA genome [69]. It is anchored to the ER membrane by a signal sequence in its C-terminus [62,69,70]. Dimerization of capsid protein is required for infectious particle formation [62,69,70]. Encapsidation appears to be partially coordinated by the viral NS2A protein (discussed under NS2A), but is also likely electrostatically driven as the highly basic nature of C gives it a high affinity for nucleic acids and lipids [62,69–71]. In addition to its role in genome encapsidation, the C protein is predominantly found in the nucleus [72]. Within the nucleus it has been implicated to interact with histones and DAXX to inhibit nucleosome formation and induce apoptosis, respectively [73,74].

The premembrane (prM) protein is a 22 kDa, integral membrane glycoprotein that is embedded in the ER [63]. During polypeptide synthesis, the prM undergoes N-glycosylation at Asn_{68} with $Glc_3Man_9GlcNAc_2$ [75]. In the ER, α-glucosidase enzymes are responsible for trimming the first 2 (and possible 3rd) glucose residues from the prM glycoprotein [75]. Inhibition of α-glucosidase activity inhibited proper folding of prM, and both delayed and destabilized the prM-E heterodimers that are necessary for assembly of immature virus particles leading to reduced viral output [75]. Under normal conditions, the immature virus particles that bud from the ER consist of 90 prM-E heterodimers that form 60 trimeric spikes [63,76,77]. During maturation in the Golgi, low pH causes dissociation of the prM-E heterodimers and leads to formation of 90 E protein homodimers which lay flat against the particle membrane [63,76,77]. This allows for furin-mediated cleavage of the pr peptide from the prM [63,76,77]. The pr peptide remains associated with the viral particle until it is released into the neutral extracellular environment [63,76,77]. This association seems to function to prevent premature fusion of viral particles within infected cells [63,76,77].

The envelope (E) glycoprotein, is ~55 kDa and is the first point of contact between DENVs and host cells [13]. It is a class II fusion protein, and is anchored to the membrane via two

antiparallel transmembrane domains in its C-terminus [13,35]. As discussed above, it can heterodimerize with prM proteins, or form homodimers. In each of these interactions, trimeric or dimeric conformations are possible [63,76,77]. The E protein is glycosylated at 2 residues: Asn_{67} and Asn_{153} [78]. The glycan attached at Asn_{67} is a high mannose glycan which is proposed to facilitate attachment to DC-SIGN and other mannose binding receptors for viral entry [79,80]. The N_{153} glycan is a complex glycan, proposed to contain terminal sialic residues [27,78]. The functionality of this residue is uncharacterized in DENVs, but is highly conserved across all flaviviruses and was demonstrated to act an "epitope shield" of the fusion loop of tick-borne encephalitis virus [78,81].

Non-structural proteins

NS1 is a multi-functional 46-55 kDa glycoprotein (glycosylation status effects molecular weight) [82]. The NS1 protein functions either as a homodimer inside the cell, or as hexameric lipoprotein when secreted [82]. It is the only viral protein secreted from cells [82]. NS1 homodimers are found in association with ER replication complexes despite the lack of a transmembrane anchor [82]. Resolution of the crystal structure of NS1 greatly advanced our understanding of how NS1 associates with membranes. The structural analysis that within the NS1 dimer, there is hydrophobic protrusion in the connector subdomain. This hydrophobic protrusion contains a prominent 'greasy finger' loop that allows for lipid-NS1 interactions [83]. In addition, structural analysis of NS1 also revealed that NS1 is glycosylated at Asn_{130} and Asn_{207}, although the type of glycan at each residue is different for intracellular and secreted NS1. Intracellular N-glycans are high mannose glycans, whereas secreted NS1 has a complex oligosaccharide glycan residue at N_{130} and a high mannose residue at N_{207} [82]. Previously, the NS1 homodimer was a proposed co-factor for RNA replication, and was thought to interact with NS4A and NS4B viral proteins [84]. It was thought that the NS1-NS4A-NS4B interaction facilitated formation of RNA replication complexes [85]. However, recent analysis determined that NS1

does not interact with mature NS4A and NS4B, but with the NS4A-2K-4B polyprotein precursor, and its role in Vp formation is independent of its interaction with the NS4A-2K-4B precursor [86]. It was proposed that NS1 temporally regulates NS4A-2K-4B cleavage as this regulation has been demonstrated to be critical for viral RNA replication of other viruses [86–89]. The mechanisms for NS1-mediated Vp formation and functional role for NS1-NS4-2K-4B precursor interactions are yet unresolved. Secreted NS1 has been demonstrated to contribute to endothelial hyperpermeability and vascular leakage in a number of studies [90–93]. NS1 is shown to induce upregulation of cellular sialidases and heparanase which cleave sialic acid residues and heparan sulfate proteoglycans which destabilizes the endothelial glycocalyx [90]. Additionally, secreted NS1 lipoprotein has been shown to inhibit thrombin activation, thus also is proposed to contribute to coagulopathy and thrombocytopenia [94].

NS2A is a transmembrane protein with a predicted molecular weight of 22 kDa [95]. NS2A has been shown to co-localize with NS3, NS5, dsRNA and other components of the viral replication complex, and is indispensable for viral replication through a yet unknown mechanism [95]. Additionally, NS2A has been shown to coordinate virion assembly by recruiting the C-prM-E polyprotein, the NS2B-NS3 protease, and nascent viral RNA to assembly sites [71]. This results in a coordinated cleavage of C, prM, E proteins, genome encapsidation, and particle assembly [71]. Importantly, these two functions of NS2A appear to be driven by separate populations of NS2A [95].

NS2B is 15 kDa transmembrane protein that primarily functions as a co-factor for the serine protease domain of NS3 (denoted NS2B-NS3 protease) [96]. It has also been shown to inhibit type I interferon and apoptosis by targeting cGAS for lysosomal degradation [97]. cGAS is a sensor that activates the IFN pathway upon detection of aberrant cytoplasmic DNA [97].

NS3 is 70 kDa elongated protein with protease activity at its N-terminus and helicase, and nucleotide triphosphatase activity occurring at its C-terminus [96,98]. It does not have a transmembrane domain, but closely associates with other viral proteins and ER membranes [14].

NS3 is vital for proteolytic processing of the viral polyprotein, as well as integral to viral RNA replication due to its helicase and triphosphatase activity [14]. During DENV infection, significant expansion of lipid membranes and perturbation of lipid metabolism is observed [99]. This is mediated, in part, through stimulation of and recruitment of fatty acid synthase to sites of viral replication by NS3 [99]. NS3 also antagonizes the interferon response by cleaving the STING protein [100].

NS4A and NS4B are transmembrane proteins with respective molecular weights of ~11 kDa and ~25 kDa are typically associated with viral replication complexes. Cleavage of the NS4A-NS4B polyprotein was demonstrated to be the key event in initiation of the membrane rearrangements required for viral replication, however the mechanism of rearrangement still remains unclear [101,102].

NS5 is a 103 kDa multifunctional protein with guanylyltransferase, methyltransferase and RNA-dependent RNA polymerase (RdRp) activity [103,104]. The RdRp domain (C-terminus) is responsible for viral genome replication while the guanylyltransferase/methyltransferase domain (N-terminus) is responsible for capping and internal methylation of the viral genome [103,104]. NS5 does not possess a transmembrane domain, but instead resides in viral replication complexes through a close association with NS3 [103]. It also contains a nuclear localization sequence (NLS) and is often found in the nucleus of infected cells [103]. In the cytoplasm, it phosphorylates STAT1 (prevents nuclear translocation) and marks STAT2 for degradation to suppress the host IFN response [105]. However, in the nucleus it has been shown to increase NF-κB-RANTES which promotes an antiviral response [106]. It was also demonstrated that NS5 binds spliceosomes in the nucleus and alters cellular gene expression [107].

1.3: Alterations of host metabolic pathways upon DENV infection

We often describe viruses as 'selfish genetic elements' as the only true 'function' of a virus is to produce more of itself. This, however, is no small task as most viral genomes encode only the genes necessary to create additional copies of themselves [108]. Thus, viruses must obtain most of their resources from their host. To accomplish this, viruses have evolved a variety of mechanisms that allow them to manipulate host metabolic pathways to their advantage [108]. This includes hijacking pathways that generate the raw materials (nucleic acids, amino acids, sugars, and lipids) and energy needed for virus production as well as inhibiting host processes that antagonize viral production (*e.g.* the host immune response) [108].

DENVs are enveloped RNA viruses whose entire life cycle is intimately entangled with highly specialized cellular membranes. Major metabolic reprogramming has been observed that is coincident with both the energetic and biosynthetic demands required to generate these specialized membranes. The major pathways altered include lipid metabolism, central carbon metabolism, and autophagy. Below we will summarize our current understanding of how DENVs interact with these pathways, what alterations occur during virus infection, and what implications these changes may have on the virus life cycle.

1.3.1 - Lipid metabolism

Lipids are the major components of all biological membranes. As such, lipids are vital molecules for DENV biogenesis. Additionally, many lipids also function as biological signaling molecules. Therefore, the outcome of perturbation of these pathways reaches beyond a mere rearrangement of biological membranes to support viral replication. Metabolomics-based analyses have begun to unravel the extent of the changes to the lipid landscape upon DENV

infection. However, there are still many functional questions to be answered, thus a complete understanding of the relationship between lipids and DENVs is unavailable.

Fatty acid metabolism

Fatty acids (FAs) are the building blocks of all cellular lipids [109]. FAs can be derived from either *de novo* biosynthesis, dietary sources, or recycling of existing lipids. The primary role for FAs is formation of the lipid bilayer of biological membranes. An overview of FA metabolism is provided in section 1.4. In this section, we will focus how FA metabolic enzymes and metabolites are altered during DENV infection.

While it was previously established that DENVs remodel membranes to form replication complexes, the first report of involvement of *de novo* FA biosynthesis in this remodeling process was published by *Heaton et al*., in 2010. This study demonstrated that FA synthase (FASN), a key enzyme in *de novo* FA biosynthesis, was recruited to sites of viral replication by the DENV NS3 protein [99]. Additionally, they reported elevated FASN activity in DENV-infected cells, and showed that pharmacological inhibition of FASN reduced viral genome replication and infectious particle release [99].

Since this initial study, various metabolomics-based studies have been conducted to characterize the lipid profile of DENV-infected cells and patient sera. Studies in *Ae. aegypti* mosquitoes as well as in mosquito cells revealed an overall increase in lipid abundance in infected mosquitoes and cells [110,111]. These studies found elevations in phosphatidylcholine (PC), lysophospholipids (LPLs), ceramide (CER), sphingomyelin (SM), glycerophospholipids (GPs), hexosylceramides, and acyl-carnitines [110,111].

Some key observations can be made from these results. First, enrichment of lipid species that can alter membrane curvature and permeability were observed in both studies [110,111]. These lipids included unsaturated PC and CER, which can both induce negative membrane curvature, and LPLs which promote positive curvature [112–114]. It should be noted that PC is

generally a planar molecule, however, incorporation of unsaturated fatty acyl chain can increase membrane flexibility and bending [115]. Enrichment of these lipids, therefore, may function to produce the Ve/Vp structures of the viral RCs and promote budding during particle assembly. LPLs and GPs support membrane permeability due to their surfactant properties [112–114]. Altered permeability of RC membranes would also be advantageous to DENVs as it allows for exchange and transport of raw materials to RCs. Second, all observed acyl-carnitines were upregulated during infection [111]. Importantly, acyl-carnitines are β-oxidation intermediates, and are therefore involved in ATP production in the mitochondria [116], thus these results signified a potential elevation in β-oxidation during DENV2 infection.

Analysis of serum samples from infected patients, revealed striking differences in the lipid profile of patients in the febrile, defervescent, and convalescent stages of dengue [117]. Elevations in polyunsaturated fatty acids, arachidonic acid, linoleic acid, docoahexaenoic acid, α-linoleic acid, acyl-carnitines, SM, and glucosylceramide (GluCer) were found in the febrile and defervescent stages but not in the convalescent [117]. This highlights a potential for use of these lipid species as prognostic biomarkers. In another study, elevated docosahexaenoic acid in sera positively correlated with progression to severe dengue (DHF/DSS) [118]. Importantly, similar alterations in host lipid metabolism upon DENV infection were observed in mosquitoes and humans. Thus, lipid metabolism is an attractive target for antiviral development and vector control methods.

Unsaturated fatty acid biosynthesis

Fatty acids are characterized as either saturated or unsaturated based either on the lack or presence of double bonds in their hydrocarbon chains. The rate limiting enzyme of *de novo* unsaturated FA biosynthesis, stearoyl-CoA desaturase 1 (SCD1), was also demonstrated to be vital for DENV replication [119]. Both pharmacological and siRNA-mediated inhibition of SCD1 resulted in a reduction of viral genome replication and viral release from cells [119]. Taken alone,

this result may be somewhat unsurprising as unsaturated fatty acids are vital components of membranes and allow for membrane curvature and fluidity. Thus, inhibition of this enzyme would result in cells with membranes that are less hospitable for DENV replication. However, a second, more consequential finding resulted from this study. Analysis of the virus particles released from SCD1 knockdown vs. control cells revealed that virions derived from SCD1 knockdown cells had more particles that were only partially mature compared to control cells, indicating that incomplete cleavage of the pr peptide occurred in the Golgi [119]. This suggested that unsaturated fatty acids are required in the viral envelope for correct structural transitions to occur during maturation [119].

Sphingolipids

Sphingolipids (SLs) are a group of structurally diverse lipids that serve as both structural components of biological membranes, and as potent bioactive signaling molecules [113]. Examples of SL involvement in signaling pathways for all major biological functions has been extensively documented [120]. Thus, disruption of SL metabolism is also linked to a wide range of human pathologies including neurological disorders, cancers, diabetes, autoimmune disease, and some viral infections [120]. A detailed overview of SL structure, metabolism, and function is presented in section 1.5.

Early evidence of SL involvement in the DENV lifecycle came from a landmark study that used high-resolution mass spectrometry to develop a comprehensive lipid profile of DENV-infected mosquito cells [110]. In this study, significant upregulation of specific ceramide (CER) and sphingomyelin (SM) species were shown during infection, while glucosylceramide (GluCer) species were predominately downregulated [110]. Another important feature of this study is that specific CER species were found to be enriched in replication complexes, implicating a possible role for CER in viral replication [110].

A follow-up study conducted in DENV-infected *Ae. aegypti* mosquitoes found elevations of CER, hexosylceramide (GluCer or galactosylceramide), SM analogs, sphinganine, and

sphingosine at 3, 7, and 11 days post infectious blood meal [111]. Additionally, this study also discovered that treatment of Aag2 cells (*Ae. aegypti* derived) with 4-hydroxyphenyl retinamide or dsRNA that targets DEGS, the enzyme responsible for the final step in *de novo* CER synthesis, reduced viral genome replication and infectious virus release from cells [111]. Taken together, both studies highlighted critical roles for CER in viral replication.

However, a later study examining the utilization of CER in DENV-infected mammalian cells contradicted these results [121]. Critical results from this study were that inhibition of CER favored DENV replication, and that CER is not incorporated in DENV replication complexes [121]. While the results of these studies are in opposition, they may underscore critical differences in CER functionality between mammals and mosquitoes. Studies of the serum of infected patients showed that CER and SM upregulation coincided with markers of inflammation [117]. As both molecules function as pro-inflammatory signaling molecules [120], elevations of these molecules in humans may be part of the host anti-viral response.

Additional reports have demonstrated roles for the sphingosine kinases (SPHK1 and SPHK2) and their products sphingosine-1-phosphates (S1Ps) in modulation of innate immune responses during DENV infection [122–125]. However, each of these studies reported conflicting information regarding expression levels of SPHKs, S1Ps, and their effect on immune signaling. Thus, it is not yet clear how these enzymes and their products are regulated during infection and whether they are pro-viral or anti-viral. Because different cell types and time points were used in each study, the results may also point to cell-specific or temporal regulation of these enzymes [122–125]. Further investigations are necessary to clarify the involvement of SPHKs and S1Ps in DENV infection.

Cholesterol biosynthesis

A final class of lipids that are altered during infections are cholesterol lipids. Cholesterols are major components of biological membranes, but are most abundant in plasma membranes [126]. Sterols provide structure and rigidity to membranes, and are often associated with sphingolipids in lipid rafts [127]. Lipid rafts are specialized microdomains where signaling molecules and receptors are organized [127].

In a study examining the effect of cholesterol on DENV2 entry, Lee *et al*., made two important observations. The first is that depletion of cholesterol/disruption of lipid rafts in the plasma membrane blocks DENV entry suggesting that lipid rafts are necessary for viral attachment/entry [128]. Of note, many of the putative receptors for DENV are found in lipid rafts [35]. The second result is that treatment of cells with excess cholesterol inhibits viral uncoating and replication suggesting that tight regulation of cholesterol levels is a requisite for DENV replication [128]. The latter result is possibly explained in a later study that found excess cholesterol taken up through the endocytic pathway blocks trafficking and viral uncoating in the late endosome, possibly through inhibition of fusion [129].

Additional studies have found that upon DENV infection upregulation of low-density lipoprotein receptors (LDLr) with concomitant increase in cellular cholesterol levels are observed [130]. These changes were observed as early as one hour post infection, indicating cholesterol may be involved in early steps in the DENV life cycle [130]. Moreover, translocation to viral RCs and increased activity of HMG-CoA reductase (HMGCR), the rate limiting enzyme for *de novo* cholesterol synthesis, was also observed at early timepoints [130,131]. Inhibition of cholesterol biosynthesis has also been shown to inhibit DENV replication [132]. Studies in similar flaviviruses have concluded that cholesterols are vital components of viral RCs, contributing to their structure and stability [133]. Taken together, these studies suggest a similar functional role for cholesterol in DENV replication.

Carro, *et al*. have argued that cholesterol is an essential component of the DENV envelope by pretreating virus particles with methyl-beta-cyclodextrin (MβCD), a substance that depletes cholesterols within membranes [134]. In this study, they found that MβCD depletion of cholesterol from virus particles dramatically reduced viral infectivity via inhibition of viral fusion in the late endosome, concluding that cholesterol is a vital component of DENV envelopes [134]. However, they failed to account for how this depletion affected the structural architecture of the virions, which would have dire effects on fusion. Thus, it remains unclear if cholesterol is a required membrane component of infectious virions, or whether its presence was merely an artifact of the membrane composition from which the viral envelope was derived.

1.3.2 - Central carbon metabolism

Central carbon metabolism collectively describes the processes involved in enzymatically transforming glucose and glutamine into metabolic precursors and energy. The primary pathways involved in central carbon metabolism are glycolysis, the tricarboxylic acid cycle (TCA cycle), and the pentose phosphate pathway. As these processes supply the energy and raw materials that would be needed for viral propagation, it is reasonable that they would be obvious targets of viral subjugation. Unfortunately, very few studies have examined how these pathways are activated/modulated during DENV infection. Below we will provide a summary of our current knowledge of the relationship between DENV and central carbon metabolism.

Glycolysis

Under standard aerobic conditions, glucose is used as central carbon source to produce ATP via oxidative phosphorylation (OXPHOS) [135]. Glycolysis is the first step of this process in which glucose is converted to pyruvate in a 10-step process [135]. Pyruvate then shuttles into the mitochondria where it undergoes additional processing in the TCA cycle (discussed in the next

section) [135]. At any step of glycolysis, intermediates may be shuttled to other pathways. Any of the 10 enzymes involved in glycolysis represent possible targets of viral modulation. However, hexokinase, phosophofructokinase, and pyruvate kinase are the most obvious targets as they represent the committal, rate-limiting, and final step, respectively [135].

Fontaine *et al.* were the first to report on DENV's influence on glycolysis. There were 3 major findings in their report. The first, was that DENV infection results in increased cellular glucose uptake via upregulation of the GLUT1 glucose transporter [136]. As well, exogenous glucose was required for productive viral infection, as infectious virus was significantly reduced in cells grown in glucose-free media [136]. Second, they found elevated hexokinase expression (mRNA and protein) and increased levels of glycolytic intermediates in DENV-infected cells [136]. Finally, they demonstrated that conversion of pyruvate to lactate by lactate dehydrogenase is necessary for viral replication [136]. Taken together, their study demonstrated that completion of glycolysis is necessary for DENV replication. However, it is unclear if glycolysis is upregulated to provide energy via completion of OXPHOS, or if it is used by DENVs to generate intermediates for fatty acid biosynthesis. The fact that pyruvate conversion to lactate was necessary for viral replication suggests that DENVs may favor energy production via lactic acid fermentation (LAF) over OXPHOS.

There is much evidence to support why DENVs might trigger a metabolic switch to lactic acid fermentation over OXPHOS. Canonically, LAF occurs under anerobic conditions, while OXPHOS proceeds in aerobic conditions [135]. The switch to LAF when oxygen is present is known as aerobic glycolysis or the Warburg Effect [135]. OXPHOS is a more efficient process as it generates 36-38 ATP per single glucose molecule, whereas LAF only generates 4 ATP per glucose molecule [135]. It would reason that OXPHOS should be a preferred pathway for a virus with high energy demands. However, kinetic analyses of these processes reveals that conversion of glucose to lactate occurs 10-100 faster than completion of OXPHOS in the mitochondria, thus,

while LAF is a less efficient means of glucose metabolism, it has the capacity to produce ATP more rapidly [137].

Interestingly, glyceraldehyde-3-phosphate dehydrogenase (GAPDH) upregulation and increased activity has been shown to positively correlate with increased LAF, moreover GAPDH was shown to be a rate-limiting enzyme for LAF [137]. GAPDH controls the sixth step of glycolysis, but has also been shown have several functions exclusive to its glycolytic activity. For example, it has been shown to regulate ER-Golgi transport, apoptosis, DNA repair and RNA stability [138]. Inhibition of GAPDH also drives increased production of metabolic precursor molecules and shuttling of G6P into the pentose phosphate pathway (PPP) [138]. In DENV-infected cells, GAPDH has been shown to interact with both the NS1 and NS3 protein at different times of infection [139,140]. At early timepoints, GAPDH-NS1 interactions prevail and GAPDH glycolytic activity is elevated [139]. At later timepoints, GAPDH-NS3 interactions prevail, and its glycolytic activity is decreased [140]. It was demonstrated that NS1 and NS3 share a similar binding site on GAPDH, but opposing allosteric effects on the enzyme [139,140]. The switch between NS1 and NS3 binding to GAPDH was proposed to be a consequence of their binding affinities for GAPDH and their relative availability to bind at early and late time points [140]. NS3 has a higher affinity for GAPDH, but is unavailable early in infection due to its functions as the viral protease [140]. This temporal regulation of GAPDH suggested that DENVs may exploit GAPDH's versatility [139,140]. Thus, increased aerobic glycolysis may support the high energy demands of early infection, however, a metabolic switch may support RNA replication, generation of metabolic precursor molecules, and ER-Golgi transport at later timepoints. This hypothesis is further supported from works by Fernandes-Siqueira *et al*. which demonstrated that glucose/glycolysis plays an anaplerotic role in fatty acid metabolism, thus supporting DENV's requirement for lipid metabolites [141]. Moreover, they determined that fatty acid oxidation (β-oxidation) is the main source of cellular energy during DENV infection [141].

The tricarboxylic acid cycle

The pyruvate generated at the completion of glycolysis has six metabolic fates, however, the general fate of pyruvate is its conversion to acetyl-CoA by pyruvate dehydrogenase [142]. Acetyl-CoA can then be shuttled into either the TCA cycle, the *de novo* cholesterol biosynthesis pathway, or the *de novo* fatty acid biosynthesis pathway [143]. The TCA cycle is series of reactions that occurs in the mitochondria that allows for the release of stored energy (ATP, NADH, and $FADH_2$) from carbohydrate molecules. The released NADH and $FADH_2$ are, in turn, used in OXPHOS to generate ATP [135]. Importantly, TCA cycle intermediates also serve as precursor molecules for both lipid and nucleotide biosynthesis [144].

Unfortunately, very few studies shed light on DENV's influence over the citric acid cycle. As Fernandes-Siqueira *et al.* demonstrated that glycolysis functions to provide substrates for fatty acid biosynthesis and β-oxidation [141], the logical conclusion is that this, in part, is through continuation of pyruvate to the TCA cycle to generate FA precursor molecules. A report analyzing metabolites in urine collected from DENV infected patients showed a marked decrease in citrate and succinate, two TCA cycle intermediates, in DENV-infected patients compared to healthy controls [145]. Under basal conditions, levels of these two intermediates are under tight homeostatic control [146], thus, these data suggest either a TCA cycle defect, or that these intermediates might be shuttled disproportionately towards other processes. Further analysis of flux of TCA cycle intermediates during DENV infection is required to clarify these results. However, the observation that mitochondrial elongation with concomitant increase in respiration and ATP synthesis occurs during DENV infection may provide some clarity [147,148]. Studies investigating the relationship between mitochondria morphodynamics and β-oxidation have shown that mitochondrial elongation maximizes β-oxidation potential [149,150]. Thus, it is entirely plausible that DENVs employ several metabolic switches to drive glycolysis and the TCA cycle towards production of fatty acids both for β-oxidation/energy production and necessary precursors for membrane biosynthesis/rearrangement and away from OXPHOS.

The pentose phosphate pathway

The first step of glycolysis is the phosphorylation of glucose to form glucose-6-phosphate (G6P) [135]. G6P can then either continue through glycolysis, or it can supply the pentose phosphate pathway (PPP) [135]. The PPP is responsible for the conversion of G6P to ribose-5-phosphate (R5P), the precursor molecule for nucleotide biosynthesis [151]. Additionally, the PPP is the main source of cellular NADPH, which is the reducing agent for cellular anabolic pathways [151]. NADPH is required for synthesis of non-essential amino acids, fatty acids, cholesterols, and nucleotides [151]. Consequently, this pathway is likely vital for DENV replication and a potential target for viral subjugation.

However, only a limited number of studies exist that examine the role of the PPP during DENV infection. In an untargeted metabolomics analysis of DENV infected Huh7 cells, our lab has shown an enrichment in purine and pyrimidine metabolism, tyrosine metabolism, and glutathione metabolism during early and peak viral replication [Gullberg RC, *et al.* unpublished]. Importantly, each of these processes are dependent upon either the ribose 5-phosphate or NADPH generated from the PPP suggesting possible upregulation of this pathway during DENV infection.

A common X-linked genetic disorder is glucose-6-phosphate dehydrogenase (G6PD) deficiency [152]. Conversion of G6P to 6-phosphoglucono-δ-lactone by G6PD is the first and rate-limiting step of the PPP [151]. The effect of this disorder on the severity of DENV infection has been examined in several studies. Interestingly, some reports show G6PD deficiency drives increased viremia and disease severity, while other studies report the deficiency has no impact on disease severity [153–155] . These results are somewhat perplexing, as decreased capacity of the pentose phosphate pathway should have an inhibitory effect on DENV. However, a possible explanation for this phenomenon is that G6PD-deficiency is demonstrated to cause marked downregulation of the pro-inflammatory immune response [152]. NADPH is a potent regulator of the immune response, and is produced by G6PD, thus intimately coupling the PPP and immune

function [156]. Therefore, is it possible that the noted increases in viremia and disease severity in G6PD-deficient DENV-infected patients was the result of a decreased antiviral response in those individuals.

1.3.3 – Autophagy

Autophagy is a homeostatic process occurring in cells that allows for degradation and recycling of cytosolic cellular components (including organelles). Cellular components are sequestered into double-membrane vesicles (autophagosomes), autophagosomes fuse with endosomes (amphisome) and traffic through endolysosomal pathway until they fuse with a lysosome (autolysosome) [157]. Once degradation is complete, permeases allow for release of molecular building blocks back into the cytoplasm that can be used for energy production or biosynthesis of macromolecules [157]. Autophagy can also be induced by cellular stress, nutrient deprivation, and accumulation of unfolded proteins and is typically involved in pro-survival processes. However, autophagy also participates in interferon induction, presentation of antigens to T lymphocytes, and can mediate cell death [157,158]. This signals that autophagy can either play pro-viral, anti-viral, or, more likely, dual roles during viral infection.

DENVs are known to induce autophagy, as an increased presence of autophagosomes in infected cells has been noted in several studies [159–163]. In each study, inhibition of autophagy resulted in decreased viral replication, release, or infectious particle generation, signaling an important role for autophagy in the DENV life cycle [159–163]. Work by Heaton *et al.* demonstrated that DENV-induced autophagy increased cellular degradation of lipid droplets [162]. Lipid droplets are storage molecules that are typically degraded when cells are under high energy demands as this process releases fatty acids that can be used in β-oxidation. Heaton *et al*. demonstrated that there was a positive correlation between DENV infection, increased lipid droplet depletion (lipolysis), and β-oxidation, and that LD depletion and subsequent β-oxidation

was required for DENV replication and release [162]. Additionally studies demonstrated that expression of the NS4A protein alone was sufficient for activating autophagy in epithelial cells, however it is not clear how viral proteins may contribute to autophagy induction in other cell types [161].

Viral dsRNA (a replication intermediate) and viral proteins have been found to co-localize with amphisomes suggesting a possible role of autophagy in early infection [159,163]. Interestingly, fusion of these structures with lysosomes resulted in a decrease of infectious particle release from cells [159,163]. This suggested that DENVs may replicate on amphisomes [159,163]. These studies were seemingly contradicted by electron tomography studies performed later that demonstrated viral replication complexes formed in vesicles that were covered by a continuous ER-derived membrane, and were not stand-alone vesicles [51]. However, endosomal trafficking requires a close association of endosomes/amphisomes with ER membranes, and endosome-ER contact sites are well described [164]. Additional electron tomography studies have revealed that ER tubules wrap around endosomes, and these associations increase as endosomes mature [165]. Thus, both observations of amphisome and ER-associated DENV replication sites are likely correct. Moreover, these discoveries of the intricate ER/mature endosome associations may shed new light on how DENVs coordinate release of their genome into appropriate membrane compartments during viral entry.

During viral infection, exosomes containing viral RNA can increase the spread of viral infection to neighboring cells and cells lacking viral receptors, thereby exacerbating infection and allowing for the virus to evade the host immune response [166]. Several viruses including DENVs have been shown to exploit this process [166]. While autophagy is largely an intracellular process, some studies have shown it also plays unconventional roles in the secretory pathway [167]. Incidentally, several recent studies have reported that DENV-containing extracellular vesicles from *in vitro* experiments and patient sera contain autophagy machinery [168–170].

Taken together, this suggests a model where autophagy may be exploited by DENVs. DENVs may utilize autophagy to generate energy and precursor molecules from lipolysis, take advantage of the unique double membrane structure of the amphisome to form viral replication complexes, facilitate its intracellular trafficking along the endosomal pathway, and evade the host antiviral response. Additional studies are needed to unravel how DENVs regulate amphisome binding with lysosomes to either complete autophagy/lipolysis or prevent degradation of replicating virus particles.

1.4: Fatty acid metabolism

In the previous sections, we have discussed how DENVs are dependent and subvert host lipid metabolic pathways. However, while changes to the lipid landscape in DENV-infected cells is well characterized, the mechanism and consequences of these changes are less so. In the next three sections, we will provide an in-depth overview of fatty acid and sphingolipid metabolic pathways, the enzymes involved, subcellular location of processes, and intracellular trafficking of lipids. We will also discuss the impact of dysregulation of sphingolipid metabolism in chronic and other infectious diseases. The goal of these sections will be to provide additional insight into how these processes may affect viral production and contribute to dengue pathogenesis. In this section, we will provide an overview of the steps of fatty acid biosynthesis, formation of complex lipids, and breakdown of fatty acids. The reactions described will be depicted in Figures 1.4 at the end of this section.

De novo fatty acid biosynthesis

De novo synthesis of FAs begins in the cytoplasm of cells. The first step is the conversion of acetyl-CoA to malonyl-CoA by acetyl-CoA carboxylase (ACC). ACC is a multi-domain enzyme with biotin carboxylase activity at its N-terminus and carboxyl transferase activity at its C-terminus,

and produces malonyl-CoA as a two-step process (depicted in Figure 1.4A) [171]. The next step is a cyclical reaction catalyzed by fatty acid synthase (FAS) that converts malonyl-CoA into palmitic acid. FAS is a multi-enzyme protein containing 7 catalytic domains: β-ketoacyl synthase (KS), malonyl/acetyltransferase (MAT), dehydrase (DH), enoyl reductase (ER), β-ketoacyl reductase (KR), acyl carrier protein (ACP), and thioesterase (TE). FAS is only active as a homodimer [172]. Although the organization of each monomer is still poorly understood, there is clear evidence to support inter- and intramonomer interactions [172]. At each 'turn' within FAS two carbons are added to a growing acyl-ACP chain through a series of condensation, reduction, and dehydration reactions (Figure 1.4B), until the C16 palmitic acid is formed, and is then released by TE [171].

After palmitic acid forms, it ligated to coenzyme A (CoA) by acyl-CoA synthetase, producing an activated palmitoyl-CoA [171]. CoA is an important cofactor for FAs as it facilitates transport and binding to FA-modifying enzymes, and can act directly as either electrophiles or neutrophiles in FA modifying reactions [173]. Palmitoyl-CoA (and other acyl-CoAs) can then be transferred to the ER, mitochondria, or peroxisome to undergo additional modifications to generate complex lipids. Throughout the remainder of this text the terms fatty acyl-CoA, fatty acid, and FAs will be used interchangeably, and free fatty acids will be described as FFAs.

Elongation and desaturation of fatty acids

Elongation of fatty acids requires the same series of condensation, reduction, and dehydration reactions as described for fatty acid synthase. However, it is catalyzed by 4 separate ER transmembrane proteins: elongation of very long chain fatty acids (ELOVL1-7), 3-keto acyl-CoA reductase (KAR), 3-hydroxy acyl-CoA dehydratase (HACD1-4), and trans 2,3 enoyl-CoA reductase (TECR) (Figure 1.4C) [171]. After each elongation series, the fatty-acyl chain is increased by 2 carbons.

Desaturation of FAs incorporates a double bond into the FA chain to generate unsaturated FAs (UFAs) (Figure 1.4D) [171]. UFAs (including mono- and polyunsaturated fatty acids, or MUFAs and PUFAs) maintain fluidity of biological membranes, are important precursors for pro- and anti-inflammatory lipid mediators (e.g. prostaglandins, leukotrienes, resolvins, and protectins), and play crucial roles as signaling molecules [174]. Desaturase enzymes are denoted as Δ#-desaturase, with the # indicating the position of the carbon-carbon double bond relative to the carboxylic acid end of a FA. There are two types of desaturase enzymes found in humans: FA desaturase (FADS1-2) and stearoyl-CoA desaturase (SCD1,5). SCD1 and 5 are both Δ-9 desaturases, however, SCD1 is predominant as SCD5 has limited tissue expression [171,175]. SCD1 is the rate-limiting enzyme for all UFA biosynthesis. Palmitic acid (C16:0) and stearic acid (C18:0) are the preferred substrates for SCD1 and are converted to palmitoleic and oleic acid, respectively [171]. FADS1 and 2 are both rate-limiting enzymes in PUFA biosynthesis. FADS1 is a Δ-5 desaturase, while FADS2 is a Δ-6 desaturase [171]. Notably, humans are not capable of introducing double bonds past the Δ9 position [171]. However, many PUFAs contain n-3 or n-6 fatty acids, which denotes the position of carbon-carbon doubles bonds relative to the methyl end of the FA. Thus, these FAs are ‘essential FAs’ and must be derived from dietary sources. Once inside cells, these FAs can be modified the same as any others.

Importantly, elongation and desaturation generate an inordinate amount of diversity in lipid species and in lipid conformation. While FAs are often incorporated into complex lipid species (glycero-, glycerophospho-, and sphingolipids), it important to remember that many FAs are also critical mediators of biological function, a concept we are only beginning to unravel [176–178]. As structure dictates function in biology, the diversity of fatty acids structures is not incidental. It is an important point to remember that when we say ‘phosphotidylcholine,’ ‘ceramide,’ ‘glucosylceramide,’ etc., that we are not discussing a specific molecule, but rather a group of molecules that share a similar base structure but can differ greatly depending upon their fatty acyl

tails, or, in the context of glycosphingolipids, their fatty acyl tails and the complexity of the sugar moieties attached to their head group.

Complex lipid synthesis

Complex lipids can be divided into three categories glycerophospholipids, glycerolipids, and sphingolipids. Sphingolipids will be discussed in depth in section 1.5, so we will only address glycerophospholipids and glycerolipids in this section.

Glycerolipids are composed of a molecule of glycerol esterified to 1, 2, or 3 fatty acyl chains (mono-, di-, and triacylglycerols, or MAGs, DAGs, and TAGs). TAGs are the main energy storage molecules in mammals. While MAGs and DAGs are important precursors for TAG synthesis, they are also recognized as vital signaling molecules [179]. *De novo* synthesis is stepwise and is carried out by glycerol-3-phosphate acyl-transferases (GPAT1-4), lysophosphatidic acid (LPA) acyltransferases (LPAAT α, β, γ, δ, and ε, formerly AGPATs), phosphatidic acid (PA) phosphatase (PAP), and diacylglycerol acyltransferases (DGAT1-2) and is depicted in Figure 1.4E [179,180]. DAGs and TAGs can be synthesized *de novo*, but MAGs are derived either from the diet or from the hydrolysis of DAGs and TAGs [179,180]. DAG can also be formed by acylation of MAG by the monoacylglycerol acyltransferases (MOGAT1-3) [181]. Once synthesized, TAGs are assembled into two types of storage molecules: lipid droplets which remain in the cell or lipoproteins which can be transported throughout the body or stored in adipocytes.

Glycerophospholipids (GPLs) are the major constituents of biological membranes and are composed of a molecule of glycerol esterified to 2 FAs (hydrophobic tail) and a phosphate head group (hydrophilic head). GPLs are named according to their head groups, with the simplest being phosphatidic acid which is comprised only of the components above [182]. The phosphate head, however, can undergo additional esterifications to choline, ethanolamine, inositol, serine, or glycerol forming phosphatidylcholine (PC), phosphatidylethanolamine (PE), phosphatidylinositol

(PI), phosphatidylserine (PS), phosphatidylglycerol (PG), or diphosphatidylglycerol (cardiolipin, or CL) [182–184]. PC and PE are the most abundant membrane lipids, however, humans are only able to synthesize small amounts of choline, making it an essential dietary nutrient [184]. While synthesis of each GPL uses DAG as a precursor and CTP for energy, there are several pathways and enzymes involved in their synthesis. They are summarized in Figure 1.4F. Importantly, the FAs that are incorporated from DAG generally consist of either saturated FAs or MUFAs [185]. After membrane incorporation, extensive remodeling of GPLs occurs to incorporate PUFAs into membrane phospholipids [185]. This process is known as the Land's Cycle and is mediated by phospholipase A_2 (PLA_2) and several enzymes with lysophospholipid acyltransferase activity [185]. Briefly, PLA_2 cleave the FA in position two of the phospholipid followed by reacylation using a PUFA donor by lysophospholipid acyltransferases [185].

Acyl-CoA Thioesterases

Accumulation of activated fatty acids (fatty acyl-CoAs) within cells can have deleterious effects on cell health. First, while activation of fatty acids is required for many of their subsequent biological functions, it also traps them as fatty acyl-CoAs are membrane impermeable [186]. This can lead to organelle overload and stress. Second, fatty acyl-CoA are good detergents due to their hydrophobic carbon chain and the highly polar characteristics of CoA [187], thus accumulation within organelles can lead to organelle damage, or sequestration of proteins and metabolic intermediates. Third, many fatty acyl-CoAs play a role in biological signaling cascades, therefore, their accumulation can lead to aberrant signaling, an example is chronic inflammation caused by DAG and ceramide accumulation [120,174,188]. Lastly, coenzyme A is an important cofactor for many cellular functions (such as β-oxidation and the TCA cycle), and accumulation of fatty acyl-CoAs reduces free CoA. However, accumulation of free fatty acids (FFAs) is also problematic. FFAs can activate PPARα, a transcription factor that upregulates lipid catabolic processes including increased cellular uptake of FFAs and mitochondrial and peroxisomal β-

oxidation [189]. In turn, this can lead to mitochondrial overload, increases in ROS, and ultimately cell death/apoptosis [189]. Moreover, elevated FFAs is one of the leading contributors of metabolic syndrome, which are a cluster of metabolic disorders that are known to result in diabetes, cardiomyopathy, and non-alcoholic fatty liver disease [190]. Thus, tight homeostatic regulation of FFAs/fatty acyl-CoAs is necessary to prevent the pernicious effects of either.

One group of enzymes responsible for regulating this balance are the acyl-CoA thioesterases (ACOTs). ACOTs are responsible for cleaving the thioester bond linking fatty acids and CoA, leading to FFA and free CoA. Humans possess 10, possibly 12 enzymes belonging to the ACOT family of enzymes [191–193]. They are localized either in the mitochondria, cytoplasm, or peroxisome, and have varying acyl-chain length specificity [191–193].

ACOTs are described as either Type I ACOTs or Type II ACOTs, and this delineation is based on their sequence and structure. Type I ACOTs (ACOT 1, 2, 4, and 6) arise from the same gene cluster, share a high degree of sequence homology, and are characterized by their α/β hydrolase domain [191–193]. Type II ACOTs (ACOTs 7-9, 11-13, THEM4, THEM5) share little to no sequence homology with Type I ACOTs or each other, are found on different chromosomes and are characterized by their “double hot dog” domain [191–193]. However, all ACOTs are functionally analogous which highlights a critical role for acyl-CoA thioesterase activity.

In the mitochondria, ACOTs have been shown to protect against ROS and decrease β-oxidation overload [194–196]. It is hypothesized that they can mediate efflux of fatty acids from the mitochondrial matrix [191]. During β-oxidation, fatty acids remain esterified to CoA, preventing their transport out of the mitochondrial matrix. However, free fatty acids have been shown to exit the mitochondria using uncoupling proteins as transporters [191]. It is proposed that ACOTs cleave CoA from fatty acyl-CoAs to mediate this process. This could protect the mitochondria from oxidative damage and overload, increase the mitochondrial pool of CoA-SH, and return shorted fatty acids to the cytoplasm where they can be re-esterified and incorporated into complex

lipids or storage lipids [191]. In the peroxisome, similar regulatory mechanisms for ACOTs have been noted [195,197–199].

In the cytoplasm, ACOT functionality may assist in fatty acid trafficking as FFAs can diffuse through the lipid bilayers of organelles and the plasma membrane [191,193,200]. ACOTs may also participate in membrane remodeling [177] . ACOT7 has been shown to have specificity towards arachidonoyl-CoA [191]. Importantly, eicosanoids and other inflammatory mediators that arise from arachidonic acid are derived from the unesterified form. Thus, ACOT7 may be an important inflammatory mediator.

We hypothesized that ACOTs may negatively regulate DENV infection by decreasing the cellular pool of activated fatty acids that are required for DENV-mediated membrane rearrangements. We examined this hypothesis using siRNA-mediated loss of function studies. Those results are discussed in Chapter 2.

Lipolysis & β-oxidation

Lipolysis is the process of breaking down TAGs stored in lipid droplets or lipoproteins by lipase enzymes into its constitutive components and proceeds in the opposite direction of TAG synthesis. Which lipases are used depends on the site of TAG hydrolysis. In the vasculature, plasma membrane bound lipoprotein lipases can hydrolyze circulating lipoproteins [201]. Endocytosed lipoproteins or autophagocytosed lipid droplets are broken down by lysosomal acid lipase [201]. In adipose tissues, triglyceride lipase, hormone-sensitive lipase, and monoacylglyceride lipases hydrolyze TAGs [201]. Hepatic and gastric lipases carry out lipolysis in the liver and intestines [201]. The released FFAs and glycerol can then be used by cells to produce energy via β-oxidation and glycolysis or can serve as precursors in fatty acid biosynthesis.

Energy is released from fatty acids via β-oxidation which occurs both in the mitochondria and peroxisomes. While carried out by different groups of enzymes, the cycle of β-oxidation is

nearly identical in the mitochondria and peroxisome. Fatty acyl-CoAs undergo a series of oxidation, hydration, and thiolytic steps that reduces the fatty acyl-CoA chain by 2 carbons at each turn [116,202]. Acetyl-CoA, $FADH_2$, and NADH are the products of these reactions [116,202]. There are a few key differences between the two processes. Mitochondrial β-oxidation is directly involved in energy production, whereas peroxisomal β-oxidation is mainly a biosynthetic/remodeling pathway indirectly involved in energy production [116,202]. Mitochondria can oxidize FAs completely to CO_2 and H_2O, whereas peroxisomes are involved in oxidation of very long chain FAs, branched chain FAs, and eicosanoids and can only oxidize down to an C8 FA chain [116,202]. The acetyl-CoA, short chain FAs, NADH, and FADH produced by peroxisomes must be shuttled to the mitochondria to complete oxidation. Electrons provided by FAD in the peroxisome are transferred to H_2O_2, whereas in the mitochondria they are transferred to electron transport chain/OXPHOS [116,202]. Another key difference is the process of acyl-CoA entry into each organelle. FFAs and fatty acyl-CoAs can transfer directly across peroxisomal membranes using ATP-binding cassette transporters [116,202]. Whereas, long chain fatty acyl-CoAs cannot cross the mitochondrial membranes (short and medium chains can), and must use the acyl-carnitine shuttle [116,202]. Carnitine palmitoyltransferase I (CPT1) is located on the outer mitochondrial membranes and coverts fatty acyl-CoAs to fatty acyl-carnitines [116,202]. Fatty acyl-carnitines then diffuse into the intermembrane space, and enter the mitochondrial matrix through a carnitine-acylcarnitine translocase located in the inner mitochondrial membrane [116,202]. Once fatty acyl-carnitines enter the mitochondrial matrix, they are converted back to fatty acyl-CoAs by CPT2 so that they can participate in β-oxidation [116,202].

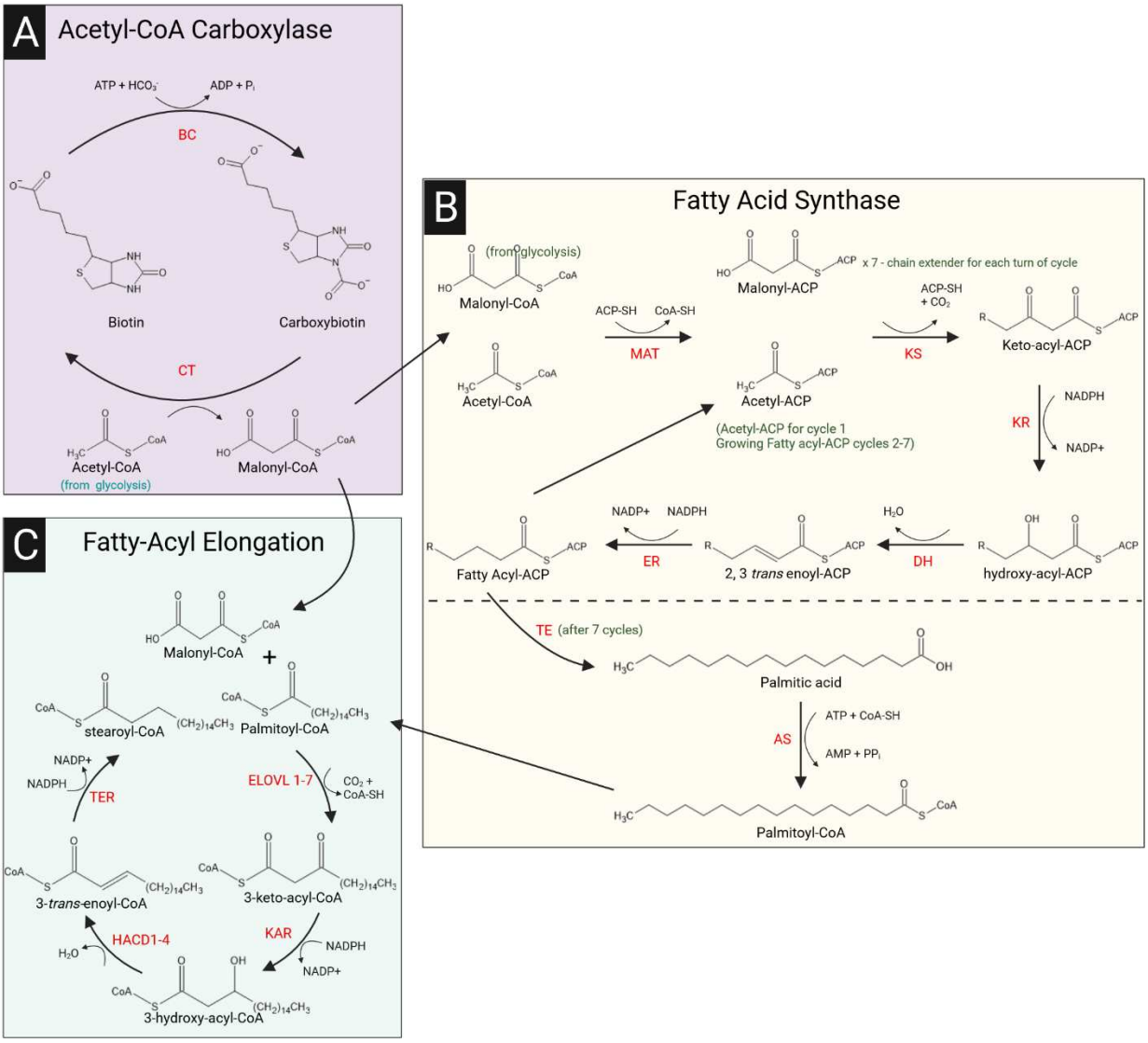
A
Acetyl-CoA Carboxylase
ATP + HCO3-
ADP + Pi
BC
Biotin
Carboxybiotin
CT
Acetyl-CoA
(from glycolysis)
Malonyl-CoA
B
Fatty Acid Synthase
(from glycolysis)
Malonyl-CoA
Malonyl-ACP
x 7 - chain extender for each turn of cycle
ACP-SH
CoA-SH
MAT
ACP-SH
+ CO2
KS
Keto-acyl-ACP
Acetyl-CoA
Acetyl-ACP
(Acetyl-ACP for cycle 1
Growing Fatty acyl-ACP cycles 2-7)
KR
NADPH
NADP+
Fatty Acyl-ACP
NADP+
NADPH
ER
2, 3 trans enoyl-ACP
H2O
DH
hydroxy-acyl-ACP
TE (after 7 cycles)
Palmitic acid
AS
ATP + CoA-SH
AMP + PPi
Palmitoyl-CoA
C
Fatty-Acyl Elongation
Malonyl-CoA
+
stearoyl-CoA
Palmitoyl-CoA
NADP+
NADPH
TER
ELOVL 1-7
CO2 +
CoA-SH
3-trans-enoyl-CoA
3-keto-acyl-CoA
HACD1-4
H2O
KAR
NADPH
NADP+
3-hydroxy-acyl-CoA

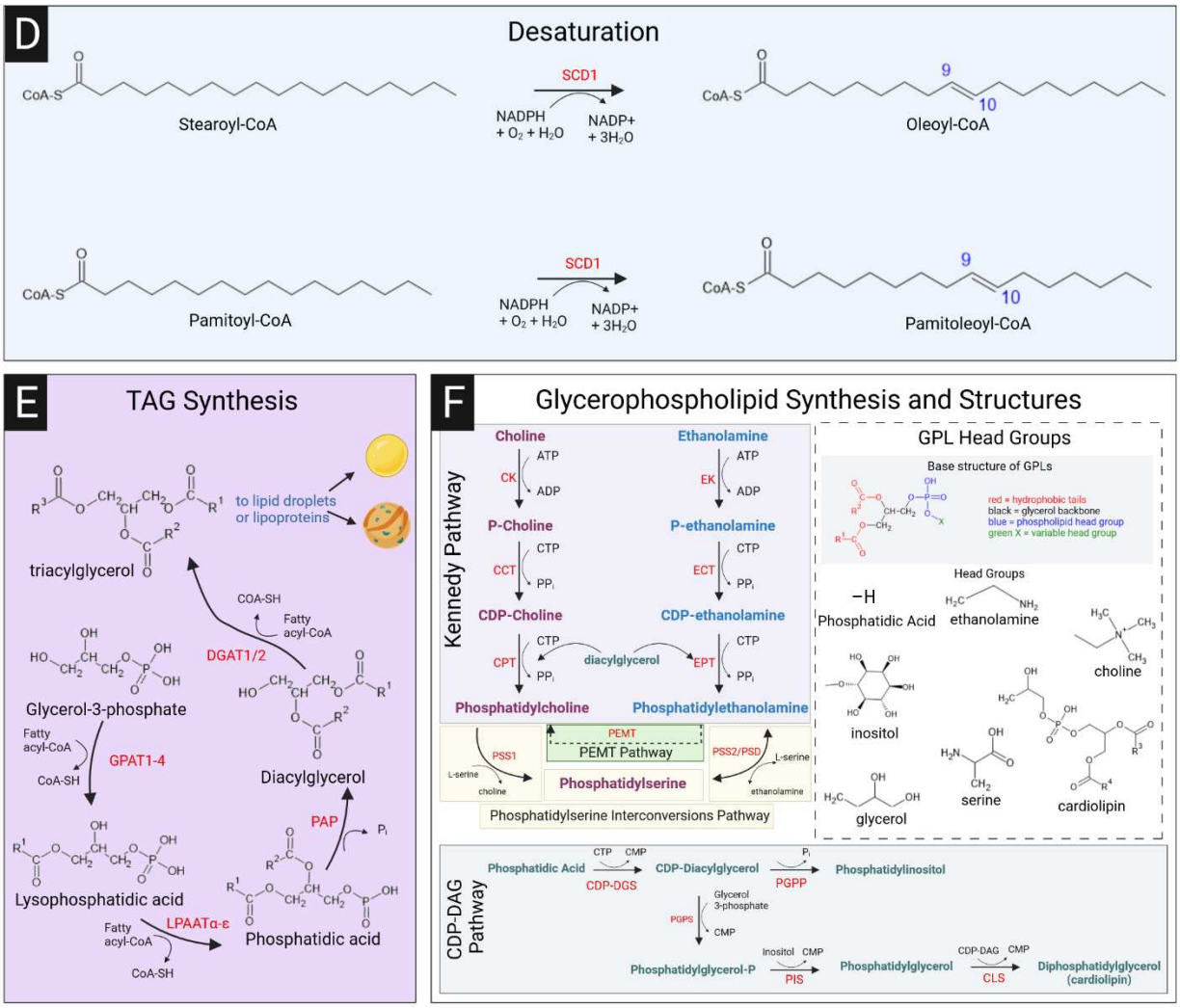

Figure 1.4 – Fatty acid synthesis pathways. A-F: Major enzymes and steps of fatty acid biosynthesis are presented. Enzymes are colored red in each panel. [Panel A]: *de novo* synthesis begins with the conversion of acetyl-CoA to malonyl-CoA by acetyl-CoA carboxylase enzyme. [Panel B]: Malonyl-CoA is remodeled into the long chain fatty acid palmitic acid through a series of condensation, reduction, and dehydratase reactions by the multi-domain enzyme FA synthase. [Panel C]: Elongation of fatty acids in the ER. Shown is the elongation of palmitoyl-CoA (C16) to stearoyl-CoA (C18). [Panel D]: Desaturation of fatty acids catalyzed by the Δ-9 desaturase SCD1. [Panel E]: Synthesis of glycerolipids including LPA, PA, DAG and TAG from glycerol-3-phosphate. [Panel F]: Synthesis of glycerophospholipids occurs through several highlighted pathways. In general, these pathways involve the addition of a variable head group onto diacylglycerol. Head group molecules are shown in right hand sub-panel. Abbreviations (starting from panel A): BC, biotin carboxylase; CT: carboxyltransferase; CoA: coenzyme A; ACP: acyl-carrier protein; MAT: malonyl/acetyl transferase domain; KS: β-ketoacyl synthase domain; DH: dehydrase domain; ER: enoyl reductase domain; KR: β-keto reductase domain; TE: thioesterase domain; AS: acyl-CoA synthetase; ELOVL: elongation of very long chain FAs; KAR: keto-acyl reductase; HACD: 3-hydroxy-acyl-CoA hydratase; TER: *trans* 2,3 enoyl reductase; SCD1: stearoyl CoA desaturase 1; GPAT: glycerophosphate acyl-transferases; LPAATs: LPA acyl-transferases; PAP: PA phosphatase; DGAT: diacylglycerol acyl-transferases; CK/EK: choline/ethanolamine kinase; CTT/ECT: CTP phosphocholine/ethanolamine cytidylyltransferase; CPT/EPT: choline/ethanolamine phosphotransferase; PEMT: phosphatidylethanolamine N-methyltransferase; DAG: diacylglycerol; CDP-DGS: CDP-diacylglycerol synthase; PGPP: phosphatidylglycerophosphatase; PIS: phosphatidylinositol synthase; CLS: cardiolipin synthase; PSS1: phosphatidyl serine synthetase; PSD: phosphatidyl serine decarboxylase. All chemical structures were generated using ACD/ChemSketch Software (Freeware) Version 2021.2.0. Composite figure was generated using Biorender.com. [Adapted from 112,171–175,179–184]

1.5: Sphingolipids as bioactive signaling molecules: the 'life raft' of cellular metabolism

1.5.1 - An overview sphingolipid metabolism

Sphingolipids (SLs) are a group of complex, extremely versatile lipid molecules that contain a sphingoid base (SB) backbone. An SB is a long chain, aliphatic amine containing 2-3 hydroxyl groups. The chain length, saturation, and number of hydroxyl groups can vary among SBs. While predominately serving as precursor molecules, SBs also have many bioactive roles (covered in 1.5.2). SBs can be *N*-acylated, forming dihydroceramide or ceramide, with ceramide being the 'central' molecule of SL metabolism (Figure 1.5). A variety of head groups can also be added to ceramide forming complex SLs. Below we will discuss synthesis and breakdown of SLs (depicted in Figure 1.5), and the key enzymes involved, as well as their general locations. In section 1.5.2 we will discuss some of the known roles of SLs in cell biology. A discussion of SL dysregulation in chronic and infectious diseases is presented in section 1.5.3. An examination of the role of SL metabolism in the DENV life cycle is presented in Chapter 4.

Sphingolipid biosynthesis

Ceramide (CER) can be synthesized *de novo* or be regenerated from the breakdown of complex SLs. The first pathway we will discuss is *de novo* CER synthesis. The first steps are catalyzed by enzymes on the cytosolic face of the ER membrane. Serine palmitoyltransferases (STPLCs) condense cytoplasm L-serine and palmitoyl-CoA to form 3-dihydrosphinganine (also called 3-ketodihydrosphingosine) [113,203]. 3-dihydrosphinganine is reduced by 3-ketosphinganine reductase (KDSR) to form sphinganine, and is then acylated by one of six CER synthases (CerS1-6) forming membrane-bound dihydroceramide (dhCer) [113,203]. The CER

synthases have distinct tissue expression patterns as well acyl-CoA chain length specificity [113,203]. Importantly, dhCer can either function as a standalone molecule, be modified by the addition of various head groups, or be desaturated by the Δ-4 dhCer desaturases (DEGS1-2) forming CER (via DEGS1) or phytoceramide (via DEGS2) [113,203]. It is not entirely clear how dhCer, CER, and phytoceramide are functionally distinct, however, some evidence suggests that CER species elicit a stronger signaling response than dhCer and phytoceramide [204]. For simplicity, we will discuss modifications to CER only with an understanding that similar reactions may also be carried out on dhCer and phytoceramide.

Following synthesis, CER can be converted to galactosylceramide (GalCer) by UDP-glycosyltransferase 8 (UGT8) found in the ER [113,203]. GalCer itself is an important component neuron myelin sheaths, but is also a precursor for sulfatides and some gangliosides [203,205]. CER is also transported to the Golgi where it can undergo additional modifications to become sphingomyelin (SM) or glucosylceramide (GluCer). CER is either transported via vesicular transport or by the CER transfer protein (CERT) [189]. Interestingly, CERT prefers ceramide with acyl chains with 22 carbons or less, and ceramides transferred to Golgi via CERT are predominantly incorporated into SM over GluCer [113]. Thus, chain length and transport mechanism may regulate SM and GluCer synthesis. SM synthases (SGMS1-2) are located in the *trans*-Golgi, and add a phosphocholine head group to CER [203]. Ceramide can also be phosphorylated by CER kinase in the Golgi, producing the bioactive ceramide-1-phosphate (C1P) molecule [189]. GluCer synthase (GCS, aka UGCG) is located in the *cis*-Golgi, and adds a glucose head group to CER [203]. Importantly, GluCer is a precursor molecule for all complex glycosphingolipids (GSLs) which represent the most diversity amongst SL structures [206]. Complex GSLs have a wide variety and variable number of additional carbohydrates attached to the initial glucose molecule. Complex GSLs consist of molecules belonging to ganglio-, globo-, isoglobo- neolacto-, and lacto-series, designations that are determined by type of carbohydrates found in their root structure [206]. While it almost a certainty that the diversity of carbohydrate

head groups drives different functionality for specific GSLs, we are only just beginning to understand GSL biology.

CER, SM, and GSLs are predominantly found in the plasma membrane where they contribute to stabilization of the plasma membrane and lipid rafts and play vital signaling roles [113,203]. However, they are also found within intracellular membranes. Some evidence suggests that their presence may mark membranes for delivery of proteins and other cargo, and that lipid concentration gradients within membranes regulate movement throughout the secretory pathway [207–209].

Degradation, Remodeling and Salvaging of Sphingolipids

Enzymes that catabolize CER, SM, and GSLs are found within lysosomes, but are also found throughout the cell and in association with the plasma membrane (illustrated in Figure 1.5). Distribution throughout the cell supports remodeling that may be vital for control of signaling within organelles or supply precursors for SL synthesis.

Sphingomyelinases (SMases) are responsible for the removal of the phosphocholine head groups to regenerate CER. There are 5 known SMases located throughout the cell and plasma membrane [113,203]. Plasma membrane associated SMases may play a role in regulating CER signaling [113]. SMases located in the ER and Golgi are thought to regenerate CER for SL synthesis, while Acid SMase in the lysosome plays a role in complete catabolism of SLs [113].

Breakdown of complex GSLs is accomplished by the activity of neuraminidases and various glycosidases on the sugar chain attached to GluCer, and finally by β-glucosylceramidase enzymes (GBA1 and GBA2) that release the glucose headgroup from ceramide [206]. GBA1 is a lysosomal enzyme, and involved in processes leading to complete degradation of SLs [203]. Whereas GBA2 is a non-lysosomal transmembrane protein that predominately associates with the ER and Golgi [203]. GBA2 is less characterized than GBA1, but it has been associated with

modulating trafficking along the secretory pathway, locomoter function, and is shown to have transglucosylation activity between GluCer and cholesterol/GluChol [210,211].

Deacylation of CER generating sphingosine represents the first step of CER catabolism, and is accomplished by one of 5 (known) ceramidase enzymes [113]. Sphingosine is then phosphorylated by sphingosine kinases (SPHK1-2) which can be found in the cytosol, plasma membrane, and nucleus [113]. Sphingosine-1-phosphate (S1P) is then degraded by S1P lyase in the ER producing the C16 aldehyde hexadecenal and phosphoethanolamine (an important precursor for glycerophospholipid synthesis) [113]. Importantly, S1P can also be excreted from cells and plays a vital role in extracellular signaling and immune cell trafficking [113]. Control of S1P signaling at the plasma membrane occurs through lipid phosphate phosphatases (PLPP1-3) [113]. S1P can also be dephosphorylated at the ER and Golgi by PLPP3 or S1P phosphatases (SPP1), allowing for the regeneration of CER catalyzed by CER synthases [113].

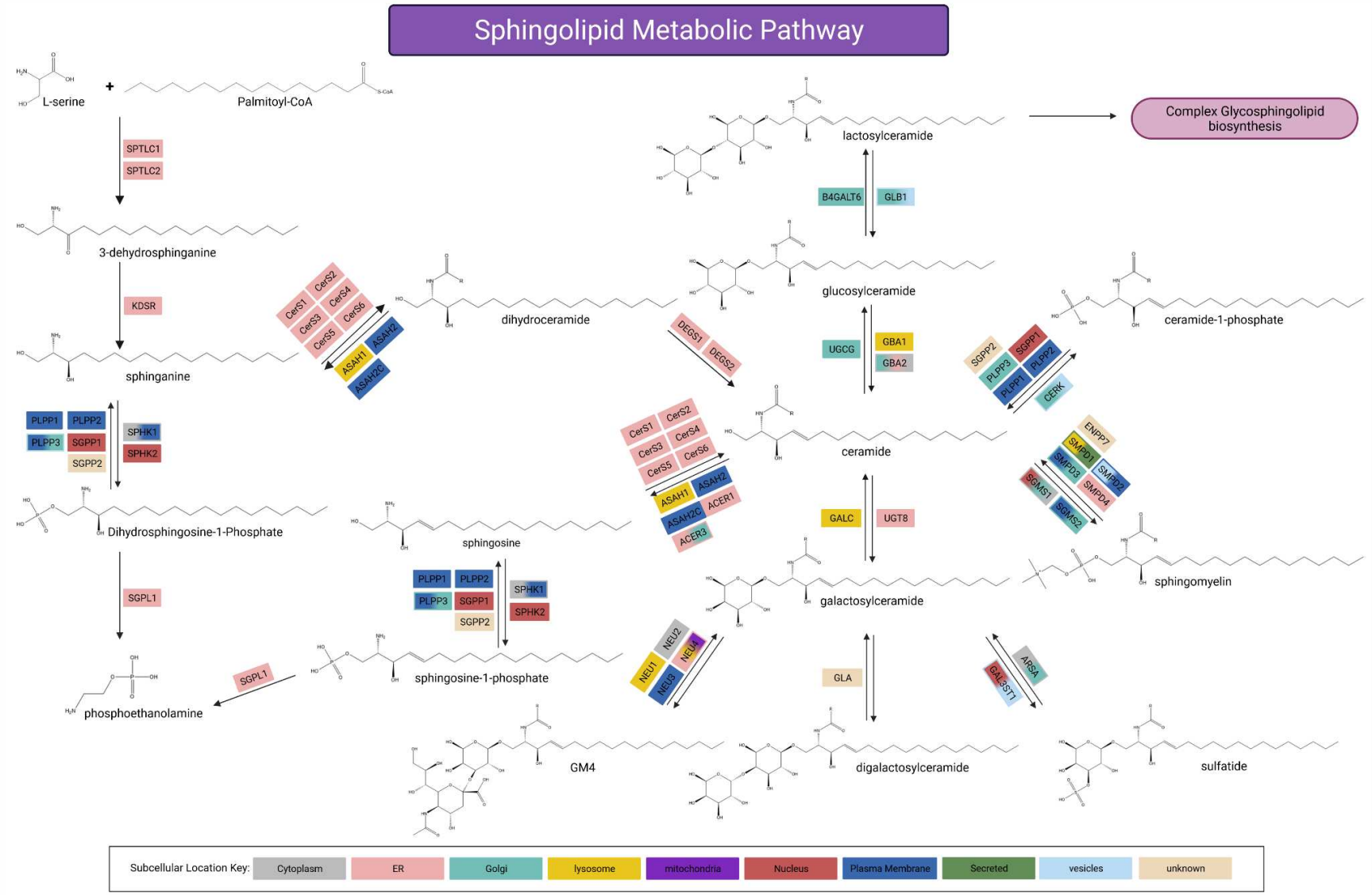

Figure 1.5 – The Sphingolipid Metabolic Pathway. Depicted are the core structures and enzymes of the sphingolipid metabolic pathway. Enzymes are colored-coded based on their known subcellular location. Chemical structures generated using ACD/ChemSketch (Freeware) version 2021.2.0. Composite image generated using Biorender.com. [Adapted from 113,203–205,206 and KEGG Pathway Database]

1.5.2 - Bioactivity of sphingolipids

In past few decades, an explosion in lipid research has determined that SL signaling is involved in nearly all aspects of cell biology. They regulate cellular traffic, pro- and anti-inflammatory immune responses, cell proliferation, apoptosis, cell differentiation, senescence, cell adhesion, cell migration, the stress response and many other functions.

There are several mechanisms by which SLs can interact and transmit signal, the most obvious being direct lipid-lipid or lipid-protein interactions. However, alterations in SL structure or levels within membranes may also exert changes on biological membranes that alter their biophysical properties [204]. Moreover, the relative concentrations of SLs are also an important factor in SL signaling. SM is the most abundant SL and is orders of magnitude higher in abundance than all other SLs [204]. Additionally, CER concentrations are much higher than C1P, sphingosine, or S1P [204]. Thus, conversion of SM to CER can have profound effects on CER signaling, and so on [204]. Transport of lipids is also a significant factor in how SLs exert signaling actions [204]. Sphingosine and S1P are able to diffuse through membranes, but larger SLs are membrane bound and require either transport proteins, vesicles, and/or the action of flippases to move within membranes [204]. Thus, regulation and mechanism of action of SL signaling is complex and a complete understanding of these processes is missing. Additional studies mapping binding partners of SLs may be beneficial but is complicated by the richness of SL structures. Thus, an understanding of how fatty-acyl chain length contributes to SL functionality is also necessary. While we are far from solving the mystery of the sphinx, advances in lipidomics continues to reveal a richness of lipid structures whose functionality may eclipse that of other macromolecules [120].

1.5.3 – Roles of sphingolipids in chronic and infectious disease

Sphingolipids are inflammatory mediators

Ceramide-1-phosphate (C1P) and sphingosine-1-phosphate (S1P) have been implicated in playing vital roles in inflammatory pathways. C1P has been implicated as playing a role in immune cell trafficking, however its biggest contribution to the immune response is its activation of cytosolic phospholipase A_2 ($cPLA_2$) [212]. It has been demonstrated that that C1P binds and allosterically activates $cPLA_2$ to increase its activity and affinity for phosphocholine [212]. Importantly, $cPLA_2$ is responsible for cleaving arachidonic acid from membrane lipids, which is the first and rate-limiting step of eicosanoid (inflammatory mediators) production [212].

S1P is a potent mediator of many cellular functions, including lymphocyte trafficking and cytokine/chemokine production [213]. S1P signaling is conducted through the S1P G-protein coupled receptors (S1PR1-5) [213]. When S1P is produced, it is exported out of the cell where it can bind S1P receptors in both autocrine and paracrine manners in what is referred to as 'inside-out signaling' [213]. S1P-S1PR1 signaling is involved in trafficking of both innate and adaptive immune cells [213]. S1P-S1PR2 signaling mediates mast-cell dependent allergic responses by triggering mast cell degranulation [213]. S1PR2 and S1PR3 signaling has also been shown to promote vascular permeability, while S1PR1 signaling protects vascular integrity, highlighting important differences amongst S1P receptors [213].

Lysosomal Storage Disorders

Many SL disorders belong to a group of diseases known as lysosomal storage disorders (LSDs). LSDs arise due to failed catabolism of molecules within lysosomes, usually due to genetic defects of catabolic enzymes. Below we will discuss some of the most well characterized SL LSDs.

Fabry's disease is caused by a deficiency in the α-galactosidase (GLA) enzyme [214]. GLA is responsible for removing terminal galactosyl residues from GSLs [214]. Specifically in Fabry's disease, deficiencies in GLA lead to accumulation of globotriaosylceramide or Gb3 [214]. Common symptoms are systemic pain, chronic kidney disease, cardiac hypertrophy, restriction of blood vessels, and the presence of skin papules in lower extremities [214]. Enzyme replacement therapy is commonly used to treat Fabry's disease [214].

Niemann-Pick Type A and B (NP-A, NP-BB) are disorders relating to deficiencies in acid sphingomyelinase (SMPD1) in the lysosome [215]. NP-A is the neuronopathic form and presents during infancy, and usually results in death by 1-3 years of age [215]. Symptoms include hepatosplenomegaly, loss of motor function, browning of skin, wasting, and macular cherry-red spots on the skin [215]. NP-B is the non-neuronopathic form and can result in a variety of symptoms. Patients with NP-B typically survive through late adulthood [215]. The most common symptoms are hepatosplenomegaly, bruising, nose-bleeding, and impaired respiratory function [215]. Currently, supportive care is the only treatment for NP-A and NP-B [215].

Gaucher disease is caused by a deficiency in the lysosomal β-glucocerebrosidase enzyme (GBA1) why breaks down glucosylceramide (GluCer) [216]. There are three distinct types of Gaucher disease. Type I Gaucher disease is the most common and mild, and has little impact on life expectancy [216]. Symptoms include splenomegaly, anemia, and bone pain/fracture [216]. Type 2 is the acute, neuronopathic form that affects infants and typically results in early childhood death [216]. Splenomegaly, long bone erosion, motor dysfunction, seizures and respiratory distress are common symptoms [216]. Type 3 is the chronic, neuronopathic form, and patients with type 3 typically live into early adulthood [216]. Symptoms include chronic pain and inflammation, anemia, hepatosplenomegaly, bruising and thrombocytopenia, and bone pain/fractures [216]. Enzyme replacement therapy is a common treatment for patients with Type 1 Gaucher, but is ineffective against Type 2 and 3 as the enzyme mimetic is unable to cross the

blood-brain barrier [216]. Miglustat, an inhibitor of GluCer synthesis, is also commonly prescribed to treat Gaucher disease [216].

Roles of sphingolipids in infectious disease

As GSLs are found in the plasma membrane, their sugar head groups are receptors and recognition moieties for many cellular proteins as well as bacterial and viral pathogens. It is well-documented that while HIV entry requires binding to CD4 and its coreceptors CCR5 or CXCR4, its envelope proteins, gp120 and g41, must bind to GSLs as well [217]. Moreover, it has been documented that HIV entry is sensitive to ceramide and cholesterol rich membranes as they prevent lateral diffusion of CD4 which inhibits association with GSLs and other co-receptors [217]. Sphingomyelin has been shown to be indispensable for entry of Sindbis virus into cell [218]. SARS-CoV-2 has been shown to rely up SMPD1 (lysosomal sphingomyelinase) conversion of SM to CER for viral entry, and GluCer synthesis was shown to be indispensable for viral replication [219,220].

S1P is known to promote pro-survival and anti-apoptotic signaling. Hepatitis B, Measles, Influenza, Respiratory Syncytial, and human cytomegaloviruses have all been shown to upregulate SPHK1 which is responsible for S1P generation [120,221]. Thus, these viruses may hijack S1P to inhibit the host antiviral and apoptotic pathways [120,221].

FAPP2 is a protein responsible for transport of GluCer from the *cis*-Golgi to the *trans*-Golgi to allow for the additional processing of GluCer that yields complex glycosphingolipids [222]. In HCV-infection, it has been documented that FAPP2 is recruited the HCV replication complex with concomitant increases in GluCer at HCV replication sites [222]. These studies concluded that GluCer was indispensable for HCV RNA synthesis [222].

In mosquitoes, our group previously showed upregulation of SLs in DENV-infected mosquitoes and mosquito cells [110,111]. *Wolbachia* is an endosymbiont introduced to *Aedes aegypti* mosquitoes that is shown to reduce DENV replication and transmission [223]. One study

found that in *Wolbachia* infected mosquitoes, the sphingolipid species that were upregulated in our previous studies were depleted [223]. Thus, the DENV life cycle in mosquitoes seems to rely on the presence of SLs. Analysis of sera from DENV-infected patients by others and our group as well as untargeted metabolomics studies of DENV-infected Huh7 cells has revealed a similar pattern of SL upregulation in humans [117,118 and Gullberg, et al., unpublished],224].

1.6: Lipid Trafficking

As we have covered, lipids play a diverse number of roles in cell biology that extend beyond their roles as biological membranes. Lipids are organized non-randomly within the plasma membrane and membranes of organelles providing even further evidence that lipids have specific functions [225]. For example, ER membranes are primarily composed of glycerophospholipids and diacylglycerols containing unsaturated fatty acids despite being the primary site of lipid biosynthesis [226]. Thus, these membranes are loosely packed, which permits membrane curvature, and easy diffusion and incorporation of newly synthesized proteins and lipids [226]. The plasma membrane is enriched in cholesterols and sphingomyelins in the outer leaflet, and plasma membrane-associated phosphatidylserine is exclusively found within the cytoplasmic leaflet [227]. In the secretory and endosomal pathways, a gradient of increasingly complex lipids is observed as those vesicles mature [227]. Mitochondrial membranes consist predominantly of glycerophospholipids (predominately PC, PE, and cardiolipin) [226]. Thus, specific mechanisms of trafficking and transporting lipids must be present in the cell.

Lipid transport that is not mediated by a transport protein or transport vesicle usually falls into one of three categories: lateral diffusion within a membrane leaflet, transmembrane diffusion (i.e. flipping), and monomeric lipid in which a lipid diffuses from the leaflet of one membrane to another in close contact with it [225]. Although transmembrane diffusion can occur without the aid of

proteins, this type of transport can be very slow for complex lipids, so it is also accomplished by enzymes known as flippases [225].

There are numerous lipid transport proteins throughout the cell that recognize and transport specific lipids [228]. For these proteins to organize lipids into specific membranes, lipid transport proteins must contain two binding domains – one that recognizes the lipid, and the other the target membrane [228]. This is one process by which precise and specific organization of lipids is maintained. There are several types of lipid transfer proteins, all characterized based on their structure, but a common feature among all is that they contain a cavity which shields the hydrophobic tail group from the cytosol during transport [228]. Lipid transport proteins can be either cytosolic or be peripheral membrane proteins [225]. Most lipid transfer proteins are selective for lipids based on their head groups, although acyl-chain length can also be a factor [228]. An example is the specificity of the ceramide transportor, CERT, it is selective for acyl chains with less than 22 carbons [113].

Vesicular trafficking along the endocytic and secretory pathways are the bulk source of lipid transport within the cell, and there is evidence for lipid sorting within budding vesicles [227]. However, our understanding of the mechanisms that drive lipid sorting withing vesicles is incomplete. One possibility is that as lipid-protein microdomains may form in the originating organelle, and interact with a specific repertoire of coat proteins that assist in vesicle formation [227]. This would ensure the correct composition of ordered microdomains arrive at their intended destination. Another possibility is the shape and saturation of lipids may exclude them from certain regions budding vesicles, driving certain lipids to concentrate in areas based on their preference for positive or negative curvature [227].

A final driver of lipid transport relies specifically on the architecture of the ER. The ER is the largest organelle within the cell, and forms a continuous network throughout the cell [225]. This allows the ER to form membrane contact sites (MCS) in which the ER membrane is within 10 nm of, but not fused with, the membrane of other organelles [225]. This close contact would facilitate

monomeric lipid transport, site-specific delivery of vesicles and of lipid transport proteins, and there is much evidence to support lipid transfer at these junctions [225]. As pointed out in Holthuis, et al., these sites are often overlooked as playing a role in lipid trafficking, but are likely the largest contributor of site-directed lipid trafficking [225].

1.7: The role of sialic acids and sialidases in infectious diseases

Sialic acids (SIAs) are a group of ~50 naturally occurring nine-carbon sugars [229]. SIAs are typically found at the terminal end of glycoproteins and glycosphingolipids (gangliosides) [229]. The vast majority of glycoconjugates are expressed on the outer leaflet of the plasma membrane, but intracellular and secreted glycoconjugates are also common [229,230]. Importantly, SIAs are largely the first point of contact between a cell and its environment as there are many SIA-containing glycoconjugates expressed on the plasma membrane. For example, there are a staggering ~10 million SIA residues on each human erythrocyte [229,230]. It is unsurprising, then, that SIAs play diverse and important roles in cell biology. They carry a high electronegative charge which can stabilize protein conformation and membrane dynamics, and dictate interactions with the extracellular environment [229,230]. They play significant roles in maintaining the integrity of the endothelial glycocalyx and vascular homeostasis [229,230]. SIAs have also been shown to play direct roles in transmembrane signaling, cell-to-cell interactions (adhesion, migration), and self versus non-self recognition [229,230]. Importantly SIAs can function as recognition or masking sites [229,230]. There are many receptors as well as pathogens that bind specifically to SIA residues, or to the penultimate galactose (Gal) residue that is usually masked by SIAs.

Glycosylation, including sialylation, occurs in the Golgi and is carried out by a number of linkage- and substrate-specific sialyltransferases (STs) [229,230]. SIA residues are typically attached to a penultimate Gal or N-acetylgalactosamine (GalNAc) residue via α2,3- or α2,6-

linkages. Oligo- and polySIAs may be linked by α2,8- and α2,9-linkages, but are more rare [229,230].

The sialidases (historically called neuraminidases, although that term is now largely reserved for viral sialidases) are enzymes responsible for cleaving sialic acid residues from glycoconjugates [231]. Humans have four (known) sialidases, NEU1-4 [231]. Each NEU is typically found in specific cellular compartments, and each has been shown to play varying roles in regulating cellular processes [231]. However, SIA and sialidase functionality remain an ongoing area of study owing to the diversity of SIAs residues and their ubiquituous expression. Thus, there are likely a great number of unknown functions of each. Below we will discuss the known functions of human sialidases, and the known interactions of SIAs and sialidases with viral pathogens, including DENVs.

1.7.1 - The sialidases and their roles in cellular metabolism

As mentioned in the previous section, sialidases are responsible for the hydrolysis of SIAs from glycoconjugates. This can mark glycoconjugates for degradation, unmask binding sites, or trigger signaling cascades [231]. In the glycocalyx, sialic residues contribute to the mechanical barrier that prevents large molecules from passing through and the chemical barrier that repels most molecules, fluids and cells and maintains vascular flow [232,233]. When the glycocalyx structure is broken down, in part by sialidases, it allows for infiltration of inflammatory molecules that are capable of disrupting cell-to-cell adhesion, ultimately allowing for immune cell infiltration and fluid leakage [232,233].

Once released, intracellular SIAs are transported to the cytoplasm where they can be reused or are degraded by N-acetylneuraminate lyase yielding *N*-acetylmannosamine and pyruvate [230]. Extracellular free SIAs are either delivered to the cytoplasm via pinocytosis, or they are filtered and removed from circulation by the kidneys [230].

NEUs are known to play vital roles in recruitment of leukocytes to sites of inflammation through desialylation of the adhesion molecule ICAM-1 on endothelial cells [234]. This allows for binding of β-2 integrin receptors to the underlying Gal or GalNAc residues [234]. Desialylation of glycoproteins is also a well-known mediator of hepatic endocytosis [235]. The hepatic asialoglycoprotein receptor (ASGP-R) is enriched in clathrin-coated pits, and is involved in removing desialylated glycoproteins and neoglycoproteins from circulation [235]. Once bound by a ligand, ASGP-R is rapidly internalized via clathrin-mediated endocytosis [235]. Common ASGP-R ligands are desialyated LDL, chylomicron, fibronectin, and IgA [235]. Many lectins have been shown to have similar endocytosis motifs indicating that sialidase activity may play a vital role in receptor-mediated endocytosis, which may mark sialidases as a particularly attractive target for viral subjugation [235].

NEU1

NEU1 is a lysosomal sialidase that must exist in complex with both β-galactosidase and carboxypeptidase protective protein/cathepsin A (PPCA) to be catalytically active [234]. It preferentially cleaves α2,3-linkages of oligosaccharides and glycoproteins over α2,6- and α2,8-linkages, and has minimal activity against gangliosides [234]. It is primarily involved in lysosomal degradation of glycoconjugates, but also regulates lysosomal exocytosis and immune cell differentiation and signaling [234]. NEU1 has been shown to translocate to the plasma membrane where it is essential for TLR4 activation (and possibly other toll-like receptors), and for desialylation of cell surface glycoconjugates that trigger IFN and cytokine production [236,237]. Moreover, it has been shown to regulate phagocytosis in macrophages and dendritic cells through desialylation of surface receptors for phagocytosis including Fcγ receptors [238].

NEU2

NEU2 is a cytosolic sialidase whose functionality is still under much debate. There is still considerable disagreement in the field as to whether cytosolic facing glycoconjugates exist and

what functional roles they have [230,234,239]. While many glycoproteins and glycolipids as well as receptors have been identified in the cytosol, their activity remains unclear [240]. NEU2 does appear to play a role in degradation of glycoconjugates delivered to the cytosol through autophagy, phagocytosis, or the unfolded protein response [230,234]. Some evidence suggest that NEU2 activity was vital for muscle cell and neuronal cell differentiation, but the mechanism was not elucidated [234]. It was also shown that NEU2 overexpression reduced tumor proliferation [234]. However, these assays were performed *in vitro*, and these functionalities have yet to be validated *in vivo* as NEU2 tissue expression is very low. Interestingly, the first *in vivo* study of a NEU2 KO mouse was recently published, and found that loss of function of NEU2 resulted in dysregulated lipid catabolism [241]. In their study, NEU2 deletion resulted increased abundance of serum TG, FFA, and lipoproteins and a downregulation of a number of sialylated glycoproteins that function in lipid transport and catabolism [241]. This lead to weight gain, decreased motor function, and hepatic steatosis in the $NEU2^{(-/-)}$ mice [241]. Interestingly, they determined these glycoproteins were downregulated at the protein level, indicating that NEU2 activity may be vital for translation of lipid mediators [241].

NEU3

NEU3 is found primarily bound to the plasma membrane and has near exclusive activity against gangliosides [230,234]. It has also been found to associate with endosomes and may play a role in endosomal trafficking [230,234]. Unsurprisingly, as NEU3 functions extracellularly, it is involved in modulation of a number of signaling cascades mainly involving cell survival and proliferation [230,234]. It has also been shown to be indispensable for inflammatory cytokine production (IL-6, IL-12p40, TNF-α) as inhibition of NEU3 with zanamivir prevented cytokine induction in LPS-treated cells [234]. NEU3 is upregulated in many forms of cancer, likely due to its roles in proliferation and inhibition of apoptosis [230,234]. NEU3 was also shown to contribute to atherosclerosis through desialylation of low-density lipoproteins (LDL) [242,243]. Desialylation

of LDL exposes Gal and GalNAc residues that are then recognized by a number of lectins as described above, thus triggering uptake of LDL into cells [235].

NEU4

NEU4 is the most recently discovered human sialidase, and very little is known about its biological roles. NEU4 has been shown to localize in the lysosome, mitochondria, and ER, and has the broadest substrate specificity of all of the human NEUs [230,234]. It is the only NEU known to hydrolyze sialyl-Lewis antigens and polySIA [230,234]. One known function is the degradation of polySIA on NCAM in neurons, which negatively regulates neurite outgrowth [244]. It's also been shown to be downregulated in many cancers, indicating it may function as a tumor suppressor [230,234]. Studies to elucidate NEU4 functionality are ongoing, but given its subcellular distribution and broad substrate specificity it likely plays a significant role in cell biology.

1.7.2 - Relationship between viruses, sialic acids, and sialidases

It is well-established that sialic acid residues are used as receptor molecules by several viruses. The most characterized relationship is between Influenza A and B and sialic acid receptors. Influenza viruses have two glycoprotein spikes embedded in their envelope: hemagglutinin and neuraminidase [245]. Hemagglutinin binds to sialic acid residues on cell surfaces, facilitating viral attachment [245]. The virus then 'walks' the surface of the cell until it encounters a yet unknown properly sialylated receptor molecule that facilitates viral uptake [245]. The viral neuraminidase facilitates this 'walking' by cleaving SIA residues from hemagglutinin which allows the virus particle to move to the next SIA residue [245]. Upon egress, neuraminidase also cleave hemagglutinin-SIA bonds to release progeny virions [245]. Human influenza is known to preferentially bind to α2,6-linked SIA residues, while avian influenza prefers α2,3-linked SIAs. Interestingly, this defines the tissue tropism and pathology for each virus in humans [246,247].

SIA residues with α2,6-linkages are predominately found in the upper respiratory tract, whereas α2,3-linkages are predominately found in the lower respiratory tract (especially in alveoli). [246,247]. Many other viruses also use sialic acids as receptors, including parainfluenza, norovirus, rotavirus, some coronaviruses, enterovirus D68, Zika virus and mumps [248]. HIV is known to express SIA in its viral envelope, which facilitates binding of HIV to Siglecs on macrophages [249]. SARS-CoV-2, the causative agent of the COVID-19 pandemic, has been shown to require SIAs as a co-receptor [220].

In DENV infections, several important observations have been made regarding a relationship between DENVs, sialic acids, and neuraminidase. The first is that the DENV envelope protein is glycosylated at 2 residues: Asn_{67} and Asn_{153} [78]. The glycosylation at Asn_{153} has been shown to consist of a complex glycan, and has been documented as either having a terminal SIA residue or a terminal GalNAc residue [78]. Thus, these residues may play important roles in viral attachment and possibly in receptor-mediated endocytosis. The second important observation was made by Eva Harris' group. They have shown that the DENV NS1 protein upregulates NEU1-3 activity *in vitro*, and this upregulation lead cleavage of SIA residues on the endothelial glycocalyx [90]. This contributed to breakdown of the glycocalyx and endothelial hyperpermeability [90]. In a follow-up *in vivo* study with our group, increased serum SIAs and circulating NS1 in a murine model was shown to be correlated with increased morbidity and mortality [91]. Combined, these studies indicated that DENV-infection upregulates host sialidase activity which, in turn, contributes to one of the hallmark pathological events of severe DENV.

Interestingly, in an siRNA-mediated loss of function study of enzymes within the sphingolipid metabolic pathway, we found that loss of function of NEU1-4 significantly reduced DENV2 release from cells. This suggested that not only was NEU1-4 activity upregulated during infection [90,91], but that it seemed to play a vital role in DENV2 replication. Thus, we sought to characterize the role of NEU1-4 in the DENV life cycle. The results of those experiments are discussed in Chapter 3.

1.8: Conclusions

Here, we have summarized our knowledge of metabolic pathways that are perturbed upon infection with DENV viruses. We have also described the biological function of these pathways, and some of the known consequences of their perturbation in chronic and infectious diseases.

It is well-established from the literature summarized herein that DENVs induce considerable metabolic changes, especially to lipids, upon infection. While many of these changes occur to meet the replicative needs of DENVs, the major pathways discussed also have significant roles in biological signaling. Thus, it remains unclear whether they are altered to provide raw materials for viral replication, are regulated by DENVs to control host functions, or are part of a host antiviral response. We identified three outstanding questions from the literature and our preliminary datasets, and will present our findings in the chapters that follow. In Chapter 2, we will discuss the unexpected reliance of DENV on the functionality of acyl-CoA thioesterases (enzymes responsible for deactivating fatty acyl-CoAs). In Chapter 3, we present the first report of a functional role for sialidase activity during DENV infection and discuss its implications. In Chapter 4, we will discuss our efforts to determine which parts of the sphingolipid metabolic pathway are critical for the DENV lifecycle, and our efforts to characterize the role of sphingolipid metabolic enzymes and metabolites in the DENV lifecycle. As well, we will present the first analysis of specific glycosphingolipids that are altered upon infection. Taken together, this dissertation will provide additional insight the reliance of DENVs on host metabolic pathways.

Hypothesis of study: Dengue viruses hijack and manipulate host metabolic pathways for their own replicative advantage. As such, alterations in metabolite levels and metabolic enzyme expression and activity are quantifiable and can be correlated with their roles in the DENV lifecycle. Moreover, these changes in the metabolic landscape can be used to identify novel therapeutics and provide insight into the DENV-induced pathology.

Chapter 2 – Acyl-CoA Thioesterases: a rheostat that controls activated fatty acids modulates dengue virus serotype 2 replication[2]

2.1: Introduction

Dengue viruses (DENVs) are arthropod-borne viruses that are transmitted by the *Aedes aegypti* mosquito [3,5]. These viruses infect over 400 million people each year. They are obligate intercellular parasites that rely on host cell metabolic pathways to fulfill their energy requirements and access substrates necessary for generating progeny virions [14]. It is widely established that the lifecycle of DENVs is reliant upon host lipid metabolic path-ways [14,42,250,251]. Specifically, these viruses alter endoplasmic reticulum membranes to form scaffolds for viral protein translation and assembly of viral replication complexes [251,252]. Moreover, during viral particle assembly, host cell membranes are co-opted and incorporated into the viral envelope as a structural component of the virus particle [14,251,252].

In our previous studies, we have shown that many lipid species are upregulated and are vital for the DENV serotype 2 (DENV2) lifecycle [110,111]. Specifically, host phospholipids and sphingolipids are increased in abundance, some to benefit viral replication and others as a host response to infection [reviewed in 14,110,111]. Precursors of these molecules are composed of fatty acyl-CoAs which are fatty acids that have been esterified to coenzyme A (CoA) [191,197]. These fatty acyl-CoAs (activated fatty acids) can then undergo further modifications to be integrated into more complex lipids or be shuttled towards β-oxidation for cellular energy production [197].

[2] Adapted from St Clair LA, Mills SA, Lian E, Soma PS, Nag A, Montgomery C, Ramirez G, Chotiwan N, Gullberg RC, Perera R. Acyl-CoA Thioesterases: A rheostat that controls activated fatty acids modulates dengue virus serotype 2 replication. *Viruses*. 2022 Jan 25; 14(2):240.

Acyl-CoA thioesterases (ACOTs) are a family of hydrolases that control the intercellular balance between fatty acyl-CoAs and free fatty acids (FFAs). Specifically, they cleave fatty acyl-CoA into FFA and coenzyme A [191,197]. There are 10 identified human ACOT enzymes further categorized into two groups by their domain motifs: α-β hydrolase (type I) and “hot dog” domain (type II) (Figure 2.1 A,B) [191,197]. These enzymes are distributed throughout the organelles of human host cells including the cytoplasm, mitochondria and peroxisomes (Figure 2.1 A,B) [191]. ACOTs have been implicated in the control of lipid metabolism by maintaining the ratios of fatty acyl-CoA and free fatty acids within each organelle [191,197]. Upon perturbation, they have been shown to cause increased proliferation of cancer cells, are implicated in neurodegenerative diseases and play a protective role against diabetic cardiac damage [198,253–255].

Given that fatty acyl-CoAs are integral to lipid metabolism and energy homeostasis, we investigated if perturbing fatty acyl-CoA homeostasis by altering ACOT enzyme ex-pression modulated DENV2 infection. We also investigated if the ACOT enzyme location (cytoplasmic vs. mitochondrial) and/or specificity type (type I vs. type II) differentially influenced DENV2 replication. We examined three representative ACOT enzymes, ACOT1, ACOT2, and ACOT7, to understand their impact on the lifecycle of DENV2 in human hepatoma (liver) cells (Huh7s). siRNA-mediated loss of function studies of the type I ACOTs 1 and 2 together significantly increased DENV2 infectious particle release. However, isolated knockdown of ACOT2 significantly decreased DENV2 protein translation, genome replication, and infectious virus release. Loss of function of ACOT7, a mitochondrial type II ACOT, also similarly suppressed DENV2. Furthermore, our studies reveal a complex relationship between type I and type II ACOTs during DENV2 infection that suggested a functional interdependency of these enzymes.

2.2: Results

2.2.1 – Combined loss of ACOT1 and ACOT2 function increases DENV2 genome replication and infectious particle release

As ACOTs act as a rheostat for intracellular levels of FFAs and fatty acyl-CoAs, we hypothesized that ACOT functionality, which purportedly limits the availability of fatty acyl-CoAs, may have an inhibitory effect on the DENV2 lifecycle. To determine if ACOT enzymes affect DENV2 replication, we used siRNA-mediated knockdown to decrease the expression of type I ACOTs 1 and 2 in Huh7 cells. ACOT1 is located in the cytoplasm and ACOT2 in the mitochondria. There is ~94% homology between the mRNAs of ACOT1 and ACOT2 with only an insertion of 90-110 nucleotides differentiating ACOT2 mRNA from ACOT1 mRNA [192,193,199]. We included a non-target, irrelevant siRNA (IRR) to control for off-target effects of siRNA treatment and a DENV2-specific siRNA as a positive control for viral inhibition. We found that loss of ACOT1 and ACOT2 together resulted in an increase (~178%) in infectious viral release (Figure 2.1C), and viral genome replication (~470%, Figure 2.1D) compared to the IRR control. Due to the sequence similarity between ACOT1 and 2, we were unable to target siRNAs specific to ACOT1, but we were able to target specific siRNAs to ACOT2. Therefore, as shown below, we were able to parse out the influence of ACOT2 on this phenotype.

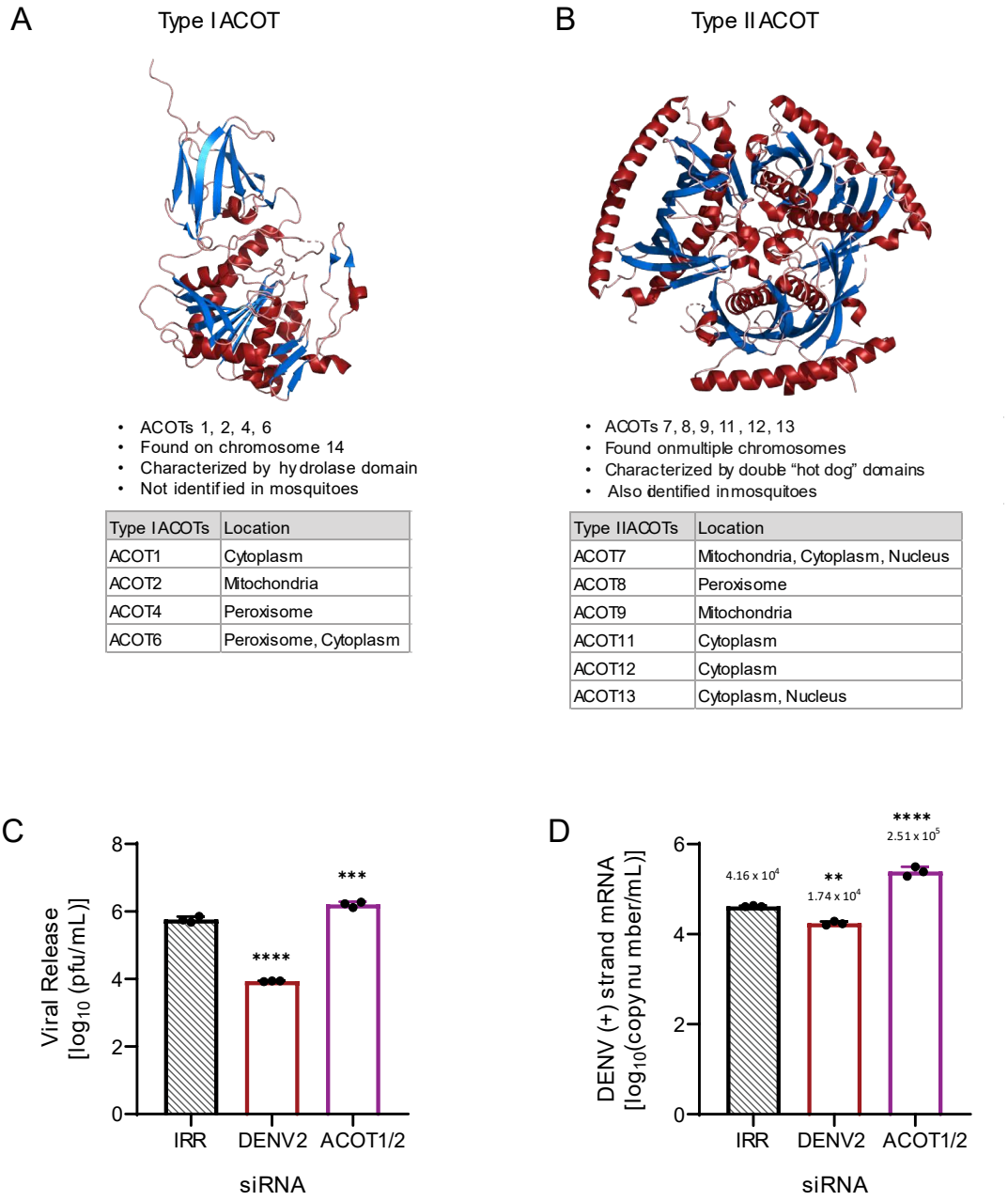

Type I ACOTs	Location
ACOT1	Cytoplasm
ACOT2	Mitochondria
ACOT4	Peroxisome
ACOT6	Peroxisome, Cytoplasm

Type II ACOTs	Location
ACOT7	Mitochondria, Cytoplasm, Nucleus
ACOT8	Peroxisome
ACOT9	Mitochondria
ACOT11	Cytoplasm
ACOT12	Cytoplasm
ACOT13	Cytoplasm, Nucleus

Figure 2.1 – ACOT enzymes categorized by structural motifs and preliminary loss of function analysis of ACOT1/2. (A) Human ACOT2, Protein Data Bank identifier 3HLK is depicted. Type I ACOTs are characterized by a hydrolase domain that contains the active site. (B) Human ACOT7, Protein Data Bank identifier 2QQ2 depicted. Type II ACOTs contain the "hot dog" domain composed of two alpha helixes surrounding a hydrophobic core. Although the composition of the active site is unknown within the "hot dog" domain, these enzymes are functionally analogous to type I ACOTs [199]. C-D: Huh7 cells were transfected with an siRNA pool targeting both the ACOT1 and ACOT2 genes as well as indicated controls (IRR and DENV2) and then infected with DENV2 for 24 hours (hr) (MOI = 3). (C) Infectious particle release was titrated via plaque assay. (D) Huh7 cells were collected, and relative copy number of viral RNA within cells was measured via qRT-PCR. qRT-PCR results were normalized to RPLP0. ACOT1/2: siRNA targeting acyl-CoA thioesterase 1 and 2, IRR: irrelevant siRNA control (no biological target for siRNA sequence), DENV2: siRNA targeting dengue virus, serotype 2. (A-B: images were generated utilizing PyMOL Molecular Graphics System, Version 1.2r3pre, Schrödinger, LLC. C-D: one-way ANOVA with Dunnett's multiple comparisons test: * = p≤0.05, ** = p≤0.01, ***= p≤0.001, **** = p≤0.0001.)

2.2.2. Loss of ACOT2 function reduces DENV2 replication, infectious particle release and infectivity

Given the above observations from combined loss of ACOT1 and ACOT2 function, and that ACOT1 and ACOT2 share the same substrate specificity [256] we hypothesized that loss of ACOT2 function alone would also result in increased viral replication and release. Therefore, we repeated knockdown studies with siRNAs specifically targeting ACOT2 in Huh7 cells. Surprisingly, we found that loss of ACOT2 function resulted in a significant reduction (~76%) in infectious virus release (Figure 2.2A) compared to the IRR control. Additionally, DENV2 genome replication was reduced by ~50% following ACOT2 knockdown (Figure 2.2B). In our previous studies, we found that inhibition of specific enzymes involved in fatty acid metabolism resulted in the release of partially immature virions, thereby reducing particle infectivity [193]. To determine if loss of ACOT2 function also reduced particle infectivity, we compared the ratios of viral RNA copies to infectious virions (particle/pfu ratio) in the supernatant of each of our treatment groups (Figure 2.2C). The data showed that there was a significant increase in the DENV particle/pfu ratio following ACOT2 knockdown compared to the IRR control; thus, suggesting a decrease in particle infectivity. We also found that viral protein translation was reduced by ~50% (Figures 2.2D and Supplemental Figure 2.1). We further confirmed that siRNA treatment was not cytotoxic to Huh7 cells (Figure 2.2E) and was also effective at reducing ACOT2 mRNA levels (Figure 2.2F). Overall, these data suggest that ACOT2 functionality is critical to the DENV2 lifecycle. This contrasts with the phenotype from the combined loss of function of ACOT1 and 2 suggesting that ACOT1 has a unique influence on viral replication.

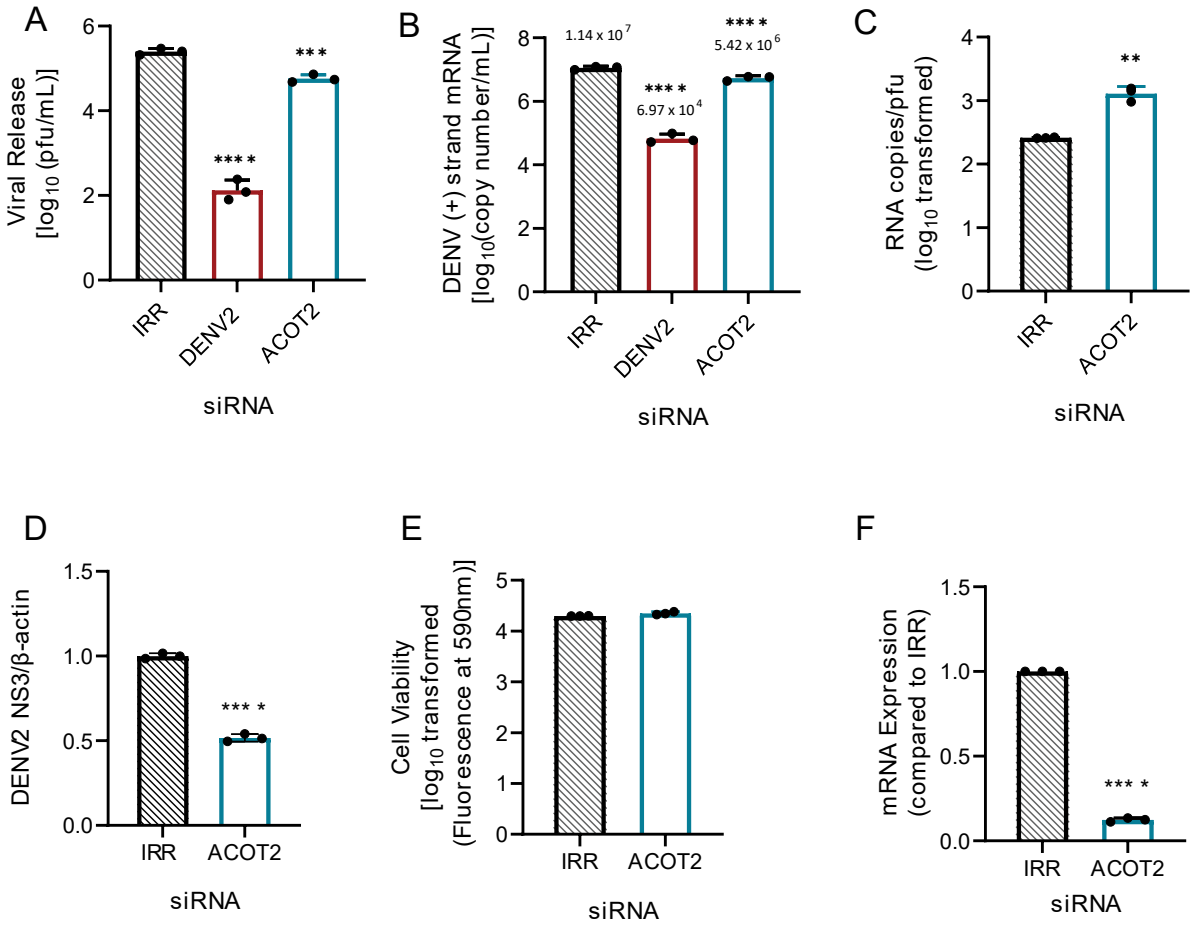

Figure 2.2 – Loss of ACOT2 function reduces DENV2 genome replication and virus release. Huh7 cells were transfected with siRNA targeting the ACOT2 gene or indicated controls (IRR and DENV2) and then infected with DENV2 for 24hr (MOI = 0.3). (A) Infectious virus release was titrated via plaque assay. (B) Huh7 cells were collected, and relative copy number of viral RNA within cells was measured via qRT-PCR. Results were normalized to RPLP0. (C) Virus supernatant was collected at 24 hpi and split into two fractions. One fraction was titrated via plaque assay, while viral RNA from the other fraction was analyzed via qRT-PCR for total copy number of DENV2 positive-strand RNA. (D) Cell lysates were collected at 24 hpi, and analyzed via western blot. Samples were probed for DENV2 nonstructural protein 3, and normalized to β-actin. Li-cor IRDyes were used as secondary antibodies, and fluorescence intensity of each band was analyzed using area under the curve analysis in ImageJ. (E) A resazurin-reduction based cell viability assay was conducted to assess cytotoxicity of siRNA treatment. (F) Knockdown of ACOT2 mRNA was confirmed at 48 hr post transfection via qRT-PCR. ACOT2: siRNA targeting acyl-CoA thioesterase 2, IRR: irrelevant siRNA control (no biological target for siRNA sequence), DENV2: siRNA targeting dengue virus, serotype 2. (A-B: one-way ANOVA with Dunnett's multiple comparisons test, C-F: unpaired t tests: * = p≤0.05, ** = p≤0.01, ***= p≤0.001, **** = p≤0.0001.)

2.2.3 – Mitochondrial ACOTs are vital for productive DENV2 infection

ACOT2 is suggested to be an important mediator of β-oxidation [194,195]. This is the process of gaining ATP from the breakdown of fatty acyl-CoA to 2-carbon acetyl-CoA molecules. As this process occurs in the mitochondria, mitochondrial ACOTs may be important in regulating

the balance of FFAs and fatty acyl-CoAs through shuttling fatty acyl-CoAs into β-oxidation [194,195]. Previous studies indicate that β-oxidation is elevated during infection of host cells by DENVs [reviewed in 14]. Both type I and type II ACOTs exist in the mitochondria. ACOT7 is a type II ACOT, and is functionally homologous to ACOT2 (both hydrolyze long-chain FAs) [193]. Therefore, we investigated if loss of ACOT7 function also resulted in suppression of DENV2 infection. Similar to ACOT2 knockdown, we found that loss of ACOT7 function significantly reduced DENV2 infectious particle release (~77%) in Huh7 cells (Figure 2.3A). Interestingly, ACOT7 inhibition resulted in a greater reduction of viral protein translation (~75% reduction, Figures 2.3D and Supplemental Figure 2.1) and viral genome replication (~70% reduction, Figure 2.3B) compared to the effect of loss of function of ACOT2 (Figure 2.2B). Similar to the ACOT2 study, loss of ACOT7 function significantly decreased particle infectivity (Figure 2.3C). We confirmed that these results were also not due to cytotoxicity of the siRNA treatment (Figure 2.3E), and that the ACOT7 siRNA effectively reduced ACOT7 mRNA levels (Figure 2.3F). Taken together, these studies suggest that two of the mitochondrial ACOTs have a vital role in the DENV2 lifecycle.

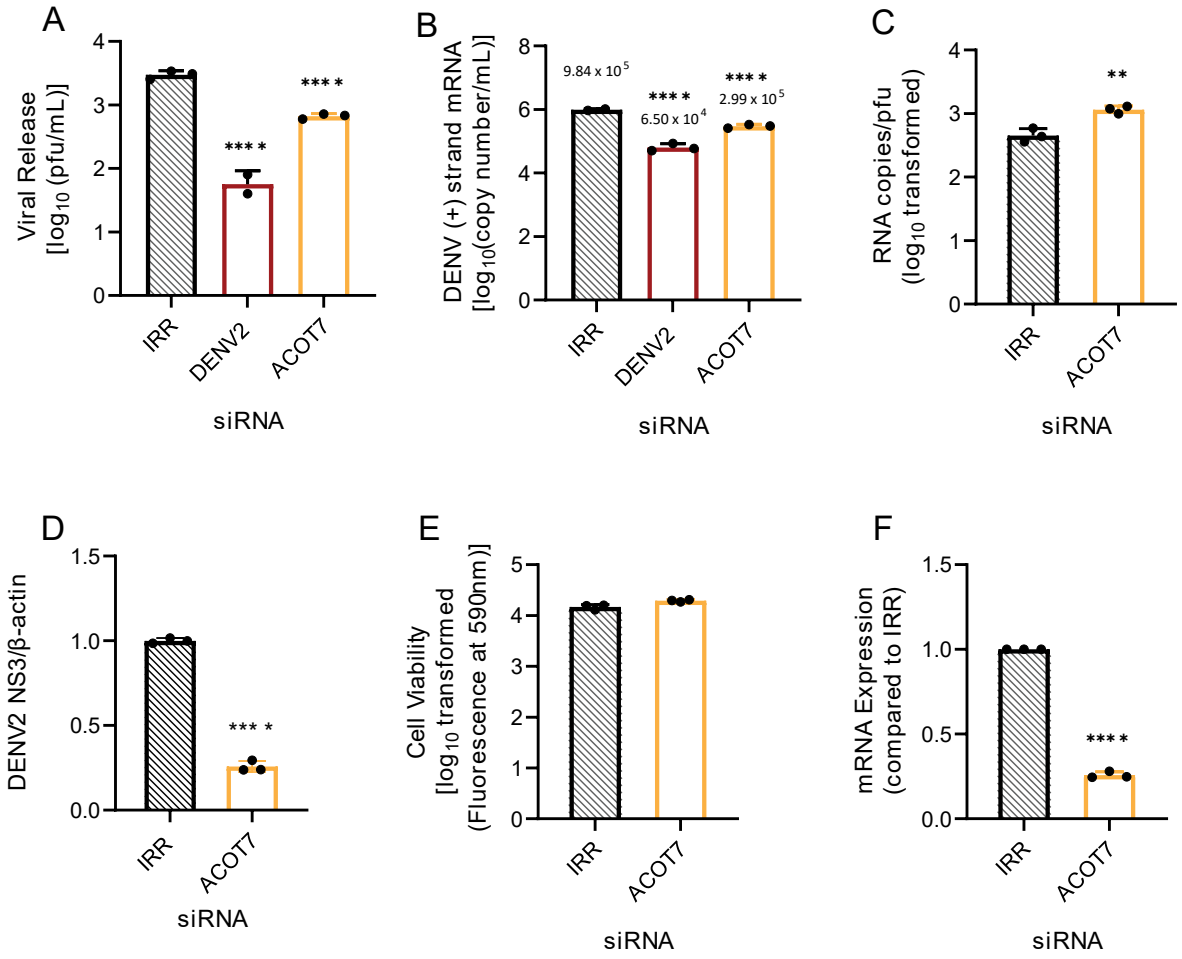

Figure 2.3 – Loss of ACOT7 function suppresses DENV2 genome replication and infectious particle release. Huh7 cells were transfected with siRNA targeting the ACOT7 gene or the indicated controls (IRR and DENV2) and then subsequently infected with DENV2 for 24hr (MOI =0.3). (A) Infectious virus release was titrated via plaque assay. (B) Huh7 cells were collected, and relative copy number of viral RNA within cells was measured via qRT-PCR. Results were normalized to RPLP0. (C) Virus supernatant was collected at 24 hpi and split into two fractions. One fraction was titrated via plaque assay, while viral RNA from the other fraction was analyzed via qRT-PCR for total copy number of DENV2 positive-strand RNA. (D) Cell lysates were collected at 24 hpi, and analyzed via western blot. Samples were probed for DENV2 nonstructural protein 3, and normalized to β-actin. Li-cor IRDyes were used as secondary antibodies, and fluorescence intensity of each band was analyzed using area under the curve analysis in ImageJ. (E) A cell viability assay using resazurin was conducted to assess cytotoxicity of siRNA treatment. (F) Knockdown of ACOT7 mRNA was confirmed at 48 hr post transfection via qRT-PCR. ACOT7: siRNA targeting acyl-CoA thioesterase 7, IRR: irrelevant siRNA control (no biological target for siRNA sequence), DENV2: siRNA targeting dengue virus, serotype 2. (A-B: one-way ANOVA with Dunnett's multiple comparisons test, C-F: unpaired t tests: * = p≤0.05, ** = p≤0.01, ***= p≤0.001, **** = p≤0.0001.)

2.2.4 – Both Type I and Type II ACOTs are differentially expressed upon ACOT2 or ACOT7 knockdown

Currently, there are ten human ACOTs known to exist in different subcellular compartments, and they have substrate specificity for a wide range of fatty acyl-CoAs [192,193]. However, the functional overlap and/or ability of each ACOT to compensate for loss of function of the others is unknown. As mitochondrial ACOTs seem to play vital roles in fatty acid metabolism and energy production, we determined whether other ACOTs could compensate for loss of ACOT2 or ACOT7 function, both within and without the context of DENV2 infection. To investigate this, we carried out similar siRNA-mediated knockdown of ACOT2 and ACOT7 in both mock-infected and DENV2-infected Huh7 cells. An IRR siRNA control was also included. 24 hours post infection (hpi), mock- and DENV2-infected cells were collected and cellular mRNA levels of each ACOT enzyme was determined via qRT-PCR.

In both mock-infected and DENV2-infected samples, we observed similar trends in the mRNA expression of other ACOTs upon knockdown of ACOT2 (Figure 2.4 A,B) or ACOT7 (Figure 2.4 C,D). Specifically, we observed that in both mock- and DENV2-infected Huh7 cells, knockdown of ACOT2 significantly reduced mRNA expression of ACOTs 1, 6, 8, and 11 (Figure 2.4 A,B). A decrease in ACOT9 and ACOT12 mRNA expression was only observed in DENV2-infected, ACOT2 knockdown samples. We found loss of ACOT7 significantly reduced mRNA expression of ACOTs 2, 4, 8, 9, and 11 in both mock- and DENV2-infected cells, (Figure 2.4 C,D). Additionally, in DENV2 infected cells, ACOT6 and ACOT13 mRNA expression was decreased in ACOT7 siRNA-treated cells. It should be noted that the siRNAs for ACOT2 and ACOT7 do not have any sequence similarity to the other ACOT mRNAs. Therefore, these data suggests that other ACOTs may be functionally dependent on the activity of ACOT2 and 7. Intriguingly, inhibiting ACOT7 also reduced expression of ACOT2 (Figure 2.4 C,D); however, inhibition of ACOT2 did not impact the expression of ACOT7 (Figure 2.4 A,B). Thus, while both mitochondrial ACOTs are

functionally similar, neither compensates for loss of the other at a transcriptional level, and ACOT2 functionality may rely upon ACOT7.

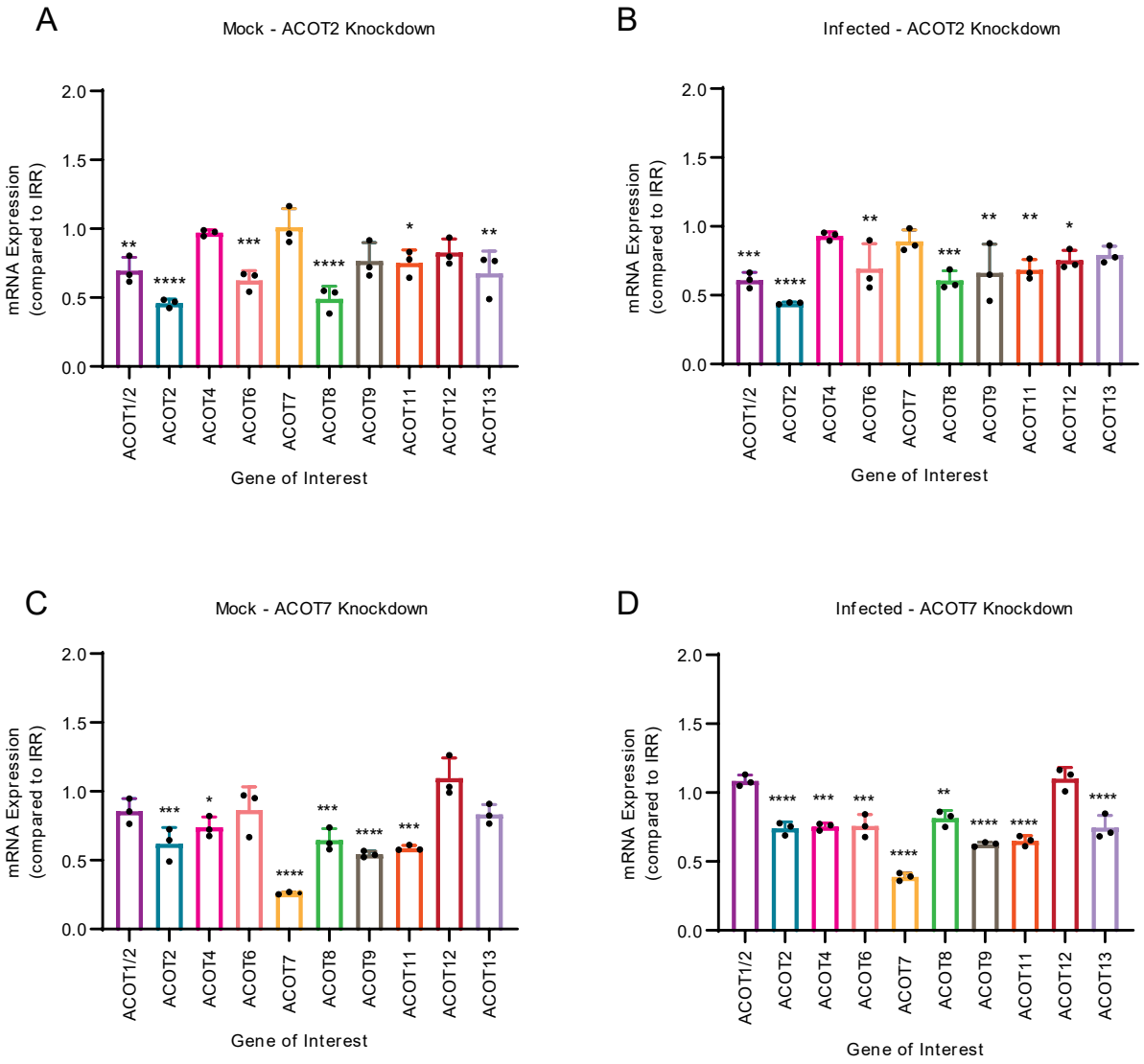

Figure 2.4 – Inhibition of mitochondrial ACOTs underlines importance of mitochondrial ACOT functionality for expression of other ACOTs. Huh7 cells were treated with either ACOT2 (A,B) or ACOT7 (C,D) siRNA or an IRR control siRNA, and then (A,C) mock-infected or (B,D) DENV2-infected (MOI = 0.3). At 24 hpi, cells were collected and mRNA levels of all 10 human ACOTs was determined via qRT-PCR. (A-D: one-way ANOVA with Dunnett's multiple comparisons tests, * = p≤0.05, ** = p≤0.01, ***= p≤0.001, **** = p≤0.0001.)

2.2.5 – Mitochondrial ACOTs are upregulated at early timepoints of infection

In previous studies, it has been demonstrated that DENV2 infection results in both viral- and host-mediated modulation of enzymes involved in fatty acid metabolism [14,42,110,111,192,250–252]. As our loss of function studies of ACOT2 and ACOT7 indicated these enzymes are vital for the DENV2 lifecycle, we analyzed whether ACOT2 and ACOT7 mRNA expression was altered over a time course of DENV2 infection. For this study, we collected both mock-infected and DENV2-infected cells at 0, 6, 24, and 48 hpi. These time points represent early, peak, and late viral replication. ACOT mRNA expression was analyzed using qRT-PCR (Figure 2.5). We observed that ACOT2 and ACOT7 mRNA expression was significantly upregulated at 6 hpi in DENV2-infected cells, but downregulated at 24 and 48 hpi (Figure 2.5A). A similar trend was noted when we compared mRNA expression between DENV2 and mock-infected samples at each timepoint although the increased expression at 6 hpi was not statistically significant (Figure 2.5B). These results combined with our results in Figures 2.2-2.3, suggest that ACOT2 and ACOT7 functionality is required for early stages of the DENV2 life cycle.

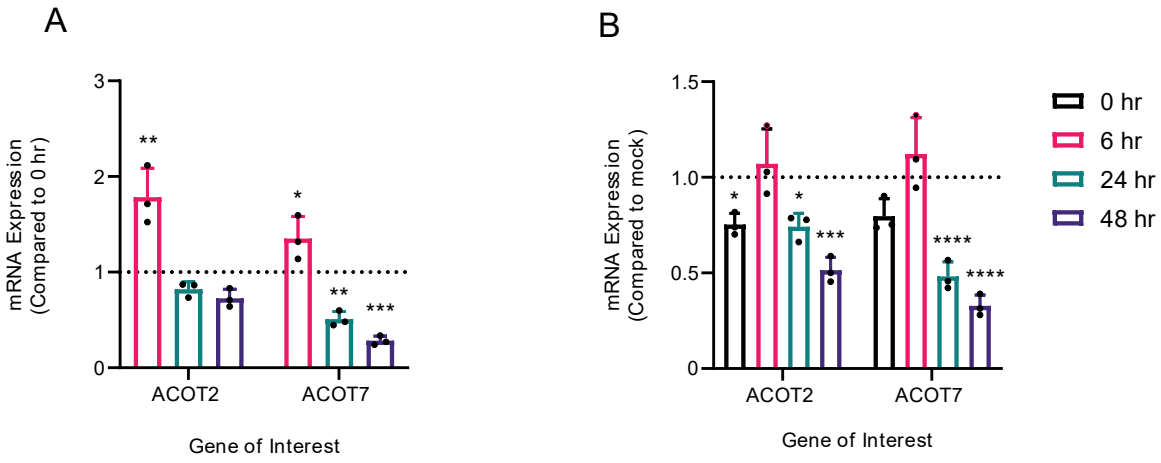

Figure 2.5 – Mitochondrial ACOT mRNA expression is temporally altered during DENV2 infection. Huh7 cells were either mock-infected or DENV2-infected (MOI = 10). At 0, 6, 24, and 48 hpi, cells were collected and mRNA levels of ACOT2 and ACOT7 were assessed via qRT-PCR. DENV2-infected samples collected at 6, 24, and 48 hpi were compared either to (A) the 0 hpi DENV2-infected samples or to (B) mock infected samples at matched timepoints. Results are reported as an expression ratio (A) between each timepoint sample and the 0 hpi sample in DENV2-infected cells, or (B)between each timepoint sample and its respective mock-infected timepoint. (A-B: one-way ANOVA with Dunnett's multiple comparisons test: * = p≤0.05, ** = p≤0.01, ***= p≤0.001, **** = p≤0.0001.)

2.3: Discussion

The ACOT family of enzymes are suggested to be key regulators of the intercellular balance of activated fatty acids (fatty acyl-CoAs) and FFAs [191,193]. As previous studies have shown that DENVs are reliant upon activated fatty acids for completion of their lifecycle [14,99,110,111,119,162,257], our present study investigated whether ACOT enzymes may be important modulators of DENV2 infection. The ACOT enzymes chosen represented both type I (ACOT1 and ACOT2) and type II ACOTs (ACOT7) as well as ACOTs found within the same organelle (ACOT2 and ACOT7 in the mitochondria). Interestingly, we found that loss of function of these enzymes had a divergent effect on the DENV2 lifecycle that was independent of their substrate specificity, and, instead, highlighted a more nuanced relationship between DENV2 and the subcellular regulation of fatty acid metabolism. Specifically, we found that the loss of function of the cytoplasmic ACOT1 enzyme resulted in increased DENV2 genome replication and infectious virus release, indicating that its normal function may be antiviral. However, loss of function of the mitochondrial ACOT2 and ACOT7 enzymes resulted in suppression of multiple stages of the DENV2 lifecycle indicating that the function of these enzymes is vital for effective DENV2 infection. Furthermore, our analyses revealed a functional dependency between enzymes within the ACOT family.

Because ACOTs act directly on activated fatty acids, it is predicted that they play a significant role in modulation of fatty acid metabolism [119,191,193,196,197]. However, mechanistic insight as to the specific functions of ACOT enzymes is limited. One challenge is that the ester bond that links coenzyme A with fatty acids is labile which limits the ability to obtain a true ratio of activated fatty acids and FFAs in cells with traditional methods [191,258]. Thus, much of what the field understands about the function of these enzymes is concluded from studies characterizing their biophysical and biochemical properties, or from mouse models studying the

impact of ACOT gene deletion on cardiac, neurological, and metabolic disorders [191–195,197–199,253–255,258]. During curation of this paper, we successfully developed an LC-MS assay that allowed us to distinguish between arachidonic acid, SH-CoA, and arachidonoyl-CoA (the primary substrate of ACOT7) [discussed in 193,194]. However, due to limitations in scalability of siRNA treatment, levels of these metabolites were below our limits of detection. As a future direction, use of knockdown cell lines may further characterize ACOT enzyme functionality. Moreover, an additional challenge was that ACOT1 and ACOT2 enzymes share 98% similarity at the protein level, and 94% nucleotide sequence homology [192,197]. This inhibited differentiation of these enzymes at the protein level. However, we were able to design specific siRNA and primer sequences that targeted the mitochondrial localization sequence of ACOT2, allowing us to characterize these enzymes based on their mRNA expression.

In an ACOT1 knockout mouse model, ACOT1 was shown to modulate liver fatty acid metabolism during fasting, and loss of function of this enzyme led to increased triglyceride turnover and beta oxidation [199]. Importantly, infection with DENV2 mimics a fasting state in the cell, and previous studies have established that triglyceride hydrolysis and beta-oxidation are increased in DENV2-infected cells [99,162,257]. Thus, inhibition of ACOT1 may further enhance these processes, leading to a more favorable environment for DENV2 replication. Moreover, as ACOT1 regulates the cytoplasmic levels of long chain fatty acyl-CoAs inhibition of ACOT1 may favor DENV2 replication by increasing the availability of the components necessary for the rearrangement and expansion of ER-derived membranes during infection [99,110,111,184,186]. Mitochondrial functional assays have suggested that ACOT2 and ACOT7 functions to decrease beta-oxidation overload, possibly by mediating efflux of fatty acids from the mitochondrial matrix [162,196,258]. Thus, loss of ACOT2 and ACOT7 function may have resulted in a buildup of fatty acyl-CoAs levels in the mitochondria, decreased turnover of CoA and fatty acid precursor molecules, and increased oxidative stress – all of which would antagonize the DENV2 lifecycle. Interestingly, we found that following ACOT2 or ACOT7 knockdown there was no compensation

by any of the other mitochondrial ACOTs (ACOT2, 7 or 9). However, ACOT2 and ACOT7 knockdown decreased peroxisomal ACOT4, ACOT6 and ACOT8 expression. Peroxisomal ACOTs are important in degradation of very long-chain fatty acids that cannot be directly shuttled to the mitochondria [191,197]. Peroxisomes are becoming recognized as important mediators for controlling or facilitating virus infection, including anti-viral immune responses, interactions with viral capsid proteins, and influencing membrane fluidity [259,260]. Therefore, another possibility is that ACOT2 or ACOT7 knockdown is indirectly suppressing DENV2 replication through altering expression of peroxisomal ACOTs which may impact peroxisomal lipid degradation activity. The role of peroxisomes in these biochemical interactions between virus and host is yet an uncharted territory.

In summary, we found there is a differential impact of ACOTs on DENV2 genome replication and infectious particle release that could be influenced by the subcellular location of these enzymes. We also observed that loss of function of a single ACOT impacted the expression of multiple ACOTs in different cellular locations highlighting the complexity of understanding how ACOTs influence viral replication. Overall, our current study underscores that DENV2 is reliant upon careful coordination of fatty acid metabolism to complete its lifecycle. Future studies aimed at characterizing the exact substrate specificities would increase our understanding of how the loss of function of specific enzymes regulate infection. Additionally, our data suggest that determining the functional relationship between ACOTs is warranted.

2.4: Materials and Methods

2.4.1 Cell lines and viruses:

The cell lines used in this study were as follows: Human hepatoma cells (Huh7) (unknown sex, From Dr. Charles Rice) [261], Clone 15 (ATCC CCL-10) of the Baby Hamster Kidney Clone

21 cells (BHK-21), and C6/36 cells (ATCC CRL-1660, larva, unknown sex). Huh7 cells were maintained in Dulbecco's Modified Eagle Medium (DMEM) (Gibco, Life-Tech) while BHK-21 and C6/36 cells were maintained in Minimum Essential (MEM) (Gibco, LifeTech). All culture media was supplemented with 2 mM L-glutamine (Hy-Clone), 2 mM nonessential amino acids (HyClone), and 10% fetal bovine serum (FBS) (At-las Biologicals). C6/36 media was also supplemented with 25 mM HEPES buffer. Cells were incubated at 37°C with 5% CO_2.

For this study, dengue virus serotype 2 was used (DENV2, strain 16681) [256,262]. The virus was passaged in C6/36 cells. Viral titer was determined via plaque assay on BHK-21 cells as previously described [263]. Virus infections were carried out at room temperature for 1 hour (hr), allowing for viral adherence. Subsequently, virus was removed, and cells were washed with 1xPBS before addition of media supplemented with 2 mM nonessential amino acids, 2 mM L-glutamine, and 2% FBS. Cells were incubated at 37°C with 5% CO_2 for 24 hours.

2.4.2 siRNA transfection and knockdown confirmation

ACOT1/2, ACOT2 and ACOT7 loss of function was conducted by transfecting Huh7 cells with pooled siRNAs (Horizon Discovery/Dharmacon, Sigma-Aldrich – see Supplemental Table 2.1) as described previously [264] using RNAiMAX (Invitrogen) and incubating for 48 hr at 37°C with 5% CO2. At 48 hr post transfection, cells were either collected for a cytotoxicity assay (described below), knockdown confirmation or infected with DENV2 (as described above). At 24 hpi, cells and viral supernatant were collected for further analysis. Viral titration was completed via plaque assay. RNA was extracted from cells, and qRT-PCR analysis was used to confirm knockdown of ACOT2 and ACOT7 mRNA transcripts. Cellular transcripts were normalized to RPLP0, and the ACOT2 and ACOT7 siRNA-treated samples were then compared to an irrelevant control (IRR) using the delta delta cq method described in [119]. The IRR control siRNA is a

scrambled RNA with no homology to any human mRNA sequences [described in 99]. Cytotoxicity of siRNA treatment was determined using a 1:10 dilution of resazurin (ThermoFisher) in cell culture media, and incubating cells for 1-2hr. Fluorescence was read on a Victor 1420 Multilabel plate reader (Perkin Elmer) at 560nm/590nm (excitation/emission).

2.4.3 RNA extraction and qRT-PCR

RNA was extracted from cells and viral supernatant using TRIzol or TRIzol LS (ThermoFisher), respectively, following standard TRIzol extraction methods. For qRT-PCR, the Brilliant III Ultra-Fast SYBR® Green one-step qRT-PCR kit (Agilent) was used, and all reactions were set up according to manufacturer's protocols on a LightCycler 96-well real-time PCR machine (Roche). The following cycling parameters were employed: 20 mins at 50°C for reverse transcription, 5 mins at 95°C, followed by 45 two-step cycles of 95°C for 5 secs, and 60°C for 60 secs. A melt curved followed each step starting at 65°C and ending at 97°C. (Primer sequences are reported in Supplemental Table 1). A standard curve was generated using in vitro transcribed viral RNA from a DENV2 cDNA sub-clone (derived from strain 16681 full-length clone) in order to quantify DENV2 genome copies. All cellular RNA transcript copy numbers were normalized to Ribosomal Protein Lateral Stalk Subunit P0 (RPLP0) RNA using the delta delta cq method as described pre-viously [119,264].

2.4.4 Western Blotting

Huh7 cells were lysed in RIPA Buffer. Total protein in each sample was measured using the Qubit BR Protein Assay (ThermoFisher) on a Qubit Flex Fluorometer. Equal total protein was loaded from each of the indicated cell lysates and run on a CriterionTM XT 4-12% Bis-Tris protein

gel (Bio-Rad). Protein was transferred at 4°C to nitrocellulose membrane for 2 hours at 50V. Following transfer, blocking was performed overnight at 4°C with a 5% milk solution in 1x PBS supplemented with 0.1% Tween 20. The primary antibodies used were a 1:300 dilution of antibody against the DENV2 NS3 protein (mouse polyclonal antibody raised against the DENV2 NS3 protein) [described in 99], and 1:100 dilution of β-actin (rabbit polyclonal antibody, Invitrogen). The secondary antibodies used were a 1:3000 dilution of goat-anti-mouse IRDye 800CW, and goat-anti-rabbit IRDye 680RD (Li-Cor Biosciences). Blots were imaged on a ChemiDoc MP Imaging System (Bio-Rad), and quantified in ImageJ utilizing area under the curve analysis.

2.4.5 Statistical analysis

In each figure and/or figure legend, statistical analysis details are noted. All results are expressed as mean values with standard deviation from three biological replicates (unless otherwise indicated). Statistical significance was deter-mined using a one-way Analysis of Variance (ANOVA) with Dunnett's multiple compar-isons test, or an unpaired t test using Prism software version 9.0 (GraphPad Software, La Jolla, California USA).

Chapter 3: Human sialidase activity is vital for dengue virus serotype 2 replication

3.1: Introduction

Sialic acids (SIAs) are a family of over 50 structurally distinct, sugar molecules with a 9-carbon backbone that are most often found at the terminal position of glycolipids and glycoproteins [229,265–267]. Given their ubiquitous occurrence, especially in cell surface molecules, SIAs are some of the most versatile and influential regulatory molecules in cell biology [229,265–267]. SIAs function either as ligands, masking molecules, or as physicochemical effectors of both their attached glycoconjugates and surrounding molecules due to their strong negative charge [229,265–267]. As such, SIAs are vital for cell signaling, cellular recognition, cell-to-cell communication, immune cell signaling and modulation, cell differentiation, cellular trafficking, and structural conformation of glycoconjugates [229,265–267]. As the roles of SIAs in biological functions are dynamic, so must be the balance between sialylated and desialylated states of glycoconjugates. This balance is mediated by sialytransferases and sialidases (neuraminidases), respectively [229,265–267]. In humans, there are 4 known sialidases (NEU1-4). Interestingly, we and others have shown that the DENV2 nonstructural protein 1 (NS1) is necessary and sufficient to cause increased activity of the human sialidase enzymes (neuraminidase 1-4, NEU1-4) in both *in vitro* and *in vivo* models [90,91]. Moreover, the upregulated sialidase activity was associated with increased endothelial hyperpermeability in *in vitro* models, and vascular leakage coupled with increased morbidity and mortality in an *in vivo* mouse model [90,91]. These studies revealed a link between increased sialidase activity and DENV pathogenesis; however, it remains unclear what advantage increased sialidase activity plays in the virus lifecycle.

In this study, we sought to characterize the role of the four human sialidase enzymes, NEU1-4, on the DENV2 lifecycle in human hepatoma cells (Huh7s). We used siRNA-mediated loss of function analysis to systematically examine the role each enzyme plays during the viral replication cycle. We uncovered that these enzymes do not only contribute to viral pathogenesis, but also play a critical role in viral replication and egress. Importantly, this study highlighted yet uncovered roles of sialic acids and sialidase enzyme activity in the DENV2 lifecycle.

3.2: Results

3.2.1 - Sialidase activity is vital for DENV2 replication and viral release

Neuraminidases were previously shown to be upregulated by DENV2 NS1 protein [90,91]. This upregulation contributed to the breakdown of endothelial barrier integrity that leads to the vascular leakage observed in severe dengue disease [90,91]. However, it was unknown whether this upregulation contributed only to viral pathogenesis or also played a role in the DENV2 lifecycle. Moreover, these previous results were intriguing given that NEU1-4 are found in different subcellular compartments (Figure 3.1A), and have different substrate specificities (Table 3.1) [268,234,reviewed in 269–271]. We hypothesized that NEU1-4 may each have specific, independent roles within the viral lifecycle. Thus, we first sought to determine the effect of siRNA-mediated loss of function of NEU1-4 on DENV2 release from Huh7 cells. Interestingly, we found that inhibition of each enzyme resulted in a significant decrease (1-2 log reduction) in infectious virus release from cells (Figure 3.1B). Similarly, we also saw a significant decrease in DENV2 genome replication (Figure 3.1C). Knockdown of NEU1-4 was validated by measuring mRNA expression using qRT-PCR (Supplemental Figure 3.1A-B). Additionally, since these experiments were conducted using a pool of four siRNAs (Dharmacon) against each NEU, we validated our

results with single siRNAs (Thermofisher) targeting NEU1-4 and saw a similar reduction in viral release upon NEU1-4 KD (Supplemental Figure 3.2).

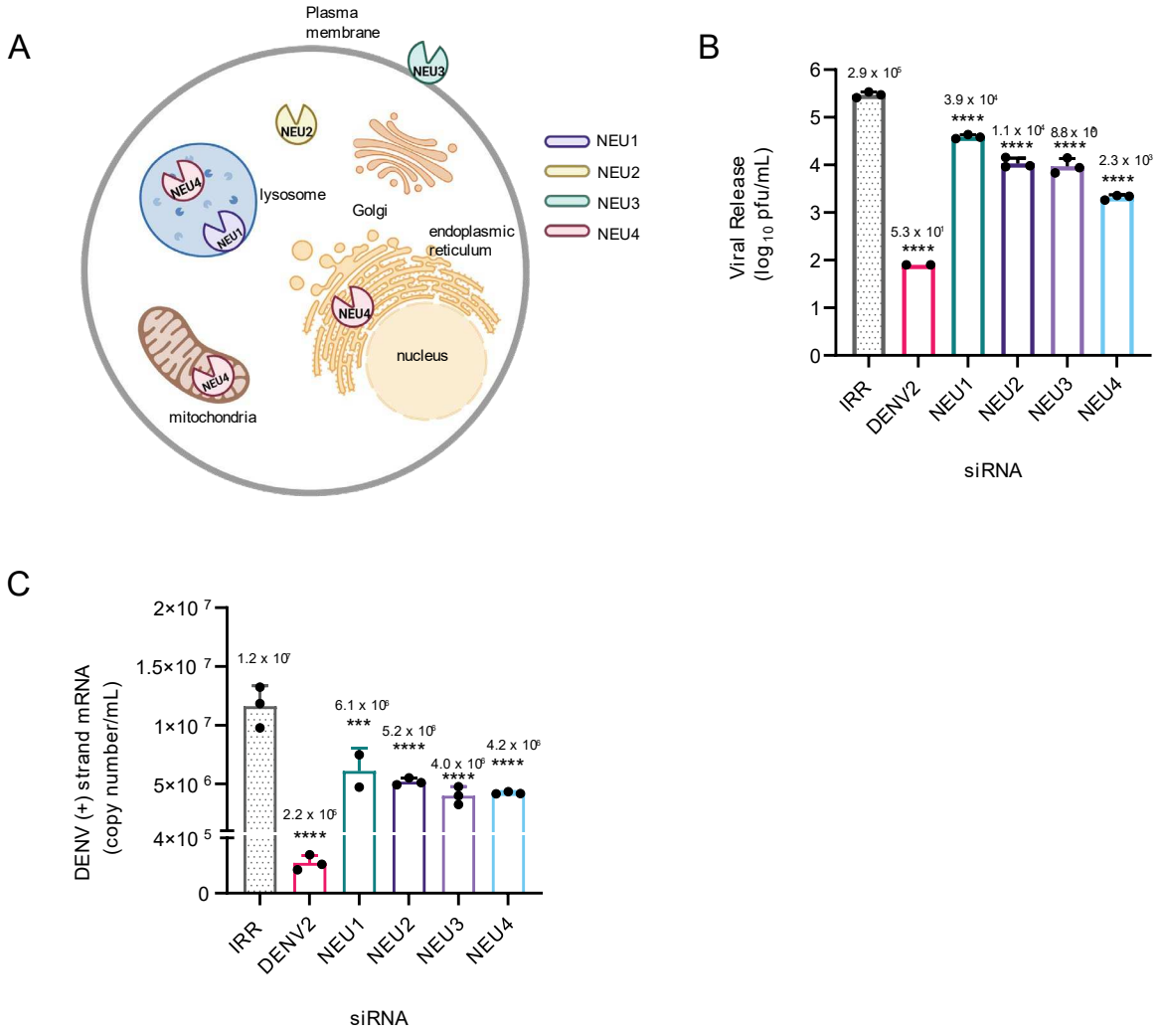

Figure 3.1 – Subcellular Location of human sialidases and preliminary loss of function analysis of NEU1-4. (A) Primary subcellular location of human sialidase enzymes. B-C: Huh7 cells were transfected with pooled siRNAs targeting NEU1-4, a DENV2-specific positive control siRNA, and an irrelevant (non-targeting) negative control siRNA, followed by DENV2 infection (MOI = 0.3) for 24 hr. (B) Supernatants were titrated via plaque assay on BHK-21 cells to measure infectious virus release. (C) Cells were collected and copy number of viral RNA was measured via qRT-PCR and normalized to the RPLP0 housekeeping gene. NEU1: human neuraminidase 1, NEU2: human neuraminidase 2, NEU3: neuraminidase 3, NEU4: neuraminidase 4, IRR: irrelevant control, DENV2: dengue virus serotype 2. (A: image generated using Biorender.com, B: one-way ANOVA with Dunnett's multiple comparison's test: * = p≤0.05, ** = p≤0.01, ***= p≤0.001, **** = p≤0.0001.)

Table 3.1 – Properties of Human Sialidases.

	Subcellular location	Glycoconjugate substrates	Linkage Preference	Chromosome Location
NEU1	lysosomes (primary), plasma membrane	oligosaccharides, glycopeptides	α-2,3- and α-2,6-	6p 21.3
NEU2	cytosol	oligosaccharides, glycopeptides, gangliosides	α-2,3- > α-2,6- = α-2,8-	2q 37
NEU3	plasma membrane (primary), endosomes	gangliosides	α-2,3- = α-2,8- > α-2,6-	11q 13.5
NEU4	lysosomes, mitochondria, endoplasmic reticulum	oligosaccharides, glycopeptides, gangliosides, sialyl-Lewis antigens	α-2,3- = α-2,6- = α-2,8-	2q 37.3

3.2.2 – Viral egress is attenuated by downregulation of NEU1-4

We next sought to determine whether defects in particle maturation, viral egress or infectivity might contribute to the reduction of viral genome replication and infectious virus released from NEU1-4 KD samples. To evaluate the effect of NEU1-4 KD on particle maturation, we measured the ratio of total particles released (genome equivalents) to infectious particles released (viral titer) in the supernatant as previously described in [119]. An increase in the particle/pfu ratio would signify impaired particle maturation as mature virus particles are more infectious than immature virus particles. We determined that loss of function of NEU1-4 had no impact on the infectivity of virus particles released from NEU1-4 KD cells (Figure 3.2A). Thus particle maturation was not impacted by loss of sialidase activity.

As neuraminidase activity is indispensable for viral entry and egress of many viruses [272, reviewed in 273,274], we next investigated whether downregulation of NEU1-4 would also inhibit DENV2 egress. Following siRNA treatment and DENV2 infection of Huh7 cells, we collected both the viral supernatant and cells (24 hpi). Cells were gently lysed using the freeze-thaw lysis method

to maintain integrity of any virions not released from the cell. We then titrated both the supernatant and cell samples on BHK-21 cells and compared the amounts of infectious DENV2 in each fraction. Overall, we found a higher amount of infectious virus in the supernatant in both the IRR control and knockdown samples compared to their corresponding internal viral titers (Figure 3.2B). However, the NEU1-4 KD samples did show an overall reduction in released infectious virus, confirming our previous results (Figure 3.1B). Intriguingly, we noticed that the internal viral titer was similar between our IRR control and NEU1-4 KD samples. Because of these combined results, we found that there was a significant decrease in the ratio of extracellular versus intracellular infectious DENV2 (Figure 3.2B). This suggested that DENV2 release may be attenuated by loss of neuraminidase activity.

To further evaluate this observation, we performed western blot analysis of DENV2-infected NEU1-4 KD cells to determine whether virus particles accumulated in cells with reduced sialidase activity. In support of our observations of similar levels of intracellular viral titer between our control and KD samples, we also observed similar levels of DENV2 E protein between our samples (Figure 3.2C-D). Importantly, measurement of 'intracellular infectious titer' and our western blot analysis of DENV2 E protein accumulation could not distinguish between infectious virus trafficking from sites of assembly in the ER to the Golgi versus infectious virus egressing from the plasma membrane following trafficking through the secretory pathway. Thus, we next performed two groups of immunofluorescence assays to clarify these results. In the first group (Figure 3.2E), cells were fixed in 4% paraformaldehyde (PFA), but not permeabilized to evaluate whether the accumulation was occurring at plasma membrane. Interestingly, we observed similar distribution of E protein at the plasma membrane in the NEU1, NEU3 and NEU4 KD samples as in the IRR control; however, in the NEU2 KD samples a significant increase in the amount of plasma membrane-associated E protein was observed. In the second group (Figure 3.2F), cells were fixed in 4% PFA and permeabilized to examine whether virus was accumulating in treated cells. As expected, the IRR control had a high number of infected cells (as indicated by significant

expression of DENV2 E protein). A decrease in the overall abundance of infected cells was noted in the NEU1-4 knockdown samples in support of our initial findings that NEU1-4 decreased infectious virus release and genome replication (Figure 3.1B-C). Interestingly, we observed that many of the infected cells in the treated samples showed a similar expression level of DENV2 E protein as the IRR control. We would expect reduced levels of E following NEU1-4 KD since genome replication was reduced in these cells. However, it seems E protein was accumulating following NEU1-4 KD. Spread of infection to neighboring cells was not observed. Taken together, these data suggest that loss of function of sialidase activity reduces viral replication and release by reducing viral egress from infected cells.

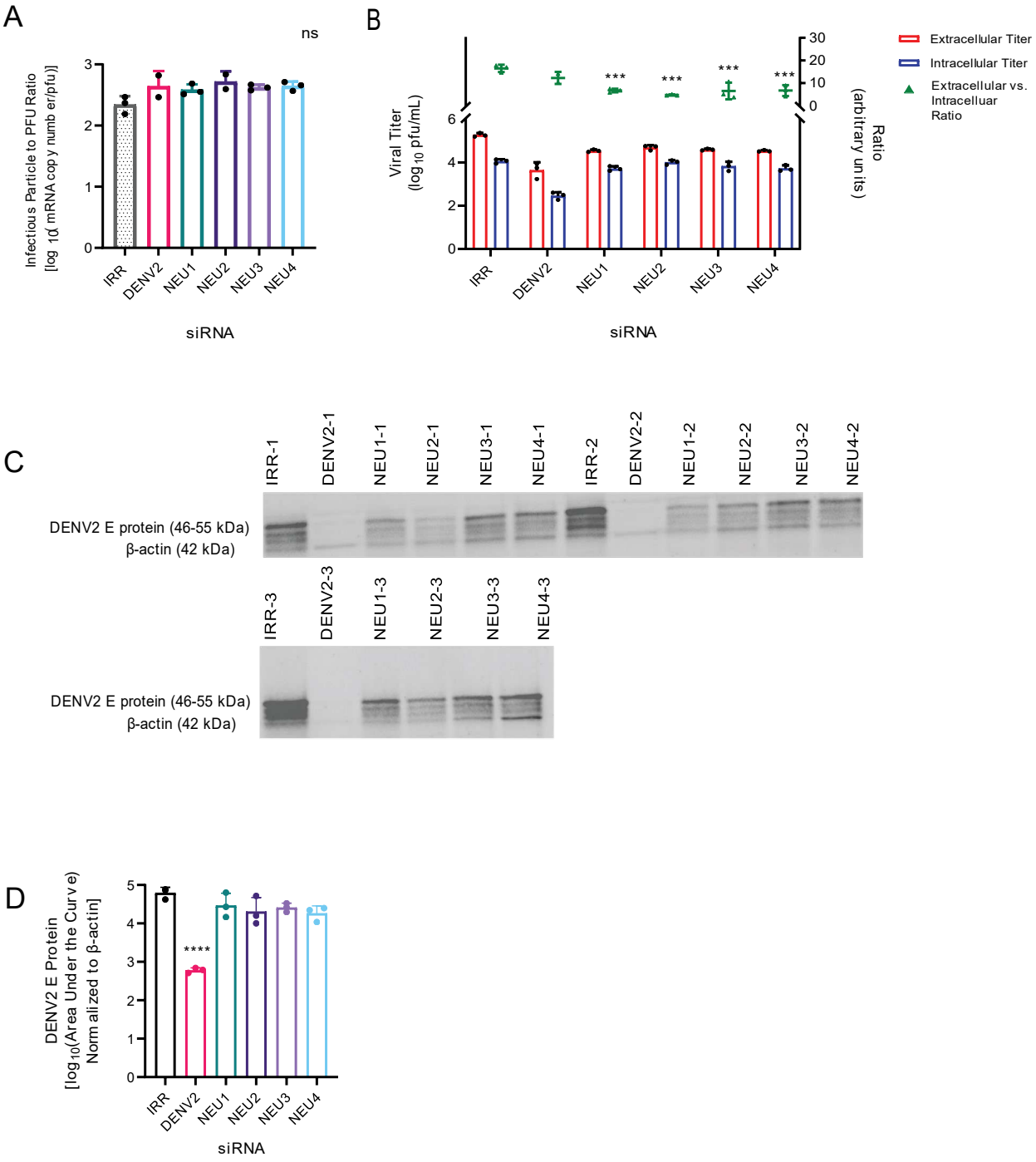
A
ns
Infectious Particle to PFU Ratio
[log 10(mRNA copy numb er/pfu)]
IRR
DENV2
NEU1
NEU2
NEU3
NEU4
siRNA
B
Viral Titer
(log 10 pfu/mL)
Ratio
(arbitrary un its)
***
Extracellular Titer
Intracellular Titer
Extracellular vs.
Intracelluar
Ratio
siRNA
C
IRR-1
DENV2-1
NEU1-1
NEU2-1
NEU3-1
NEU4-1
IRR-2
DENV2-2
NEU1-2
NEU2-2
NEU3-2
NEU4-2
DENV2 E protein (46-55 kDa)
β-actin (42 kDa)
IRR-3
DENV2-3
NEU1-3
NEU2-3
NEU3-3
NEU4-3
DENV2 E protein (46-55 kDa)
β-actin (42 kDa)
D
DENV2 E Protein
[log10(Area Under the Curve)
Norm alized to β-actin]
****
IRR
DENV2
NEU1
NEU2
NEU3
NEU4
siRNA

E

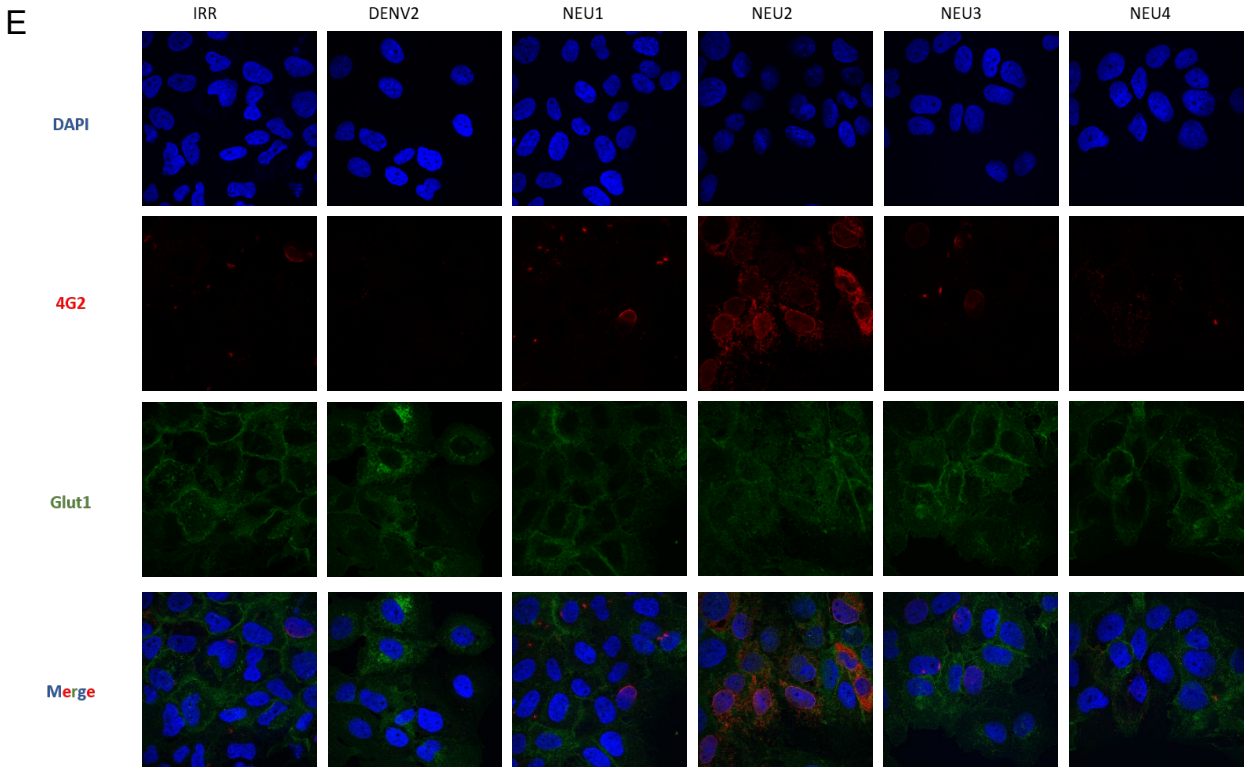
IRR
DENV2
NEU1
NEU2
NEU3
NEU4
DAPI
4G2
Glut1
Merge

F

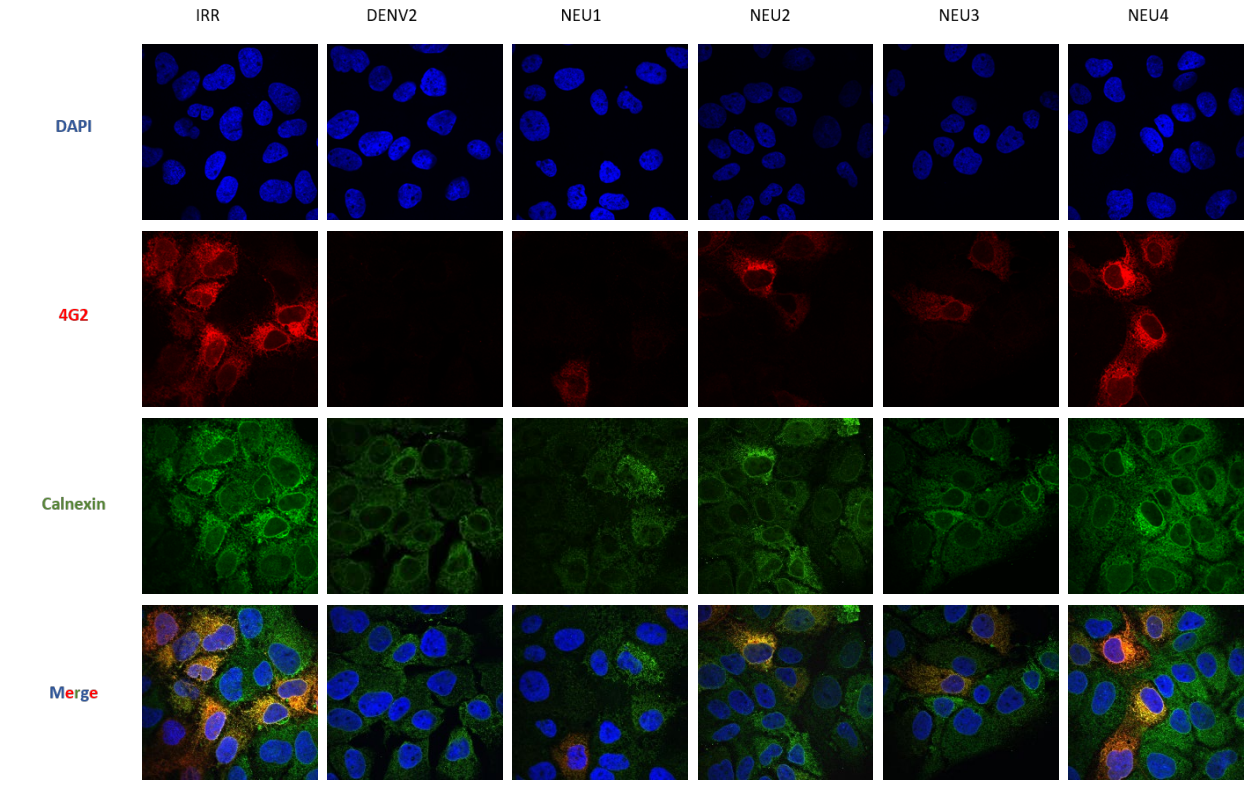
IRR
DENV2
NEU1
NEU2
NEU3
NEU4
DAPI
4G2
Calnexin
Merge

Figure 3.2 – Dengue release, but not particle infective is affected by loss of function of NEU1-4. Huh7 cells were transfected with siRNAs targeting NEU1-4 and indicated controls, followed by infection with DENV2 (24 hr, MOI = 0.3). (A) At 24 hpi, viral supernatants were collected and split to be analyzed via plaque assay for infectious virus released from cells, and via qRT-PCR to measure total viral particles release (genome equivalents) release. A ratio of infectious virus particle to viral titer was taken to determine the effect of NEU1-4 KD on DENV2 particle infectivity. (B) At 24 hpi, viral supernatants were collected, and then cells were trypsinized, collected and counted. The cells were subjected to freeze-thaw lysis, and then both the viral supernatants and cell fractions were analyzed via plaque assay to examine the effect of NEU1-4 KD on viral release. A ratio of extracellular vs. intracellular virus was calculated and is displayed on the right y-axis. Extracellular and intracellular titer values were normalized to total cell count. (C) At 24 hpi, cells were collected and the amount of DENV2 E protein in each sample was measured via Western Blot. (D) Western blot was analyzed using image under the curve analysis in ImageJ, and normalized to β-actin to determine the relative amount of DENV2 E protein in each sample. (E-F) At 24 hpi, cells were fixed in 4% paraformaldehyde, and either not permeabilized (E) or permeabilized (F) to determine whether NEU1-4 KD inhibits viral egress from cells. Primary antibodies used were mouse anti-4G2 (DENV2 E protein) , rabbit anti-Glut1 (plasma membrane marker), or rabbit anti-Calnexin (ER marker). Cells were counterstained with goat anti-mouse AlexaFluor 488, goat anti-rabbit AlexaFluor 647, and DAPI nuclear stain and imaged on an Olympus inverted laser scanning confocal microscope and processed using Volocity software v6.3. (A, B, D: one-way ANOVA with Dunnett's multiple comparison's test: * = $p \leq 0.05$, ** = $p \leq 0.01$, ***= $p \leq 0.001$, **** = $p \leq 0.0001$.)

3.2.3 NEU1-4 mRNA levels are regulated during DENV2 infection

Previously, DENV NS1 was shown to increase expression of NEU1-3 proteins by 3 hours post treatment [90]. This lead to a decrease in plasma membrane sialic acid residues at early timepoints (6 and 12 hpt) with a return to normal levels by 24 hpt [90]. As this previous work used recombinant NS1 protein alone to examine its effect on NEU proteins, we sought to characterize whether NEU1-4 mRNA might be transcriptionally or post-transcriptionally altered during DENV2 infection. Huh7 cells were infected with DENV2, and then collected at timepoints representing early (0, 6, 12), peak (18, 24, 36), and late (48) viral replication. We then analyzed the mRNA expression of NEU1-4 and hexokinase II at each timepoint using qRT-PCR (Figure 3.3). Hexokinase II was used as a positive control as it has been previously established that it is upregulated during DENV infection [136]. NEU1 mRNA expression was elevated at 6 hpi (Figure 3.3A), but otherwise remained at or near basal levels at later timepoints (Figure 3.3B-F). NEU2 mRNA expression was elevated between 6-18 hpi (Figure 3.3A-C), but returned to near basal levels between 24-36 hpi (Figure 3.3D,E), and decreased at 48 hpi (Figure 3.3F). These results suggested that NEU1 and NEU2 functionality may support early events of the DENV lifecycle.

NEU3 mRNA expression increased at 18 and 36 hpi (Figure 3.3C,E), but remained at normal levels at other timepoints (Figure 3.3A,B, D,F). This suggested that NEU3 may play a role during peak viral replication. Surprisingly, NEU4 mRNA expression began to decrease at 12 hpi (Figure 3.3B-F), and was dramatically reduced by 48 hpi (Figure 3.3F). As our previous data showed that loss of function of NEU4 resulted in the most significant decrease in viral release (Figure 3.1B) and viral genome replication (Figure 3.1C), these results indicated that NEU4 must play a vital role during early events of the DENV lifecycle but may be detrimental during later timepoints.

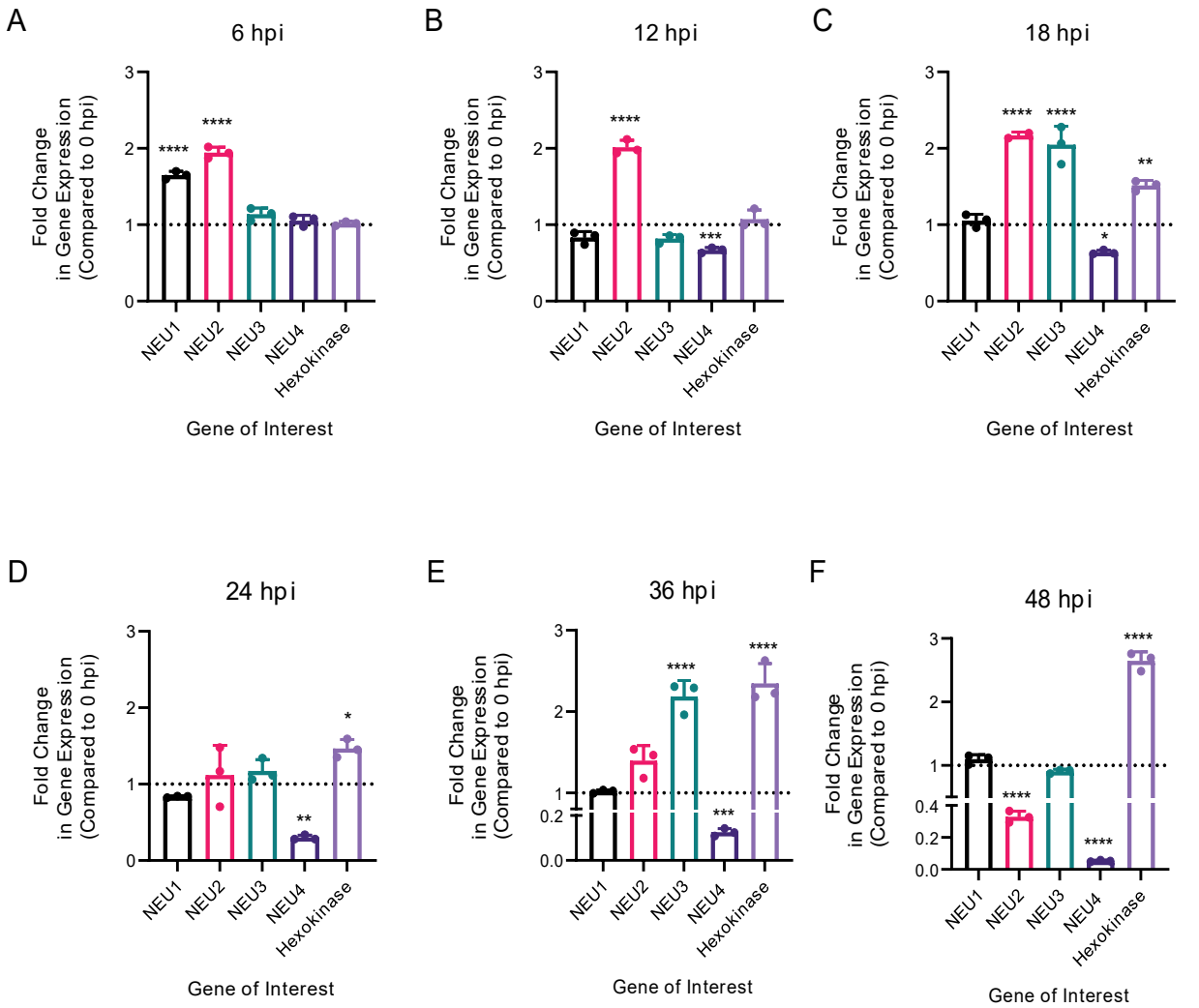

Figure 3.3 – NEU1-4 mRNA is transcriptionally regulated during DENV2 infection. (A-F) Huh7 cells were infected with DENV2 (MOI = 10), and infected cells were collected at the indicated timepoints, processed, and analyzed via qRT-PCR for mRNA expression of NEU1-4 and hexokinase II (positive control) to determine relative mRNA expression. Results were normalized to the RPLP0 housekeeping gene, and compared to samples collected at 0 hpi. (A-F: one-way ANOVA with Dunnett's multiple comparison's test: * = p≤0.05, ** = p≤0.01, ***= p≤0.001, **** = p≤0.0001.)

3.2.4 Loss of function of NEU1-4 differentially affects other NEUs

NEU1-4 have been shown to translocate between cellular compartments during infection with DENVs and other viruses [90,234,275,276]. Because there is some overlap in functionality between NEU1-4 [234,270,271], we next evaluated whether each neuraminidase could compensate for loss of function of the others. Upon examining mRNA expression in our mock infected samples (Figure 3.4A), NEU4 expression ($p < 0.01$) was elevated upon knockdown of NEU1. As NEU1 and NEU4 are both found within the lysosome [277], this indicated that NEU4 may be able to compensate for loss of function of NEU1. Interestingly, in many of our samples we observed that loss of function of one NEU resulted in decreased mRNA expression of the others. In the NEU1 knockdown samples, NEU3 mRNA expression was significantly ($p < 0.01$) reduced. Downregulation of NEU3 resulted in a decrease in NEU1 ($p < 0.01$) and NEU4 ($p < 0.05$) mRNA expression. In the NEU4 knockdown samples, NEU1 mRNA expression was significantly reduced ($p < 0.05$). Loss of function of NEU2 had no significant impact on mRNA expression of the other NEUs. Importantly, there is very little sequence homology between each NEU [231], and our BLAST results indicated that each of our siRNAs was specific to each NEU, thus, it is not likely that these results are due to off-target effects of our siRNAs. The results in DENV2 infected cells (Fig 3.4B) varied from the mock infected samples supporting our previous observations that NEU1-4 mRNA expression is altered upon DENV2 infection (Figure 3.3). In our NEU1 knockdown, we saw significant elevations in mRNA expression of both NEU2 ($p < 0.001$) and NEU4 ($p < 0.0001$). In the NEU2 knockdown, NEU4 mRNA expression was reduced ($p < 0.01$). There were no changes to mRNA expression of other NEUs upon knockdown of NEU3. Finally, loss of function of NEU4 in DENV2 infected cells resulted in significant knockdown ($p > 0.0001$) of NEU1-3. Our results in both our mock and infected samples suggested that the neuraminidases may have some functional dependence on each other or on the products from other NEUs and this functional dependance changes with infection.

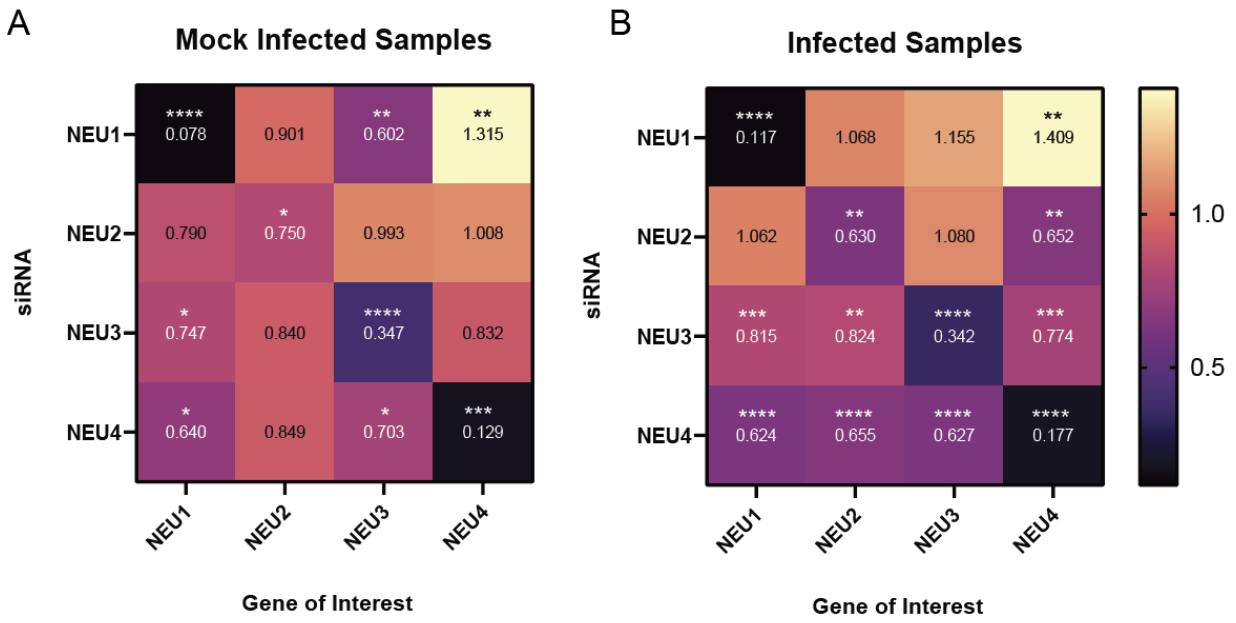

Figure 3.4 – loss of function of NEU1-4 impacts mRNA expression of other NEUs. Huh7 cells were transfected with pooled siRNAs targeting NEU1-4 and an IRR control siRNA, and either mock-infected (A) or DENV2-infected (B). At 24 hpi, cells were collected and analyzed via qRT-PCR to determine the relative mRNA expression of each NEU upon KD of other NEUs. Results were normalized to the RPLP0 housekeeping gene and compared to the IRR control (not shown) for each group. Results are displayed as a heatmap showing the fold change of each gene under each condition, written values inside boxes are average fold change values. Stars represent statistical significance in fold change compared to the corresponding IRR control. (A-B: One-way ANOVA with Dunnett's multiple comparison's test: * = p≤0.05, ** = p≤0.01, ***= p≤0.001, **** = p≤0.0001.)

3.3: Discussion

Viruses such as DENVs are reliant upon and hijack host metabolic pathways to fulfill their replicative needs [2,13,14,111,119,278,279]. Dysregulation of host metabolic pathways leads to some of the pathogenesis seen in DENV infection, as was shown in studies that discovered NS1-mediated upregulation of sialidase activity was linked with endothelial hyperpermeability and vascular leakage [90,91]. However, a functional role for the increased sialidase activity remained unexplored. In this study, we sought to further characterize the relationship between DENV and the human sialidase enzymes. Here, we have shown that functionality of NEU1-3 is required for DENV2 replication and viral egress. In addition, we have now demonstrated that NEU4, previously

unstudied in DENV infection, appears to not only be the most consequential sialidase to the DENV2 lifecycle, but that its expression is also necessary for the expression of NEU1-3.

Recent studies have highlighted there is much ambiguity in the functional roles of NEUs. Each NEU retains some activity towards SIA residues beyond their preferred substrates [268,269,280,281], and some NEUs have been shown to be capable of translocating and acting in different subcellular compartments beyond their primary locations [236,276,282,283]. Moreover, the regulatory elements that govern NEUs remain unknown [284]. This level of ambiguity presented a challenge to determining the mechanism by which desialylation impacts DENV2 replication and viral release from cells. Thus, we chose to limit our study to determining which parts of the viral lifecycle were inhibited by loss of function of sialidase activity.

However, there are several possibilities that have emerged to explain the influence of sialidases on the DENV2 lifecycle. Desialylation of low density lipoproteins (LDLs) by NEU1 and NEU3 has been shown to increase cellular uptake of LDLs and increase intracellular cholesterol, possibly through the removal of steric hindrance on apo B-100, a ligand for the LDL receptor [285,243,242,286]. During DENV infection, LDL uptake increases at early timepoints of infection [130], thus, upregulation of NEUs may augment LDL uptake, providing DENVs with some of the lipid precursors necessary for membrane restructuring that drive formation of replication complexes. Another possibility is that intracellular trafficking along the endocytic and lysosomal pathways are, in part, modulated by the sialylation state of glycoconjugates within endocytic vesicles [287,288]. Importantly, DENVs are critically dependent upon endosomes to enter cells, have been shown to traffic between intercellular compartments using the endolysosomal system, and viral replication complexes have been found in components of the autophagolysosomal system [37,42,58,163,169]. Alternately, sialidases may act on the conserved glycosylation site at N154 (in most flaviviruses, N153) in the viral envelope (E) protein that has been proposed to shield the fusion loop preventing premature fusion [63,79,81]. Thus, sialidase activity in the late endosome may partially drive the fusion event necessary to release the viral RNA into the

cytoplasm. Taken together, this suggests a model by which cellular sialidase activity supports the events necessary for viral uncoating, the membrane remodeling necessary to support viral replication, and intracellular trafficking of virus particles within infected cells. Further studies are necessary to parse these or other potential mechanisms by which NEUs influence the DENV2 lifecycle.

In summary, we have demonstrated that sialidase activity is vital for several steps in the DENV2 lifecycle. Moreover, we provided the first known evidence of a transcriptional co-dependence between the human sialidase enzymes. Importantly, although previous studies established that the DENV NS1 protein modulated NEU1-3 activity, our present study highlights that manipulation of these enzymes, and thus cellular glycosylation, benefits DENVs. Future studies using NEU knockout cell lines, coupled with LC-MS/MS analysis of cellular glycoconjugates may help delineate which glycoconjugates are desialylated during DENV2 infection shedding light on the mechanism by which desialyation benefits DENV2 replication.

3.4: Materials and Methods

3.4.1 Cell lines

The cell lines used were the following: Clone 15(ATCC CCL-10) of the Baby Hamster Kidney Clone 21 cells (BHK-21), human hepatoma cells (Huh7) (unknown sex, From Dr. Charles Rice) [261], African Green Monkey kidney epithelial (Vero) cells (ATCC CRL-1586), and C6/36 cells (ATCC CRL-1660, larva, unknown sex). Huh7 and Vero cells were maintained in Dulbecco's Modified Eagle Medium (DMEM) (Gibco, LifeTech), while BHK-21 and C6/36 cells were maintained in Minimum Essential Media (MEM) (Gibco, LifeTech). All media was supplemented with 10% heat-inactivated fetal bovine serum (FBS) (Atlas Biologicals), 2 mM nonessential amino

acids (HyClone), 2 mM L-glutamine (Hyclone), and C6/36 media was also supplemented with 25 mM HEPES buffer. Huh7, BHK-21, and Vero cells were maintained at 37°C with 5% CO_2, and C6/36 cells were maintained at 28°C with 5% CO_2.

3.4.2 Viruses

The virus strain used was: DENV2 (16681) [256]. DENV2 was passaged in C6/36 cells. Viral titers were obtained via plaque assay on BHK-21 cells [263]. Viral infections were performed at room temperature for 1 hr to allow for viral adherence. Afterwards, virus was removed, cells were washed with 1X PBS, and cell were overlaid with MEM or DMEM supplemented with 2% FBS, 2mM non-essential amino acids, and 2 mM L-glutamine. Cells were incubated at 37°C with 5% CO_2 for indicated time periods.

3.4.3 RNA extraction and qRT-PCR

Standard TRIzol extraction methods using either TRIzol or TRIzol LS (ThermoFisher) were used to extract RNA from cells and from viral supernatant. The Brilliant III Ultra-Fast SYBR® Green one-step qRT-PCR kit (Agilent) was used for all qRT-PCR reactions. The cycling parameters used were as follows: 20 mins at 50°C for reverse transcription, followed by 5 minutes at 95°C, and then 45 two-step cycles of 95°C for 5 secs and 60°C for 60 secs. A melt curve followed each cycle starting at 65°C and ending at 97°C. (Primer sequences are reported in Supplemental Table 1) To quantify DENV2 genome copies, *in vitro* transcribed viral RNA from a DENV2 cDNA subclone was used to generate a standard curve. All cellular RNA was normalized to Ribosomal Protein Lateral Stalk Subunit P0 (RPLP0) using the delta delta ct method as described in [119,264].

3.4.4 siRNA transfection and confirmation of loss of function

Loss of function of NEU1-4 was conducted by transfecting cells with pooled siRNAs (Supplemental Table 1) (Dharmacon) or single siRNAs (Supplemental Table 1) (ThermoFisher) using RNAiMAX (Invitrogen) as described in [110]. Subsequently, cells were either infected with indicated viruses (described above), assessed for cytotoxicity of siRNA treatment (described below), or collected for confirmation of gene knockdown. Following indicated timeframes, viral supernatant and cells were collected. Viral supernatant was titrated via plaque assay. RNA from cells was analyzed via qRT-PCR to confirm knockdown of mRNA transcripts as described above. All siRNA treated samples were also compared to an irrelevant (IRR) siRNA control. Cytotoxicity of siRNA treatment was determined by replacing cell media with a 1:10 dilution of alamarBlue (ThermoFisher) in appropriate cell culture media and incubating for 1-2 hrs. A Victor 1420 Multilabel plate reader (Perkin Elmer) was used to measure fluorescence output with excitation at 560 nM and emission at 590 nM.

3.4.5 Western Blot Analysis

Huh7 cells from IRR control and NEU1-4 KD samples were lysed in RIPA Buffer. Total protein in each sample was measured using the Pierce™ BCA Protein Assay Kit (ThermoFisher) according to manufacturer's instructions. Equal total protein was loaded onto on a Criterion™ XT 4-12% Bis-Tris protein gel (Bio-Rad) and the was run for 2 hours at 100V. Protein was transferred at 4°C to nitrocellulose membrane for 2 hours at 50V. Following transfer, blots were blocked overnight at 4°C in a 5% milk solution in 1x PBS supplemented with 0.1% Tween 20. The primary antibodies used were a 1:500 dilution of the flavivirus group antigen antibody (D1-4G2-4-15, or 4G2) which binds domain II of the DENV E protein (mouse monoclonal antibody, BioVision) and

1:100 dilution of β-actin (rabbit polyclonal antibody, Invitrogen). A 1:3000 dilution of goat-anti-mouse IRDye 800CW, and goat-anti-rabbit IRDye 680RD (Li-Cor Biosciences) were used as secondary antibodies. Blots were imaged on a ChemiDoc MP Imaging System (Bio-Rad), and quantified in ImageJ utilizing area under the curve analysis.

3.4.6 Immunofluorescence Assays

Huh7 cells were seeded in 12 well plates containing sterilized glass cover slips, and subjected to siRNA transfection and viral infection as described above. At 24 hpi, viral supernatants were collected and used to confirm reduction in viral release via plaque assay on BHK-21. Cells were then washed twice in 1x PBS, and fixed with a 4% paraformaldehyde solution for 20 minutes at room temperature, and then quenched with a 30 mM glycine/PBS (1x, pH 7.5) solution for 5 minutes. Following fixation, indicated samples were permeabilized in a 0.1% Triton X-100 (Sigma Aldrich), 1% Bovine Serum Albumin (BSA, Gold Biotechnology) in 1x PBS solution at room temperature, and then blocked with a 0.01% Triton X-100, 1% BSA in 1x PBS solution overnight at 4°C. Non-permeabilized samples were blocked with a 1% BSA in 1x PBS solution overnight at 4°C. The primary antibodies used were a 1:1000 dilution of 4G2 (mouse monoclonal antibody, described above), a 1:500 dilution of anti-Glut1 (rabbit monoclonal antibody, ThermoFisher) or a 1:500 dilution anti-Calnexin (rabbit polyclonal antibody, ThermoFisher). Glut1 and Calnexin were used as cellular markers for the plasma membrane and endoplasmic reticulum, respectively. The secondary antibodies were a 1:500 dilution of goat anti-mouse Alexa Fluor 647 (ThermoFisher), 1:500 dilution of goat anti-rabbit Alexa Fluor 488 (ThermoFisher). Coverslips were counterstained with a 1:1000 dilution of the DAPI nuclear stain, and then fixed to slides with FluoroSave Reagent (Calbiochem). Slides were imaged using an Olympus inverted IX81 FV1000 laser scanning confocal microscope under the 100x oil objective using Fluoview

FV10-AS2 4.2 software (Olympus). Images were processed with Volocity software version 6.3 (PerkinElmer). A total of 20 representative images from each slide/condition were taken.

3.4.7 Quantification and statistical analysis

Statistical details are noted in each figure and corresponding figure legend. Results are expressed as mean values with standard deviation from three biological replicates (unless stated otherwise). Statistical significance was determined using either a one-way Analysis of Variance (ANOVA) with Tukey's or Dunnett's multiple comparisons test using Prism software version 9.0 (GraphPad Software, La Jolla, California, USA).

Chapter 4: Subcellular location of glucosylceramide hydrolysis drives different outcomes for DENV2 infection.

4.1: Introduction

Sphingolipids (SLs) are a class of potent, bioactive signaling molecules which play critical roles in nearly all biological responses [120,reviewed in 204]. As such, perturbations of SL metabolism are now linked to several chronic human diseases, such as Alzheimer's disease, amyotrophic lateral sclerosis, diabetes, atherosclerosis, and metabolic disorders such as Gaucher disease [214,reviewed in 289,290]. Recent studies have also emerged linking dysregulation of SL metabolism with the pathology of viral infections, including infection with DENVs [122,124,reviewed in 217,218,222,291]. In our previous work, we have established that DENVs are reliant upon and cause significant dysregulation of host lipid metabolism, including significant changes to SLs [99,110,111,119]. However, despite our increased understanding of how SLs may contribute to viral pathology, the role of SL metabolism in the DENV lifecycle remains poorly understood.

In this study, we sought to begin characterizing the interaction with and dependency of DENV2 on SL metabolism. We completed a preliminary siRNA-mediated loss of function study to analyze the effect of 46 of the enzymes involved in SL metabolism. This preliminary study identified that DENV2 relies upon enzymes found in the salvage and sphingomyelinase pathways of ceramide synthesis as opposed to *de novo* ceramide (CER) synthesis. We uncovered that glycosphingolipids (GSLs) such as galactosylceramide (GalCer) and glucosylceramide (GluCer) and their derivatives are vital for the DENV2 lifecycle. Moreover, we observed opposing effects between the lysosomal (GBA1) and non-lysosomal (GBA2) β-glucocerebrosidase enzymes on DENV2 release implicating the latter enzyme as vital for the DENV2 lifecycle. Further analysis

allowed us to characterize a yet undefined role for the enzyme in glycosphingolipid remodeling, and identify the antiviral potential of Ambroxol hydrochloride, a modulator of glucocerebrosidases.

4.2: Results

4.2.1 - The salvage and sphingomyelinase pathways of sphingolipid biosynthesis are vital for DENV2 release

Due the dynamic roles of sphingolipids as bioactive signaling molecules, we hypothesized that perturbations of sphingolipid homeostasis during DENV2 infection were both viral- and host-mediated. Specifically, we hypothesized that certain components of the sphingolipid pathway were altered by DENV2 to both meet its replicative needs and to subvert the host immune response, while other components were altered as part of the host anti-viral response to infection. To determine which arms of the sphingolipid metabolic pathway might be pro-viral or anti-viral, we used a library of pooled siRNAs (Dharmacon, Supplemental Table 4.1) targeting the main enzymes in the pathway (based on KEGG pathway database) in human hepatoma (Huh7) cells. A non-targeting, irrelevant siRNA (IRR) was used as a negative control, and an siRNA targeting the DENV2 genome was used as a positive control for viral inhibition. Following transfection of siRNAs, Huh7 cells were either mock-infected or DENV2-infected for 24 hr, and then viral supernatants were analyzed via plaque assay (Figure 4.1A). Cytotoxic effects of siRNA treatment on mock-infected cells were not observed (Supplemental Figure 4.1). We validated select hits in this initial screen in human adenocarcinoma cells (A549s) using fluorescence cytometry to quantify the relative expression of DENV2 E protein in infected cells (Supplemental Figure 4.2). We found similar effects in both cell lines.

The results of this initial screen of the SL metabolic pathway allowed for 3 critical observations. First, we identified that loss of function of many of the enzymes in the sphingomyelinase and salvage pathways of CER biosynthesis as opposed to *de novo* CER synthesis resulted in a significant reduction in infectious DENV2 release (Figure 4.1A and Supplemental Figure 4.3). Second, we determined that loss of function of the enzymes involved in the formation and degradation of the glycosphingolipid (GSL) precursors, galactosylceramide (GalCer) and glucosylceramide (GluCer) (Figure 4.1A – enzyme names in blue), were vital for DENV2 release, implicating GSLs as important metabolites for the DENV2 lifecycle. Finally, we observed that loss of function of glucocerebrosidases (the lysosomal GBA1, and non-lysosomal GBA2 enzymes) had opposite effects on DENV2 release (Figure 4.1A). In follow-up analysis of the latter observation, we also determined that inhibition of GBA1 and GBA2 had opposite effects on DENV2 genome replication (Figure 4.1B). Importantly, the observed effect on DENV2 genome replication were of less magnitude than DENV2 release indicating that GBA1/GBA2 and GSLs may play significant roles during post-replication stages of the viral lifecycle (assembly, maturation, or egress). As these results were intriguing, we decided to focus our efforts on characterizing the role of glucocerebrosidases (GCases) in the DENV2 lifecycle.

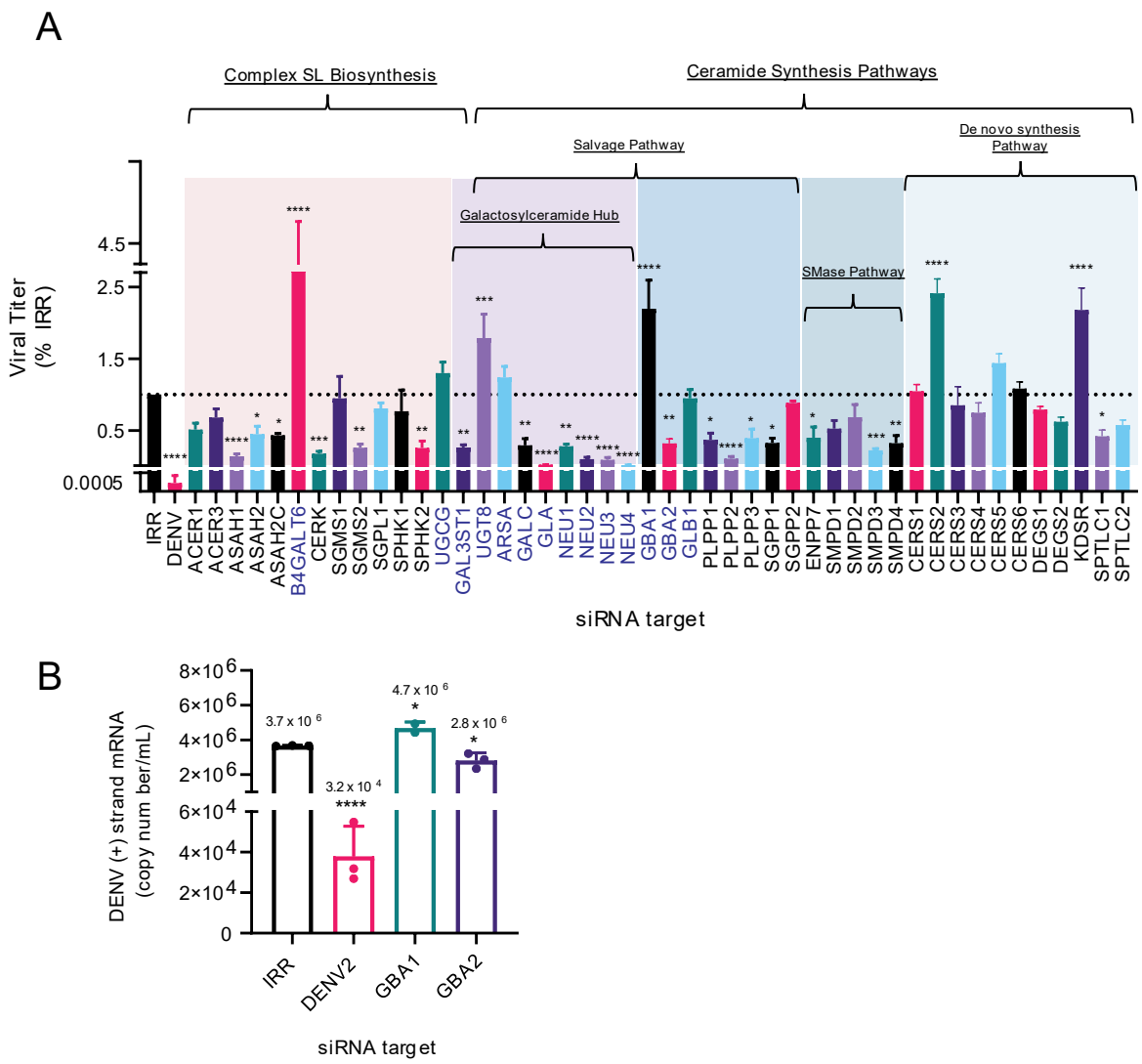

Figure 4.1 – Effect of loss of function of sphingolipid pathway enzymes on DENV2 release. Huh7 cells were transfected with siRNAs targeting enzymes within the SL metabolic pathway (as identified via KEGG pathway database), a non-targeting irrelevant (IRR) negative control, and a DENV2-specific positive control siRNA. Following transfection, cells were infected DENV2 (MOI = 0.1) for 24 hr. (A) At 24 hpi, viral supernatants were collected and analyzed via plaque assays. Results are represented as fold change compared to the IRR control, and are organized according to which parts of the SL pathway they belong. Enzyme names colored in blue are involved in GluCer and GalCer synthesis and degradation. (B) In a follow-up study on GBA1 and GBA2 cells were collected and analyzed via qRT-PCR for total copy number of DENV2 genome. Results were normalized to the RPLP0 housekeeping gene. Numbers above bars represent the mean copy number/µL of each treatment group. (A-B one-way ANOVA with Dunnett's multiple comparison's test: * = p≤0.05, ** = p≤0.01, ***= p≤0.001, **** = p≤0.0001.) [Abbreviations: IRR, irrelevant, non-targeting siRNA; DENV, DENV2-specific siRNA; ACER1, alkaline ceramidase 1; ACER3, alkaline ceramidase 3; ASAH1, acid ceramidase; ASAH2, neutral ceramidase 2; ASAH2C, neutral ceramidase 2C; B4GALT6, β-1, 4-galactosyltransferase 6; CERK, ceramide kinase; SGMS1-2, sphingomyelin synthase 1-2; SGPL1, sphingosine-1-phosphate lyase 1; SPHK1-2, sphingosine kinase 1-2; UGCG, glucosylceramide synthase; GAL3ST1, galatosylceramide sulfotransferase; UGT8, galactosylceramide synthase; ARSA, arylsulfatase A; GALC, galactocerebrosidase; GLA, α-galatosidase A; NEU1-4, neuraminidase 1-4; GBA1, β-glucocerebrosidase 1; GBA2, β-glucocerebrosidase 2; GLB1, β-galactosidase; PLPP1-3, phospholipid phosphatase 1-3; SGPP1, sphingosine-1-phosphate phosphatase 1; ENPP7, ectonucleotide pyrophosphatase/phosphodiesterase family member 7; SMPD1-4; sphingomyelin phosphodiesterase 1-4; CERS1-6, ceramide synthase 1-6; DEGS1, sphingolipid delta(4) desaturase 1; DEGS2, sphingolipid delta(4)-desaturase/C4-monooxygenase 2; KDSR, 3-ketodihydrosphingosine reductase; SPTLC1-2, serine palmitoyltransferase 1-2.]

4.2.2 – Pharmacological inhibition of enzymes involved in GluCer/GalCer synthesis and degradation validates select siRNA screen results

We next sought to both validate the results of our siRNA screen and identify candidate pharmacological agents to use in the remainder of our investigations. We investigated the effect of several well-characterized pharmacological agents that are known to inhibit the activity of GBA1, GBA2, glucosylceramide synthase (UGCG), and galactosylceramide synthase (UGT8). Conduritol B epoxide (CBE) and n-butyldeoxynojirimycin (NB-DNJ or miglustat) have been used widely to investigate Gaucher disease, which is a lysosomal storage disorder characterized by defects in GBA1 [214,292]. At the concentrations tested, we found that CBE had differential effects on DENV2 release from Huh7 cells (Figure 4.2A), while miglustat significantly reduced viral release at all concentrations tested (Figure 4.2B). Importantly, CBE and miglustat are known to have inhibitory effects on several enzymes depending on their concentrations. CBE is known to inhibit α-glucosidase as well as GBA1, with higher concentrations typically used to inhibit GBA1 [293]. This may explain why treatment with CBE at concentrations between 6.25-25 μM resulted in a decrease in DENV2 release, but higher concentrations resulted increased viral release. Previously, it was established that α-glucosidase activity is indispensable for virion formation in DENV2 infection [75]. Thus, our results supported these earlier studies as well as support our siRNA results indicating that GBA1 inhibition results in increased viral production. Miglustat is a glucose analog that has been shown to have activity against UGCG, GBA1, and GBA2 in a concentration-dependent manner due to its different binding affinities with each enzyme [reviewed in 292]. At concentrations below 20 μM, miglustat has been shown to inhibit GBA2 only, while at concentrations between 20 μM-400 μM it inhibits GBA2 and UGCG, and inhibits GBA1 at concentrations above 400 μM [reviewed in 292]. In our studies, concentrations above 100 μM resulted in complete cell death, so were not tested for efficacy against DENV2. However, our results did confirm the loss of function of UGCG and GBA2 activity resulted in decreased

infectious virus release from DENV2 infected cells. We next evaluated pharmacological agents with specific activities towards GBA2 and UGCG. OM-2 (a gift from Michael Spedding and The Pasteur Institute) is a specific inhibitor of GBA2, and was shown to reduce DENV2 release at high concentrations (Figure 4.2C). PDMP hydrochloride and GENZ-123346 are both potent CER analogs and known inhibitors of UGCG [294–297]. We found that both drugs significantly reduced DENV2 release from cells (Figure 4.2D-E), although GENZ-123346 had a lower IC_{50} than PDMP. Finally, we evaluated the GalCer synthase (UGT8) inhibitor, UGT8 inhibitor 19, and found a dramatic decrease in DENV2 release from cells (Figure 4.2F). These results were opposite of our siRNA screen which indicated that loss of function of UGT8 resulted in an increase in DENV2 release from cells. One possibility is that the drug also has activity against other UDP-glucuronosyltransferase enzymes (UGTs) [298], thus these results may be due to off-target effects of the drug and warrant additional scrutiny. Taken together, our evaluation of these pharmacological inhibitors provided additional insights into the importance of GluCer synthesis as well as GluCer hydrolysis via GBA2 on DENV2 viral production. Moreover, as our siRNA treatments showed only 50-60% knockdown of GBA1 and GBA2 (Supplemental Figure 4.4) and siRNA treatment has reduced scalability, these results identified candidate drug targets to use in further analyses.

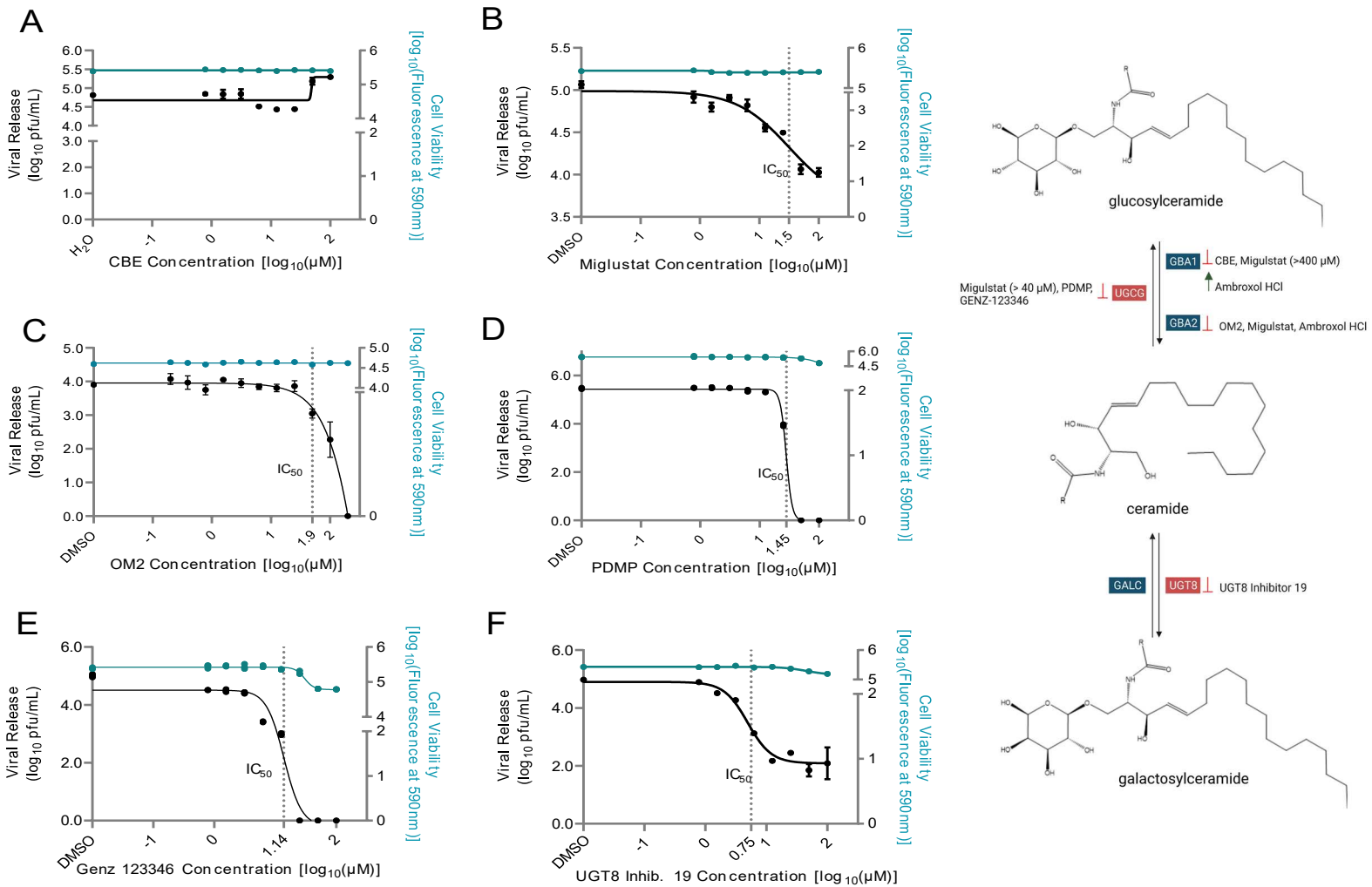

Figure 4.2 – Evaluation of pharmacological inhibitors of GluCer and GalCer synthesis and degradation. Huh7 cells were either mock-infected or DENV2-infected (MOI = 0.1), followed by overlay with media containing either CBE (A), Miglustat (B), OM2 (C), PDMP (D), Genz-123346 (E), or UGT8 Inhibitor 19 (F) at concentrations ranging from 391 nm-100 μM. At 24 hpi, an AlamarBlue cytotoxicity assay was performed on mock cells (right y axis in blue), and viral supernatants from DENV2-infected were evaluated via plaque assay. As the inhibitors in B-F reduced DENV2 release, IC_{50} values were calculated and are displayed on each graph. A schematic depicting which enzymes are inhibited by each compound is provided on the right. Enzymes involves in GSL synthesis are colored in red, while enzymes involved in GSL degradation are colored in blue. (A-F: one-way ANOVA with Dunnett's multiple comparison's test was used to determine significance of each inhibitor on viral release and cytotoxicity, while non-linear regression was used to calculate the IC_{50} of each drug. Inset figure was generated using Biorender.com)

4.2.3 – Ambroxol hydrochloride emerges as a pharmacological inhibitor of interest

Ambroxol hydrochloride is a well-characterized, over-the-counter mucolytic agent [299]. Recently, it has emerged as a potential therapeutic agent for the treatment of neurodegenerative disorders such as Gaucher disease, Parkinson's disease and amyotrophic lateral sclerosis due to its activity as a molecular chaperone of GBA1 and inhibitor of GBA2 [300–304]. As our data thus far indicated that GBA1 activity seemed to have an antiviral effect on the DENV2 lifecycle (as downregulation of GBA1 enhanced viral production) and GBA2 activity was vital for viral genome replication and release, we next sought to evaluate the antiviral potential of Ambroxol HCl against DENV2. We determined that Ambroxol significantly reduced DENV2 release at concentrations of 6.25 μM and above when Huh7 cells were infected at a low multiplicity of infection (MOI = 0.1, Figure 4.3A). Surprisingly, we also found that Ambroxol concentrations of 12.5 μM and above also significantly reduced DENV2 release when cells were infected at a high MOI (MOI = 5, Figure 4.3B). These results combined with our previous analyses suggested that the subcellular location of GluCer hydrolysis was a critical factor in the DENV2 lifecycle.

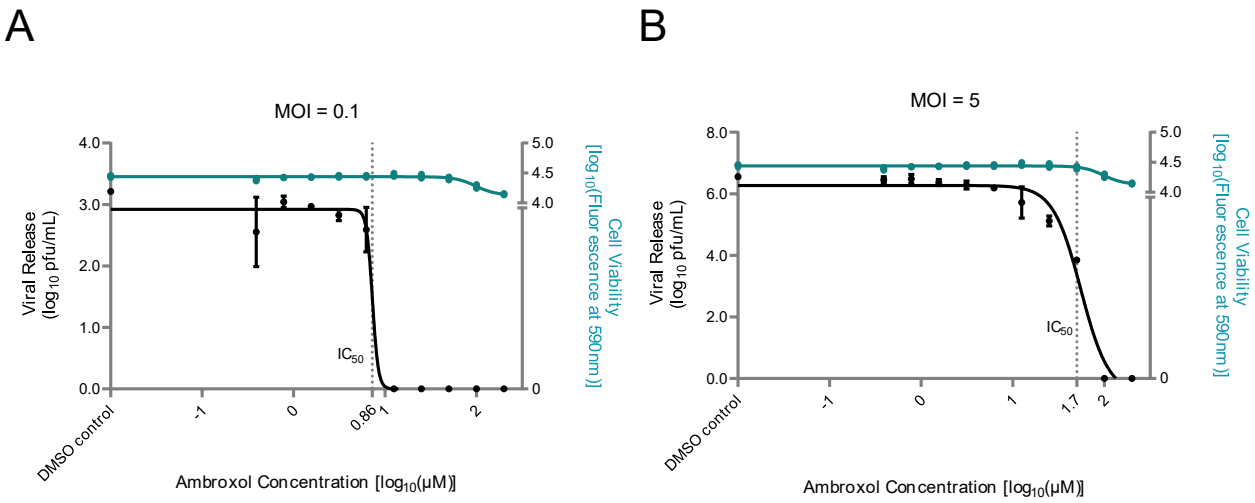

Figure 4.3 – Ambroxol is a potent inhibitor of DENV2 release. Huh7 cells were either mock-infected or DENV2-infected with MOI = 0.1 (A) or MOI = 5 (B) followed by overlay with media containing Ambroxol HCl at the indicated concentrations. At 24 hpi, an AlamarBlue cytotoxicity assay was performed on mock cells (right y axis in blue), and viral supernatants from DENV2-infected were evaluated via plaque assay. IC_{50} values were calculated for Ambroxol for each MOI and are displayed on each graph. (A-B: one-way ANOVA with Dunnett's multiple comparison's test was used to determine significance of Ambroxol treatment on viral release and cytotoxicity, while non-linear regression was used to calculate the IC_{50} of each drug.)

4.2.4 – DENV2 infection results in upregulation of glycosphingolipids

Our results thus far were seemingly contradictory as we found that loss of function of both UGCG and GBA2 both had an inhibitory effect on DENV2 release. This suggested that both GluCer synthesis and location-specific hydrolysis were vital for the viral lifecycle. Thus, we next sought to evaluate the effect of DENV2 infection on glycosphingolipid (GSL) levels in Huh7 cells. Huh7 cells were either mock infected or DENV2 infected, and collected at 0, 36, and 72 hours post infection. GSLs were extracted from the sample and analyzed via normal-phase high-performance liquid chromatography (NP-HPLC) [described in 305,306]. As expected, we observed no significant changes in the GSL profiles of mock and DENV2-infected cells collected at 0 hpi (Figure 4.4A, D). At 36 hpi (representing peak viral replication), we observed significant upregulation in the relative abundance of several GSL species in the DENV2-infected cells compared to mock-infected cells (Figure 4.4B,D). At 72 hpi, the level of most GSL species returned basal levels (Figure 4.4C,D). While all the results represented in Figures 4.4A-D represent various GSL species, we have thus far only identified the molecular structures of 7 specific GSL species (Figures 4.4E-H). Importantly, these results suggested that DENV2 requires specific GSL species during peak viral replication, but not during late-stage infection.

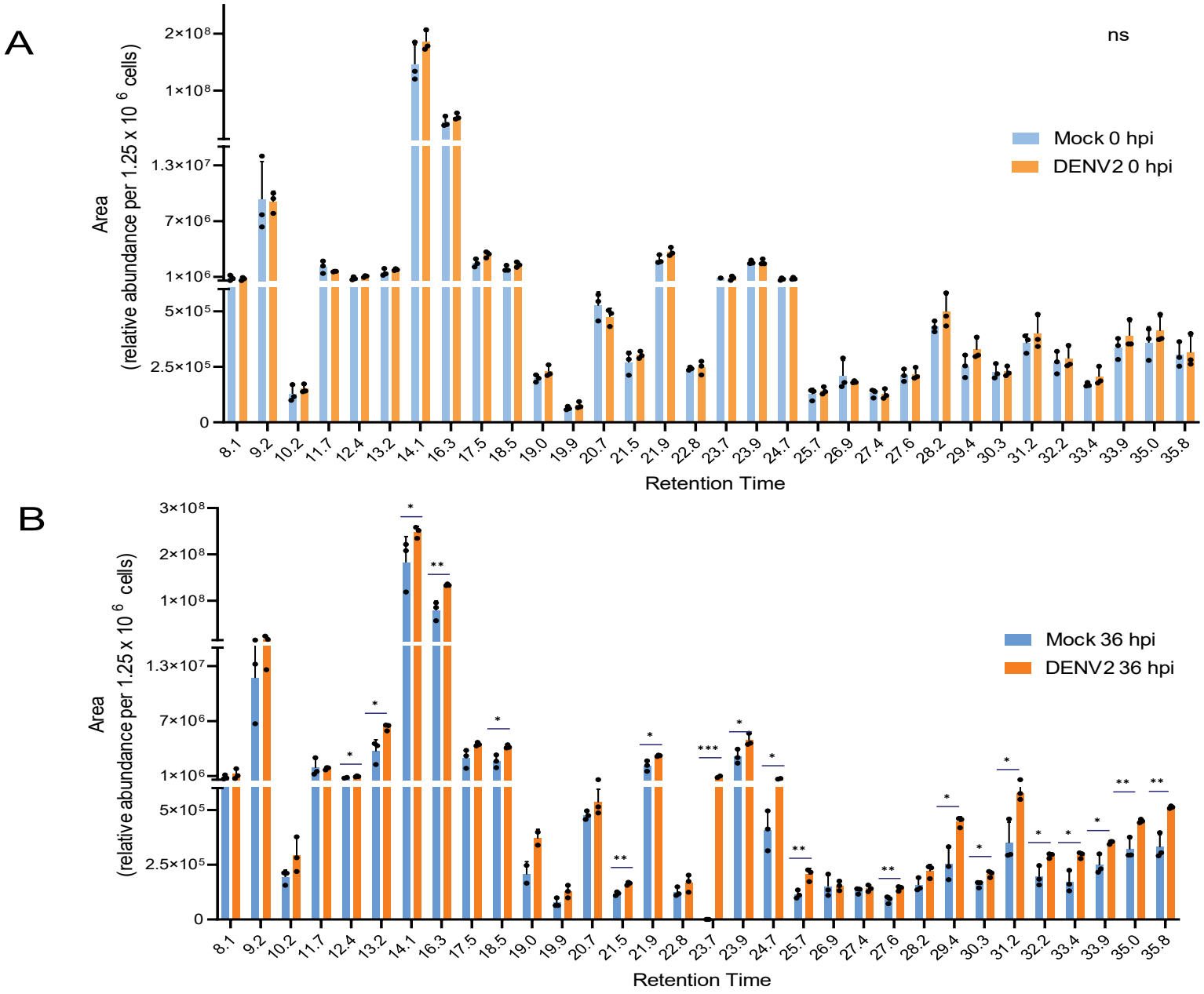
A
ns
Mock 0 hpi
DENV2 0 hpi
Area
(relative abundance per 1.25 x 10 6 cells)
2×10⁸
1×10⁸
1.3×10⁷
7×10⁶
1×10⁶
5×10⁵
2.5×10⁵
0
8.1 9.2 10.2 11.7 12.4 13.2 14.1 16.3 17.5 18.5 19.0 19.9 20.7 21.5 21.9 22.8 23.7 23.9 24.7 25.7 26.9 27.4 27.6 28.2 29.4 30.3 31.2 32.2 33.4 33.9 35.0 35.8
Retention Time
B
Mock 36 hpi
DENV2 36 hpi
Area
(relative abundance per 1.25 x 10 6 cells)
3×10⁸
2×10⁸
1×10⁸
1.3×10⁷
7×10⁶
1×10⁶
5×10⁵
2.5×10⁵
0
8.1 9.2 10.2 11.7 12.4 13.2 14.1 16.3 17.5 18.5 19.0 19.9 20.7 21.5 21.9 22.8 23.7 23.9 24.7 25.7 26.9 27.4 27.6 28.2 29.4 30.3 31.2 32.2 33.4 33.9 35.0 35.8
Retention Time

C

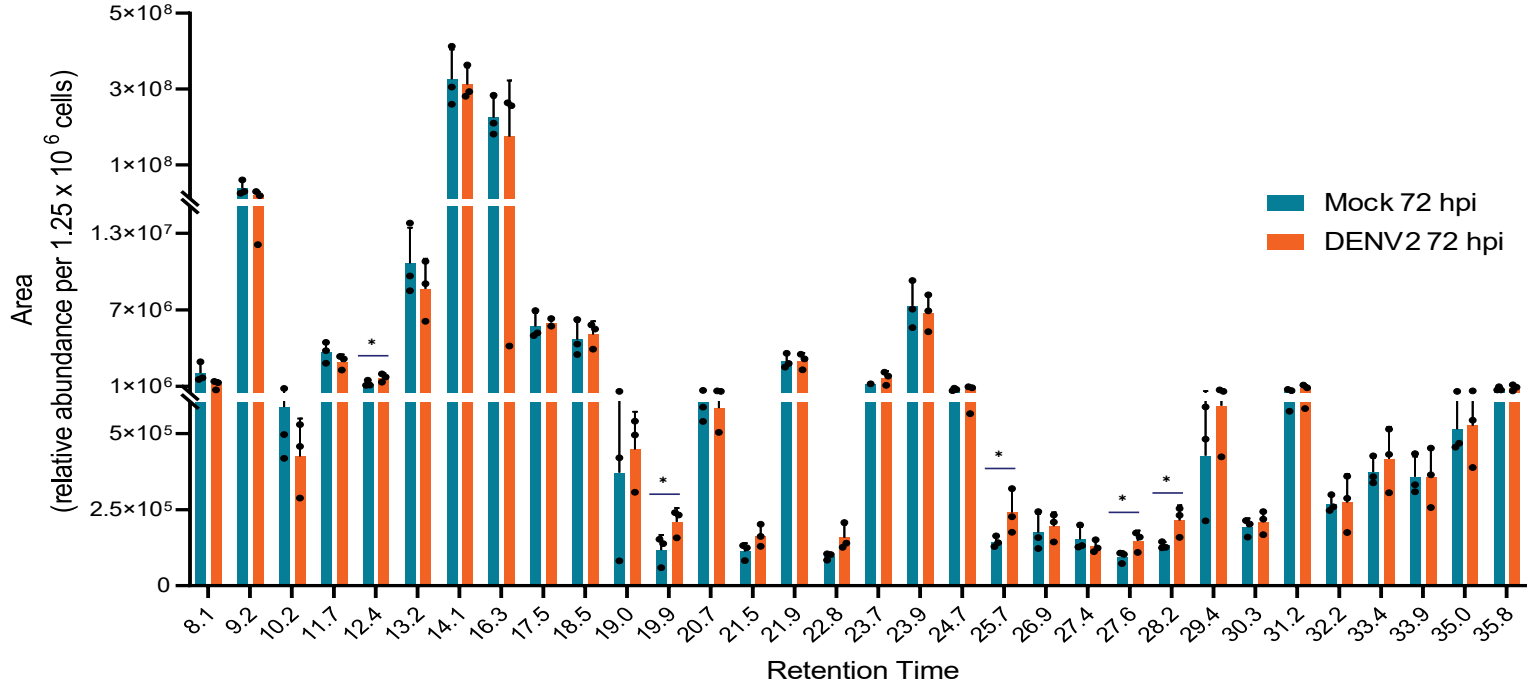
Area
(relative abundance per 1.25 x 10 6 cells)
5×10⁸
3×10⁸
1×10⁸
1.3×10⁷
7×10⁶
1×10⁶
5×10⁵
2.5×10⁵
0
Mock 72 hpi
DENV2 72 hpi
8.1
9.2
10.2
11.7
12.4
13.2
14.1
16.3
17.5
18.5
19.0
19.9
20.7
21.5
21.9
22.8
23.7
23.9
24.7
25.7
26.9
27.4
27.6
28.2
29.4
30.3
31.2
32.2
33.4
33.9
35.0
35.8
Retention Time

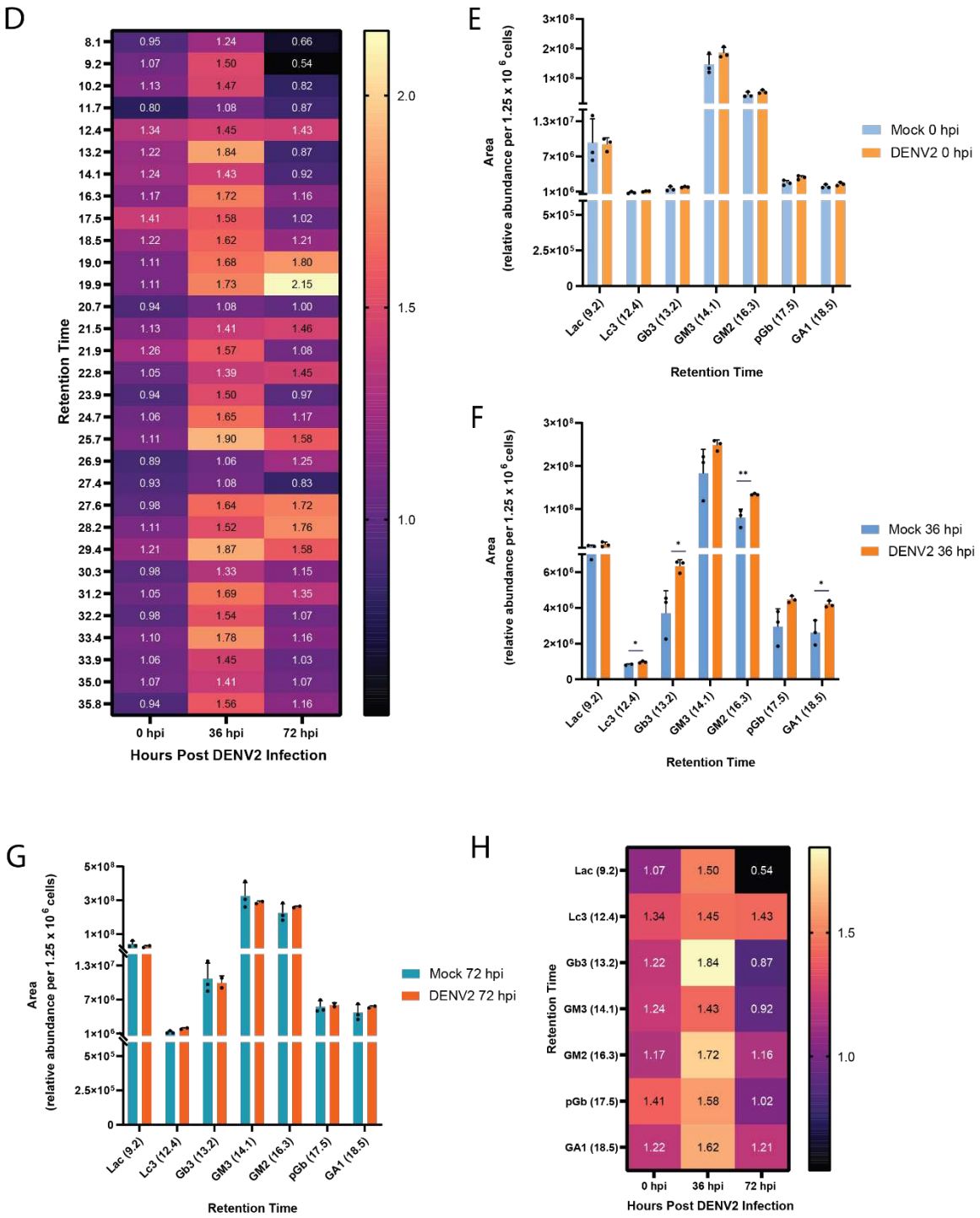

Figure 4.4 – Glycosphingolipids are elevated during peak viral replication. Huh7 cells were either mock-infected or DENV2-infected (MOI = 0.1) and collected at indicated timepoints. Glycosphingolipids were then extracted and analyzed via NP-HPLC using a fluorescence detection method. (A-C) The relative abundance (area under the curve) and retention times of GSLs species detected at 0 (A), 36 (B), and 72 hpi (C) are depicted. (D) A heatmap of fold change of each GSL species (identified by retention time) in DENV2-infected cells compared matched mock samples. Values in each box represents the mean fold change. Graphs E-H highlight the data from graphs A-D of GSLs that were positively identified using GSL standards. (E-F) Depicts the relative abundance of each identified species at 0, 36, and 72 hpi, respectively. (H) Fold change of identified GSL species in DENV2-infected samples compared to matched mock samples are depicted. (A-H: multiple unpaired t tests with Holm-Šídák multiple comparisons test: : * = p≤0.05, ** = p≤0.01, ***= p≤0.001)

4.2.5 – Ambroxol abolishes DENV2-induced elevation of glycosphingolipids

We next sought to evaluate the impact of Ambroxol treatment on GSLs during DENV2 infection. Similar to the above analysis, Huh7 cells were treated with either DMSO (vehicle control) or 50 μM of Ambroxol for 24 hours prior to infection, and then either mock-infected or DENV2-infected. GSLs were extracted and analyzed via NP-HPLC. In our preliminary analyses (n = 2), we found that treatment with Ambroxol results in a ~50% reduction in total GSL abundance (Figure 4.5A) in both mock and DENV2-infected cells. Moreover, we saw a reduction in the abundance (40-60%) of the GSLs we were able to positively identify in Figures 4.4E-I (Figure 4.5B). Taken together with our previous results, these results suggested that while GBA2 is involved in GluCer hydrolysis, it may play critical roles in GSL remodeling since its inhibition with Ambroxol resulted in a significant reduction in total GSL abundance.

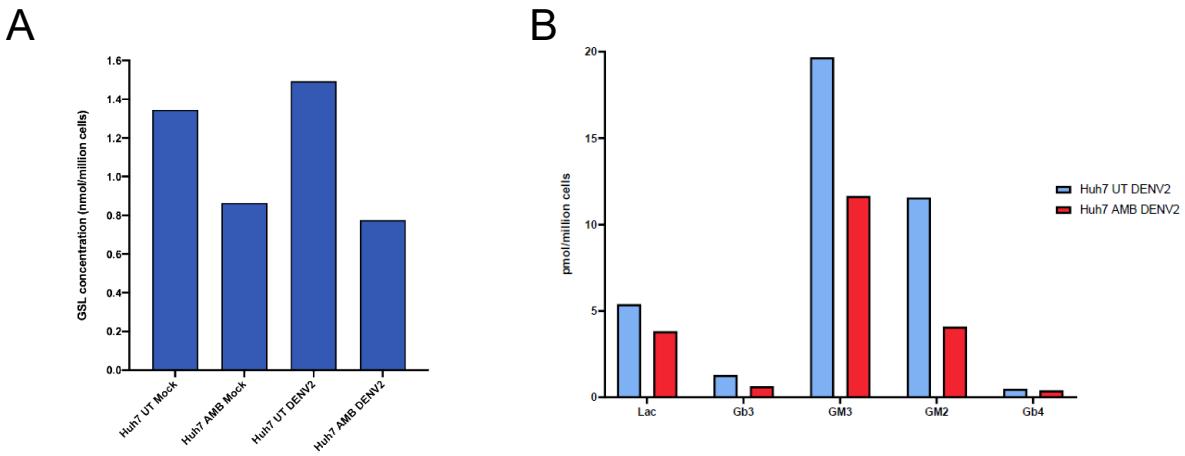

Figure 4.5 – Ambroxol HCl reduces glycosphingolipid abundance in mock and infected cells. Huh7 cells were treated with Ambroxol or 0.1% DMSO for 24 hours prior to infection, and then mock infected or infected with DENV2 (MOI = 0.1). At 24 hours post infection, cells were collected, counted, and GSLs were extracted from a equal number of cells per sample. Total (A) and specific (B) GSL abundances were measured using NP-HPLC with fluorescence detection. A significant reduction in total GSL concentration (A) as well as lowered abundance of specific GSL species identified with standards (B) was observed in each sample. (Representative preliminary data, n=2)

4.3: Discussion

Previously, we have established that DENV2 infection resulted in significant alterations of host lipid metabolism, including SL metabolism [99,110,111,119]. SLs are potent bioactive signaling molecules, and disruption of SL homeostasis has been linked with the pathology of several chronic and infectious diseases [120,122,124,204,217,218,222,289,291]. Here we investigated the importance of SLs in the DENV2 lifecycle through loss of function studies. To our knowledge, this study provides the first profiling of enzymes in the entire SL metabolic pathway during DENV2 infection and has allowed for several critical observations.

First, in previous studies, CERs have been shown to be elevated in DENV2-infected mosquitoes and mosquito cells, as well as in patient sera [110,111,117]. Here we show that enzymes involved in the salvage and sphingomyelinase pathways of CER biosynthesis as opposed to *de novo* CER synthesis were critical to DENV2 release from human cells. Importantly, the enzymes involved in SL biosynthesis and degradation are housed in discrete subcellular compartments and membranes [reviewed in 113]. Interestingly, the DENV2 lifecycle is also dependent upon host cellular membranes with each stage occurring in specific subcellular compartments connected through membrane contact sites [reviewed in 14]. Thus, these observations together are not coincidental but provide insight as to which parts of the viral lifecycle are impacted by the functionality of specific SL metabolic enzymes based on their subcellular location.

Second, we observed that enzymes involved in both biosynthesis and degradation of GluCer and GalCer were critical to DENV2 release. While these results are seemingly contradictory, they provided initial clues that GSLs may be involved in DENV2 replication. This prompted us to investigate whether GSLs are altered during infection. Here, we found several GSL species were upregulated at 36 hpi, representing peak viral replication, but not at later timepoints (72 hpi). This finding coupled with our earlier results showing that loss of function of

GBA1 and GBA2 has a greater effect on infectious virus release versus genome replication suggests that GSLs may play important roles in viral assembly, maturation or egress.

Of the GSLs we were able to chemically identify using standards, we saw increases in LacCer, Lc3, Gb3, GM2 and GA1 GSLs. LacCer is a precursor molecule for globo-, ganglio-, and lacto/neolacto-series GSLs, and is therefore required for complex GSL biosynthesis. However, LacCer itself also serves important physiological functions, including organization of plasma membrane microdomains, regulation of autophagy, induction of pro-inflammatory signaling, and activation of the cytosolic phospholipase A2 enzyme ($cPLA_2$) [307,308]. Importantly, each of these processes has been shown to be either vital to or a consequence of DENV2 replication [2,reviewed in 14,309 and Lian E, et al., unpublished]. Interestingly, we have shown DENV2 infection results in increased levels of arachidonic acid (AA) in Huh7 cells [Lian E, et al., unpublished]. PLA_2 enzymes are key mediators of AA in cells, as they are responsible for cleaving AA from membrane lipids [171]. Upon further investigation, we have shown that PLA_2 activity (cytosolic and secreted) was vital for DENV2 replication and viral genome replication through a yet unresolved mechanism [Lian E, et al., unpublished]. Thus, our observations here may provide additional insight into the regulation of AA in DENV2 infected cells. The functionality of Lc3 and Gb3, precursor molecules of lacto/neolacto- and globo-series glycosphingolipids, respectively, is less understood, although the latter has been linked to Fas/FasL induction of apoptosis and interferon signaling so may be upregulated as part of the host antiviral response [310,311]. GM2 and GA1 are gangliosides which are major constituents of cell membranes in nervous tissues where they are indispensable for signal transduction; however, very little is known about their functional roles in other tissues [312].

Finally, the results of this study revealed that the DENV2 lifecycle was differentially affected by the subcellular location of GluCer hydrolysis. Our analyses revealed that lysosomal degradation of GluCer by GBA1 was detrimental for virus production, whereas non-lysosomal degradation by GBA2 was required for virus production. The key difference between lysosomal

and non-lysosomal degradation of GluCer is the fate of CER. CER cannot freely exit the lysosome, so it must be further catabolized into free fatty acids and sphingosine by ceramidase [313]. In contrast, the CER that is released from GBA2 hydrolysis at the ER and Golgi has several possible fates. CERs formed in the ER/Golgi can either be converted to GalCer in the ER, or trafficked through specific Golgi compartments to be converted to ceramide-1-phosphate, sphingomyelin, or GluCer [reviewed in 113,206]. Interestingly, CER chain length determines to which Golgi compartment it is delivered. The CER transport protein, CERT, has been shown to only transport CER with acyl chains of C22 or shorter, and delivers them to the *cis*-Golgi where they are converted to sphingomyelin or ceramide-1-phosphate [314,reviewed in 113]. In contrast, CERs with larger acyl-chains are delivered via vesicular transport to the *trans*-Golgi where they are converted to GluCer and can then undergo additional modifications to form complex GSLs as they traffic through the Golgi [reviewed in 113,315]. Given that DENV2 infection results in increased GSL levels, we propose a novel function of GBA2 as a driver of GluCer/CER recycling during DENV2 infection. Ambroxol HCl abolishes this process by decreasing GBA2 activity, and increasing GBA1 activity resulting in complete degradation of GluCer/CER. While the concentrations of Ambroxol HCl used in this study were above the current approved dosing regimen of 30 mg (0.24 μM steady state plasma concentration) [299], our study revealed that higher concentrations of Ambroxol HCl were not cytotoxic and positioned Ambroxol HCl as a valuable tool for glycosphingolipid analysis. Moreover, studies demonstrating the safety and effectiveness of higher doses of Ambroxol HCl in mouse models of ALS and in clinical trials of Parkison's disease have prompted the re-evaluation of the approved recommended dosing by the European Medicines Agency and FDA [300-302, 316].

In summary, we have provided the first analysis of the role of SL metabolic enzymes in DENV2 infection and have demonstrated that enzymes involved in the sphingomyelinase and salvage pathways of ceramide synthesis were critical for DENV2 replication. Moreover, we determined that enzymes involved in glycosphingolipid synthesis and degradation were

necessary for DENV2 release, and have provided the first analysis of changes to glycosphingolipids levels during DENV2 infection. These analyses allowed us to propose a novel role for the non-lysosomal GBA2 enzyme as a driver of GluCer/CER recycling and identify Ambroxol HCl as a potential therapeutic agent against DENV2 infection. Future studies will be aimed at identifying the remainder of GSLs upregulated during DENV2 infection and determining how specific GSL populations contribute to viral replication. These studies will employ the use of UGCG/GBA1/GBA2 knockdown cell lines, exogenous addition of GSLs, and animal models of DENV2 infection. These studies will not only improve our understanding of DENV infection, but will also help to elucidate unknown biological functions of GSLs.

4.4: Materials and Methods

4.4.1 – Cell Lines

The following cell lines were used in this study: human alveolar adenocarcinoma cells (A549s, ATCC CCL-185), clone 15 (ATCC CCL-10) of the baby hamster kidney clone 21 cells (BHK-21), human hepatoma cells (Huh7s, unknown sex, a gift from Dr. Charles Rice) [261], and *Aedes albopictus* larval cells (C6/36, ATCC CRL-1660). A549s and Huh7s were maintained in Dulbecco's Modified Eagle Medium (DMEM) (Gibco, LifeTech), and BHK-21 and C6/36 cells were maintained in Minimum Essential Media (MEM) (Gibco, LifeTech). Media for A549s, Huh7s and C6/36 cells were supplemented with 10% heat inactivated fetal bovine serum (FBS, Atlas Biologicals), 2 mM nonessential amino acids (NEAA, HyClone), 2 mM L-glutamine (L-glut, HyClone), and 25 mM HEPES buffer (pH 7.0-7.4). Media for BHK-21 cells was supplemented with 10% heat-inactivated FBS, 2 mM NEAA, and 2 mM L-glut. A549s, Huh7s, and BHK-21 cells were maintained at 37°C with 5% CO_2, and C6/36 cells were maintained at 28°C with 5% CO_2.

4.4.2 – Viral infection

DENV2 (strain 16681) [256] was used throughout this study. The virus was passaged in C6/36 cells, and viral titers were obtained via plaque assay on BHK-21 cells as described in [263]. All viral infections were performed at room temperature for 1 hr to allow for viral adherence. Following infection, viral inoculums were removed, cells were washed with 1x PBS, and cells were overlaid with cell-appropriate media supplemented with 2% heat inactivated FBS. Cells were incubated at 37°C with 5% CO_2 for time periods indicated in each experiment.

4.4.3 – siRNA transfection

Initial loss of function experiments were conducted by transfecting Huh7 or A549 cells with a library of pooled siRNAs targeting enzymes in the sphingolipid metabolic pathway (Horizon Discovery, Supplemental Table 4.1) as described in [110] using the RNAiMAX lipofectamine reagent (ThermoFisher). Subsequently, cells were either infected with DENV2 (described in 4.4.2) or mock infected. Following completion of siRNA experiments, infected cells and corresponding supernatants were collected additional analysis; while mock-infected cells were either assessed for cytotoxicity of siRNA treatment (described in 4.4.6) or confirmation of gene knockdown. Viral supernatants were analyzed via plaque assay, while RNA from DENV2-infected and mock-infected cells were analyzed via qRT-PCR (described in 4.4.7). All siRNA experiments included a non-targeting siRNA (irrelevant or IRR) negative control and DENV2-specific positive control. All siRNA treated samples were compared to the IRR control sample.

4.4.5 – Pharmacological inhibition of select sphingolipid pathway enzymes

The inhibitors used in this study were conduritol B epoxide (CBE, Cayman Chemical), N-butyldeoxynojirimycin (Migulstat, Cayman Chemical), OM2 (a gift from The Pasteur Institute), N-[2-hydroxy-1-(4-morpholinylmethyl)-2-phenylethyl]-decanamide, monohydrochloride (PDMP, Cayman Chemical), GENZ-123346 (Cayman Chemical), UGT8 inhibitor 19 (Cayman Chemical) and Ambroxol hydrochloride (Millipore Sigma – European pharmacopoeia reference standard). All inhibitors except CBE were solubilized and diluted in DMSO before being mixed with 2% DMEM at indicated concentrations and added to cells. CBE was solubilized and diluted in RNase-free, sterile water. The final concentration of DMSO in drug treated and vehicle treated samples was kept at 0.1% to avoid cytotoxic effects of DMSO on cells. Drug treatments were either added to cells following virus attachment, or at 24 hours prior to infection. Viral supernatants and cells were collected at indicated timepoints. Viral supernatants were titrated via plaque assay, and collected cells were analyzed as indicated in each experiment.

4.4.6 – Analysis of cytotoxicity

Cytotoxicity was measured using a resazurin-based cell viability assay (Resazurin sodium salt, Millipore Sigma). All cytotoxicity/cell viability assays were performed in parallel to the experiments evaluating the effect of siRNA-mediated loss of function or pharmacological inhibition of all enzymes on viral infection in this study. A 10x stock solution of resazurin was diluted 1:10 in in 2% DMEM. Media was removed from cells, and replaced with the 1x resazurin/2% DMEM solution, and cells were incubated 1-2 hours at 37°C and 5% CO_2. Fluorescence output was detected using either a Victor 1420 Multilabel plate reader (Perkin Elmer) or Biotek Synergy HTX Multi-Mode plate reader (Agilent) with excitation at 560 nm and emission at 590 nm.

4.4.7 – RNA extraction and qRT-PCR analysis

RNA was extracted from cells following standard TRIzol (ThermoFisher) extraction methods. Agilent's Brillant III Ultra-Fast SYBR® Green one-step qRT-PCR kit was used in all qRT-PCR reactions. DENV2 genome copies were quantified using an *in vitro* transcribed viral RNA from a DENV2 cDNA subclone to generate a standard curve. All cellular RNA was normalized to Ribosomal Protein Lateral Stalk Subunit P0 (RPLP0) using the delta delta ct method as described in [119,264].The cycling parameters used were as follows: 20 mins at 50°C for reverse transcription, followed by 5 minutes at 95°C, and then 45 two-step cycles of 95°C for 5 secs and 60°C for 60 secs. A melt curve followed each cycle starting at 65°C and ending at 97°C.

4.4.8 – Glycosphingolipid extraction, purification, and analysis

Cells prepared for glycosphingolipid analysis were grown in T75 culture flasks (VWR). For infection experiments, cells were either mock infected or infected with DENV2 for 1 hr at room temperature. Following infection, cells were washed with 1x PBS, and then overlaid with 2% DMEM and incubated for indicated time periods. For Ambroxol experiments, cells were treated with Ambroxol HCl as described in 4.4.5 or with 0.1% DMSO (vehicle control) for 24 hours, followed by either mock infection or DENV2 infection for 1 hr at room temperature. Following infection, 2% DMEM containing fresh drug was applied to cells and cells were incubated for indicated time periods. At time of collection, viral supernatants were collected to validate infection and inhibition phenotype via plaque assay. Cells were trypsinized and counted using a hemocytometer and trypan blue reagent (ThermoFisher). For each sample set, an equal number of cells were centrifuged for 10 minutes at 10,000 RPM and 4°C.

GSLs were extracted as described in [317,306]. Following centrifugation, media was aspirated, and cell pellets were washed with 1x, and then resuspended in 400 µL of LC-MS grade water (Millipore Sigma). Cells were then subjected to 5x freeze thaw cycles to lyse cells, and then 1.6 mL of a 1:2 chloroform/methanol ($CHCl_3$/MeOH, v/v) solution was added and vortexed and samples were stored overnight at 4°C. Samples were then centrifuged at 16,000 RPM for 10 minutes at room temperature, and supernatants were transferred to separate tubes. Cell pellets were retained to analyze total protein content using a standard BCA colorimetric assay as described in [306]. A 1:1 solution of PBS and chloroform was added to supernatants for phase separation, and samples were centrifuged at 16,000 RPM for 10 minutes at room temperature. The upper phase was removed and saved, and the lower organic phase was dried on a 42°C heat block under a stream of nitrogen. After drying, the lower phase was resuspended in 20 µL $CHCl_3$/MeOH (1:3) and then added to the reserved upper phase and vortexed.

GSLs were then purified on C18 solid-phase extraction columns that were pre-equilibrated with methanol and deionized water (4 x and 3 x 1 mL, respectively). Sample tubes were washed with deionized water, and wash was added to the column. Columns were washed 3x with 1mL water. GSLs were eluted into new tubes by adding 2 mL $CHCl_3$/MeOH (98:2, v/v), 2 mL of $CHCl_3$/MeOH (1:3, v/v), and 1 mL methanol. Eluates were dried on a 42°C heat block under a stream of nitrogen until ~150 µL remained. Samples were transferred to new tubes. 200 µL of $CHCl_3$/MeOH (2:1 v/v) was used to wash tubes, and wash was added to the samples in new collection tubes. Samples were dried again on a 42°C heat block under a stream of nitrogen, followed be resuspension in 50 µL $CHCl_3$/MeOH (2:1, v/v), vortexed, and then dried down once more to concentrate GSLs.

To analyze GSL content, glycan head groups were enzymatically released from GSLs using recombinant endoglycoceramidase I (rEGCase I, custom synthesis from GenScript). 4 µL of rEGCase I (0.47 mg/mL) was added to 86 µL of a 0.6% Triton X-100 in 50 mM sodium acetate buffer (pH 5.2) and then added to each sample. Samples were vortexed and incubated at 37°C

for 16 hours. Following digest, the released oligosaccharides in each 90 µL tube were labelled with 310 µL 2-anthranillic acid (2AA) solution to allow for fluorescence detection by HPLC as described in [305,306]. The 2AA labeling mixture was prepared by adding 30 mg/mL 2AA and 45 mg/mL sodium cyanoborohydride to 2AA labeling buffer (4% sodium acetate, 2% boric acid in methanol). Samples were incubated at 80°C for 1 hr, cooled to room temperature, and then 3mL acetonitrile/water (97:3, v/v) was added to wash. Excess 2AA label was removed by purifying samples on Discovery DPA-6S columns (Sigma-Aldrich) pre-equilibrated with 1 mL acetonitrile/2 mL deionized water/2 mL acetonitrile. Samples were loaded onto columns, columns were washed with 4 mL acetonitrile/water (95:5, v/v), and then labeled oligosaccharides were eluted into new tubes using 600 µL deionized water and stored at -20°C until analyzed via HPLC. A standards mixture of commercially available GSLs (Table 4.1) was also dried, digested, and 2AA labeled as described above to help identify specific GSL species.

NP-HPLC was carried out on a Waters Alliance 2695 HPLC system with a Waters 2475 multi λ fluorescence detector (set to 360/425 nm excitation and emission). The solid phase used was a 4.6 x 250 mm TSK gel-Amine 80 column (Anachem) that was maintained at 30°C. The mobile phases consist of acetonitrile, deionized water, and 100 mM ammonium acetate (pH 3.85) used at gradient conditions (Table 4.2). GSL species were identified using Waters Empowers software to calculate glucose unit values compared to a 2AA-labelled homopolymer dextran ladder (Waters). Peak integration was performed in Waters Empower software to determine peak area, and a 2.5 pmol 2-AA labelled chitotriose standard was included with samples in the Ambroxol treated groups to calculate molar quantities from integrated peaks.

Table 4.1 – GSL standards mixture

Name	Vendor	Catalog number	GSL content	Concentration	Volume added
Neutral GSL mix	Matreya	1505	GluCer, LacCer, Gb3, Gb4	1.0 mg/mL	50 µL
Ganglioside Mix	Matreya	1510	Lac-Cer, GM3, GD3	0.5 mg/mL	100 µL
Ganglioside Mix	Matreya	1511	GA1, GM1a, GD1a, GD1b, GT1b	0.5 mg/mL	100 µL
GM2 Ganglioside	Matreya	1502	GM2	0.5 mg/mL	30 µL
Asialo-GM2	Sigma-Aldrich	G9398	GA2	1.0 mg/mL	30 µL

Table 4.2 – Gradient conditions and flow rate used in NP-HPLC [table adapted from 306]**.**

Time (min)	0	6	35	37	39	41	42	54	60
Flow (mL/min)	0.8	0.8	0.8	0.8	0.8	0.8	1.2	1.2	0.8
% acetonitrile	71.6	71.6	52.8	23.0	71.6	71.6	71.6	71.6	71.6
% DI-H_2O	8.4	8.4	27.2	57.0	57.0	8.4	8.4	8.4	8.4
% 100 mM ammonium acetate (pH 3.85)	20.0	20.0	20.0	20.0	20.0	20.0	20.0	20.0	20.0

4.4.9 – Fluorescence Imaging Cytometry

A549 cells were seeded in 48 well plates and transfected with siRNA as described in 4.4.3, followed by viral infection described in 4.4.2. At 24 hpi, viral supernatants were collected and stored at -80°C, and cells were washed with 1x PBS. Cells were fixed for 20 minutes at room temperature using 200 µL ice-cold MeOH, and then washed 3x with 1x PBS. Following washing, cells were permeabilized for 20 minutes at room temperature with a 0.1% Triton X-100/1% bovine serum albumin (BSA, Gold Biotechnology) solution in 1x PBS. Cells were then blocked overnight at 4°C in a 0.01% Triton X-100/1% BSA solution in 1x PBS. Cells were then incubated for 1 hr at 37°C with a 1:500 dilution of the flavivirus group antigen antibody (D1-4G2-4-15, or 4G2) which binds to domain II of the DENV E protein (mouse monoclonal antibody, BioVision). Following primary antibody staining, cells were washed 3x with blocking buffer (described above), and then counterstained with a 1:1000 dilution of goat anti-mouse FITC (ThermoFisher) for 1 hr at 37°C. Cells were again washed in blocking buffer, and counterstained with DAPI nuclear stain for 1 minute at room temperature (ThermoFisher), followed by 3 additional washes. 100 µL of blocking buffer was added to wells prior to imaging. Imaging was carried out using a Celigo Image Cytometer and Celigo software (Nexcelom Biosciences, a division of Perkin Elmer). The Celigo software application “Target 1 + 2 + 3” was used to visualize the cells in the brightfield channel, identify total number of cells (DAPI positive) in the blue channel (Ex/Em: 359/457 nm), and to quantify levels of E protein (FITC-positive) in the green channel (Ex/Em: 491/520 nm). For

analysis, E protein fluorescence values were normalized to total cell count in each well, and samples were compared to the non-targeting irrelevant control siRNA sample.

4.4.10 – Statistical analysis

The statistical tests used are noted in each figure legend. Results, where applicable, are expressed as mean values with standard deviation from three biological replicates (unless otherwise indicated). Statistical significance was determined using either a one-way analysis of variance (ANOVA) with Dunnett's multiple comparisons test, or multiple unpaired t-tests with Holm-Šídák multiple comparisons test in GraphPad Prism version 9 or higher (GraphPad software, La Jolla, California, USA). The half-maximal inhibitory concentration (IC_{50}) and half-maximal cytotoxic concentration (CC_{50}) of each pharmacological inhibitor used in this study was determined using non-linear regression/dose-response analysis in GraphPad Prism version 9 or higher. For IC_{50} analysis, viral titers (y-axis) were also log transformed in order to assess which concentrations of inhibitors used produced significant reductions (> 1 log) in viral titer and where therefore appropriate concentrations to use in the remainder of our studies.

Chapter 5: Conclusions

5.1: Summary and Future Directions

DENVs are the etiological agents of one of the world's most aggressive arthropod-borne diseases [1,2]. At present, there are no antivirals available to treat dengue, and only a single, suboptimal vaccine is available [1,2]. Vaccine development is greatly hindered by the fact that antibodies against one serotype are not cross-protective against but rather enhance infection by a secondary, heterotypic virus (antibody-dependent enhancement) [5]. These facts have prompted us to explore novel antiviral approaches by examining host-virus interactions.

As DENVs are obligate intracellular parasites, successful infection requires careful control and coordination of a variety of host factors both to fulfill their replicative needs, and to control the host antiviral response [reviewed in 14]. In fact, it is now well-documented that upon infection with DENVs, several host pathways are significantly altered, including: the unfolded protein response, autophagy, lipid metabolism, and central carbon metabolism [reviewed in 14 discussed in detail in section 1.3 of this dissertation]. In this dissertation, we have capitalized on this existing knowledge as well as our previous studies investigating alterations to host lipid metabolism and changes to sialic acids during DENV2 infection [99,110,111,119,90,91 Gullberg et al., unpublished, and Lian E, et al. unpublished]. Here, we have employed Huh7 cells as an *in vitro* model system of human DENV infection, and explored how loss of function of enzymes involved in regulating fatty acyl-CoA homeostasis (Chapter 2), desialylation of glycoconjugates (Chapter 3), and the synthesis and degradation of sphingolipids (Chapter 4) impacts the DENV2 lifecycle.

Importantly, while each of these studies have broadened our understanding of the reliance of DENVs upon these different host factors, they also allowed us to uncover novel functional roles

for the enzymes that we studied. Below I have summarized the key findings of each of these studies and highlighted important future directions for each.

5.1.1 – Acyl-CoA Thioesterases

Summary

The ACOT family of enzymes are predicted to control the intracellular balance of activated fatty acids (fatty acyl-CoAs), free fatty acids (FFA), and coenzyme A (CoA-SH) [191,193,196,197]. Specifically, they are responsible for the hydrolysis of fatty acyl-CoAs, resulting in formation of FFA and CoA-SH [191,193,196,197]. Importantly, fatty acyl-CoAs are precursor molecules for generation of phospholipids and sphingolipids. During infection with DENVs, we had previously shown that many lipid species, including phospholipids and sphingolipids, are upregulated and vital for the DENV2 lifecycle [110,111,119]. In initial loss of function studies examining enzymes within fatty acid biosynthesis pathways, we found that inhibition of the type I ACOTs, ACOT1 (cytoplasmic) and ACOT2 (mitochondrial), combined resulted in a significant increase DENV2 genome replication and infectious particle release. Thus, we initially hypothesized that the ACOT family of enzymes may antagonize DENV2. As ACOT1 and ACOT2 are splice variants [192,197], it was not possible to design siRNAs or primer sequences that targeted ACOT1 specifically, but were able to target ACOT2 by targeting its the mitochondrial localization sequence. This allowed us to parse out the influence of ACOT1 and ACOT2 leading to the discovery that loss of function of ACOT1 increased DENV2 genome replication and release, while loss of function of ACOT2 significantly decreased DENV2 genome replication and release. These results were unexpected and intriguing, and led us to question whether subcellular location was a key determinant of the effect of ACOT functionality on DENV2. Thus, we evaluated the effect of loss of function of ACOT7, a type II mitochondrial ACOT, and found that it similarly suppressed DENV2 replication

and release. Moreover, we uncovered that reduced expression of ACOT2 and ACOT7 also resulted in reduced expression of other ACOTs located in multiple organelle compartments highlighting a yet unknown functional relationship between ACOTs.

Future directions

Mechanistic insight into the role of each ACOT in the field is limited. One challenge is that the ester linkage between CoA and fatty acids is labile, and traditional methods of analysis are unable to determine a true ratio between activated fatty acids and FFA [191,258]. This prevented us from profiling which specific fatty acyl-CoAs were impacted in our study which would have provided additional insight into specific fatty acid/lipid requirements of DENVs. To address this, we were able to successfully develop an LC-MS assay that allowed us to distinguish between arachidonic acid, arachidonyl-CoA, and CoA-SH as proof of principle (arachidonyl-CoA is the primary substrate of ACOT7). However, due to limitations in scalability of siRNA treatment, the level of these metabolites in our model system fell below our limits of detection for the LC-MS assay. Thus, a future direction of this project will employ the use of knockout cell lines to identify specific lipid species impacted by loss of function of ACOTs 1, 2, and 7 in both mock and infected cell subtypes.

5.1.2 – Neuraminidases

Summary

While viruses rely upon and hijack host metabolic pathways to fulfill their replicative needs, these alterations to host cellular metabolism often have pathological consequences on the host [reviewed in 14,309,318]. Previously, it was established that the DENV2 NS1 protein upregulated host sialidase activity [90,91]. This increased sialidase activity was linked with endothelial

hyperpermeability and vascular leakage, which are hallmarks of severe dengue disease [90,91]. However, a functional role for the increased sialidase activity remained unexplored until our studies detailed in Chapter 3.

During our siRNA-mediated loss of function analysis of enzymes involved in the sphingolipid metabolic pathways (presented in Chapter 4), we uncovered that loss of function of NEU1-4 significantly reduced DENV2 infectious particle release from cells. In terms of sphingolipid metabolism, NEU1-4 are involved in the catabolism of gangliosides through the hydrolysis of their sialic acid residues [reviewed in 319]. However, sialic acids are found at the terminal position of many other glycoconjugates as well [reviewed in 229]. Thus, while this discovery was made in the context of investigating sphingolipid pathway enzymes, we recognized that the functional roles of NEU1-4 extended far beyond their involvement in ganglioside catabolism. However, the fact that we now had direct evidence that sialidases not only contributed to DENV pathogenesis but were also vital for DENV2 infectious particle release prompted us to investigate how loss of function of sialidase activity influenced the viral lifecycle. We found that NEU1-4 functionality was vital for both viral replication and viral egress. Moreover, we provided the first characterization of the inter-relationship between NEUs, highlighting that NEU1-3 expression is decreased upon loss of function of NEU4. Importantly, NEU4 is found in multiple subcellular compartments and has the broadest substrate specificity among NEUs [reviewed in 231,234], but its biological function is the least characterized. This discovery provides some insight that NEU4, or its downstream products, are involved in transcriptional regulation of NEU1-3.

Future directions

One challenge to this study is that biological function of each sialidase enzyme is ambiguous due to the overwhelming number of glycoconjugates containing terminal sialic acid residues that exist in the cell. Moreover, the regulatory elements involved in governing sialidase

activity remain unknown. This prevented us from providing mechanistic insight into how desialylation impacts DENV2 genome replication and egress. Future studies using DENV2 infected/wild-type and DENV2-infected/NEU$^{-/-}$ cell lines coupled with LC-MS analysis of cellular glycoconjugates would assist in identifying which cellular glycoconjugates are desialylated by each NEU during infection. While these analyses alone will not provide mechanistic insight into how desialyation impacts the DENV2 lifecycle, they can serve as a tool to narrow in on specific glycoconjugates of interest.

5.1.3 – Sphingolipid Metabolism

Sphingolipids are potent bioactive signaling molecules, and perturbation of SL metabolism is known to be associated with the pathology of several chronic and infectious diseases [reviewed in 120]. In our previous studies, we established that many SLs are upregulated during dengue infection in both the human and mosquito host [110,111 Gullberg RC, et al., unpublished]. Here we provided the first profiling of enzymes of the SL metabolic pathway during DENV2 infection. These loss of function studies allowed for several critical observations.

First, we determined that the salvage and sphingomyelinase pathways of ceramide synthesis as opposed to *de novo* ceramide synthesis were critical for DENV2 release from human cells. It was previously established that ceramide levels were elevated during DENV2 infection [110,111,117]. Thus, this finding suggests that the elevation of ceramide during DENV2 infection is caused by activation of enzymes involved in degradation of complex sphingolipids.

Second, we determined that enzymes involved in glycosphingolipid synthesis and degradation are vital for DENV2 release. This seemingly contradictory finding prompted us to examine whether glycosphingolipid levels are altered during infection. We found that several GSL species were, in fact, elevated during peak viral replication, but not at later timepoints. This

suggested that GSLs may be vital for the events of viral replication through yet undefined mechanisms. We were able to chemically identify several of the GSL species elevated during infection including LacCer, Lc3, Gb3, GM2 and GA1. The functionality of Lc3, Gb3, GM2, and GA1 GSLs are poorly understood, but provide us with specific metabolites to target in future studies. LacCer is an important precursor for all complex glycosphingolipids, but is, itself, a vital regulatory molecule. One intriguingly link between this study and ongoing work by other researchers in our lab is that LacCer is involved in the activation of the cytosolic phospholipase A2 enzyme ($cPLA_2$) [307,308]. One role for PLA_2 enzymes is they mediate cellular arachidonic acid levels [308]. In other works by our group, we have established that arachidonic acid is elevated during DENV2 infection, and that PLA_2 (both cytosolic and secreted) activity is vital for DENV2 genome replication and release [Gullberg RC, et al., and Lian E, et al., unpublished]. However, those studies have yet to uncover how PLA_2 activity is regulated during infection. These results provide exciting new insight and directions to pursue.

Finally, this study allowed us to determine that lysosomal and non-lysosomal glucocerebrosidase activity has differential effects on DENV2 genome replication and infectious virus release. Specifically, the lysosomal GBA1 enzyme inhibits DENV2 release and the non-lysosomal GBA2 enzyme is vital for DENV2 release. Each of these enzymes is responsible for breaking down GluCer into ceramide and glucose [reviewed in 113] . However, the difference between these enzymes lies in what happens to ceramide after it is released from GluCer. In the lysosome, it is fully catabolized to sphingosine and free fatty acids, but in the ER/Golgi it can be recycled to form the GalCer and GluCer precursor for complex GSLs [reviewed in 113]. Based on these data, we have proposed a novel function of GBA2 as a driver of GluCer/CER recycling during DENV2 infection. Importantly, these findings also lead to our investigation of Ambroxol HCl (a GBA1 chaperone/GBA2 inhibitor) as potential therapeutic agent against DENVs. We found that it is a potent inhibitor of DENV2 at both low and high MOI *in vitro* (MOI = 0.1 and 5, respectively).

Moreover, we found that it abolished the elevation of GSLs seen during DENV2 infection supporting our proposed model.

Future directions

Further characterization of GBA1/GBA2 activity during DENV2 infection is ongoing to identify which part of the DENV2 lifecycle is specifically impacted by these enzymes. These analyses include time of addition studies using Ambroxol HCl, as well as NB-DGJ (a GBA2 specific inhibitor) and enzyme activity analysis over a time course of infection; and assays to determine whether DENV2 proteins interact directly with each enzyme. Additionally, we have revised our protocols for GSL analysis to allow for chemical identification of a broader subset of GSLs than our initial analyses provided. These experiments will aid us in determining the mechanism by which GBA2 and GSLs impact release of infectious DENV2 particles.

In addition, the success of our *in vitro* study of Ambroxol HCl has prompted a collaboration between our group and the Teixeira lab at the Universidade Federal de Minas Gerais in Brazil to investigate the efficacy of Ambroxol HCl against DENV2 in a murine model. The preliminary results of these studies are promising and showed reduced DENV2 titers, reduced inflammatory cytokine production, and reduced hepatic damage in treated vs. untreated DENV2-infected mice. We excluded those results from this dissertation as the *in vivo* experiments were not conducted directly by our group and are still being optimized. However, the efforts of this collaboration will allow for a better understanding of how the elevation of GSLs during infection contribute to DENV2 pathogenesis.

Finally, this study identified many sphingolipid pathway enzymes that are critical to infectious virus release that we have yet to evaluate further since we focused our efforts on characterizing GBA1 and GBA2. Further evaluation of these enzymes will provide additional insight into how sphingolipids support DENV2 production.

5.2: Concluding Remarks

The unifying theme that was explicit throughout this dissertation was that infection with DENVs results in an altered metabolic environment in the cell. These alterations can be both host-induced as part of the antiviral response or caused directly through viral subjugation of host metabolic processes. It is well understood that perturbation of metabolic homeostasis can have dire pathological effects on the host. As an example, Gaucher disease is a chronic metabolic disorder characterized by genetic mutations in the GBA1 enzyme which results in build-up of GluCer within the lysosome and overall accumulation of cellular GSLs [214,reviewed in 216]. The accompanying pathology associated with Gaucher disease is increased inflammatory signaling, anemia, hepatosplenomegaly, bruising/thrombocytopenia, and bone pain/fractures/and/or arthritis [214,reviewed in 216]. Interestingly, each of these pathologies also accompanies severe dengue disease [reviewed in 4]. Herein, we have demonstrated that GSLs are elevated in a human *in vitro* model of DENV2 infection. While our studies thus far cannot conclude that elevated GSLs are directly associated with DENV2 pathology, the similarities between these two diseases are striking. Moreover, these similarities point out a more implicit theme woven throughout this dissertation which is that viral infections are themselves acute metabolic disorders. By reframing our view of viruses as diseases of metabolism we can connect viral infection with broader themes within human disease. This provides a greater advantage towards understanding host-virus interactions, viral pathology, and the identification of novel therapeutics to improve patient outcomes (e.g. identification of Ambroxol HCl in Chapter 4). Further mapping of the similarities between viral infection-induced metabolic changes and chronic metabolic disorders represents a next and exciting step within this field.

References

1. World Health Organization. Dengue and severe dengue [Internet]. Available from: https://www.who.int/news-room/fact-sheets/detail/dengue-and-severe-dengue

2. Halstead S. Recent advances in understanding dengue. F1000Res. 2019;8:F1000 Faculty Rev-1279.

3. Messina JP, Brady OJ, Scott TW, Zou C, Pigott DM, Duda KA, Bhatt S, Katzelnick L, Howes RE, Battle KE, Simmons CP, Hay SI. Global spread of dengue virus types: mapping the 70 year history. Trends Microbiol. 2014 Mar;22(3):138–46.

4. Ministry of Health - Sri Lanka. National Guidelines for the Clinical Management of Dengue Infection in Pregnancy [Internet]. Colombo, Sri Lanka: Epidemiology Unit; 2019 Jul. Available from: www.epid.gov.lk

5. Halstead SB. Dengue Antibody-Dependent Enhancement: Knowns and Unknowns. Microbiol Spectr. 2014 Dec;2(6).

6. Narayan R, Tripathi S. Intrinsic ADE: The Dark Side of Antibody Dependent Enhancement During Dengue Infection. Front Cell Infect Microbiol. 2020 Oct 2;10:580096.

7. Begum F, Das S, Mukherjee D, Mal S, Ray U. Insight into the Tropism of Dengue Virus in Humans. Viruses. 2019 Dec 9;11(12):1136.

8. Martinez DR, Metz SW, Baric RS. Dengue Vaccines: The Promise and Pitfalls of Antibody-Mediated Protection. Cell Host & Microbe. 2021 Jan 13;29(1):13–22.

9. Shukla R, Ramasamy V, Shanmugam RK, Ahuja R, Khanna N. Antibody-Dependent Enhancement: A Challenge for Developing a Safe Dengue Vaccine. Front Cell Infect Microbiol. 2020 Oct 22;10:572681.

10. Thomas SJ, Yoon IK. A review of Dengvaxia®: development to deployment. Hum Vaccin Immunother. 2019 Oct 7;15(10):2295–314.

11. World Health Organization. Global Advisory Committee on Vaccine Safety, 6-7 December 2017. Weekly Epidemiology Record. 2018 Jan 19;93(3):17–32.

12. Wilder-Smith A. Dengue vaccine development by the year 2020: challenges and prospects. Curr Opin Virol. 2020 Aug;43:71–8.

13. Kuhn RJ. The Flaviviruses. In: Acheson NH, editor. *Fundamentals of Molecular Virology*. 2nd ed. Hoboken, NJ, U.S.: John Wiley & Sons Ltd; p. 137–47.

14. Perera R, Kuhn RJ. Host Metabolism and its Contribution in Flavivirus Biogenesis. In: *Arboviruses: Molecular Biology, Evolution and Control*. Caister Academic Press; 2016. p. 45–60.

15. Skehel JJ, Wiley DC. Receptor binding and membrane fusion in virus entry: the influenza hemagglutinin. Annu Rev Biochem. 2000;69:531–69.

16. Wilen CB, Tilton JC, Doms RW. HIV: cell binding and entry. Cold Spring Harb Perspect Med. 2012 Aug 1;2(8):a006866.

17. Laureti M, Narayanan D, Rodriguez-Andres J, Fazakerley JK, Kedzierski L. Flavivirus Receptors: Diversity, Identity, and Cell Entry. Front Immunol. 2018;9:2180.

18. Balsitis SJ, Coloma J, Castro G, Alava A, Flores D, McKerrow JH, Beatty PR, Harris E. Tropism of dengue virus in mice and humans defined by viral nonstructural protein 3-specific immunostaining. Am J Trop Med Hyg. 2009 Mar;80(3):416–24.

19. Jessie K, Fong MY, Devi S, Lam SK, Wong KT. Localization of dengue virus in naturally infected human tissues, by immunohistochemistry and in situ hybridization. J Infect Dis. 2004 Apr 15;189(8):1411–8.

20. Kangwanpong D, Bhamarapravati N, Lucia HL. Diagnosing dengue virus infection in archived autopsy tissues by means of the in situ PCR method: a case report. Clinical and Diagnostic Virology. 1995 Feb 1;3(2):165–72.

21. Póvoa TF, Alves AMB, Oliveira CAB, Nuovo GJ, Chagas VLA, Paes MV. The Pathology of Severe Dengue in Multiple Organs of Human Fatal Cases: Histopathology, Ultrastructure and Virus Replication. PLoS One. 2014 Apr 15;9(4):e83386.

22. Durbin AP, Vargas MJ, Wanionek K, Hammond SN, Gordon A, Rocha C, Balmaseda A, Harris E. Phenotyping of peripheral blood mononuclear cells during acute dengue illness demonstrates infection and increased activation of monocytes in severe cases compared to classic dengue fever. Virology. 2008 Jul 5;376(2):429–35.

23. Gao F, Duan X, Lu X, Liu Y, Zheng L, Ding Z, Li J. Novel binding between pre-membrane protein and claudin-1 is required for efficient dengue virus entry. Biochem Biophys Res Commun. 2010 Jan 1;391(1):952–7.

24. Navarro-Sanchez E, Altmeyer R, Amara A, Schwartz O, Fieschi F, Virelizier JL, Arenzana-Seisdedos F, Desprès P. Dendritic-cell-specific ICAM3-grabbing non-integrin is essential for the productive infection of human dendritic cells by mosquito-cell-derived dengue viruses. EMBO Rep. 2003 Jul;4(7):723–8.

25. Tassaneetrithep B, Burgess TH, Granelli-Piperno A, Trumpfheller C, Finke J, Sun W, Eller MA, Pattanapanyasat K, Sarasombath S, Birx DL, Steinman RM, Schlesinger S, Marovich MA. DC-SIGN (CD209) mediates dengue virus infection of human dendritic cells. J Exp Med. 2003 Apr 7;197(7):823–9.

26. Dejnirattisai W, Webb AI, Chan V, Jumnainsong A, Davidson A, Mongkolsapaya J, Screaton G. Lectin switching during dengue virus infection. J Infect Dis. 2011 Jun 15;203(12):1775–83.

27. Miller JL, de Wet BJM, deWet BJM, Martinez-Pomares L, Radcliffe CM, Dwek RA, Rudd PM, Gordon S. The mannose receptor mediates dengue virus infection of macrophages. PLoS Pathog. 2008 Feb 8;4(2):e17.

28. Chen Y, Maguire T, Hileman RE, Fromm JR, Esko JD, Linhardt RJ, Marks RM. Dengue virus infectivity depends on envelope protein binding to target cell heparan sulfate. Nat Med. 1997 Aug;3(8):866–71.

29. Jindadamrongwech S, Thepparit C, Smith DR. Identification of GRP 78 (BiP) as a liver cell expressed receptor element for dengue virus serotype 2. Arch Virol. 2004 May;149(5):915–27.

30. Thepparit C, Smith DR. Serotype-Specific Entry of Dengue Virus into Liver Cells: Identification of the 37-Kilodalton/67-Kilodalton High-Affinity Laminin Receptor as a Dengue Virus Serotype 1 Receptor. J Virol. 2004 Nov;78(22):12647–56.

31. Aoki C, Hidari KIPJ, Itonori S, Yamada A, Takahashi N, Kasama T, Hasebe F, Islam MA, Hatano K, Matsuoka K, Taki T, Guo CT, Takahashi T, Sakano Y, Suzuki T, Miyamoto D, Sugita M, Terunuma D, Morita K, Suzuki Y. Identification and characterization of carbohydrate molecules in mammalian cells recognized by dengue virus type 2. J Biochem. 2006 Mar;139(3):607–14.

32. Reyes-del Valle J, del Angel RM. Isolation of putative dengue virus receptor molecules by affinity chromatography using a recombinant E protein ligand. J Virol Methods. 2004 Mar 1;116(1):95–102.

33. Chen YC, Wang SY, King CC. Bacterial lipopolysaccharide inhibits dengue virus infection of primary human monocytes/macrophages by blockade of virus entry via a CD14-dependent mechanism. J Virol. 1999 Apr;73(4):2650–7.

34. Meertens L, Carnec X, Lecoin MP, Ramdasi R, Guivel-Benhassine F, Lew E, Lemke G, Schwartz O, Amara A. The TIM and TAM families of phosphatidylserine receptors mediate dengue virus entry. Cell Host Microbe. 2012 Oct 18;12(4):544–57.

35. Cruz-Oliveira C, Freire JM, Conceição TM, Higa LM, Castanho MARB, Da Poian AT. Receptors and routes of dengue virus entry into the host cells. FEMS Microbiology Reviews. 2015 Mar 1;39(2):155–70.

36. van der Schaar HM, Rust MJ, Chen C, van der Ende-Metselaar H, Wilschut J, Zhuang X, Smit JM. Dissecting the cell entry pathway of dengue virus by single-particle tracking in living cells. PLoS Pathog. 2008 Dec;4(12):e1000244.

37. Acosta EG, Castilla V, Damonte EB. Differential Requirements in Endocytic Trafficking for Penetration of Dengue Virus. PLoS One. 2012 Sep 7;7(9):e44835.

38. Elkin SR, Lakoduk AM, Schmid SL. Endocytic Pathways and Endosomal Trafficking: A Primer. Wien Med Wochenschr. 2016 May;166(7–8):196–204.

39. Kuhn RJ, Zhang W, Rossmann MG, Pletnev SV, Corver J, Lenches E, Jones CT, Mukhopadhyay S, Chipman PR, Strauss EG, Baker TS, Strauss JH. Structure of dengue virus: implications for flavivirus organization, maturation, and fusion. Cell. 2002 Mar 8;108(5):717–25.

40. Zhang X, Sheng J, Austin SK, Hoornweg TE, Smit JM, Kuhn RJ, Diamond MS, Rossmann MG. Structure of Acidic pH Dengue Virus Showing the Fusogenic Glycoprotein Trimers. J Virol. 2014 Dec 16;89(1):743–50.

41. Stiasny K, Fritz R, Pangerl K, Heinz FX. Molecular mechanisms of flavivirus membrane fusion. Amino Acids. 2011 Nov;41(5):1159–63.

42. Zaitseva E, Yang ST, Melikov K, Pourmal S, Chernomordik LV. Dengue virus ensures its fusion in late endosomes using compartment-specific lipids. PLoS Pathog. 2010 Oct 7;6(10):e1001131.

43. Gruenberg J. Lipids in endocytic membrane transport and sorting. Curr Opin Cell Biol. 2003 Aug;15(4):382–8.

44. Gebhard LG, Filomatori CV, Gamarnik AV. Functional RNA Elements in the Dengue Virus Genome. Viruses. 2011 Sep 15;3(9):1739–56.

45. Sanford TJ, Mears HV, Fajardo T, Locker N, Sweeney TR. Circularization of flavivirus genomic RNA inhibits de novo translation initiation. Nucleic Acids Res. 2019 Oct 10;47(18):9789–802.

46. Filomatori CV, Lodeiro MF, Alvarez DE, Samsa MM, Pietrasanta L, Gamarnik AV. A 5′ RNA element promotes dengue virus RNA synthesis on a circular genome. Genes Dev. 2006 Aug 15;20(16):2238–49.

47. Choi KH. The Role of the Stem-Loop A RNA Promoter in Flavivirus Replication. Viruses. 2021 Jun 9;13(6):1107.

48. Lescar J, Soh S, Lee LT, Vasudevan SG, Kang C, Lim SP. The Dengue Virus Replication Complex: From RNA Replication to Protein-Protein Interactions to Evasion of Innate Immunity. Adv Exp Med Biol. 2018;1062:115–29.

49. Paranjape SM, Harris E. Control of Dengue Virus Translation and Replication. In: Rothman AL, editor. Dengue Virus. Berlin, Heidelberg: Springer; 2010. p. 15–34. (Current Topics in Microbiology and Immunology).

50. Junjhon J, Pennington JG, Edwards TJ, Perera R, Lanman J, Kuhn RJ. Ultrastructural characterization and three-dimensional architecture of replication sites in dengue virus-infected mosquito cells. J Virol. 2014 May;88(9):4687–97.

51. Welsch S, Miller S, Romero-Brey I, Merz A, Bleck CKE, Walther P, Fuller SD, Antony C, Krijnse-Locker J, Bartenschlager R. Composition and three-dimensional architecture of the dengue virus replication and assembly sites. Cell Host Microbe. 2009 Apr 23;5(4):365–75.

52. Westaway EG, Mackenzie JM, Kenney MT, Jones MK, Khromykh AA. Ultrastructure of Kunjin virus-infected cells: colocalization of NS1 and NS3 with double-stranded RNA, and of NS2B with NS3, in virus-induced membrane structures. J Virol. 1997 Sep;71(9):6650–61.

53. Friedrich S, Engelmann S, Schmidt T, Szczepankiewicz G, Bergs S, Liebert UG, Kümmerer BM, Golbik RP, Behrens SE. The Host Factor AUF1 p45 Supports Flavivirus Propagation by Triggering the RNA Switch Required for Viral Genome Cyclization. J Virol. 2018 Feb 26;92(6):e01647-17.

54. Villordo SM, Alvarez DE, Gamarnik AV. A balance between circular and linear forms of the dengue virus genome is crucial for viral replication. RNA. 2010 Dec;16(12):2325–35.

55. Li MY, Grandadam M, Kwok K, Lagache T, Siu YL, Zhang JS, Sayteng K, Kudelko M, Qin CF, Olivo-Marin JC, Bruzzone R, Wang PG. KDEL Receptors Assist Dengue Virus Exit from the Endoplasmic Reticulum. Cell Reports. 2015 Mar 10;10(9):1496–507.

56. Lewis MJ, Pelham HR. A human homologue of the yeast HDEL receptor. Nature. 1990 Nov 8;348(6297):162–3.

57. Cancino J, Jung JE, Luini A. Regulation of Golgi signaling and trafficking by the KDEL receptor. Histochem Cell Biol. 2013 Oct;140(4):395–405.

58. Jia J, Yue X, Zhu L, Jing S, Wang Y, Gim B, Qian Y, Lee I. KDEL receptor is a cell surface receptor that cycles between the plasma membrane and the Golgi via clathrin-mediated transport carriers. Cell Mol Life Sci. 2021 Feb;78(3):1085–100.

59. Friberg H, Jaiswal S, West K, O'Ketch M, Rothman AL, Mathew A. Analysis of human monoclonal antibodies generated by dengue virus-specific memory B cells. Viral Immunol. 2012 Oct;25(5):348–59.

60. da Silva Voorham JM, Rodenhuis-Zybert IA, Ayala Nuñez NV, Colpitts TM, van der Ende-Metselaar H, Fikrig E, Diamond MS, Wilschut J, Smit JM. Antibodies against the envelope glycoprotein promote infectivity of immature dengue virus serotype 2. PLoS One. 2012;7(3):e29957.

61. Perera R, Kuhn RJ. Structural proteomics of dengue virus. Curr Opin Microbiol. 2008 Aug;11(4):369–77.

62. Ma L, Jones CT, Groesch TD, Kuhn RJ, Post CB. Solution structure of dengue virus capsid protein reveals another fold. Proc Natl Acad Sci U S A. 2004 Mar 9;101(10):3414–9.

63. Li L, Lok SM, Yu IM, Zhang Y, Kuhn RJ, Chen J, Rossmann MG. The flavivirus precursor membrane-envelope protein complex: structure and maturation. Science. 2008 Mar 28;319(5871):1830–4.

64. Modis Y, Ogata S, Clements D, Harrison SC. A ligand-binding pocket in the dengue virus envelope glycoprotein. Proc Natl Acad Sci U S A. 2003 Jun 10;100(12):6986–91.

65. Edeling MA, Diamond MS, Fremont DH. Structural basis of Flavivirus NS1 assembly and antibody recognition. Proc Natl Acad Sci U S A. 2014 Mar 18;111(11):4285–90.

66. Xie X, Gayen S, Kang C, Yuan Z, Shi PY. Membrane topology and function of dengue virus NS2A protein. J Virol. 2013 Apr;87(8):4609–22.

67. Luo D, Xu T, Hunke C, Grüber G, Vasudevan SG, Lescar J. Crystal structure of the NS3 protease-helicase from dengue virus. J Virol. 2008 Jan;82(1):173–83.

68. El Sahili A, Soh TS, Schiltz J, Gharbi-Ayachi A, Seh CC, Shi PY, Lim SP, Lescar J. NS5 from Dengue Virus Serotype 2 Can Adopt a Conformation Analogous to That of Its Zika Virus and Japanese Encephalitis Virus Homologues. J Virol. 2019 Dec 12;94(1):e01294-19.

69. Byk LA, Gamarnik AV. Properties and Functions of the Dengue Virus Capsid Protein. Annu Rev Virol. 2016 Sep 29;3(1):263–81.

70. Jones CT, Ma L, Burgner JW, Groesch TD, Post CB, Kuhn RJ. Flavivirus capsid is a dimeric alpha-helical protein. J Virol. 2003 Jun;77(12):7143–9.

71. Xie X, Zou J, Zhang X, Zhou Y, Routh AL, Kang C, Popov VL, Chen X, Wang QY, Dong H, Shi PY. Dengue NS2A Protein Orchestrates Virus Assembly. Cell Host & Microbe. 2019 Nov 13;26(5):606-622.e8.

72. Wang SH, Syu WJ, Huang KJ, Lei HY, Yao CW, King CC, Hu ST. Intracellular localization and determination of a nuclear localization signal of the core protein of dengue virus. J Gen Virol. 2002 Dec;83(Pt 12):3093–102.

73. Colpitts TM, Barthel S, Wang P, Fikrig E. Dengue virus capsid protein binds core histones and inhibits nucleosome formation in human liver cells. PLoS One. 2011;6(9):e24365.

74. Netsawang J, Noisakran S, Puttikhunt C, Kasinrerk W, Wongwiwat W, Malasit P, Yenchitsomanus P thai, Limjindaporn T. Nuclear localization of dengue virus capsid protein is required for DAXX interaction and apoptosis. Virus Res. 2010 Feb;147(2):275–83.

75. Courageot MP, Frenkiel MP, Duarte Dos Santos C, Deubel V, Desprès P. α-Glucosidase Inhibitors Reduce Dengue Virus Production by Affecting the Initial Steps of Virion Morphogenesis in the Endoplasmic Reticulum. J Virol. 2000 Jan;74(1):564–72.

76. Yu IM, Zhang W, Holdaway HA, Li L, Kostyuchenko VA, Chipman PR, Kuhn RJ, Rossmann MG, Chen J. Structure of the immature dengue virus at low pH primes proteolytic maturation. Science. 2008 Mar 28;319(5871):1834–7.

77. Zhang Y, Zhang W, Ogata S, Clements D, Strauss JH, Baker TS, Kuhn RJ, Rossmann MG. Conformational changes of the flavivirus E glycoprotein. Structure. 2004 Sep;12(9):1607–18.

78. Yap SSL, Nguyen-Khuong T, Rudd PM, Alonso S. Dengue Virus Glycosylation: What Do We Know? Frontiers in Microbiology. 2017;8.

79. Hacker K, White L, de Silva AM. N-linked glycans on dengue viruses grown in mammalian and insect cells. J Gen Virol. 2009 Sep;90(Pt 9):2097–106.

80. Pokidysheva E, Zhang Y, Battisti AJ, Bator-Kelly CM, Chipman PR, Xiao C, Gregorio GG, Hendrickson WA, Kuhn RJ, Rossmann MG. Cryo-EM reconstruction of dengue virus in

complex with the carbohydrate recognition domain of DC-SIGN. Cell. 2006 Feb 10;124(3):485–93.

81. Rey FA, Heinz FX, Mandl C, Kunz C, Harrison SC. The envelope glycoprotein from tick-borne encephalitis virus at 2 A resolution. Nature. 1995 May 25;375(6529):291–8.

82. Muller DA, Young PR. The flavivirus NS1 protein: molecular and structural biology, immunology, role in pathogenesis and application as a diagnostic biomarker. Antiviral Res. 2013 May;98(2):192–208.

83. Akey DL, Brown WC, Dutta S, Konwerski J, Jose J, Jurkiw TJ, DelProposto J, Ogata CM, Skiniotis G, Kuhn RJ, Smith JL. Flavivirus NS1 crystal structures reveal a surface for membrane association and regions of interaction with the immune system. Science. 2014 Feb 21;343(6173):881–5.

84. Lindenbach BD, Rice CM. Genetic interaction of flavivirus nonstructural proteins NS1 and NS4A as a determinant of replicase function. J Virol. 1999 Jun;73(6):4611–21.

85. Youn S, Ambrose RL, Mackenzie JM, Diamond MS. Non-structural protein-1 is required for West Nile virus replication complex formation and viral RNA synthesis. Virol J. 2013 Nov 18;10:339.

86. Płaszczyca A, Scaturro P, Neufeldt CJ, Cortese M, Cerikan B, Ferla S, Brancale A, Pichlmair A, Bartenschlager R. A novel interaction between dengue virus nonstructural protein 1 and the NS4A-2K-4B precursor is required for viral RNA replication but not for formation of the membranous replication organelle. PLoS Pathog. 2019 May 9;15(5):e1007736.

87. Shirako Y, Strauss JH. Regulation of Sindbis virus RNA replication: uncleaved P123 and nsP4 function in minus-strand RNA synthesis, whereas cleaved products from P123 are required for efficient plus-strand RNA synthesis. J Virol. 1994 Mar;68(3):1874–85.

88. Harris KS, Xiang W, Alexander L, Lane WS, Paul AV, Wimmer E. Interaction of poliovirus polypeptide 3CDpro with the 5’ and 3’ termini of the poliovirus genome. Identification of viral and cellular cofactors needed for efficient binding. J Biol Chem. 1994 Oct 28;269(43):27004–14.

89. Romero-Brey I, Berger C, Kallis S, Kolovou A, Paul D, Lohmann V, Bartenschlager R. NS5A Domain 1 and Polyprotein Cleavage Kinetics Are Critical for Induction of Double-Membrane Vesicles Associated with Hepatitis C Virus Replication. mBio. 2015 Jul 7;6(4):e00759.

90. Puerta-Guardo H, Glasner DR, Harris E. Dengue Virus NS1 Disrupts the Endothelial Glycocalyx, Leading to Hyperpermeability. PLoS Pathog. 2016 Jul;12(7):e1005738.

91. Espinosa DA, Beatty PR, Puerta-Guardo H, Islam MN, Belisle JT, Perera R, Harris E. Increased serum sialic acid is associated with morbidity and mortality in a murine model of dengue disease. J Gen Virol. 2019 Nov;100(11):1515–22.

92. Wang C, Puerta-Guardo H, Biering SB, Glasner DR, Tran EB, Patana M, Gomberg TA, Malvar C, Lo NTN, Espinosa DA, Harris E. Endocytosis of flavivirus NS1 is required for

NS1-mediated endothelial hyperpermeability and is abolished by a single N-glycosylation site mutation. PLoS Pathog. 2019 Jul 29;15(7):e1007938.

93. Chen HR, Chao CH, Liu CC, Ho TS, Tsai HP, Perng GC, Lin YS, Wang JR, Yeh TM. Macrophage migration inhibitory factor is critical for dengue NS1-induced endothelial glycocalyx degradation and hyperpermeability. PLoS Pathog. 2018 Apr;14(4):e1007033.

94. Lin SW, Chuang YC, Lin YS, Lei HY, Liu HS, Yeh TM. Dengue virus nonstructural protein NS1 binds to prothrombin/thrombin and inhibits prothrombin activation. J Infect. 2012 Mar;64(3):325–34.

95. Xie X, Zou J, Puttikhunt C, Yuan Z, Shi PY. Two distinct sets of NS2A molecules are responsible for dengue virus RNA synthesis and virion assembly. J Virol. 2015 Jan 15;89(2):1298–313.

96. Wahaab A, Mustafa BE, Hameed M, Stevenson NJ, Anwar MN, Liu K, Wei J, Qiu Y, Ma Z. Potential Role of Flavivirus NS2B-NS3 Proteases in Viral Pathogenesis and Anti-flavivirus Drug Discovery Employing Animal Cells and Models: A Review. Viruses. 2021 Dec 28;14(1):44.

97. Aguirre S, Luthra P, Sanchez-Aparicio MT, Maestre AM, Patel J, Lamothe F, Fredericks AC, Tripathi S, Zhu T, Pintado-Silva J, Webb LG, Bernal-Rubio D, Solovyov A, Greenbaum B, Simon V, Basler CF, Mulder LCF, García-Sastre A, Fernandez-Sesma A. Dengue virus NS2B protein targets cGAS for degradation and prevents mitochondrial DNA sensing during infection. Nat Microbiol. 2017 Mar 27;2:17037.

98. Swarbrick CMD, Basavannacharya C, Chan KWK, Chan SA, Singh D, Wei N, Phoo WW, Luo D, Lescar J, Vasudevan SG. NS3 helicase from dengue virus specifically recognizes viral RNA sequence to ensure optimal replication. Nucleic Acids Res. 2017 Dec 15;45(22):12904–20.

99. Heaton NS, Perera R, Berger KL, Khadka S, Lacount DJ, Kuhn RJ, Randall G. Dengue virus nonstructural protein 3 redistributes fatty acid synthase to sites of viral replication and increases cellular fatty acid synthesis. Proc Natl Acad Sci U S A. 2010 Oct 5;107(40):17345–50.

100. Stabell AC, Meyerson NR, Gullberg RC, Gilchrist AR, Webb KJ, Old WM, Perera R, Sawyer SL. Dengue viruses cleave STING in humans but not in nonhuman primates, their presumed natural reservoir. Elife. 2018 Mar 20;7:e31919.

101. Roosendaal J, Westaway EG, Khromykh A, Mackenzie JM. Regulated cleavages at the West Nile virus NS4A-2K-NS4B junctions play a major role in rearranging cytoplasmic membranes and Golgi trafficking of the NS4A protein. J Virol. 2006 May;80(9):4623–32.

102. Mackenzie JM, Khromykh AA, Jones MK, Westaway EG. Subcellular localization and some biochemical properties of the flavivirus Kunjin nonstructural proteins NS2A and NS4A. Virology. 1998 Jun 5;245(2):203–15.

103. El Sahili A, Lescar J. Dengue Virus Non-Structural Protein 5. Viruses. 2017 Apr 24;9(4):91.

104. Issur M, Geiss BJ, Bougie I, Picard-Jean F, Despins S, Mayette J, Hobdey SE, Bisaillon M. The flavivirus NS5 protein is a true RNA guanylyltransferase that catalyzes a two-step reaction to form the RNA cap structure. RNA. 2009 Dec;15(12):2340–50.

105. Castillo Ramirez JA, Urcuqui-Inchima S. Dengue Virus Control of Type I IFN Responses: A History of Manipulation and Control. J Interferon Cytokine Res. 2015 Jun;35(6):421–30.

106. Khunchai S, Junking M, Suttitheptumrong A, Yasamut U, Sawasdee N, Netsawang J, Morchang A, Chaowalit P, Noisakran S, Yenchitsomanus PT, Limjindaporn T. Interaction of dengue virus nonstructural protein 5 with Daxx modulates RANTES production. Biochem Biophys Res Commun. 2012 Jun 29;423(2):398–403.

107. De Maio FA, Risso G, Iglesias NG, Shah P, Pozzi B, Gebhard LG, Mammi P, Mancini E, Yanovsky MJ, Andino R, Krogan N, Srebrow A, Gamarnik AV. The Dengue Virus NS5 Protein Intrudes in the Cellular Spliceosome and Modulates Splicing. PLoS Pathog. 2016 Aug;12(8):e1005841.

108. Acheson NH. Fundamentals of Molecular Virology. 2nd ed. Hoboken, NJ, U.S.: John Wiley & Sons Ltd; 2011. 528 p.

109. Ma Y, Nenkov M, Chen Y, Press AT, Kaemmerer E, Gassler N. Fatty acid metabolism and acyl-CoA synthetases in the liver-gut axis. World J Hepatol. 2021 Nov 27;13(11):1512–33.

110. Perera R, Riley C, Isaac G, Hopf-Jannasch AS, Moore RJ, Weitz KW, Pasa-Tolic L, Metz TO, Adamec J, Kuhn RJ. Dengue virus infection perturbs lipid homeostasis in infected mosquito cells. PLoS Pathog. 2012;8(3):e1002584.

111. Chotiwan N, Andre BG, Sanchez-Vargas I, Islam MN, Grabowski JM, Hopf-Jannasch A, Gough E, Nakayasu E, Blair CD, Belisle JT, Hill CA, Kuhn RJ, Perera R. Dynamic remodeling of lipids coincides with dengue virus replication in the midgut of *Aedes aegypti* mosquitoes. PLoS Pathog. 2018 Feb;14(2):e1006853.

112. van Meer G, Voelker DR, Feigenson GW. Membrane lipids: where they are and how they behave. Nat Rev Mol Cell Biol. 2008 Feb;9(2):112–24.

113. Gault CR, Obeid LM, Hannun YA. An overview of sphingolipid metabolism: from synthesis to breakdown. Adv Exp Med Biol. 2010;688:1–23.

114. Rivera R, Chun J. Biological effects of lysophospholipids. Rev Physiol Biochem Pharmacol. 2008;160:25–46.

115. Szule JA, Fuller NL, Peter Rand R. The Effects of Acyl Chain Length and Saturation of Diacylglycerols and Phosphatidylcholines on Membrane Monolayer Curvature. Biophysical Journal. 2002 Aug 1;83(2):977–84.

116. Adeva-Andany MM, Carneiro-Freire N, Seco-Filgueira M, Fernández-Fernández C, Mouriño-Bayolo D. Mitochondrial β-oxidation of saturated fatty acids in humans. Mitochondrion. 2019 May;46:73–90.

117. Cui L, Lee YH, Kumar Y, Xu F, Lu K, Ooi EE, Tannenbaum SR, Ong CN. Serum Metabolome and Lipidome Changes in Adult Patients with Primary Dengue Infection. PLoS Negl Trop Dis. 2013 Aug 15;7(8):e2373.

118. Villamor E, Villar LA, Lozano A, Herrera VM, Herrán OF. Serum fatty acids and progression from dengue fever to dengue hemorrhagic fever / dengue shock syndrome. Br J Nutr. 2018 Oct;120(7):787–96.

119. Gullberg RC, Steel JJ, Pujari V, Rovnak J, Crick DC, Perera R. Stearoly-CoA desaturase 1 differentiates early and advanced dengue virus infections and determines virus particle infectivity. PLoS Pathog. 2018 Aug;14(8):e1007261.

120. Hannun YA, Obeid LM. Sphingolipids and their metabolism in physiology and disease. Nat Rev Mol Cell Biol. 2018 Mar;19(3):175–91.

121. Aktepe TE, Pham H, Mackenzie JM. Differential utilisation of ceramide during replication of the flaviviruses West Nile and dengue virus. Virology. 2015 Oct 1;484:241–50.

122. Al-Shujairi WH, Clarke JN, Davies LT, Pitman MR, Calvert JK, Aloia AL, Pitson SM, Carr JM. In vitro and in vivo roles of sphingosine kinase 2 during dengue virus infection. J Gen Virol. 2019 Apr;100(4):629–41.

123. Aloia AL, Calvert JK, Clarke JN, Davies LT, Helbig KJ, Pitson SM, Carr JM. Investigation of sphingosine kinase 1 in interferon responses during dengue virus infection. Clin Transl Immunology. 2017 Jul;6(7):e151.

124. Clarke JN, Davies LK, Calvert JK, Gliddon BL, Shujari WHA, Aloia AL, Helbig KJ, Beard MR, Pitson SM, Carr JMY 2016. Reduction in sphingosine kinase 1 influences the susceptibility to dengue virus infection by altering antiviral responses. Journal of General Virology. 97(1):95–109.

125. Morchang A, Lee RCH, Yenchitsomanus PT, Sreekanth GP, Noisakran S, Chu JJH, Limjindaporn T. RNAi screen reveals a role of SPHK2 in dengue virus-mediated apoptosis in hepatic cell lines. PLoS One. 2017;12(11):e0188121.

126. Luo J, Yang H, Song BL. Mechanisms and regulation of cholesterol homeostasis. Nat Rev Mol Cell Biol. 2020 Apr;21(4):225–45.

127. Ripa I, Andreu S, López-Guerrero JA, Bello-Morales R. Membrane Rafts: Portals for Viral Entry. Frontiers in Microbiology. 2021;12.

128. Lee CJ, Lin HR, Liao CL, Lin YL. Cholesterol Effectively Blocks Entry of Flavivirus. J Virol. 2008 Jul;82(13):6470–80.

129. Poh MK, Shui G, Xie X, Shi PY, Wenk MR, Gu F. U18666A, an intra-cellular cholesterol transport inhibitor, inhibits dengue virus entry and replication. Antiviral Research. 2012 Jan 1;93(1):191–8.

130. Soto-Acosta R, Mosso C, Cervantes-Salazar M, Puerta-Guardo H, Medina F, Favari L, Ludert JE, del Angel RM. The increase in cholesterol levels at early stages after dengue

virus infection correlates with an augment in LDL particle uptake and HMG-CoA reductase activity. Virology. 2013 Aug 1;442(2):132–47.

131. Soto-Acosta R, Bautista-Carbajal P, Cervantes-Salazar M, Angel-Ambrocio AH, Del Angel RM. DENV up-regulates the HMG-CoA reductase activity through the impairment of AMPK phosphorylation: A potential antiviral target. PLoS Pathog. 2017 Apr;13(4):e1006257.

132. Rothwell C, Lebreton A, Young Ng C, Lim JYH, Liu W, Vasudevan S, Labow M, Gu F, Gaither LA. Cholesterol biosynthesis modulation regulates dengue viral replication. Virology. 2009 Jun 20;389(1–2):8–19.

133. Mackenzie JM, Khromykh AA, Parton RG. Cholesterol Manipulation by West Nile Virus Perturbs the Cellular Immune Response. Cell Host & Microbe. 2007 Oct 11;2(4):229–39.

134. Carro AC, Damonte EB. Requirement of cholesterol in the viral envelope for dengue virus infection. Virus Res. 2013 Jun;174(1–2):78–87.

135. Jones W, Bianchi K. Aerobic Glycolysis: Beyond Proliferation. Front Immunol. 2015 May 15;6:227.

136. Fontaine KA, Sanchez EL, Camarda R, Lagunoff M. Dengue virus induces and requires glycolysis for optimal replication. J Virol. 2015 Feb;89(4):2358–66.

137. Shestov AA, Liu X, Ser Z, Cluntun AA, Hung YP, Huang L, Kim D, Le A, Yellen G, Albeck JG, Locasale JW. Quantitative determinants of aerobic glycolysis identify flux through the enzyme GAPDH as a limiting step. eLife. 2014 Jul 9;3:e03342.

138. Tristan C, Shahani N, Sedlak TW, Sawa A. The diverse functions of GAPDH: views from different subcellular compartments. Cell Signal. 2011 Feb;23(2):317–23.

139. Allonso D, Andrade IS, Conde JN, Coelho DR, Rocha DCP, da Silva ML, Ventura GT, Silva EM, Mohana-Borges R. Dengue Virus NS1 Protein Modulates Cellular Energy Metabolism by Increasing Glyceraldehyde-3-Phosphate Dehydrogenase Activity. J Virol. 2015 Sep 16;89(23):11871–83.

140. Silva EM, Conde JN, Allonso D, Ventura GT, Coelho DR, Carneiro PH, Silva ML, Paes MV, Rabelo K, Weissmuller G, Bisch PM, Mohana-Borges R. Dengue virus nonstructural 3 protein interacts directly with human glyceraldehyde-3-phosphate dehydrogenase (GAPDH) and reduces its glycolytic activity. Sci Rep. 2019 Feb 25;9:2651.

141. Fernandes-Siqueira LO, Zeidler JD, Sousa BG, Ferreira T, Da Poian AT. Anaplerotic Role of Glucose in the Oxidation of Endogenous Fatty Acids during Dengue Virus Infection. mSphere. 2018 Jan 31;3(1):e00458-17.

142. Prochownik EV, Wang H. The Metabolic Fates of Pyruvate in Normal and Neoplastic Cells. Cells. 2021 Mar 30;10(4):762.

143. Zheng H, Wu J, Jin Z, Yan LJ. Protein Modifications as Manifestations of Hyperglycemic Glucotoxicity in Diabetes and Its Complications. Biochem Insights. 2016 Mar 23;9:1–9.

144. Martínez-Reyes I, Chandel NS. Mitochondrial TCA cycle metabolites control physiology and disease. Nat Commun. 2020 Jan 3;11(1):102.

145. Shahfiza N, Osman H, Hock TT, Abdel-Hamid AHZ. Metabolomics approach for multibiomarkers determination to investigate dengue virus infection in human patients. Acta Biochimica Polonica. 2017 Jul 11;64(2):215–9.

146. Werner C, Doenst T, Schwarzer M. Chapter 4 - Metabolic Pathways and Cycles. In: Schwarzer M, Doenst T, editors. The Scientist's Guide to Cardiac Metabolism. Boston: Academic Press; 2016. p. 39–55.

147. Barbier V, Lang D, Valois S, Rothman AL, Medin CL. Dengue virus induces mitochondrial elongation through impairment of Drp1-triggered mitochondrial fission. Virology. 2017 Jan;500:149–60.

148. Chatel-Chaix L, Cortese M, Romero-Brey I, Bender S, Neufeldt CJ, Fischl W, Scaturro P, Schieber N, Schwab Y, Fischer B, Ruggieri A, Bartenschlager R. Dengue Virus Perturbs Mitochondrial Morphodynamics to Dampen Innate Immune Responses. Cell Host Microbe. 2016 Sep 14;20(3):342–56.

149. Rambold AS, Cohen S, Lippincott-Schwartz J. Fatty Acid Trafficking in Starved Cells: Regulation by Lipid Droplet Lipolysis, Autophagy, and Mitochondrial Fusion Dynamics. Developmental Cell. 2015 Mar 23;32(6):678–92.

150. Song JE, Alves TC, Stutz B, Šestan-Peša M, Kilian N, Jin S, Diano S, Kibbey RG, Horvath TL. Mitochondrial Fission Governed by Drp1 Regulates Exogenous Fatty Acid Usage and Storage in Hela Cells. Metabolites. 2021 May 18;11(5):322.

151. Ge T, Yang J, Zhou S, Wang Y, Li Y, Tong X. The Role of the Pentose Phosphate Pathway in Diabetes and Cancer. Frontiers in Endocrinology. 2020;11.

152. Yang HC, Ma TH, Tjong WY, Stern A, Chiu DTY. G6PD deficiency, redox homeostasis, and viral infections: implications for SARS-CoV-2 (COVID-19). Free Radic Res. :1–11.

153. Al-Alimi AA, Ali SA, Al-Hassan FM, Idris FM, Teow SY, Mohd Yusoff N. Dengue virus type 2 (DENV2)-induced oxidative responses in monocytes from glucose-6-phosphate dehydrogenase (G6PD)-deficient and G6PD normal subjects. PLoS Negl Trop Dis. 2014 Mar;8(3):e2711.

154. Chao YC, Huang CS, Lee CN, Chang SY, King CC, Kao CL. Higher infection of dengue virus serotype 2 in human monocytes of patients with G6PD deficiency. PLoS One. 2008 Feb 13;3(2):e1557.

155. May WL, Kyaw MP, Blacksell SD, Pukrittayakamee S, Chotivanich K, Hanboonkunupakarn B, Thein KN, Lim CS, Thaipadungpanit J, Althaus T, Jittamala P. Impact of glucose-6-phosphate dehydrogenase deficiency on dengue infection in Myanmar children. PLoS One. 2019;14(1):e0209204.

156. Muri J, Kopf M. Redox regulation of immunometabolism. Nat Rev Immunol. 2021 Jun;21(6):363–81.

157. Kundu M, Thompson CB. Autophagy: basic principles and relevance to disease. Annu Rev Pathol. 2008;3:427–55.

158. Choi Y, Bowman JW, Jung JU. Autophagy during viral infection — a double-edged sword. Nat Rev Microbiol. 2018;16(6):341–54.

159. Khakpoor A, Panyasrivanit M, Wikan N, Smith DR. A role for autophagolysosomes in dengue virus 3 production in HepG2 cells. J Gen Virol. 2009 May;90(Pt 5):1093–103.

160. Mateo R, Nagamine CM, Spagnolo J, Méndez E, Rahe M, Gale M, Yuan J, Kirkegaard K. Inhibition of cellular autophagy deranges dengue virion maturation. J Virol. 2013 Feb;87(3):1312–21.

161. McLean JE, Wudzinska A, Datan E, Quaglino D, Zakeri Z. Flavivirus NS4A-induced autophagy protects cells against death and enhances virus replication. J Biol Chem. 2011 Jun 24;286(25):22147–59.

162. Heaton NS, Randall G. Dengue virus-induced autophagy regulates lipid metabolism. Cell Host Microbe. 2010 Nov 18;8(5):422–32.

163. Panyasrivanit M, Khakpoor A, Wikan N, Smith DR. Co-localization of constituents of the dengue virus translation and replication machinery with amphisomes. J Gen Virol. 2009 Feb;90(Pt 2):448–56.

164. Di Mattia T, Tomasetto C, Alpy F. Faraway, so close! Functions of Endoplasmic reticulum-Endosome contacts. Biochim Biophys Acta Mol Cell Biol Lipids. 2020 Jan;1865(1):158490.

165. Friedman J, DiBenedetto JR, West M, Rowland AA, Voeltz G. Endoplasmic reticulum–endosome contact increases as endosomes traffic and mature. Molecular biology of the cell. 2013;

166. Reyes-Ruiz JM, Osuna-Ramos JF, De Jesús-González LA, Palacios-Rápalo SN, Cordero-Rivera CD, Farfan-Morales CN, Hurtado-Monzón AM, Gallardo-Flores CE, Alcaraz-Estrada SL, Salas-Benito JS, del Ángel RM. The Regulation of Flavivirus Infection by Hijacking Exosome-Mediated Cell–Cell Communication: New Insights on Virus–Host Interactions. Viruses. 2020 Jul 16;12(7):765.

167. Raudenska M, Balvan J, Masarik M. Crosstalk between autophagy inhibitors and endosome-related secretory pathways: a challenge for autophagy-based treatment of solid cancers. Mol Cancer. 2021 Oct 27;20(1):140.

168. Wu YW, Mettling C, Wu SR, Yu CY, Perng GC, Lin YS, Lin YL. Autophagy-associated dengue vesicles promote viral transmission avoiding antibody neutralization. Sci Rep. 2016 Aug 25;6:32243.

169. Wu SY, Chen YL, Lee YR, Lin CF, Lan SH, Lan KY, Chu ML, Lin PW, Yang ZL, Chen YH, Wang WH, Liu HS. The Autophagosomes Containing Dengue Virus Proteins and Full-Length Genomic RNA Are Infectious. Viruses. 2021 Oct 9;13(10):2034.

170. Li MY, Naik TS, Siu LYL, Acuto O, Spooner E, Wang P, Yang X, Lin Y, Bruzzone R, Ashour J, Evans MJ, Sanyal S. Lyn kinase regulates egress of flaviviruses in autophagosome-derived organelles. Nat Commun. 2020 Oct 15;11(1):5189.

171. Clarke SD, Nakamura MT. Lipids | Fatty Acid Structure and Synthesis. In: Jez J, editor. Encyclopedia of Biological Chemistry III (Third Edition). Oxford: Elsevier; 2013. p. 478–82.

172. Asturias FJ, Chadick JZ, Cheung IK, Stark H, Witkowski A, Joshi AK, Smith S. Structure and molecular organization of mammalian fatty acid synthase. Nat Struct Mol Biol. 2005 Mar;12(3):225–32.

173. Strauss E. 7.11 - Coenzyme A Biosynthesis and Enzymology. In: Liu HW (Ben), Mander L, editors. Comprehensive Natural Products II. Oxford: Elsevier; 2010. p. 351–410.

174. Brown HA, Marnett LJ. Introduction to Lipid Biochemistry, Metabolism, and Signaling. Chem Rev. 2011 Oct 12;111(10):5817–20.

175. Igal RA, Sinner DI. Stearoyl-CoA desaturase 5 (SCD5), a Δ-9 fatty acyl desaturase in search of a function. Biochim Biophys Acta Mol Cell Biol Lipids. 2021 Jan;1866(1):158840.

176. van Meer G, Voelker DR, Feigenson GW. Membrane lipids: where they are and how they behave. Nat Rev Mol Cell Biol. 2008 Feb;9(2):112–24.

177. Rivera R, Chun J. Biological effects of lysophospholipids. Rev Physiol Biochem Pharmacol. 2008;160:25–46.

178. Brown HA, Marnett LJ. Introduction to Lipid Biochemistry, Metabolism, and Signaling. Chem Rev. 2011 Oct 12;111(10):5817–20.

179. Alves-Bezerra M, Cohen DE. Triglyceride metabolism in the liver. Compr Physiol. 2017 Dec 12;8(1):1–8.

180. Coleman RA, Lee DP. Enzymes of triacylglycerol synthesis and their regulation. Prog Lipid Res. 2004 Mar;43(2):134–76.

181. Hall AM, Kou K, Chen Z, Pietka TA, Kumar M, Korenblat KM, Lee K, Ahn K, Fabbrini E, Klein S, Goodwin B, Finck BN. Evidence for regulated monoacylglycerol acyltransferase expression and activity in human liver. J Lipid Res. 2012 May;53(5):990–9.

182. Henneberry AL, Wright MM, McMaster CR. The Major Sites of Cellular Phospholipid Synthesis and Molecular Determinants of Fatty Acid and Lipid Head Group Specificity. Mol Biol Cell. 2002 Sep;13(9):3148–61.

183. Blunsom NJ, Cockcroft S. CDP-Diacylglycerol Synthases (CDS): Gateway to Phosphatidylinositol and Cardiolipin Synthesis. Frontiers in Cell and Developmental Biology. 2020;8.

184. Gibellini F, Smith TK. The Kennedy pathway—De novo synthesis of phosphatidylethanolamine and phosphatidylcholine. IUBMB Life. 2010;62(6):414–28.

185. Hishikawa D, Hashidate T, Shimizu T, Shindou H. Diversity and function of membrane glycerophospholipids generated by the remodeling pathway in mammalian cells. J Lipid Res. 2014 May;55(5):799–807.

186. Grevengoed TJ, Klett EL, Coleman RA. Acyl-CoA Metabolism and Partitioning. Annu Rev Nutr. 2014;34:1–30.

187. Kirkby B, Roman N, Kobe B, Kellie S, Forwood JK. Functional and structural properties of mammalian acyl-coenzyme A thioesterases. Prog Lipid Res. 2010 Oct;49(4):366–77.

188. Jani S, Da Eira D, Hadday I, Bikopoulos G, Mohasses A, de Pinho RA, Ceddia RB. Distinct mechanisms involving diacylglycerol, ceramides, and inflammation underlie insulin resistance in oxidative and glycolytic muscles from high fat-fed rats. Sci Rep. 2021 Sep 27;11(1):19160.

189. Swarbrick CMD, Nanson JD, Patterson EI, Forwood JK. Structure, function, and regulation of thioesterases. Prog Lipid Res. 2020 Jul;79:101036.

190. Wakil SJ, Abu-Elheiga LA. Fatty acid metabolism: target for metabolic syndrome. J Lipid Res. 2009 Apr;50(Suppl):S138–43.

191. Tillander V, Alexson SEH, Cohen DE. Deactivating Fatty Acids: Acyl-CoA Thioesterase-Mediated Control of Lipid Metabolism. Trends Endocrinol Metab. 2017 Jul;28(7):473–84.

192. Hunt MC, Rautanen A, Westin MAK, Svensson LT, Alexson SEH. Analysis of the mouse and human acyl-CoA thioesterase (ACOT) gene clusters shows that convergent, functional evolution results in a reduced number of human peroxisomal ACOTs. FASEB J. 2006 Sep;20(11):1855–64.

193. Brocker C, Carpenter C, Nebert DW, Vasiliou V. Evolutionary divergence and functions of the human acyl-CoA thioesterase gene (ACOT) family. Hum Genomics. 2010 Aug;4(6):411–20.

194. Bekeova C, Anderson-Pullinger L, Boye K, Boos F, Sharpadskaya Y, Herrmann JM, Seifert EL. Multiple mitochondrial thioesterases have distinct tissue and substrate specificity and CoA regulation, suggesting unique functional roles. J Biol Chem. 2019 Dec 13;294(50):19034–47.

195. Svensson LT, Engberg ST, Aoyama T, Usuda N, Alexson SE, Hashimoto T. Molecular cloning and characterization of a mitochondrial peroxisome proliferator-induced acyl-CoA thioesterase from rat liver. Biochem J. 1998 Feb 1;329 (Pt 3):601–8.

196. Moffat C, Bhatia L, Nguyen T, Lynch P, Wang M, Wang D, Ilkayeva OR, Han X, Hirschey MD, Claypool SM, Seifert EL. Acyl-CoA thioesterase-2 facilitates mitochondrial fatty acid oxidation in the liver. J Lipid Res. 2014 Dec;55(12):2458–70.

197. Hunt MC, Siponen MI, Alexson SEH. The emerging role of acyl-CoA thioesterases and acyltransferases in regulating peroxisomal lipid metabolism. Biochim Biophys Acta. 2012 Sep;1822(9):1397–410.

198. Yang S, Chen C, Wang H, Rao X, Wang F, Duan Q, Chen F, Long G, Gong W, Zou MH, Wang DW. Protective effects of Acyl-coA thioesterase 1 on diabetic heart via PPARα/PGC1α signaling. PLoS One. 2012;7(11):e50376.

199. Franklin MP, Sathyanarayan A, Mashek DG. Acyl-CoA Thioesterase 1 (ACOT1) Regulates PPARα to Couple Fatty Acid Flux With Oxidative Capacity During Fasting. Diabetes. 2017 Aug;66(8):2112–23.

200. Jay AG, Simard JR, Huang N, Hamilton JA. SSO and other putative inhibitors of FA transport across membranes by CD36 disrupt intracellular metabolism, but do not affect FA translocation. Journal of Lipid Research. 2020 May 1;61(5):790–807.

201. Zechner R, Zimmermann R, Eichmann TO, Kohlwein SD, Haemmerle G, Lass A, Madeo F. FAT SIGNALS - Lipases and Lipolysis in Lipid Metabolism and Signaling. Cell Metab. 2012 Mar 7;15(3):279–91.

202. Wanders RJA, Waterham HR, Ferdinandusse S. Metabolic Interplay between Peroxisomes and Other Subcellular Organelles Including Mitochondria and the Endoplasmic Reticulum. Frontiers in Cell and Developmental Biology. 2016;3.

203. Futerman AH. Chapter 10 - Sphingolipids. In: Ridgway ND, McLeod RS, editors. Biochemistry of Lipids, Lipoproteins and Membranes (Sixth Edition). Boston: Elsevier; 2016. p. 297–326.

204. Hannun YA, Obeid LM. Principles of bioactive lipid signalling: lessons from sphingolipids. Nat Rev Mol Cell Biol. 2008 Feb;9(2):139–50.

205. Vos JP, Lopes-Cardozo M, Gadella BM. Metabolic and functional aspects of sulfogalactolipids. Biochim Biophys Acta. 1994 Mar 3;1211(2):125–49.

206. Merrill AH. Sphingolipid and Glycosphingolipid Metabolic Pathways in the Era of Sphingolipidomics. Chem Rev. 2011 Oct 12;111(10):6387–422.

207. Lippincott-Schwartz J, Phair RD. Lipids and Cholesterol as Regulators of Traffic in the Endomembrane System. Annu Rev Biophys. 2010 Jun 9;39:559–78.

208. Prinz WA. Bridging the gap: membrane contact sites in signaling, metabolism, and organelle dynamics. J Cell Biol. 2014 Jun 23;205(6):759–69.

209. Young MM, Wang HG. Sphingolipids as Regulators of Autophagy and Endocytic Trafficking. Adv Cancer Res. 2018;140:27–60.

210. Körschen HG, Yildiz Y, Raju DN, Schonauer S, Bönigk W, Jansen V, Kremmer E, Kaupp UB, Wachten D. The non-lysosomal β-glucosidase GBA2 is a non-integral membrane-associated protein at the endoplasmic reticulum (ER) and Golgi. J Biol Chem. 2013 Feb 1;288(5):3381–93.

211. Woeste MA, Wachten D. The Enigmatic Role of GBA2 in Controlling Locomotor Function. Frontiers in Molecular Neuroscience. 2017;10.

212. Subramanian P, Stahelin RV, Szulc Z, Bielawska A, Cho W, Chalfant CE. Ceramide 1-Phosphate Acts as a Positive Allosteric Activator of Group IVA Cytosolic Phospholipase A2α and Enhances the Interaction of the Enzyme with Phosphatidylcholine *. Journal of Biological Chemistry. 2005 May 6;280(18):17601–7.

213. Spiegel S, Milstien S. The outs and the ins of sphingosine-1-phosphate in immunity. Nat Rev Immunol. 2011 Jun;11(6):403–15.

214. Platt FM, d'Azzo A, Davidson BL, Neufeld EF, Tifft CJ. Lysosomal storage diseases. Nat Rev Dis Primers. 2018 Oct 1;4(1):27.

215. Vanier MT. Chapter 176 - Niemann–Pick diseases. In: Dulac O, Lassonde M, Sarnat HB, editors. Handbook of Clinical Neurology. Elsevier; 2013. p. 1717–21. (Pediatric Neurology Part III; vol. 113).

216. Platt FM. Emptying the stores: lysosomal diseases and therapeutic strategies. Nat Rev Drug Discov. 2018 Feb;17(2):133–50.

217. Avota E, Bodem J, Chithelen J, Mandasari P, Beyersdorf N, Schneider-Schaulies J. The Manifold Roles of Sphingolipids in Viral Infections. Front Physiol. 2021 Sep 29;12:715527.

218. Ng CG, Griffin DE. Acid sphingomyelinase deficiency increases susceptibility to fatal alphavirus encephalomyelitis. J Virol. 2006 Nov;80(22):10989–99.

219. Carpinteiro A, Gripp B, Hoffmann M, Pöhlmann S, Hoertel N, Edwards MJ, Kamler M, Kornhuber J, Becker KA, Gulbins E. Inhibition of acid sphingomyelinase by ambroxol prevents SARS-CoV-2 entry into epithelial cells. J Biol Chem. 2021 Jun;296:100701.

220. Vitner EB, Achdout H, Avraham R, Politi B, Cherry L, Tamir H, Yahalom-Ronen Y, Paran N, Melamed S, Erez N, Israely T. Glucosylceramide synthase inhibitors prevent replication of SARS-CoV-2 and influenza virus. J Biol Chem. 2021 Feb 25;296:100470.

221. Schneider-Schaulies J, Schneider-Schaulies S. Viral infections and sphingolipids. Handb Exp Pharmacol. 2013;(216):321–40.

222. Khan I, Katikaneni DS, Han Q, Sanchez-Felipe L, Hanada K, Ambrose RL, Mackenzie JM, Konan KV. Modulation of hepatitis C virus genome replication by glycosphingolipids and four-phosphate adaptor protein 2. J Virol. 2014 Nov;88(21):12276–95.

223. Molloy JC, Sommer U, Viant MR, Sinkins SP. Wolbachia Modulates Lipid Metabolism in *Aedes albopictus* Mosquito Cells. Appl Environ Microbiol. 2016 May 15;82(10):3109–20.

224. Suvarna JC, Rane PP. Serum lipid profile: a predictor of clinical outcome in dengue infection. Trop Med Int Health. 2009 May;14(5):576–85.

225. Holthuis JCM, Levine TP. Lipid traffic: floppy drives and a superhighway. Nat Rev Mol Cell Biol. 2005 Mar;6(3):209–20.

226. Jackson CL, Walch L, Verbavatz JM. Lipids and Their Trafficking: An Integral Part of Cellular Organization. Developmental Cell. 2016 Oct;39(2):139–53.

227. Maxfield FR, Hao M. Lipid Trafficking in Cells. In: Roberts GCK, editor. Encyclopedia of Biophysics. Berlin, Heidelberg: Springer; 2013. p. 1289–96.

228. Wong LH, Gatta AT, Levine TP. Lipid transfer proteins: the lipid commute via shuttles, bridges and tubes. Nat Rev Mol Cell Biol. 2019 Feb;20(2):85–101.

229. Schauer R, Kamerling JP. Exploration of the Sialic Acid World. Adv Carbohydr Chem Biochem. 2018;75:1–213.

230. Varki A, Schnaar RL, Schauer R. Sialic Acids and Other Nonulosonic Acids. In: Varki A, Cummings RD, Esko JD, Stanley P, Hart GW, Aebi M, Darvill AG, Kinoshita T, Packer NH, Prestegard JH, Schnaar RL, Seeberger PH, editors. Essentials of Glycobiology. 3rd ed. Cold Spring Harbor (NY): Cold Spring Harbor Laboratory Press; 2015.

231. Monti E, Miyagi T. Structure and Function of Mammalian Sialidases. In: Gerardy-Schahn R, Delannoy P, von Itzstein M, editors. SialoGlyco Chemistry and Biology I: Biosynthesis, structural diversity and sialoglycopathologies. Berlin, Heidelberg: Springer; 2015. p. 183–208. (Topics in Current Chemistry).

232. Ushiyama A, Kataoka H, Iijima T. Glycocalyx and its involvement in clinical pathophysiologies. J Intensive Care. 2016;4(1):59.

233. Kumar P, Shen Q, Pivetti CD, Lee ES, Wu MH, Yuan SY. Molecular mechanisms of endothelial hyperpermeability: implications in inflammation. Expert Rev Mol Med. 2009 Jun 30;11:e19.

234. Miyagi T, Yamaguchi K. Mammalian sialidases: physiological and pathological roles in cellular functions. Glycobiology. 2012 Jul;22(7):880–96.

235. Weigel PH, Yik JHN. Glycans as endocytosis signals: the cases of the asialoglycoprotein and hyaluronan/chondroitin sulfate receptors. Biochimica et Biophysica Acta (BBA) - General Subjects. 2002 Sep 19;1572(2):341–63.

236. Amith SR, Jayanth P, Finlay T, Franchuk S, Gilmour A, Abdulkhalek S, Szewczuk MR. Detection of Neu1 sialidase activity in regulating Toll-like receptor activation. J Vis Exp. 2010 Sep 7;(43):2142.

237. Natori Y, Nasui M, Edo K, Sato S, Sakurai T, Kizaki T, Kihara-Negishi F. NEU1 sialidase controls gene expression and secretion of IL-6 and MCP-1 through NF-κB pathway in 3T3-L1 adipocytes. J Biochem. 2017 Aug 1;162(2):137–43.

238. Seyrantepe V, Iannello A, Liang F, Kanshin E, Jayanth P, Samarani S, Szewczuk MR, Ahmad A, Pshezhetsky AV. Regulation of phagocytosis in macrophages by neuraminidase 1. J Biol Chem. 2010 Jan 1;285(1):206–15.

239. Glanz VY, Myasoedova VA, Grechko AV, Orekhov AN. Sialidase activity in human pathologies. Eur J Pharmacol. 2019 Jan 5;842:345–50.

240. Funakoshi Y, Suzuki T. Glycobiology in the cytosol: the bitter side of a sweet world. Biochim Biophys Acta. 2009 Feb;1790(2):81–94.

241. Oh M, Ha DI, Son C, Kang JG, Hwang H, Moon SB, Kim M, Nam J, Kim JS, Song SY, Kim YS, Park S, Yoo JS, Ko JH, Park K. Defect in cytosolic Neu2 sialidase abrogates lipid metabolism and impairs muscle function in vivo. Sci Rep. 2022 Feb 25;12:3216.

242. Grewal T, Bartlett A, Burgess JW, Packer NH, Stanley KK. Desialylated LDL uptake in human and mouse macrophages can be mediated by a lectin receptor. Atherosclerosis. 1996 Mar;121(1):151–63.

243. Demina EP, Smutova V, Pan X, Fougerat A, Guo T, Zou C, Chakraberty R, Snarr BD, Shiao TC, Roy R, Orekhov AN, Miyagi T, Laffargue M, Sheppard DC, Cairo CW, Pshezhetsky AV. Neuraminidases 1 and 3 Trigger Atherosclerosis by Desialylating Low-Density Lipoproteins and Increasing Their Uptake by Macrophages. J Am Heart Assoc. 2021 Feb 16;10(4):e018756.

244. Takahashi K, Mitoma J, Hosono M, Shiozaki K, Sato C, Yamaguchi K, Kitajima K, Higashi H, Nitta K, Shima H, Miyagi T. Sialidase NEU4 hydrolyzes polysialic acids of neural cell adhesion molecules and negatively regulates neurite formation by hippocampal neurons. J Biol Chem. 2012 Apr 27;287(18):14816–26.

245. Dou D, Revol R, Östbye H, Wang H, Daniels R. Influenza A Virus Cell Entry, Replication, Virion Assembly and Movement. Front Immunol. 2018 Jul 20;9:1581.

246. Varki A. Sialic acids in human health and disease. Trends Mol Med. 2008 Aug;14(8):351–60.

247. Role of receptor binding specificity in influenza A virus transmission and pathogenesis. The EMBO Journal. 2014 Apr 16;33(8):823–41.

248. Tan CW, Huan Hor CH, Kwek SS, Tee HK, Sam IC, Goh ELK, Ooi EE, Chan YF, Wang LF. Cell surface α2,3-linked sialic acid facilitates Zika virus internalization. Emerg Microbes Infect. 2019;8(1):426–37.

249. Burke JM, St Clair LA, Perera R, Parker R. SARS-CoV-2 infection triggers widespread host mRNA decay leading to an mRNA export block. RNA. 2021 Nov;27(11):1318–29.

250. Neufeldt CJ, Cortese M, Acosta EG, Bartenschlager R. Rewiring cellular networks by members of the Flaviviridae family. Nat Rev Microbiol. 2018 Feb 12;16(3):125–42.

251. Chatel-Chaix L, Bartenschlager R. Dengue virus- and hepatitis C virus-induced replication and assembly compartments: the enemy inside--caught in the web. J Virol. 2014 Jun;88(11):5907–11.

252. Gillespie LK, Hoenen A, Morgan G, Mackenzie JM. The endoplasmic reticulum provides the membrane platform for biogenesis of the flavivirus replication complex. J Virol. 2010 Oct;84(20):10438–47.

253. Jung SH, Lee HC, Hwang HJ, Park HA, Moon YA, Kim BC, Lee HM, Kim KP, Kim YN, Lee BL, Lee JC, Ko YG, Park HJ, Lee JS. Acyl-CoA thioesterase 7 is involved in cell cycle progression via regulation of PKCζ-p53-p21 signaling pathway. Cell Death Dis. 2017 May 18;8(5):e2793.

254. Wang F, Wu J, Qiu Z, Ge X, Liu X, Zhang C, Xu W, Wang F, Hua D, Qi X, Mao Y. ACOT1 expression is associated with poor prognosis in gastric adenocarcinoma. Hum Pathol. 2018 Jul;77:35–44.

255. Ellis JM, Wong GW, Wolfgang MJ. Acyl coenzyme A thioesterase 7 regulates neuronal fatty acid metabolism to prevent neurotoxicity. Mol Cell Biol. 2013 May;33(9):1869–82.

256. Kinney RM, Butrapet S, Chang GJ, Tsuchiya KR, Roehrig JT, Bhamarapravati N, Gubler DJ. Construction of infectious cDNA clones for dengue 2 virus: strain 16681 and its attenuated vaccine derivative, strain PDK-53. Virology. 1997 Apr 14;230(2):300–8.

257. Samsa MM, Mondotte JA, Iglesias NG, Assunção-Miranda I, Barbosa-Lima G, Da Poian AT, Bozza PT, Gamarnik AV. Dengue virus capsid protein usurps lipid droplets for viral particle formation. PLoS Pathog. 2009 Oct;5(10):e1000632.

258. Fujita M, Momose A, Ohtomo T, Nishinosono A, Tanonaka K, Toyoda H, Morikawa M, Yamada J. Upregulation of Fatty Acyl-CoA Thioesterases in the Heart and Skeletal Muscle of Rats Fed a High-Fat Diet. Biological and Pharmaceutical Bulletin. 2011;34(1):87–91.

259. Cook KC, Moreno JA, Jean Beltran PM, Cristea IM. Peroxisome Plasticity at the Virus-Host Interface. Trends Microbiol. 2019 Nov;27(11):906–14.

260. You J, Hou S, Malik-Soni N, Xu Z, Kumar A, Rachubinski RA, Frappier L, Hobman TC. Flavivirus Infection Impairs Peroxisome Biogenesis and Early Antiviral Signaling. J Virol. 2015 Dec;89(24):12349–61.

261. Blight KJ, McKeating JA, Rice CM. Highly permissive cell lines for subgenomic and genomic hepatitis C virus RNA replication. J Virol. 2002 Dec;76(24):13001–14.

262. Yoksan S, Bhamarapravati N, Halstead SB. Dengue virus vaccine development: study on biological markers of uncloned dengue 1-4 viruses serially passaged in primary kidney cells. In: Arbovirus research in Australia Proceedings of the Fourth Symposium. Brisbane, Australia: CSIRO/QIMR; p. 35–8.

263. Dulbecco R, Vogt M. Some problems of animal virology as studied by the plaque technique. Cold Spring Harb Symp Quant Biol. 1953;18:273–9.

264. Livak KJ, Schmittgen TD. Analysis of relative gene expression data using real-time quantitative PCR and the 2(-Delta Delta C(T)) Method. Methods. 2001 Dec;25(4):402–8.

265. Angata T, Varki A. Chemical Diversity in the Sialic Acids and Related α-Keto Acids: An Evolutionary Perspective. Chem Rev. 2002 Feb 1;102(2):439–70.

266. Byrne B, Donohoe GG, O'Kennedy R. Sialic acids: carbohydrate moieties that influence the biological and physical properties of biopharmaceutical proteins and living cells. Drug Discovery Today. 2007 Apr 1;12(7):319–26.

267. Varki A, Gagneux P. Multifarious roles of sialic acids in immunity. Ann N Y Acad Sci. 2012 Apr;1253(1):16–36.

268. Smutova V, Albohy A, Pan X, Korchagina E, Miyagi T, Bovin N, Cairo CW, Pshezhetsky AV. Structural Basis for Substrate Specificity of Mammalian Neuraminidases. PLoS One. 2014 Sep 15;9(9):e106320.

269. Yuan L, Zhao Y, Sun XL. Sialidase substrates for Sialdiase assays - activity, specificity, quantification and inhibition. Glycoconj J. 2020 Oct;37(5):513–31.

270. Monti E, Bonten E, D'Azzo A, Bresciani R, Venerando B, Borsani G, Schauer R, Tettamanti G. Sialidases in vertebrates: a family of enzymes tailored for several cell functions. Adv Carbohydr Chem Biochem. 2010;64:403–79.

271. Lipničanová S, Chmelová D, Ondrejovič M, Frecer V, Miertuš S. Diversity of sialidases found in the human body - A review. Int J Biol Macromol. 2020 Apr 1;148:857–68.

272. Zou Z, Chastain A, Moir S, Ford J, Trandem K, Martinelli E, Cicala C, Crocker P, Arthos J, Sun PD. Siglecs Facilitate HIV-1 Infection of Macrophages through Adhesion with Viral Sialic Acids. PLoS One. 2011 Sep 8;6(9):e24559.

273. Matrosovich M, Herrler G, Klenk HD. Sialic Acid Receptors of Viruses. SialoGlyco Chemistry and Biology II. 2013 Jul 20;367:1–28.

274. Miyagi T, Takahashi K, Yamamoto K, Shiozaki K, Yamaguchi K. Biological and Pathological Roles of Ganglioside Sialidases. Prog Mol Biol Transl Sci. 2018;156:121–50.

275. Shiozaki K, Takahashi K, Hosono M, Yamaguchi K, Hata K, Shiozaki M, Bassi R, Prinetti A, Sonnino S, Nitta K, Miyagi T. Phosphatidic acid-mediated activation and translocation to the cell surface of sialidase NEU3, promoting signaling for cell migration. FASEB J. 2015 May;29(5):2099–111.

276. Cirillo F, Ghiroldi A, Fania C, Piccoli M, Torretta E, Tettamanti G, Gelfi C, Anastasia L. NEU3 Sialidase Protein Interactors in the Plasma Membrane and in the Endosomes. J Biol Chem. 2016 May 13;291(20):10615–24.

277. Seyrantepe V, Landry K, Trudel S, Hassan JA, Morales CR, Pshezhetsky AV. Neu4, a novel human lysosomal lumen sialidase, confers normal phenotype to sialidosis and galactosialidosis cells. J Biol Chem. 2004 Aug 27;279(35):37021–9.

278. Lindenbach BD, Thiel HJ, Rice CM. Flaviviridae: The Viruses and Their Replication. In: Knipe DM, Howley OM, editor. *Fields Virology*. 5th ed. Lippincott William & Wilkins Ltd; 2011. p. 1101–51.

279. Katzelnick LC, Coloma J, Harris E. Dengue: knowledge gaps, unmet needs, and research priorities. Lancet Infect Dis. 2017 Mar;17(3):e88–100.

280. Tomar S, Sun XL. Investigation of substrate specificity of sialidases with membrane mimetic glycoconjugates. Glycoconj J. 2020 Apr 1;37(2):175–85.

281. Li Y, Cao H, Yu H, Chen Y, Lau K, Qu J, Thon V, Sugiarto G, Chen X. Identifying selective inhibitors against the human cytosolic sialidase NEU2 by substrate specificity studies. Mol Biosyst. 2011 Apr;7(4):1060–72.

282. Amith SR, Jayanth P, Franchuk S, Finlay T, Seyrantepe V, Beyaert R, Pshezhetsky AV, Szewczuk MR. Neu1 desialylation of sialyl alpha-2,3-linked beta-galactosyl residues of TOLL-like receptor 4 is essential for receptor activation and cellular signaling. Cell Signal. 2010 Feb;22(2):314–24.

283. Bonardi D, Papini N, Pasini M, Dileo L, Orizio F, Monti E, Caimi L, Venerando B, Bresciani R. Sialidase NEU3 dynamically associates to different membrane domains specifically modifying their ganglioside pattern and triggering Akt phosphorylation. PLoS One. 2014;9(6):e99405.

284. Wei M, Wang PG. Desialylation in physiological and pathological processes: New target for diagnostic and therapeutic development. Prog Mol Biol Transl Sci. 2019;162:25–57.

285. Orekhov AN, Tertov VV, Sobenin IA, Smirnov VN, Via DP, Guevara J, Gotto A, Morrisett J. Sialic acid content of human low density lipoproteins affects their interaction with cell receptors and intracellular lipid accumulation. Journal of Lipid Research. 1992 Jun;33(6):805–17.

286. Fujioka Y, Taniguchi T, Ishikawa Y, Yokoyama M. Significance of acidic sugar chains of apolipoprotein B-100 in cellular metabolism of low-density lipoproteins. Journal of Laboratory and Clinical Medicine. 2000 Nov;136(5):355–62.

287. Ravindran MS, Tanner LB, Wenk MR. Sialic acid linkage in glycosphingolipids is a molecular correlate for trafficking and delivery of extracellular cargo. Traffic. 2013 Nov;14(11):1182–91.

288. Yogalingam G, Bonten EJ, van de Vlekkert D, Hu H, Moshiach S, Connell SA, d'Azzo A. Neuraminidase 1 is a negative regulator of lysosomal exocytosis. Dev Cell. 2008 Jul;15(1):74–86.

289. Quinville BM, Deschenes NM, Ryckman AE, Walia JS. A Comprehensive Review: Sphingolipid Metabolism and Implications of Disruption in Sphingolipid Homeostasis. International Journal of Molecular Sciences. 2021 Jan;22(11):5793.

290. Czubowicz K, Jęśko H, Wencel P, Lukiw WJ, Strosznajder RP. The Role of Ceramide and Sphingosine-1-Phosphate in Alzheimer's Disease and Other Neurodegenerative Disorders. Mol Neurobiol. 2019 Aug;56(8):5436–55.

291. Drews K, Calgi MP, Harrison WC, Drews CM, Costa-Pinheiro P, Shaw JJP, Jobe KA, Nelson EA, Han JD, Fox T, White JM, Kester M. Glucosylceramidase Maintains Influenza Virus Infection by Regulating Endocytosis. J Virol. 2019 Jun 15;93(12):e00017-19.

292. Ridley CM, Thur KE, Shanahan J, Thillaiappan NB, Shen A, Uhl K, Walden CM, Rahim AA, Waddington SN, Platt FM, van der Spoel AC. β-Glucosidase 2 (GBA2) Activity and Imino Sugar Pharmacology. J Biol Chem. 2013 Sep 6;288(36):26052–66.

293. Rempel BP, Withers SG. Covalent inhibitors of glycosidases and their applications in biochemistry and biology. Glycobiology. 2008 Aug 1;18(8):570–86.

294. Lee L, Abe A, Shayman JA. Improved inhibitors of glucosylceramide synthase. J Biol Chem. 1999 May 21;274(21):14662–9.

295. Zhao H, Przybylska M, Wu IH, Zhang J, Maniatis P, Pacheco J, Piepenhagen P, Copeland D, Arbeeny C, Shayman JA, Aerts JM, Jiang C, Cheng SH, Yew NS. Inhibiting glycosphingolipid synthesis ameliorates hepatic steatosis in obese mice. Hepatology. 2009 Jul;50(1):85–93.

296. Natoli TA, Smith LA, Rogers KA, Wang B, Komarnitsky S, Budman Y, Belenky A, Bukanov NO, Dackowski WR, Husson H, Russo RJ, Shayman JA, Ledbetter SR, Leonard JP, Ibraghimov-Beskrovnaya O. Inhibition of glucosylceramide accumulation results in effective blockade of polycystic kidney disease in mouse models. Nat Med. 2010 Jul;16(7):788–92.

297. Shen W, Henry AG, Paumier KL, Li L, Mou K, Dunlop J, Berger Z, Hirst WD. Inhibition of glucosylceramide synthase stimulates autophagy flux in neurons. Journal of Neurochemistry. 2014;129(5):884–94.

298. Thurairatnam S, Lim S, Barker RH, Choi-Sledeski YM, Hirth BH, Jiang J, Macor JE, Makino E, Maniar S, Musick K, Pribish JR, Munson M. Brain Penetrable Inhibitors of Ceramide Galactosyltransferase for the Treatment of Lysosomal Storage Disorders. ACS Med Chem Lett. 2020 Jun 16;11(10):2010–6.

299. Abdelwahab NS. Determination of Ambroxol Hydrochloride, Guaifenesin, and Theophylline in Ternary Mixtures and in the Presence of Excipients in Different Pharmaceutical Dosage Forms. Journal of AOAC INTERNATIONAL. 2012 Nov 1;95(6):1629–38.

300. Bouscary A, Quessada C, Mosbach A, Callizot N, Spedding M, Loeffler JP, Henriques A. Ambroxol Hydrochloride Improves Motor Functions and Extends Survival in a Mouse Model of Familial Amyotrophic Lateral Sclerosis. Front Pharmacol. 2019 Aug 7;10:883.

301. McNeill A, Magalhaes J, Shen C, Chau KY, Hughes D, Mehta A, Foltynie T, Cooper JM, Abramov AY, Gegg M, Schapira AHV. Ambroxol improves lysosomal biochemistry in glucocerebrosidase mutation-linked Parkinson disease cells. Brain. 2014 May;137(5):1481–95.

302. Ambrosi G, Ghezzi C, Zangaglia R, Levandis G, Pacchetti C, Blandini F. Ambroxol-induced rescue of defective glucocerebrosidase is associated with increased LIMP-2 and saposin C levels in GBA1 mutant Parkinson's disease cells. Neurobiology of Disease. 2015 Oct 1;82:235–42.

303. Migdalska-Richards A, Ko WKD, Li Q, Bezard E, Schapira AHV. Oral ambroxol increases brain glucocerebrosidase activity in a nonhuman primate. Synapse. 2017 Jul;71(7):e21967.

304. Luan Z, Li L, Higaki K, Nanba E, Suzuki Y, Ohno K. The chaperone activity and toxicity of ambroxol on Gaucher cells and normal mice. Brain and Development. 2013 Apr;35(4):317–22.

305. Neville DCA, Coquard V, Priestman DA, te Vruchte DJM, Sillence DJ, Dwek RA, Platt FM, Butters TD. Analysis of fluorescently labeled glycosphingolipid-derived oligosaccharides following ceramide glycanase digestion and anthranilic acid labeling. Anal Biochem. 2004 Aug 15;331(2):275–82.

306. Priestman DA, Vruchte D te, Wallom KL, Fernández-Suárez ME, Leondaraki M, Drake C, Platt FM. Analysis of glycosphingolipids from human plasma. protocols.io. 2021.

307. Chatterjee S, Balram A, Li W. Convergence: Lactosylceramide-Centric Signaling Pathways Induce Inflammation, Oxidative Stress, and Other Phenotypic Outcomes. Int J Mol Sci. 2021 Feb 12;22(4):1816.

308. Nakamura H, Moriyama Y, Makiyama T, Emori S, Yamashita H, Yamazaki R, Murayama T. Lactosylceramide interacts with and activates cytosolic phospholipase A2α. J Biol Chem. 2013 Aug 9;288(32):23264–72.

309. Nanaware N, Banerjee A, Mullick Bagchi S, Bagchi P, Mukherjee A. Dengue Virus Infection: A Tale of Viral Exploitations and Host Responses. Viruses. 2021 Sep 30;13(10):1967.

310. Togayachi A, Kozono Y, Ikehara Y, Ito H, Suzuki N, Tsunoda Y, Abe S, Sato T, Nakamura K, Suzuki M, Goda HM, Ito M, Kudo T, Takahashi S, Narimatsu H. Lack of lacto/neolacto-glycolipids enhances the formation of glycolipid-enriched microdomains, facilitating B cell activation. Proc Natl Acad Sci U S A. 2010 Jun 29;107(26):11900–5.

311. Celi AB, Goldstein J, Rosato-Siri MV, Pinto A. Role of Globotriaosylceramide in Physiology and Pathology. Frontiers in Molecular Biosciences [Internet]. 2022 [cited 2022 Apr 17];9. Available from: https://www.frontiersin.org/article/10.3389/fmolb.2022.813637

312. Schnaar RL. The Biology of Gangliosides. Adv Carbohydr Chem Biochem. 2019;76:113–48.

313. Chatelut M, Leruth M, Harzer K, Dagan A, Marchesini S, Gatt S, Salvayre R, Courtoy P, Levade T. Natural ceramide is unable to escape the lysosome, in contrast to a £uorescent analogue. FEBS Letters. 1998;5.

314. Kudo N, Kumagai K, Tomishige N, Yamaji T, Wakatsuki S, Nishijima M, Hanada K, Kato R. Structural basis for specific lipid recognition by CERT responsible for nonvesicular trafficking of ceramide. Proc Natl Acad Sci U S A. 2008 Jan 15;105(2):488–93.

315. Watson P, Stephens DJ. ER-to-Golgi transport: form and formation of vesicular and tubular carriers. Biochim Biophys Acta. 2005 Jul 10;1744(3):304–15.

316. University College, London. A Phase IIA Prospective, Single-Centre, Open Label Clinical Trial to Evaluate the Safety, Tolerability and Pharmacodynamic Effects of Ambroxol in Patients With Parkinson Disease: Ambroxol in Disease Modification in Parkinson Disease [Internet]. clinicaltrials.gov; 2020 Apr [cited 2022 May 24]. Report No.: NCT02941822. Available from: https://clinicaltrials.gov/ct2/show/NCT02941822

317. Svennerholm L, Fredman P. A procedure for the quantitative isolation of brain gangliosides. Biochimica et Biophysica Acta (BBA) - Lipids and Lipid Metabolism. 1980 Jan 18;617(1):97–109.

318. Fernandez-Garcia MD, Mazzon M, Jacobs M, Amara A. Pathogenesis of flavivirus infections: using and abusing the host cell. Cell Host Microbe. 2009 Apr 23;5(4):318–28.

319. Miyagi T, Takahashi K, Yamamoto K, Shiozaki K, Yamaguchi K. Chapter Four - Biological and Pathological Roles of Ganglioside Sialidases. In: Schnaar RL, Lopez PHH, editors. Progress in Molecular Biology and Translational Science. Academic Press; 2018. p. 121–50. (Gangliosides in Health and Disease; vol. 156).

320. WHO Coronavirus (COVID-19) Dashboard [Internet]. Available from: https://covid19.who.int

321. Commissioner O of the. Coronavirus (COVID-19) Update: FDA Authorizes First Oral Antiviral for Treatment of COVID-19 [Internet]. FDA. FDA; 2021. Available from: https://www.fda.gov/news-events/press-announcements/coronavirus-covid-19-update-fda-authorizes-first-oral-antiviral-treatment-covid-19

322. Frediansyah A, Nainu F, Dhama K, Mudatsir M, Harapan H. Remdesivir and its antiviral activity against COVID-19: A systematic review. Clin Epidemiol Glob Health. 2021 Mar;9:123–7.

323. Imran M, Kumar Arora M, Asdaq SMB, Khan SA, Alaqel SI, Alshammari MK, Alshehri MM, Alshrari AS, Mateq Ali A, Al-Shammeri AM, Alhazmi BD, Harshan AA, Alam MT, Abida null. Discovery, Development, and Patent Trends on Molnupiravir: A Prospective Oral Treatment for COVID-19. Molecules. 2021 Sep 24;26(19):5795.

324. Parums DV. Editorial: Current Status of Oral Antiviral Drug Treatments for SARS-CoV-2 Infection in Non-Hospitalized Patients. Med Sci Monit. 2022 Jan 1;28:e935952.

325. Masci AL, Menesale EB, Chen WC, Co C, Lu X, Bergelson S. Integration of Fluorescence Detection and Image-Based Automated Counting Increases Speed, Sensitivity, and Robustness of Plaque Assays. Mol Ther Methods Clin Dev. 2019 Sep 13;14:270–4.

326. Jorquera PA, Mishin VP, Chesnokov A, Nguyen HT, Mann B, Garten R, Barnes J, Hodges E, De La Cruz J, Xu X, Katz J, Wentworth DE, Gubareva LV. Insights into the antigenic advancement of influenza A(H3N2) viruses, 2011-2018. Sci Rep. 2019 Feb 25;9(1):2676.

327. Shambaugh C, Azshirvani S, Yu L, Pache J, Lambert SL, Zuo F, Esser MT. Development of a High-Throughput Respiratory Syncytial Virus Fluorescent Focus-Based Microneutralization Assay. Clin Vaccine Immunol. 2017 Dec;24(12):e00225-17.

328. Yang ML, Wang CT, Yang SJ, Leu CH, Chen SH, Wu CL, Shiau AL. IL-6 ameliorates acute lung injury in influenza virus infection. Sci Rep. 2017 Mar 6;7:43829.

329. Ramos I, Smith G, Ruf-Zamojski F, Martínez-Romero C, Fribourg M, Carbajal EA, Hartmann BM, Nair VD, Marjanovic N, Monteagudo PL, DeJesus VA, Mutetwa T, Zamojski M, Tan GS, Jayaprakash C, Zaslavsky E, Albrecht RA, Sealfon SC, García-Sastre A, Fernandez-Sesma A. Innate Immune Response to Influenza Virus at Single-Cell Resolution in Human Epithelial Cells Revealed Paracrine Induction of Interferon Lambda 1. J Virol. 2019 Oct 15;93(20):e00559-19.

330. Rosen O, Chan LLY, Abiona OM, Gough P, Wang L, Shi W, Zhang Y, Wang N, Kong WP, McLellan JS, Graham BS, Corbett KS. A high-throughput inhibition assay to study

MERS-CoV antibody interactions using image cytometry. J Virol Methods. 2019 Mar;265:77–83.

331. Martinez Viedma MDP, Pickett BE. Characterizing the Different Effects of Zika Virus Infection in Placenta and Microglia Cells. Viruses. 2018 Nov 18;10(11):E649.

332. Amanat F, White KM, Miorin L, Strohmeier S, McMahon M, Meade P, Liu WC, Albrecht RA, Simon V, Martinez-Sobrido L, Moran T, García-Sastre A, Krammer F. An In Vitro Microneutralization Assay for SARS-CoV-2 Serology and Drug Screening. Curr Protoc Microbiol. 2020 Sep;58(1):e108.

333. Miorin L, Kehrer T, Sanchez-Aparicio MT, Zhang K, Cohen P, Patel RS, Cupic A, Makio T, Mei M, Moreno E, Danziger O, White KM, Rathnasinghe R, Uccellini M, Gao S, Aydillo T, Mena I, Yin X, Martin-Sancho L, Krogan NJ, Chanda SK, Schotsaert M, Wozniak RW, Ren Y, Rosenberg BR, Fontoura BMA, García-Sastre A. SARS-CoV-2 Orf6 hijacks Nup98 to block STAT nuclear import and antagonize interferon signaling. Proc Natl Acad Sci U S A. 2020 Nov 10;117(45):28344–54.

334. Chu H, Chan JFW, Yuen TTT, Shuai H, Yuan S, Wang Y, Hu B, Yip CCY, Tsang JOL, Huang X, Chai Y, Yang D, Hou Y, Chik KKH, Zhang X, Fung AYF, Tsoi HW, Cai JP, Chan WM, Ip JD, Chu AWH, Zhou J, Lung DC, Kok KH, To KKW, Tsang OTY, Chan KH, Yuen KY. Comparative tropism, replication kinetics, and cell damage profiling of SARS-CoV-2 and SARS-CoV with implications for clinical manifestations, transmissibility, and laboratory studies of COVID-19: an observational study. Lancet Microbe. 2020 May;1(1):e14–23.

335. Pommerenke C, Rand U, Uphoff CC, Nagel S, Zaborski M, Hauer V, Kaufmann M, Meyer C, Denkmann SA, Riese P, Eschke K, Kim Y, Safranko ZM, Kurolt IC, Markotic A, Cicin-Sain L, Steenpass L. Identification of cell lines CL-14, CL-40 and CAL-51 as suitable models for SARS-CoV-2 infection studies. PLoS One. 2021;16(8):e0255622.

336. Wang M, Cao R, Zhang L, Yang X, Liu J, Xu M, Shi Z, Hu Z, Zhong W, Xiao G. Remdesivir and chloroquine effectively inhibit the recently emerged novel coronavirus (2019-nCoV) in vitro. Cell Res. 2020 Mar;30(3):269–71.

337. Xie X, Muruato A, Lokugamage KG, Narayanan K, Zhang X, Zou J, Liu J, Schindewolf C, Bopp NE, Aguilar PV, Plante KS, Weaver SC, Makino S, LeDuc JW, Menachery VD, Shi PY. An Infectious cDNA Clone of SARS-CoV-2. Cell Host Microbe. 2020 May 13;27(5):841-848.e3.

338. Xie X, Lokugamage KG, Zhang X, Vu MN, Muruato AE, Menachery VD, Shi PY. Engineering SARS-CoV-2 using a reverse genetic system. Nat Protoc. 2021 Mar;16(3):1761–84.

339. Harcourt J, Tamin A, Lu X, Kamili S, Sakthivel SK, Murray J, Queen K, Tao Y, Paden CR, Zhang J, Li Y, Uehara A, Wang H, Goldsmith C, Bullock HA, Wang L, Whitaker B, Lynch B, Gautam R, Schindewolf C, Lokugamage KG, Scharton D, Plante JA, Mirchandani D, Widen SG, Narayanan K, Makino S, Ksiazek TG, Plante KS, Weaver SC, Lindstrom S, Tong S, Menachery VD, Thornburg NJ. Severe Acute Respiratory Syndrome Coronavirus 2 from Patient with Coronavirus Disease, United States. Emerg Infect Dis. 2020 Jun;26(6):1266–73.

340. Holshue ML, DeBolt C, Lindquist S, Lofy KH, Wiesman J, Bruce H, Spitters C, Ericson K, Wilkerson S, Tural A, Diaz G, Cohn A, Fox L, Patel A, Gerber SI, Kim L, Tong S, Lu X, Lindstrom S, Pallansch MA, Weldon WC, Biggs HM, Uyeki TM, Pillai SK, Washington State 2019-nCoV Case Investigation Team. First Case of 2019 Novel Coronavirus in the United States. N Engl J Med. 2020 Mar 5;382(10):929–36.

341. Chan LLY. High-Throughput Direct Cell Counting Method for Immuno-Oncology Functional Assays Using Image Cytometry. In: Tan SL, editor. Immuno-Oncology: Cellular and Translational Approaches. New York, NY: Springer US; 2020. p. 13–34. (Methods in Pharmacology and Toxicology).

342. Kessel S, Cribbes S, Déry O, Kuksin D, Sincoff E, Qiu J, Chan LLY. High-Throughput 3D Tumor Spheroid Screening Method for Cancer Drug Discovery Using Celigo Image Cytometry. SLAS Technol. 2017 Aug;22(4):454–65.

343. Pearson M, LaVoy A, Chan LLY, Dean GA. High-throughput viral microneutralization method for feline coronavirus using image cytometry. J Virol Methods. 2020 Dec;286:113979.

344. Zhang H, Chan LLY, Rice W, Kassam N, Longhi MS, Zhao H, Robson SC, Gao W, Wu Y. Novel high-throughput cell-based hybridoma screening methodology using the Celigo Image Cytometer. J Immunol Methods. 2017 Aug;447:23–30.

345. Unal MA, Bitirim CV, Summak GY, Bereketoglu S, Cevher Zeytin I, Besbinar O, Gurcan C, Aydos D, Goksoy E, Kocakaya E, Eran Z, Murat M, Demir N, Aksoy Ozer ZB, Somers J, Demir E, Nazir H, Ozkan SA, Ozkul A, Azap A, Yilmazer A, Akcali KC. Ribavirin shows antiviral activity against SARS-CoV-2 and downregulates the activity of TMPRSS2 and the expression of ACE2 in vitro. Can J Physiol Pharmacol. 2021 May;99(5):449–60.

Appendix A – Supplemental Figures and Tables

A.1: Overview

In the following sections (Appendix A), supplemental figures and tables referenced in Chapters 2-4 are presented in order. Supplemental figures and tables are numbered according to chapter and order (e.g. first supplemental figure from Chapter 2 will be labeled as Supplemental Figure 2.1)

A.2: Supplemental Figures and Tables accompanying Chapter 2

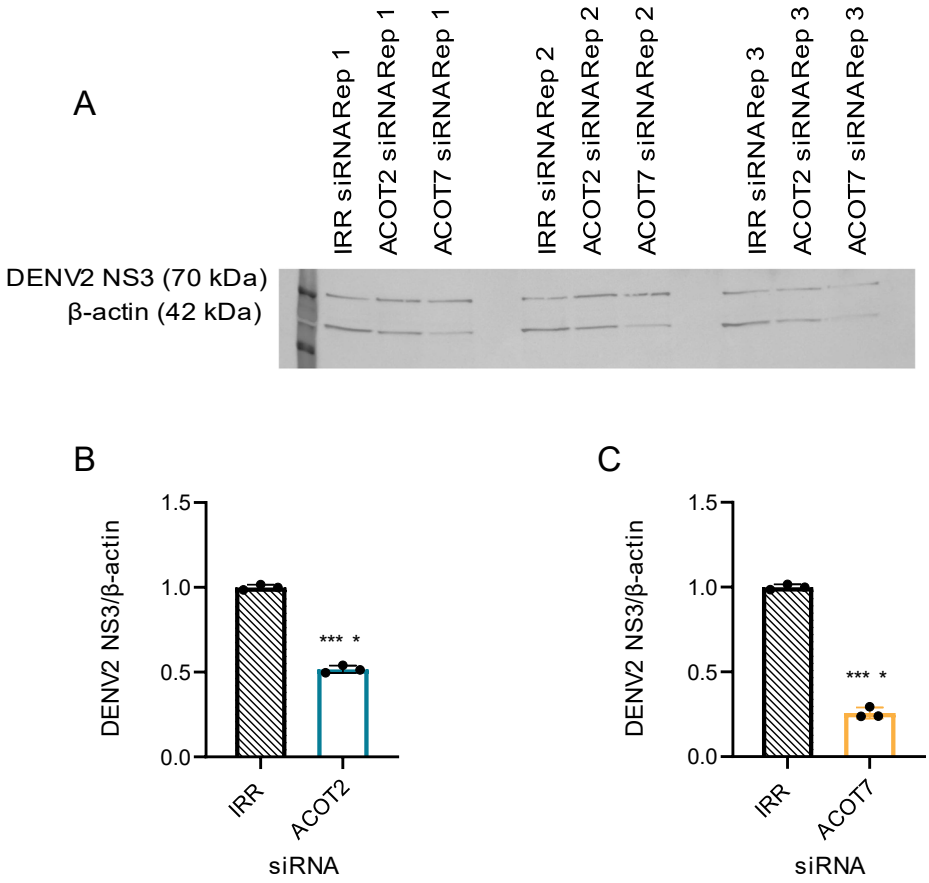

Supplemental Figure 2.1 – Loss of function of mitochondrial ACOTs inhibits viral protein translation. Huh7 cells where transfected with either ACOT2, ACOT7, or an IRR siRNA, and then subsequently infected with DENV2 (MOI = 0.3) for 24hr. (A) Cell lysates were prepared and analyzed via western blot. Samples were probed for DENV2 nonstructural protein 3, and β-actin (for normalization). Li-cor IRDyes were used as secondary antibodies. (B-C) and fluorescence intensity of each band was analyzed using area under the curve analysis in ImageJ.

Supplemental Table 2.1. siRNA and oligonucleotide resources used in this study.

siRNA resources		
Reagent	Source	Product Identifier
SMARTPool ACOT1 siRNA	Horizon Discovery/Dharmacon	M-034967-00
MISSION® esiRNA human ACOT2	Sigma-Aldrich	EHU104751-20UG
MISSION® esiRNA human ACOT7	Sigma-Aldrich	EHU112971-20UG
Oligonucleotides		
	Forward Primer (5'-3')	Reverse Primer (5'-3')
ACOT1/2	AGAGGAAGAGTTGGGCAGAG	TTCGTCCCAGCAGCAGCG
ACOT2	GCCCGAGAGGATGTCTAACA	TCAGGCTCCATTGGTACAGC
ACOT4	AGGAG GGTACAAGAACCCCA	GAGGCTCGATGTAATGCCCA
ACOT6	AGCCGTGGACTTTATGCTGC	AGTACAGTGGCTGTGATGCC
ACOT7	CTGCACCCTGCACGGCTTTG	CGGAAGCTGTGACGATGTTG
ACOT8	GCTCTCGCATTCATAGAGCAT	AAGTTCAGTGGCCATGTTAGC
ACOT9	AAGTTCAGTGGCCATGTTAGC	AATGCCGGCCCTTTATTTTCA
ACOT11	AATCACCAGGGCAACACCTT	CAATGGCCTTCAGCGTAGGG
ACOT12	ACGCTATCGGGGAGCTATTG	TTGCTGTCACTCAGGGATGC
ACOT13	CTCTTCGCCCTTTGTGTCCT	GAGTAATCTTTCCCAAAACTCTCTC

A.3: Supplemental Figures and Tables accompanying Chapter 3

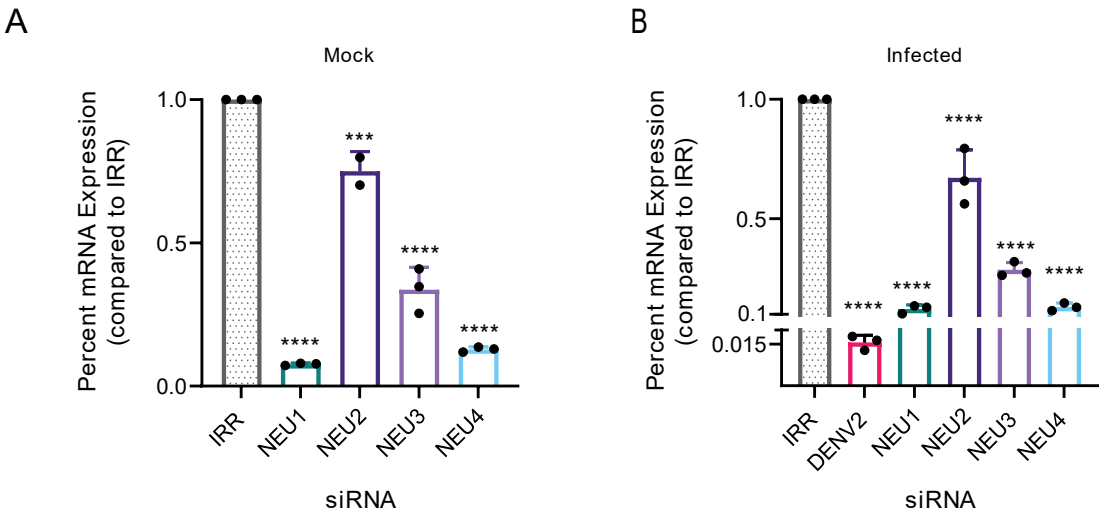

Supplemental Figure 3.1 – Confirmation of knockdown of siRNA-mediated knockdown of sialidase mRNA levels. (A-B): Huh7 cells were transfected with pooled siRNAs targeting NEU1-4 and the indicated controls followed by mock-infection (A) or DENV2-infection (B). At 24 hpi, cells were collected, processed, and relative mRNA expression was analyzed via qRT-PCR. Values were normalized to the RPLP0 housekeeping gene. (A-B: one-way ANOVA with Tukey's multiple comparisons test: * = p≤0.05, ** = p≤0.01, ***= p≤0.001, **** = p≤0.0001.)

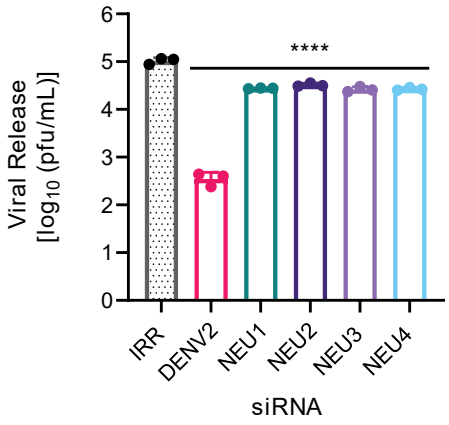

Supplemental Figure 3.2 – Validation of reduction of DENV2 release upon NEU1-4 knockdown using single siRNAs. Huh7 cells were transfected with single siRNAs targeting NEU1-4 and the indicated controls followed by DENV2 infection. At 24 hpi, supernatants were collected and analyzed via plaque assay on BHK-21 cells. (One-way ANOVA with Tukey's multiple comparisons test: * = p≤0.05, ** = p≤0.01, ***= p≤0.001, **** = p≤0.0001.)

Supplemental Table 3.1 – siRNA reagents and primer sequences used in this study.

siRNA reagents and sequences			
siRNA	**Manufacturer**	**Product Identifier**	**Sequence(s)**
Irrelavant control siRNA (custom)	Horizon Discovery	Custom siRNA	GGACUUCCAGAAGAACAUCTT
DENV2 control siRNA (custom)	Horizon Discovery	Custom siRNA	CGGGAAAGACGAAGAGAUAUU
Neuraminidase 1 (SMARTpool)	Horizon Discovery	M-011092-00	GAAAGAGACAGUCCAGCUA
			CGGAAUCUCUCCCUGGAUA
			CGAUGGAGCUUCAGCAAUG
			AGUGAGCGAUGUUGAGACA
Neuraminidase 2 (SMARTpool)	Horizon Discovery	M-012058-00	GUACGAAGCCAAUGAUUAC
			CCAAUGACGGGCUUGAUUU
			CAAGAAGGAUGAGCACGCA
			GGCAAGUCACGGAGCAACA
Neuraminidase 3 (SMARTpool)	Horizon Discovery	M-010641-01	GAAGAUGACAGAGGGAUUA
			GAUCUACAGUGAUGACCUA
			GUGCAGAGGUCAUGGAAGA
			GAACCCAAGCCAAUUCAAA
Neuraminidase 4 (SMARTpool)	Horizon Discovery	M-013263-00	GAUGAGAUUUCCUUUUGUA
			GUGCAGAUCGCCACGGGAA
			GCUCGGCUACACAUGGGUA
			GGCCACGGGAUGACAGUUG
NEU1 silencer siRNA	ThermoFisher	AM16708 / assay ID 8573	AUUUCUUUUCUACUCCCUUU
NEU2 silencer siRNA	ThermoFisher	AM16708 / assay ID 45117	UUACGAGGAGAUUGUCUUUC
NEU3 silencer siRNA	ThermoFisher	AM16708 / assay ID 135986	CAGUUGGUACAGUGGGGGCC
NEU4 silencer siRNA	ThermoFisher	AM16708 / assay ID 36069	UCUUUAGGAAGGGGAGCAGC
Primer Sequences			
Target	Abbreviation	**Forward**	**Reverse**
Ribosomal protein lateral stalk subunit P0	RPLP0	AGATGCAGCAGATCCGCAT	GGATGGCCTTGCGCA
Hexokinase II	Hexokinase	ATCCCTGAGGACATCATGCGA	CTTATCCATGAAGTTAGCCAGGCA
Neuraminidase 1	NEU1	GTCAGCCCAAGCAGGAAAATG	CGGGCATTGATGACGACTGA
Neuraminidase 2	NEU2	GCGCAGAGGAGACTACGAC	GTCATACAAGGGGCATGGGTT
Neuramindase 3	NEU3	GACCATGAACCCCTGTCCTG	AGCATTCCTGCCTGACACAA
Neuraminidase 4	NEU4	ACCGCCGAGAGTGTTTTGG	CGTGGTCATCGCTGTAGAAGG

A.4 Supplemental Figures and Tables Accompanying Chapter 4

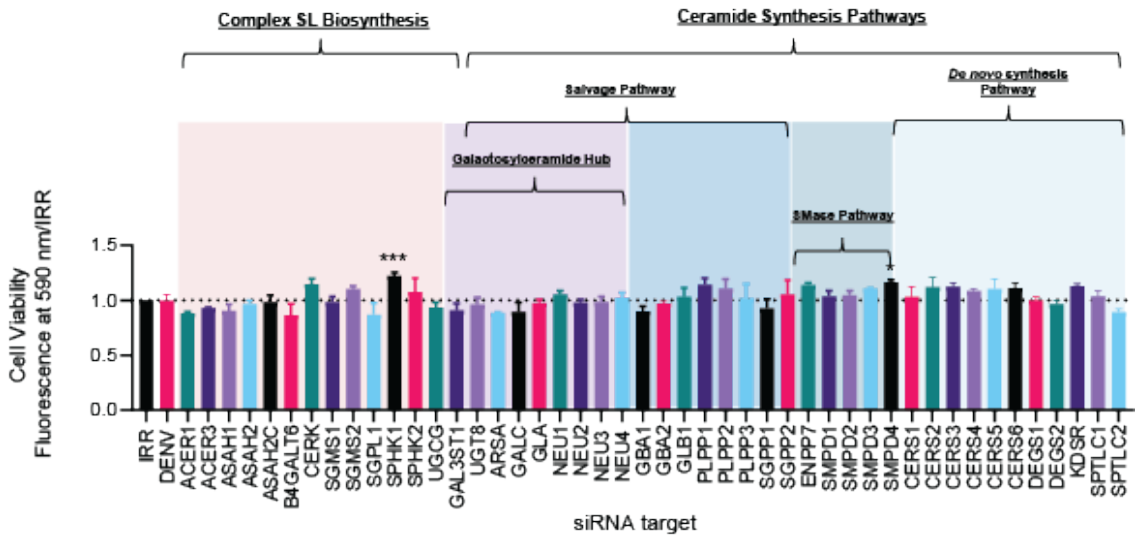

Supplemental Figure 4.1 – Cytotoxic effects of siRNAs targeting enzymes within the sphingolipid metabolic pathway. Huh7 cells were transfected with indicated siRNAs, an IRR control, or DENV2-specific control siRNA. Following transfection, cells were mock-infected. At 24 hpi, an AlamarBlue cytotoxicity assay was performed. Results are displayed as fold change in fluorescence at 590 nm of each treatment group compared to the irrelevant control. (One-way ANOVA with Dunnett's multiple comparison's test: * = p≤0.05, ** = p≤0.01, ***= p≤0.001, **** = p≤0.0001.)

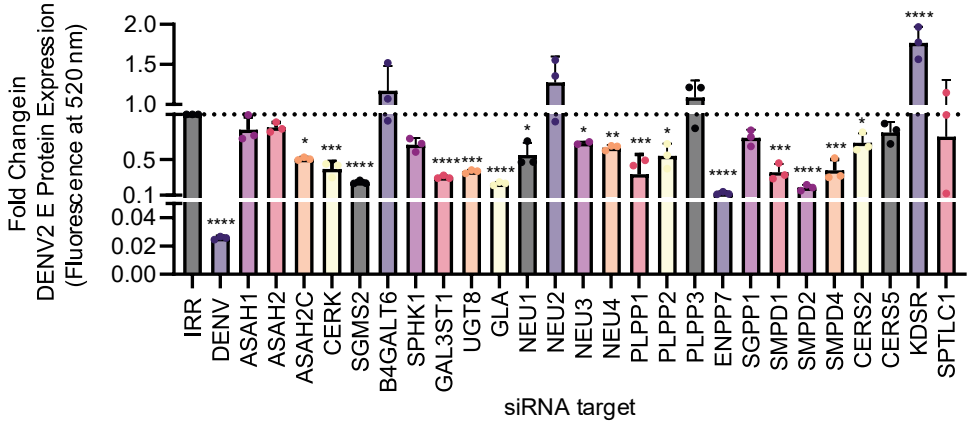

Supplemental Figure 4.2 – Validation of siRNA screen results in an alternate cell line using fluorescence cytometry. A549 cells were transfected with indicated siRNAs, an IRR control, or DENV2-specific control siRNA, followed by infection with DENV2 (MOI = 0.1). At 24 hpi, viral supernatants were collected and stored at -80°C. Cells were washed with 1x PBS and fixed with 100% MeOH. Following fixation, cells were washed, blocked overnight in a 1% BSA solution, and then probed with 4G2 antibody (anti-DENV E protein). Cells were counterstained with goat anti-mouse FITC and DAPI, and then analyzed using a Celigo Imaging Cytometer to determine total fluorescence of DENV2 E protein in each sample. Results are displayed as fold change in fluorescence at 520 nm compared to the irrelevant control. (One-way ANOVA with Dunnett's multiple comparison's test: * = p≤0.05, ** = p≤0.01, ***= p≤0.001, **** = p≤0.0001.)

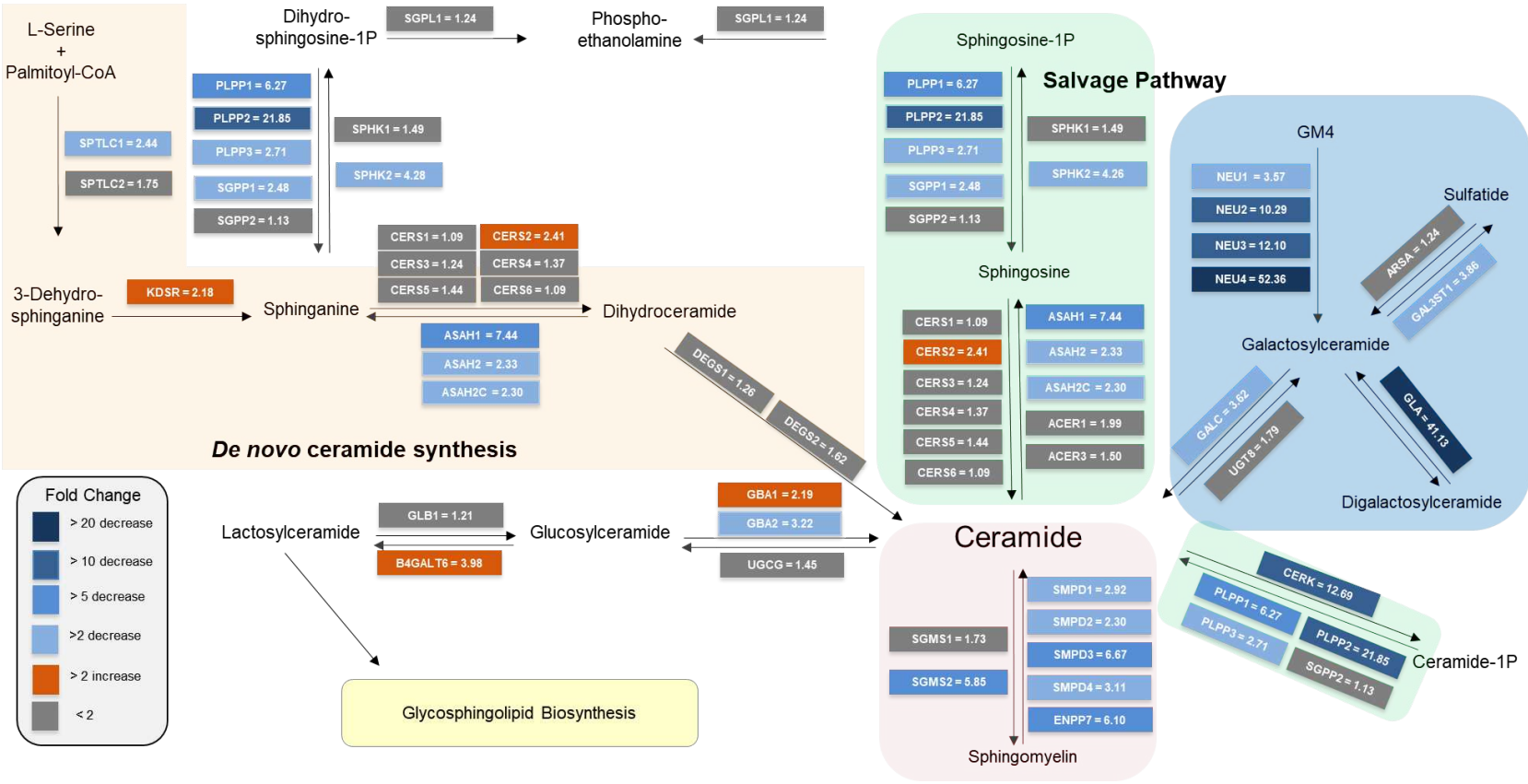

Supplemental Figure 4.3 – Effect of loss of function of sphingolipid pathway enzymes on DENV2 release (map representation). The results from Figure 4.1A are displayed over a map of the sphingolipid metabolic pathway (derived from KEGG pathway database). Different 'arms' of the pathway are highlighted (beige = *de novo* ceramide synthesis, green = salvage pathway, pink = sphingomyelinase pathway, blue = galactosylceramide hub). Enzyme names are highlighted in boxes that are colored to represent the fold change in DENV2 viral release compared to the IRR control. Blue boxes correspond to enzymes whose loss of function decreased DENV2 release, and darker shades of blue indicate a greater fold change. Orange boxes represent enzymes whose loss of function increased DENV2 release. Grey boxes indicate a change in DENV2 release less than 2-fold, which was below our threshold for further evaluation. The mean fold change for each enzyme provided next to each enzyme name.

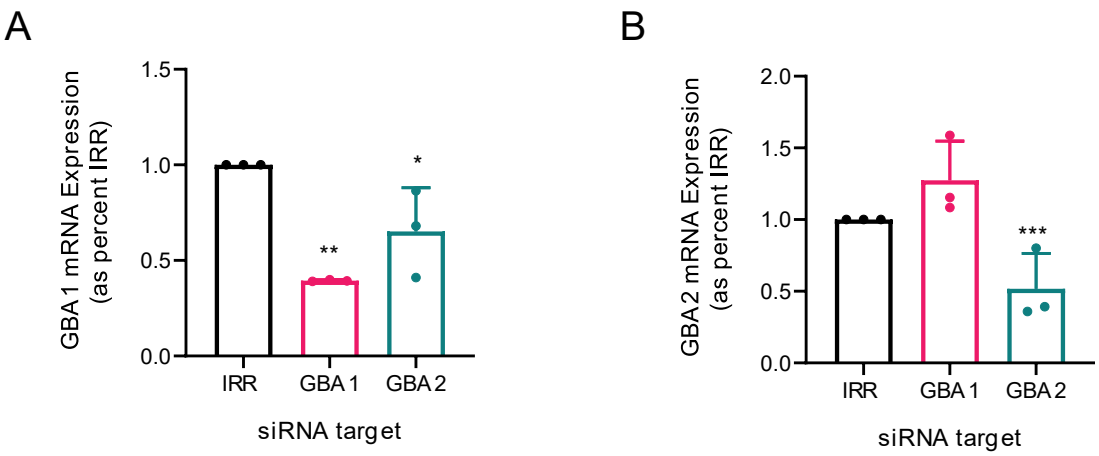

Supplemental Figure 4.4 – Confirmation of GBA1 and GBA2 mRNA knockdown using siRNA inhibitors. Huh7 cells were transfected with siRNAs targeting GBA1 and GBA2 and an IRR control. At 72 hours post transfection (corresponding to time of collection following viral infection), cells were collected and analyzed for mRNA expression of GBA1 (A) and GBA2 (B). (A-B one-way ANOVA with Dunnett's multiple comparison's test: * = p≤0.05, ** = p≤0.01, ***= p≤0.001.)

Supplemental Table 4.1 – Horizon Discover SMARTpool siRNA Resources

Catalog #	Gene Symbol	Sequence		Catalog #	Gene Symbol	Sequence
M-010298-00	ACER1	UACAACACGUUCUCCAAUA		M-009936-03	KDSR	GGAAGUGCAUUGCUAUCGA
		GAGCUUCGGCACCUGAUUG				GCAUUGCUAUCGAGUGCUA
		GGCCUGUUCUCCAUGUAUU				UAACUUCUAUUACUGAGGG
		GGCAGUGGCUAUAGCAUAU				GCAAAGAAACUUCGAAAUC
M-009430-01	ACER3	GAUUAUACCUCCAAUGUUC		M-011092-00	NEU1	GAAAGAGACAGUCCAGCUA
		CCACAUGACUCUGAAAUAU				CGGAAUCUCUCCCUGGAUA
		AACGGUACAUUGCUUCUUA				CGAUGGAGCUUCAGCAAUG
		GGACUGGGUUAUACAUCAU				AGUGAGCGAUGUUGAGACA
M-009558-01	ARSA	CAUCAGGGCUUCCAUCGAU		M-012058-00	NEU2	GUACGAAGCCAAUGAUUAC
		GACCUGAGACCAUGCGUAU				CCAAUGACGGGCUUGAUUU
		UCUAUGACCUGUCCAAGGA				CAAGAAGGAUGAGCACGCA
		GCCAGAACCUGACCUGCUU				GGCAAGUCACGGAGCAACA
M-005228-01	ASAH1	CACCAUAAAUCUUGACUUA		M-010641-01	NEU3	GAAGAUGACAGAGGGAUUA
		GGUCAUAACUGAGCAACUA				GAUCUACAGUGAUGACCUA
		UAUAUGAACUCGAUGCUAA				GUGCAGAGGUCAUGGAAGA
		GAAAAUAGCACAAGUUAUG				GAACCCAAGCCAAUUCAAA
M-005229-00	ASAH2	CACAUUACAUUACCACUUA		M-013263-00	NEU4	GAUGAGAUUUCCUUUUGUA
		GGAAAGCCAUCUGAAGAAA				GUGCAGAUCGCCACGGGAA
		GAACAACAGUAACCAUCUU				GCUCGGCUACACAUGGGUA
		GACCAUGUCUGGACGAAGA				GGCCACGGGAUGACAGUUG
M-039945-00	ASAH2C	ACAGAUAGUUUACUGCUAA		M-019098-01	PLPP1	GAGGAGGACUCUCAUACAA
		AAUACCAGGCUCAGCGAUA				CUACAUAUGUCGAGGGAAU
		GACCAUGUCUGGACGAAGA				CAACAACUGGGAAUCACUA
		GAUCAACAGAAGUCCGUAU				CUGUAUAUGUAUCGGAUUU
M-011933-00	B4GALT6	AGAGUUAGCUCCAAUCGAA		M-011500-00	PLPP2	UGACAGACCUGGCCAAGUA
		UCGAUGGACUGAACAAUUU				GCACGACUCUGUUGGAAGU
		GCUCAACGGUACAGAUUAU				GCUCGGACUUCAACAACUA
		CAACGUAUCUCCCGGAAAA				CCGCGUGUCUGAUUACAAA
M-004061-02	CERK	GAUCAUCGCCGUUGAGGAA		M-017312-01	PLPP3	GGGACUGUCUCGCGUAUCA
		CAACGGACUGCGUGUGUUA				UCUAUUACCUGAAGAAGUC
		CCACUGACAUCAUCGUUAC				CAGUUCACCUUGAUCAUGA

Catalog #	Gene Symbol	Sequence	Catalog #	Gene Symbol	Sequence
M-010298-00	ACER1	UACAACACGUUCUCCAAUA	M-009936-03	KDSR	GGAAGUGCAUUGCUAUCGA
		GAGCUUCGGCACCUGAUUG			GCAUUGCUAUCGAGUGCUA
		GGCCUGUUCUCCAUGUAUU			UAACUUCUAUUACUGAGGG
		GGCAGUGGCUAUAGCAUAU			GCAAAGAAACUUCGAAAUC
M-009430-01	ACER3	GAUUAUACCUCCAAUGUUC	M-011092-00	NEU1	GAAAGAGACAGUCCAGCUA
		CCACAUGACUCUGAAAUAU			CGGAAUCUCUCCCUGGAUA
		AACGGUACAUUGCUUCUUA			CGAUGGAGCUUCAGCAAUG
		GGACUGGGUUAUACAUCAU			AGUGAGCGAUGUUGAGACA
M-009558-01	ARSA	CAUCAGGGCUUCCAUCGAU	M-012058-00	NEU2	GUACGAAGCCAAUGAUUAC
		GACCUGAGACCAUGCGUAU			CCAAUGACGGGCUUGAUUU
		UCUAUGACCUGUCCAAGGA			CAAGAAGGAUGAGCACGCA
		GCCAGAACCUGACCUGCUU			GGCAAGUCACGGAGCAACA
M-005228-01	ASAH1	CACCAUAAAUCUUGACUUA	M-010641-01	NEU3	GAAGAUGACAGAGGGAUUA
		GGUCAUAACUGAGCAACUA			GAUCUACAGUGAUGACCUA
		UAUAUGAACUCGAUGCUAA			GUGCAGAGGUCAUGGAAGA
		GAAAAUAGCACAAGUUAUG			GAACCCAAGCCAAUUCAAA
		CAAGGCAAGCGGAUAUAUG			GGAAUUCUACCGGAUCUAU
M-010275-01-0005	CERS1	UCACCAAGCUCAACAUUUA	M-019477-00	SGMS1	GCUAACACUUACCUACUUA
		CGAGAGCGUUGGAAGUUU			GGAAGUGGUUUAUUGGUCA
		CACCAUCUGUCUUCUACGA			GCCCAACUGCGAAGAAUAA
		CCAUCUACGCUACGCUAUA			GAACGAGUACCUCCUAAGG
M-010282-01-0005	CERS2	UAACAACCAUCGUAAGAAU	M-018775-01	SGMS2	CAACGGAUUCUACGAUUGA
		GAAAGCUGGUAGAAGAUGA			GGGAUUAUAUUAGUUGGAU
		UGAUUGAACUUUCCUUCUA			UACGAACACUUAUGCAAGA
		GCACUAUCCCUUCCCAGUA			GCACACGAACACUACACUA
m-017860-02-0005	CERS3	GCAAAGAGAUGGAUUGUUU	M-008747-00	SGPL1	GAAUAUGGUUGCAGAAUUG
		GAAAGAUGGUUUAGGAGUC			GGACAAAGAGUAUGUGAAA
		UGAUAAACCUUGGCUAUAU			GAACAUGUCAUUCCUGAAA
		CCACAGGAGAGGUCGGCUU			GAAGAGCUAUCUCCAGGAA
M-014364-00-0005	CERS4	UCAACUACAUGCAGUAUCA	M-014653-00	SGPP1	GAACUUCCUUAUCGGUAUA
		GGACAGAGGUAGAAGACCG			AAUCUUAGCUGUCUUCUAU
		GCAGGACAGGUUCUGGUUA			GCAACGAACUCUUCUACAU

Catalog #	Gene Symbol	Sequence
M-010298-00	ACER1	UACAACACGUUCUCCAAUA
		GAGCUUCGGCACCUGAUUG
		GGCCUGUUCUCCAUGUAUU
		GGCAGUGGCUAUAGCAUAU
M-009430-01	ACER3	GAUUAUACCUCCAAUGUUC
		CCACAUGACUCUGAAAUAU
		AACGGUACAUUGCUUCUUA
		GGACUGGGUUAUACAUCAU
M-009558-01	ARSA	CAUCAGGGCUUCCAUCGAU
		GACCUGAGACCAUGCGUAU
		UCUAUGACCUGUCCAAGGA
		GCCAGAACCUGACCUGCUU
M-005228-01	ASAH1	CACCAUAAAUCUUGACUUA
		GGUCAUAACUGAGCAACUA
		UAUAUGAACUCGAUGCUAA
		GAAAAUAGCACAAGUUAUG
		GAGAAGGACAUUCGUAGUG
M-016077-02-005	CERS5	CAAUAUGGUUCGAGUGGGA
		CUACCUAAUUGCACGGAUU
		CUUUGAGAGUUGGGAGAUA
		GGAUUGGAAUGUCCGAAAA
M-032207-00-0005	CERS6	GAAGUGAUAUUGAGUCUAG
		CAAGCACGCUGACGAGGUU
		CGCCAUAGCCCUCAACAUU
		CUUCUGGUCUUACUUGAUU
M-006675-01	DEGS	GAGAUAAAGUCCUUGAUGA
		GGAAUUAAAUCCUUAGUCU
		GGGAGAUCCUGGCAAAGUA
		GCGUUUGGCAGUUGCAUUA
M-010296-01	DEGS2	GGCUCAAGCCCGUGGUCUA
		AGAAGUACCACGUGGACCA
		CAGCACCACUCCUGGGUGA
M-009936-03	KDSR	GGAAGUGCAUUGCUAUCGA
		GCAUUGCUAUCGAGUGCUA
		UAACUUCUAUUACUGAGGG
		GCAAAGAAACUUCGAAAUC
M-011092-00	NEU1	GAAAGAGACAGUCCAGCUA
		CGGAAUCUCUCCCUGGAUA
		CGAUGGAGCUUCAGCAAUG
		AGUGAGCGAUGUUGAGACA
M-012058-00	NEU2	GUACGAAGCCAAUGAUUAC
		CCAAUGACGGGCUUGAUUU
		CAAGAAGGAUGAGCACGCA
		GGCAAGUCACGGAGCAACA
M-010641-01	NEU3	GAAGAUGACAGAGGGAUUA
		GAUCUACAGUGAUGACCUA
		GUGCAGAGGUCAUGGAAGA
		GAACCCAAGCCAAUUCAAA
		UCACAAAUAUGCUCCAUUC
M-015727-00	SGPP2	UGAAGUGCCUUACAAGUUU
		AGAAGUACGUCGUGAAGAA
		CAUCUGCGCUACAACCUUU
		ACUGGAAUAUUGACCCUUA
M-006676-01	SMPD1	GCAUAUAAUUGGCCACAUU
		AGACCUACAUCCUGAAUCU
		CUCUACAGGGCUCGAGAAA
		GCUGGAAUUAUUACCGAAU
M-006677-01	SMPD2	GCAGAGAGGUCGCCGUUGA
		GGAGGUCAAUGGCUUAUAU
		CAAGGCAGUUUCUGGGUUU
		UGAAACCACUACAGGCUUU
M-006678-01	SMPD3	CAACAGCGGCCUCCUCUUU
		CAAGCGAGCAGCCACCAAA
		ACCAAAGAAUCGUCGGGUA

Catalog #	Gene Symbol	Sequence
M-010298-00	ACER1	UACAACACGUUCUCCAAUA
		GAGCUUCGGCACCUGAUUG
		GGCCUGUUCUCCAUGUAUU
		GGCAGUGGCUAUAGCAUAU
M-009430-01	ACER3	GAUUAUACCUCCAAUGUUC
		CCACAUGACUCUGAAAUAU
		AACGGUACAUUGCUUCUUA
		GGACUGGGUUAUACAUCAU
M-009558-01	ARSA	CAUCAGGGCUUCCAUCGAU
		GACCUGAGACCAUGCGUAU
		UCUAUGACCUGUCCAAGGA
		GCCAGAACCUGACCUGCUU
M-005228-01	ASAH1	CACCAUAAAUCUUGACUUA
		GGUCAUAACUGAGCAACUA
		UAUAUGAACUCGAUGCUAA
		GAAAAUAGCACAAGUUAUG
		CCGCCUCCUUCAAGAAGUA
M-009059-00	ENPP7	GCAAAUAUAUCGAGAACCA
		GAAUUAACGUCCAGUUCAA
		GAGCACCGGUACAAAGUCA
		ACACAGUGAUGGCGUGGUU
M-011956-01	GAL3ST1	GGAAGUUCAUUCGCGAUUU
		GAAACCUGCUCUUCUUCGA
		GCUACAACCUCAAGAAGAG
		GCGACAAGCUGACCGAGUU
M-011038-01	GALC	CUGGCAACGCCGAGCGAAA
		GAGAAUUAUUUCCGAGGAU
		GAAAGGAGGAAGCUACGUA
		GAUUAUCUCUUUAAGCCGA
M-006366-02	GBA	GAAGAAGGAAUCGGAUAUA
		CCAAUUGGGUGCGUAACUU
		CAACAUCCUUGCCCUGUCA
M-009936-03	KDSR	GGAAGUGCAUUGCUAUCGA
		GCAUUGCUAUCGAGUGCUA
		UAACUUCUAUUACUGAGGG
		GCAAAGAAACUUCGAAAUC
M-011092-00	NEU1	GAAAGAGACAGUCCAGCUA
		CGGAAUCUCUCCCUGGAUA
		CGAUGGAGCUUCAGCAAUG
		AGUGAGCGAUGUUGAGACA
M-012058-00	NEU2	GUACGAAGCCAAUGAUUAC
		CCAAUGACGGGCUUGAUUU
		CAAGAAGGAUGAGCACGCA
		GGCAAGUCACGGAGCAACA
M-010641-01	NEU3	GAAGAUGACAGAGGGAUUA
		GAUCUACAGUGAUGACCUA
		GUGCAGAGGUCAUGGAAGA
		GAACCCAAGCCAAUUCAAA
		CGAACGGCCUGUACGAUGA
M-020681-02	SMPD4	UGAAUCCGUUCGAGUAUUA
		CCAACGACCUGGACGAGAU
		GGCCAGGACUGCAAGUACA
		AGGUGAAGAGCCACGUCUA
M-004172-03	SPHK1	GGGAAUUGAUGGUUAGCGA
		CGACGAGGACUUUGUGCUA
		AGGGCAGGCAUAUGGAGUA
		CUGACCAACUGCACGCUAU
M-004831-00	SPHK2	CAAGGCAGCUCUACACUCA
		GAGACGGGCUGCUCCAUGA
		GCUCCUCCAUGGCGAGUUU
		CCACUGCCCUCACCUGUCU
M-006673-02	SPTLC1	GGGUUAAGGCAGCAGCUUU
		GUAUAAACUUCGCCUCAUU
		UUCUUGGAUUGUUGGAUAA

Catalog #	Gene Symbol	Sequence
M-010298-00	ACER1	UACAACACGUUCUCCAAUA
		GAGCUUCGGCACCUGAUUG
		GGCCUGUUCUCCAUGUAUU
		GGCAGUGGCUAUAGCAUAU
M-009430-01	ACER3	GAUUAUACCUCCAAUGUUC
		CCACAUGACUCUGAAAUAU
		AACGGUACAUUGCUUCUUA
		GGACUGGGUUAUACAUCAU
M-009558-01	ARSA	CAUCAGGGCUUCCAUCGAU
		GACCUGAGACCAUGCGUAU
		UCUAUGACCUGUCCAAGGA
		GCCAGAACCUGACCUGCUU
M-005228-01	ASAH1	CACCAUAAAUCUUGACUUA
		GGUCAUAACUGAGCAACUA
		UAUAUGAACUCGAUGCUAA
		GAAAAUAGCACAAGUUAUG
		GCACAGGCCUGCUACUGAC
L-009375-01-0005	GBA2	GUCCACUACAGGCGGUAUA
		GGUACAAAUCUGCGCUGUU
		GAACCAUGGCUCCGCGUCA
		GCUGAAGGCUGCUACCGUA
M-012538-02	GLA	AAGCUAGGGUUCUAUGAAU
		AGGCAGACCCUCAGCGCUU
		GAGUAGAUCUGCUAAAAUU
		GGUUAUAAGCACAUGUCCU
M-012539-01	GLB1	GUGCAUAUAUCAACGAUUU
		GAAUGGAGGGCCAGUUAUA
		UGAAACAGCAUUAUGGGUU
		GGUCCUAUCCCUCCAUCUA

Catalog #	Gene Symbol	Sequence
M-009936-03	KDSR	GGAAGUGCAUUGCUAUCGA
		GCAUUGCUAUCGAGUGCUA
		UAACUUCUAUUACUGAGGG
		GCAAAGAAACUUCGAAAUC
M-011092-00	NEU1	GAAAGAGACAGUCCAGCUA
		CGGAAUCUCUCCCUGGAUA
		CGAUGGAGCUUCAGCAAUG
		AGUGAGCGAUGUUGAGACA
M-012058-00	NEU2	GUACGAAGCCAAUGAUUAC
		CCAAUGACGGGCUUGAUUU
		CAAGAAGGAUGAGCACGCA
		GGCAAGUCACGGAGCAACA
M-010641-01	NEU3	GAAGAUGACAGAGGGAUUA
		GAUCUACAGUGAUGACCUA
		GUGCAGAGGUCAUGGAAGA
		GAACCCAAGCCAAUUCAAA
		ACUUGUGGACCCAGAGGAU
M-006674-01	SPTLC2	UCAAACAGAUACCGGUUAA
		CAUACUAUAACCAGGUAAA
		CCGAGGAUGUGGAUGUUAU
		GUACAAAGCUGCUCCGUAG
M-006441-02	UGCG	GAUAUGAAGUUGCAAAGUA
		GCGAAUCCAUGACAAUAUA
		GGACCAAACUACGAAUUAA
		GAUUUGUGAUAGUGGAAUA
M-010270-02	UGT8	ACACUAAACUCAUAGAAUG
		CGAGAGAGGCCACCAUACA
		GAUGCUGUGUACUGACGUA
		CAGUCCAAGAUGCGGAAUA

Appendix B – Additional Works

Overview

In the following sections (Appendix B1 and Appendix B2), additional non-dissertation works (first authorships and published/under review collaborations and patents) will be presented. Appendix B1 is a methods paper entitled “Development of a high-throughput SARS-CoV-2 antiviral testing method using plate-based image cytometry,” that is currently under review at *The Journal of Virological Methods*, and is included here with the permission of all authors. Appendix B2 will provide and outline of additional collaborative works presented with citation, abstract, and an overview of my contributions to each project.

Appendix B1 – Development of a high-throughput SARS-CoV-2 antiviral testing method using plate-based image cytometry.[3]

B1.1: Introduction

Since January of 2020, the COVID-19 pandemic has created a major public health crisis across the globe. Since the start of the pandemic, approximately 400 million cases and 5.8 million deaths have been reported worldwide [320]. In response, researchers around the world have engaged in rapid vaccine development, surveillance programs, and antiviral testing. These combined efforts within the community led to the development and delivery of multiple vaccine candidates, where an estimated 10.2 billion doses of vaccines have been administered worldwide [320]. To date, there have been numerous drugs tested and repurposed as antivirals that have either received approval or emergency use authorization such as remdesivir, molnupiravir, nirmatrelvir/ritonavir (Paxlovid^{TM}), while testing and clinical trials are ongoing for many others [321–324]. However, each of these drugs has its limitations for use, and are not yet available to many low-income communities throughout the world. Additionally, with the emergence of new highly transmissible variants that are showing an increased ability to circumvent the immunity conferred by vaccination, like the Omicron variant that emerged in November 2021, there has been a renewed interest in the discovery of novel antiviral candidates effective against emerging variants of concern.

Traditional antiviral or vaccine testing methods utilize plaque-reduction neutralization tests (PRNTs) or RT-PCR analysis to investigate the effects of antiviral drugs and vaccines to

[3] Adapted from: St Clair LA, Chan LL, Boretsky A, Lin B, Spedding M, and Perera R. Development of a high-throughput SARS-CoV-2 antiviral testing method using plate-based image cytometry. Under review at *Journal of Virological Methods*.

neutralize viral infections. However, both assays are time-consuming, requiring days to either form visually clear plaques or to prepare cell extractions for PCR analysis. These assays are also low-throughput and can have high operator-to-operator variation. Furthermore, digital images of the viral reduction are not typically recorded [325]. These facts underpin a critical need to develop high-throughput testing methods of new antiviral drugs and vaccine candidates to improve the efficiency of research and development.

Plate-based image cytometry systems have demonstrated high-throughput screening for potential vaccine candidates [325–328]. The Celigo Image Cytometer has been employed for high-speed and high-throughput counting of viral plaques, foci, and individual virus-infected cells in 96-well microplates using bright field or fluorescence imaging. Image cytometric analysis can significantly reduce the plaque counting time and minimize operator-to-operator variation, which can improve the efficiency of identifying new or novel candidates for viral diseases [329–331]. Current publications have shown the improvement in assay time and precision for fluorescence detection of plaques, foci, or individual infected cells via immunostaining or fluorescent protein reporter for COVID-19 vaccine development [332,333]. In this work, we developed a high-throughput antiviral testing method employing the Celigo Image Cytometer to investigate the effects of antiviral drugs candidates on infection rates using a SARS-CoV-2 reporter virus that stably expresses a fluorescent mNeonGreen reporter protein as well as their cytotoxicity effects on the healthy host cell line using fluorescent viability stains. During the method development, the host cell line, MOI, and cell seeding density were first selected for the antiviral testing method. The optimized image cytometry method was then used to demonstrate antiviral testing of four drug compounds repurposed for potential COVID-19 treatment at different concentrations. The high-throughput antiviral testing method using Celigo Image Cytometer can provide a more efficient platform to rapidly identify potential antiviral drugs, which is highly critical during a global pandemic to combat the rapidly spreading SARS-CoV-2 virus and its variants.

B1.2: Results

B1.2.1 – Selection of the optimal host cell line and MOI

To develop a high-throughput SARS-CoV-2 antiviral testing method, we first sought to determine an appropriate host cell line and the respective MOI. The purpose was to identify the potential cell types that were permissive to infection with the mNeonGreen SARS-CoV-2 reporter virus and provide robust and biologically relevant results for the antiviral testing method. In this initial experiment, we compared the infection of Calu3, Huh7, ACE2-A549, Detroit 562, and Fadu cells at various MOIs. The fluorescent overlay images of Hoechst and mNeonGreen are displayed in Figure B1.1, which visually showed higher infection for Calu3 in comparison to Huh7. The ACE2-A549 also showed high infection, however, a significant cell loss was observed.

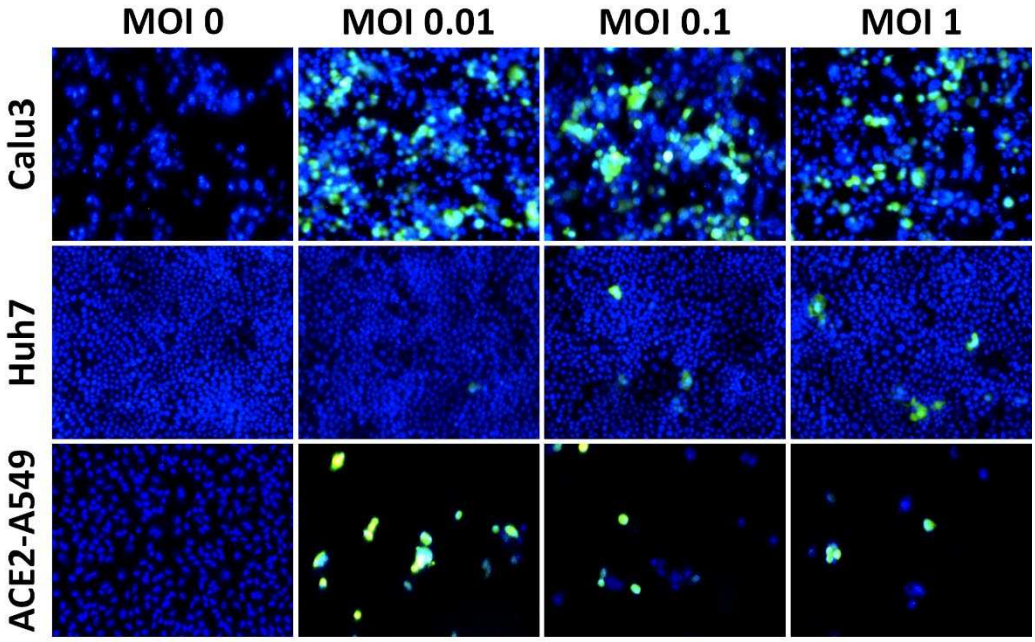

Figure B1.1. Fluorescent overlay images of Hoechst and mNeonGreen SARS-CoV-2-infected Calu3, Huh7, and ACE2-A529 at MOIs 0.01, 0.1, and 1. Visually, Calu3 and ACE2-A549 cells both showed permissibility to the SARS-CoV-2 virus, but only the ACE2-A549 showed significant cell loss.

The normalized mNeonGreen cell count results are shown in Figure B1.2a-d, which indicated that ACE2-A549, Huh7, and Calu3 were permissive to SARS-CoV-2 at low MOI and were viable candidate host cell lines. The Detroit 562 and Fadu cell lines did not show any mNeonGreen fluorescence, indicating that they were not permissive to SARS-CoV-2 infection (Supplemental Figure B1.1). In addition, we observed significant cytopathic effect in SARS-CoV-2-infected ACE2-A549 cells causing cell loss that was not observed in other human cell lines (Figure B1.2e-f), which suggested that overexpression of ACE2 in these cells may increase SARS-CoV-2 replication kinetics. The Calu3 cells represent a more biologically relevant cell line (compared to Huh7 cells) and are naturally permissive to infection [334], and thus were selected as the most appropriate cell line for the antiviral testing method. The MOI of 0.1 for Calu3 was also selected based on its lower standard deviation.

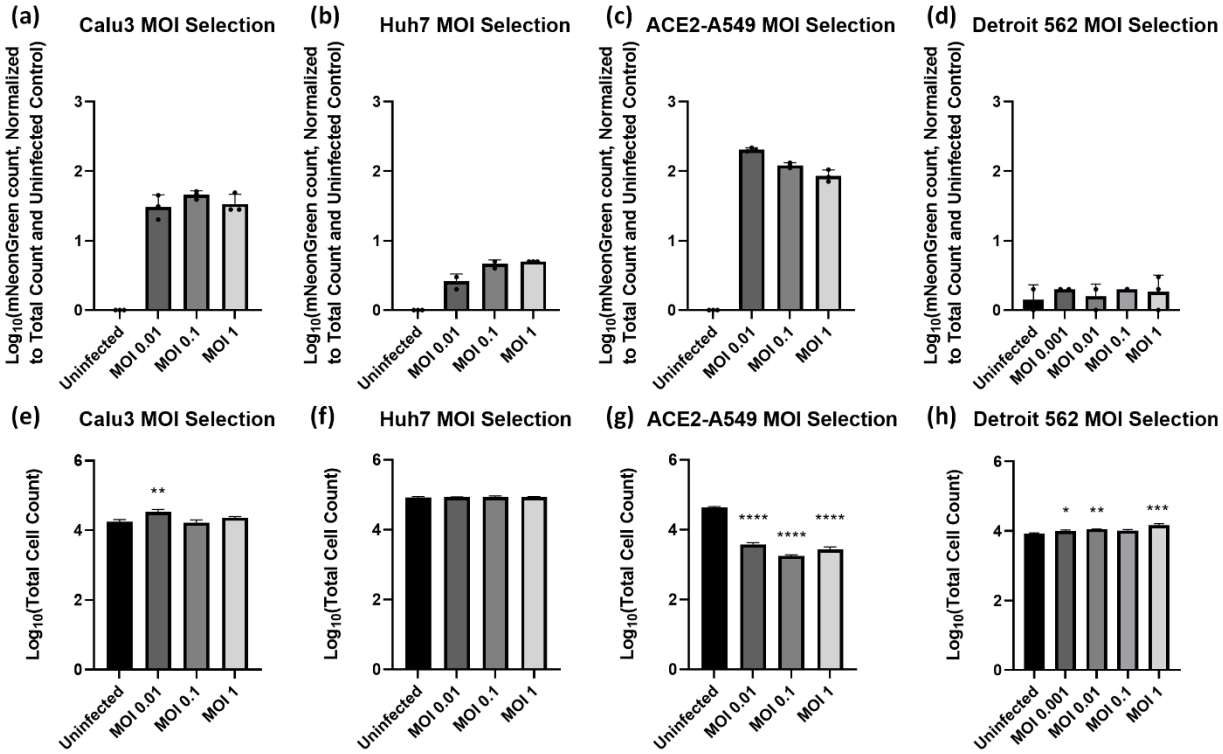

Figure A.1.2. Cell counting results measured by the image cytometer. (a-d) The mNeonGreen positive cell counting results normalized to the total cell count (e-h) measured by Hoechst staining. The Calu3 and ACE2-A549 cells showed significant increase to the mNeonGreen positive cell count, while Huh7 and Detroit 562 did not. The ACE2-A549 also showed a significant reduction in the total cell count. E-H: One way ANOVA with Dunnett's multiple comparisons test: * = p≤0.05, ** = p≤0.01, ***= p≤0.001, **** = p≤0.0001).

A.1.2.2 – Optimization of cell seeding density

To further optimize the image-based antiviral testing method, we performed a cell seeding density experiment to determine the optimal cell seeding per well. It was previously demonstrated that SARS-CoV-2 has a peak viral replication cycle at approximately 36 - 72 hours post-infection (hpi) [334]. Therefore, the seeding density should allow for adequate detection of the antivirals efficacy, visualization of the viral spread, and should not result in overgrowth/cell stress by 72 hpi. The cell proliferation bright field images are shown in Figure B1.3 and Supplemental Figure B1.2 for 1 x 10^5, 8 x 10^4, 6 x 10^4, 4 x 10^4, 2 x 10^4, and 1 x 10^4 cells/well. For seeding densities above 4 x 10^4 cells/well at 96 hours post seeding (representing 72 hours post infection), the confluence percentages were 85 – 100%, which may stress the host cells (Figure B1.4). The seeding density of 2 x 10^4 cells/well provided a clear visualization of host cells in the well and did not show overgrowth over the 96 hours.

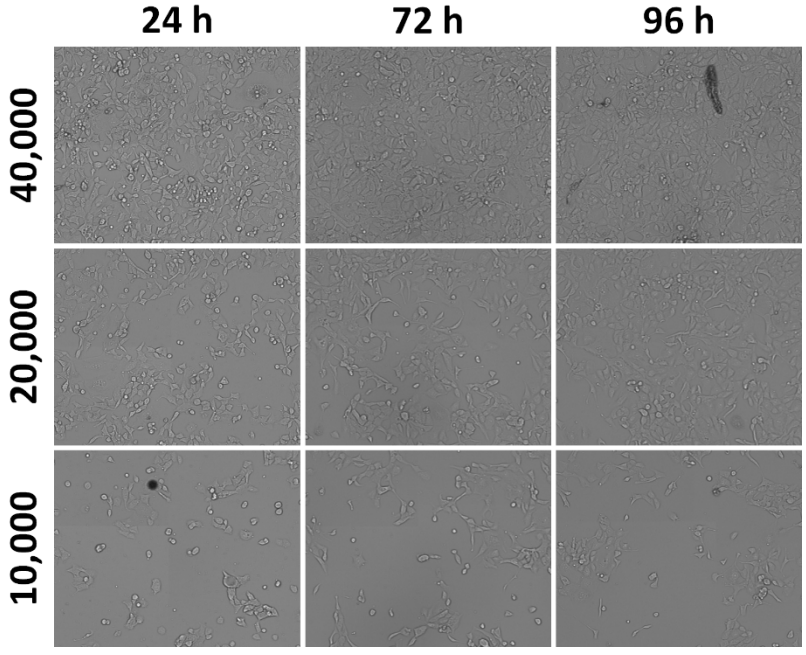

Figure B1.3. The bright field images of Calu3 confluency at seeding densities 1 x 10^4, 2 x 10^4, and 4 x 10^4 cells/well from 24 to 96 h. Visually, 2 x 10^4 cells/well is the most appropriate density.

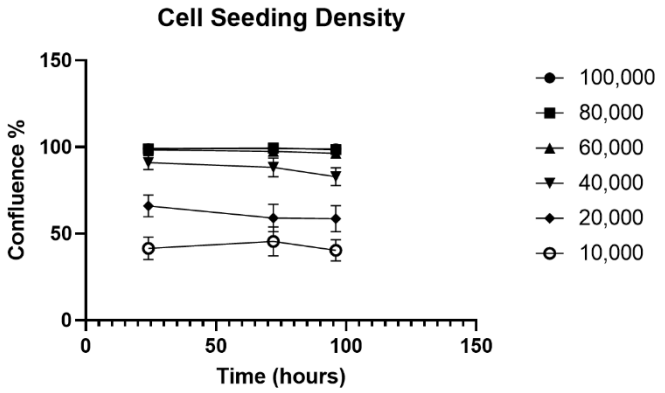

Figure B1.4. Time-course confluence percentages of Calu3 at seeding densities from 1 x 10^4 to 1 x 10^5 cells/well. The 2 x 10^4 cells/well showed a consistent 60 – 70% confluence over time, while densities at 4 x 10^4 or above showed closer to 100% confluence.

A.1.2.3 – Demonstration of the high-throughput antiviral testing method

The selected host cell line (Calu3), MOI (0.1), and seeding density (2 x 10^4 cells/well) were employed to develop the antiviral testing method. To demonstrate the image-based antiviral testing method, we investigated the effects of four drug compounds that were repurposed for treatment of SARS-CoV-2 infection. Each of the drug compounds (Remdesivir, Ribavirin, Ambroxol HCl, GENZ-123346) showed different antiviral effects on the SARS-CoV-2-infected Calu3 cells (Figure B1.5). Remdesivir showed the highest effect, Ribavirin and GENZ-123346 showed similar effects, and Ambroxol HCl was the least effective drug, but still showed ~0.5 log reduction in viral replication.

In addition, we investigated the cytotoxic effects of the drug compounds on healthy Calu3 cells. The live/dead ratio results are shown in Figure B1.6, and the normalized live and dead cell counts are shown in Supplemental Figure B1.3. Remdesivir seemed to have no effects on the live/dead ratio except for 5 μM. Both Ambroxol HCl and Ribavirin showed cytoprotective effects as the concentration increased. Finally, GENZ-123346 showed cytoprotective effects at low concentrations, but significant cytotoxic effects at high concentrations. It is interesting to note that

each drug compound showed different effects on the live and dead cell counts, specifically, Ambroxol HCl showed increase in live cell counts, while Ribavirin showed decrease in dead cell counts, and GENZ-123346 showed both increase and decrease in live cell counts and increase in dead cell counts.

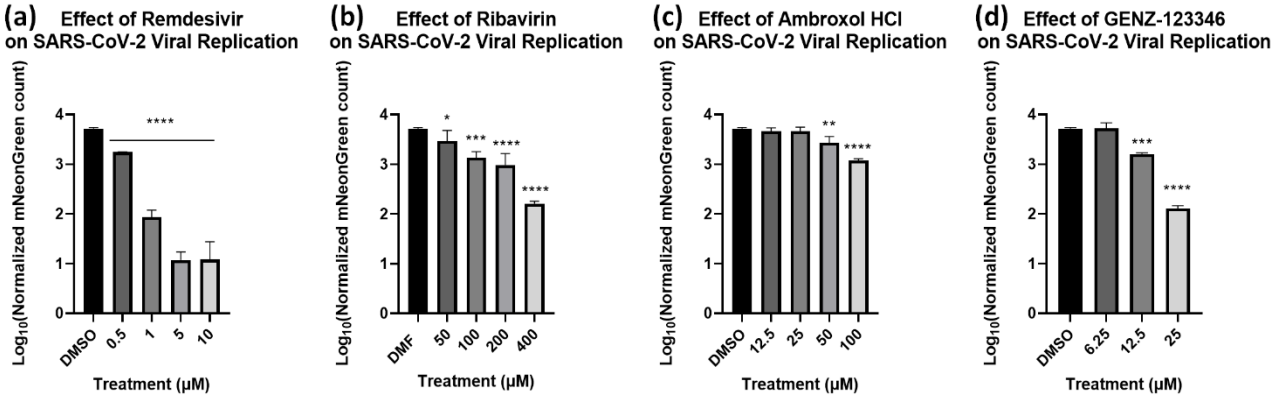

Figure 5. Concentration-dependent effects of drug compounds on SARS-CoV-2 viral replication for (a) Remdesivir, (b) Ribavirin, (c) Ambroxol HCl, and (d) GENZ-123346. All the tested drug compounds showed reduction in the mNeonGreen positive cells, with the following ranking: Remdesivir > Ribavirin ≅ GENZ-123346 > Ambroxol HCl (One way ANOVA with Dunnett's multiple comparisons test: * = p≤0.05, ** = p≤0.01, ***= p≤0.001, **** = p≤0.0001).

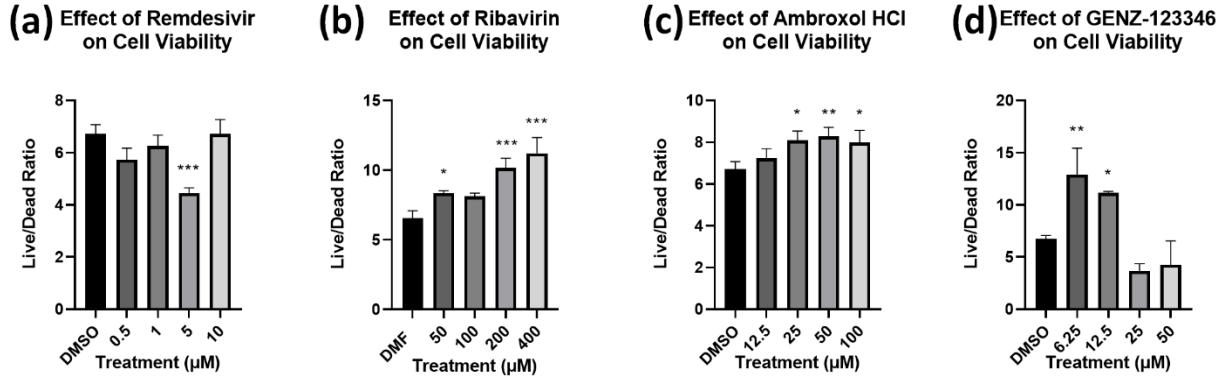

Figure 6. Concentration-dependent effects of drug compounds on host cell viability (live/dead ratio) for (a) Remdesivir, (b) Ribavirin, (c) Ambroxol HCl, and (d) GENZ-123346. Remdesivir showed no notable changes to cell viability, while both Ribavirin and GENZ-123346 showed cytoprotective effects with increased viability. GENZ-123346 showed increased viability at low MOI and vice versa at high MOI (One way ANOVA with Dunnett's multiple comparisons test: * = p≤0.05, ** = p≤0.01, ***= p≤0.001).

B1.3: Discussion

The SARS-CoV-2 viral outbreak has spread rapidly across the globe prompting the urgent need for discovery of novel antiviral and vaccine candidates. To increase the efficiency of screening of viable candidates, it is important to develop a high-throughput antiviral testing method that can show significant improvement from the traditional assays such as PRNT or RT-PCR. Plate-based image cytometry can increase the speed of data acquisition and analysis in a high-speed and high-throughput manner, enables bright field- and fluorescence-based detection, as well as provide image-based digital records.

We demonstrated the use of the Celigo Image Cytometer for high-throughput SARS-CoV-2 antiviral testing by first optimizing the methodology by selecting a host cell line and optimizing the MOI and seeding density. Of the five host cell lines tested, only Calu3 showed a high increase in normalized mNeonGreen positive cells on an order of ~2 logs without inducing cytopathic effects on the host cells. The ACE2-A549 showed greater than 2 decades of increase in mNeonGreen positive cells, however, severe cytopathic effects and cell death were observed rendering this cell line inappropriate for this assay. The MOI of 0.1 for Calu3 showed the most stable infection rate, thus was selected for the testing method. Due to variations of cell counts during initial seeding and potential cell loss after infection, the total cell counts were used to normalize the mNeonGreen positive cell counts to minimize the variations in the results.

The seeding density required optimization to ensure the host cells are not over-confluent 96 h post-seeding, which can stress the cells and potentially affect the infectivity of SARS-CoV-2 virus on the host cells. Seeding densities at 4×10^4 cells/well or above showed confluence percentages approximately 85 – 98%, which was too high for the assay. Both 1×10^4 and 2×10^4 seemed to be in the appropriate range for cell seeding. Interestingly, the seeded Calu3 cells did

not proliferate, and remained consistent from 24 – 96 h, which indicated that Calu3 is a slow growing cell type and is consistent with other published studies [335].

After optimizing the high-throughput antiviral testing method, two experiments were performed to test four pre-selected compounds repurposed for COVID-19 treatment. The first experiment explored the infectivity of SARS-CoV-2 virus, which was accomplished by measuring the number of mNeonGreen positive cells and total cell count for normalization. Both Remdesivir and Ribavirin have previously shown *in vitro* and had clinical efficacy against the SARS-CoV-2 virus [336]. In this experiment, those results were recapitulated using the image cytometry method showing strong concentration-dependent antiviral effects against SARS-CoV-2 at higher concentrations. Ambroxol HCl and GENZ-123346 also showed concentration-dependent antiviral effects at the two highest concentrations. It is important to note that the 50 μM treatment of GENZ-123346 was not included in the results as it was cytotoxic and complete loss of cells was observed.

The second experiment investigated the cytotoxic effects of the drug compounds on the host cells. The cell viability was calculated by the normalized live cell count divided by the normalized dead cell count, which combined the effects of the drugs on live and dead cells. For example, except for 5 μM Remdesivir the remaining concentrations showed consistent live and dead cell count, which resulted in consistent live/dead ratios over the dosages. The Ribavirin treatment showed no effects on the live cell counts but reduced the number of dead cells with increasing concentrations, which resulted in an increase in live/dead ratio. In contrast, Ambroxol HCl showed no effects on the dead cell counts but increased the number of live cells with increasing concentrations, which also resulted in an increase in live/dead ratio. The most interesting results were characterized for GENZ-123346, where the live and dead cell counts were indirectly correlated as the concentrations increased. At the two lower dosages, the live and dead cell counts increased and decreased, respectively, and reversed at the two higher dosages. The

GENZ-123346 results indicated that this drug was cytoprotective at lower dosages and cytotoxic at higher dosages, thus further characterization is required to ensure the safe use of this drug compound.

In conclusion, the development of an image-based high-throughput antiviral testing method allowed rapid characterization of potential antiviral drug candidates, which enabled direct quantification of the antiviral effects on SARS-CoV-2 viral infectivity and their cytotoxic and/or cytoprotective effects to the host cells, which are both critical to ensure the efficacy and safety of the potential antiviral drug candidates. Furthermore, the versatility of the methodology developed in this work may also be adopted for screening antiviral candidates for other diseases.

B1.4: Materials and Methods

B1.4.1 – Cell lines and viruses used

The cell lines used to develop the plate-based image cytometry method for SARS-CoV-2 antiviral testing have been published previously: Human lung adenocarcinoma cells stably transfected to express ACE2 (ACE2-A549s) [249], Human lung adenocarcinoma (Calu3) cells (ATCC HTB-55), two human pharyngeal carcinoma (Fadu, Detroit 562) cell lines (ATCC HTB-43 and ATCC CCL-138), human hepatoma (Huh7) cells (unknown sex, a gift from Dr. Charles Rice) [261], and African green monkey kidney epithelial (Vero E6) cells (ATCC CRL-1586).

ACE2-A549s, Huh7, and Vero E6 cells were maintained in Dulbecco's Modified Eagle Medium (DMEM) (Gibco/Life Technologies, Carlsbad, CA) and supplemented with 10% heat-inactivated fetal bovine serum (FBS) (Atlas Biologicals, Fort Collins, CO). Calu3 cells were maintained in DMEM and supplemented with 15% non-heat inactivated FBS. Fadu and Detriot 562 cells were maintained in Minimum Essential Media (MEM) (Gibco/Life Technologies)

supplemented with 10% non-heat inactivated FBS. All media was also supplemented with 2 mM nonessential amino acids (HyClone, Logan, UT), 2 mM L-glutamine (HyClone), and 25 mM HEPES buffer. All cell lines were maintained at 37°C with 5% CO_2.

The mNeonGreen SARS-CoV-2 virus strain was provided by the World Reference Center for Emerging Viruses and Arboviruses at the University of Texas Medical Branch, Galveston, TX [337]. This infectious clone was constructed by Xie et al. based on the virus strain (2019-nCOV/USA_WA01/2020) isolated from the first reported SARS-CoV-2 case in the US [338–340]. Viral stocks were amplified in Vero E6 cells to passage 1 (P1) with a titer of 9.67 x 10^5 PFU/mL and were stored at -80°C. Viral infections were carried out at specific multiplicity of infection (MOI) and incubation time for assay development. During all infections, cells were overlaid with either MEM or DMEM supplemented with 2% heat-inactivated FBS, 2 mM non-essential amino acids, 2 mM L-glutamine, and 25 mM HEPES buffer.

B1.4.2 – Celigo instrumentation and software application

The Celigo Image Cytometer has been described previously, which utilizes one bright field (BF) and four fluorescence (FL) imaging channels: Blue (Ex/Em: 377/470 nm), Green (Ex/Em: 483/536 nm), Red (Ex/Em: 531/629 nm), and Far Red (Ex/Em: 628/688 nm) in combination with high-power light-emitting diodes [341–344].

The Celigo software application “Confluence 1” was used to measure the host cell confluence percentages using the acquired bright field images. The preset ANALYZE parameters were optimized to automatically measure confluence percentages. The confluence percentages were calculated as the ratio of cell surface area coverage divided by total surface area in the well measured directly from the image cytometer. The results were used to optimize Calu3 seeding density.

The Celigo software application “Target 1 + 2 + Mask” was used to identify the total number of Hoechst-positive host cells (Ex/Em: 352/461 nm) in the Blue channel and the number of mNeonGreen fluorescent infected cells (Ex/Em: 506/517 nm) in the Green channel. The Celigo instrument was set up to acquire images in the Target 1 (BF), Target 2 (Green), and Mask (Blue) channels, where the exposure times for mNeonGreen and Hoechst were 60,000 and 145,000 µs, respectively. Image-based autofocus was used to focus in the BF channel, and the focus offsets were applied for the BF (-2 µm), Green (0 µm) and Blue (-15 µm) channels. The preset ANALYZE parameters were optimized to identify the Hoechst-positive host cells above an intensity threshold of 2, then the gating feature was used to determine the mNeonGreen-positive infected cell number.

The Celigo software application “Target 1 + 2 + 3 + 4” was used to identify the total number of Hoechst-positive cells (Ex/Em: 352/461 nm) in the Blue channel, the number of live/metabolically active Calcein AM-positive cells (Ex/Em: 488/520 nm) in the Green channel, and dead propidium iodide-positive cells (PI, Ex/Em: 496/636 nm). The Celigo instrument was set up to acquire images in the Target 1 (BF), Target 2 (Blue), Target 3 (Green), and Target 4 (Red) channels, where the exposure times for Hoechst, Calcein AM, and PI were 23,000, 10,000, and 10,000 µs, respectively. Image-based autofocus was used to focus in the BF channel, and the focus offsets were applied for the BF (-8 µm), Blue (-13 µm), Green (+7 µm) and Red (0 µm) channels. The preset ANALYZE parameters were optimized to identify the fluorescent positive cells above an intensity threshold of 4.

B1.4.3 – Host cell line and MOI selection

Multiple host cell lines were infected with different MOIs of the mNeonGreen SARS-CoV-2 virus to select the most appropriate cell type for antiviral testing. First, the ACE2-A549, Calu3, Huh7, Fadu, Detroit 562, and Vero E6 cell types were seeded in a 96-well plate (Greiner 655180)

at 20,000 cells/well and allowed to adhere overnight. After 24 hours post-seeding, the ACE2-A549, Calu3, and Huh7 were infected with MOIs of 0.01, 0.1, and 1. The Fadu and Detroit 562 were infected with MOIs of 0.001, 0.01, 0.1, and 1. After 72 hours post-infection (hpi), the cells were stained with ViaStain^{TM} Hoechst 33342 (Nexcelom Bioscience, Lawrence, MA) following manufacturer's instructions. Subsequently, the wells were scanned using the image cytometer to determine the total cell count and infected cell count for selecting the most optimal cell type. The infected cell count results were normalized to the average total cell count.

B1.4.4 – Cell seeding density selection

A cell proliferation experiment was conducted to optimize the seeding density for the antiviral testing method using Calu3 that was selected from the experiment described previously. The Calu3 cells were seeded at densities of 1 x 10^5, 8 x 10^4, 6 x 10^4, 4 x 10^4, 2 x 10^4, and 1 x 10^4 cells/well in a 96-well plate. The cells were allowed to incubate for 96 hours post-seeding, where the plate was scanned using the image cytometer at 24, 72, and 96 hours. The confluence percentages were measured at each time point to select a seeding density that can generate 50 – 70% confluence.

B1.4.5 – High- image-based antiviral testing method

To demonstrate the optimized antiviral testing method, an experiment was performed to measure the antiviral effects of four drugs on SARS-CoV-2-infected Calu3 cells. The four drugs chosen were Remdesivir, Ribavirin, Ambroxol hydrochloride (#A0363700, Sigma-Aldrich, St. Louis, MO), and GENZ-123346 (#28500, Cayman Chemical, Ann Arbor, MI). Remdesivir and Ribavirin were selected for the assay as positive controls since they were already shown to be relatively effective at inhibiting SARS-CoV-2 *in vitro* [336,345]. Ambroxol HCl and GENZ-123346

are both modulators of glucosylceramide, a lipid metabolite that may be vital for SARS-CoV-2 replication [220]. Ambroxol HCl is a molecular chaperone of β-glucocerebrosidase 1, and inhibitor of β-glucocerebrosidase 2, and can modulate glycosphingolipid metabolism in pathophysiological situations by these mechanisms [300]. GENZ-123346 is an inhibitor of glucosylceramide synthase. These compounds were chosen as part of an ongoing study in our laboratory investigating the role of sphingolipid metabolism in SARS-CoV-2 infections.

The Calu3 cells were first seeded at a density of 2 x 10^5 cells/well in 96-well plates and incubated overnight. Approximately 1 – 3 hours prior to infection, the growth media was removed from cells, and subsequently overlaid with DMEM supplemented with 2% heat-inactivated FBS, 2 mM NEAA, 2 mM L-glutamine, 25 mM HEPES buffer, containing each compound at different concentrations: Remdesivir (10, 5, 1, 0.5 μM), Ribavirin (400, 200, 100, 50 μM), Ambroxol HCl (100, 50, 25, 12.5 μM), and GENZ-123346 (50, 25, 12.5, 6.25 μM). The concentrations selected were based on published IC_{50} values for Remdesivir and Ribavirin [336] and previous optimization in our studies for Ambroxol HCl and GENZ-123346. The cells were then infected with the mNeonGreen SARS-CoV-2 virus at MOI of 0.1 for 72 hours. Each drug compound and its corresponding vehicle control (DMSO or DMF) were tested in triplicate. It is important to note that the 96-well plates were made in duplicate to investigate the antiviral activity as well as assessing cytotoxicity effects of the compounds on host cells in parallel.

Following the infection experiment, the supernatant from infected Calu3 cells was harvested and stored at -80°C. The remaining cells were washed with 1X PBS, and then stained with the ViaStain™ Hoechst 33342 following manufacturer's instructions. To determine viral replication, the plates were imaged and analyzed using the image cytometer to count the total number of Calu3 cells with Hoechst staining and mNeonGreen SARS-CoV-2 infection. The infected cell count results were normalized to the average total cell count.

In contrast, the cytotoxicity plates were not infected with the mNeonGreen reporter virus, but all other conditions and timeframes were maintained. Following the experiment, the media from uninfected cells was aspirated, cells were washed with 1X PBS, and then were stained with the ViaStain^{TM} Calcein AM/Hoechst/PI Viability Kit following manufacturer's instructions. The viability kit allowed for determination of the effects of various compounds and their respective concentrations on host cell viability. To determine the cell viability, the plates were imaged and analyzed using the image cytometer to count the total number of cells with Hoechst, the live cells with Calcein AM, and dead cells with PI. The live and dead cell count results were also normalized to the average total cell count.

B1.4.6 – Statistical Analysis

The statistical analysis method used is noted in each applicable figure. Determination of statistical significance for antiviral effect, cell viability, and live/dead cell counts was performed using a one-way Analysis of Variance (ANOVA) with Dunnett's multiple comparisons using version 9.3.1 of Prism software (GraphPad Software, La Jolla, California, USA).

B1.5 – Supplemental Figures

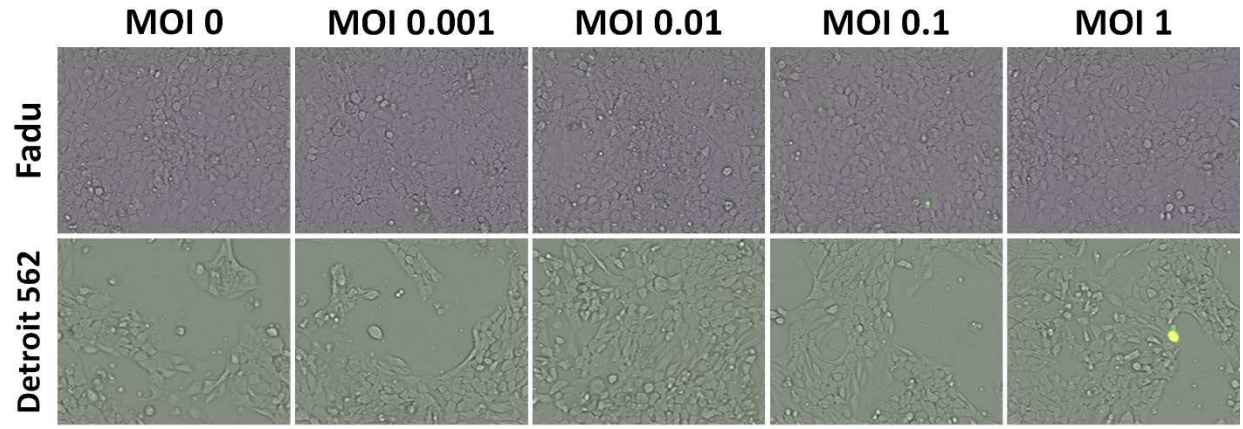

Supplemental Figure B1.1. Bright field and fluorescent overlay images of mNeonGreen SARS-CoV-2-infected Fadu and Detroit 562 at MOIs 0.001, 0.01, 0.1, and 1. Visually, both cell lines showed low to no permissibility to the SARS-CoV-2 virus.

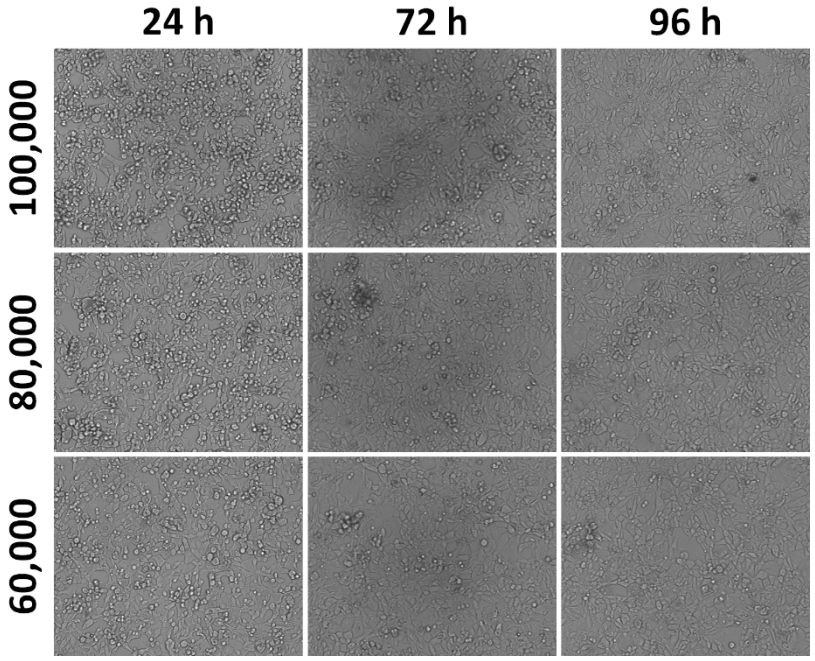

Supplemental Figure B1.2. The bright field images of Calu3 confluency at seeding densities 6 x 10^4, 8 x 10^4, and 1 x 10^5 cells/well from 24 to 96 h. Visually, these densities are over-confluent.

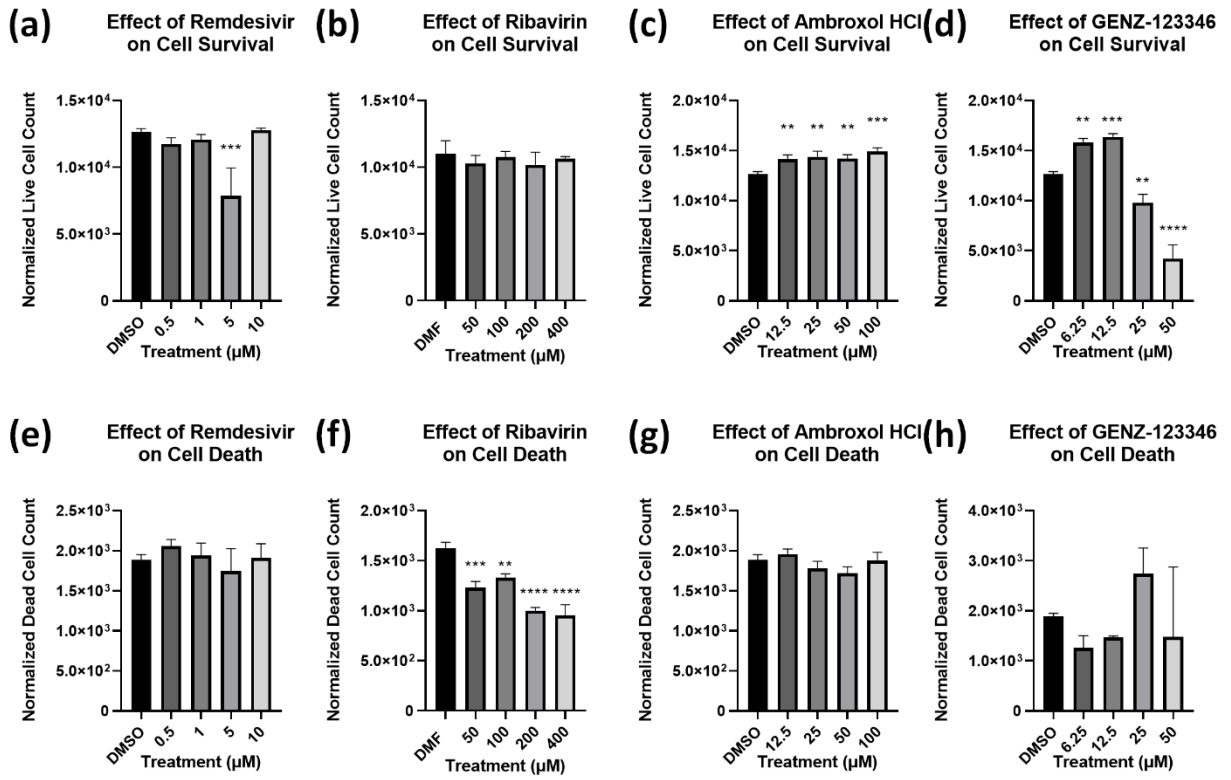

Supplemental Figure B1.3. Concentration-dependent effects of drug compounds on live and dead cell count for (a, e) Remdesivir, (b, f) Ribavirin, (c, g) Ambroxol HCl, and (d, h) GENZ-123346 (One way ANOVA with Dunnett's multiple comparisons test: * = p≤0.05, ** = p≤0.01, ***= p≤0.001, **** = p≤0.0001).

Appendix B2 – Collaborations and Other Works

B2.1 – Additional Flavivirus Related Works

1. Trammell CE, Ramirez G, Sanchez-Vargas I, **St Clair LA**, Ratnayake OC, Luckhart S, Perera R, Goodman AG. Coupled small molecules target RNA interference and JAK/STAT signaling to reduce Zikva virus infection in *Aedes aegypti* (2022). PLoS Pathogens, 18(4): e1010411. DOI: 10.1371/journal.ppat.1010411

Abstract: The recent global Zika epidemics have revealed the significant threat that mosquito-borne viruses pose. There are currently no effective vaccines or prophylactics to prevent Zika virus (ZIKV) infection. Limiting exposure to infected mosquitoes is the best way to reduce disease incidence. Recent studies have focused on targeting mosquito reproduction and immune responses to reduce transmission. Previous work has evaluated the effect of insulin signaling on antiviral JAK/STAT and RNAi in vector mosquitoes. Specifically, insulin-fed mosquitoes resulted in reduced virus replication in an RNAi-independent, ERK-mediated JAK/STAT-dependent mechanism. In this work, we demonstrate that targeting insulin signaling through the repurposing of small molecule drugs results in the activation of both RNAi and JAK/STAT antiviral pathways. ZIKV-infected *Aedes aegypti* were fed blood containing demethylasterriquinone B1 (DMAQ-B1), a potent insulin mimetic, in combination with AKT inhibitor VIII. Activation of this coordinated response additively reduced ZIKV levels in *Aedes aegypti*. This effect included a quantitatively greater reduction in salivary gland ZIKV levels up to 11 d post-bloodmeal ingestion, relative to single pathway activation. Together, our study indicates the potential for field delivery of these small molecules to substantially reduce virus transmission from mosquito to human. As infections

like Zika virus are becoming more burdensome and prevalent, understanding how to control this family of viruses in the insect vector is an important issue in public health.

Project contributions: Experimental design, data curation, formal analysis, manuscript editing. Data curation entailed mosquito rearing and colony maintenance of *Aedes aegypti* mosquitoes, as well as all experimentation for Figure 2 (sugar-bait delivery of DMAQ-B1 and AKT Inhibitor VIII inhibitors model and survival analysis).

2. Gullberg RC, Chotiwan N, Lian E, Islam N, St Clair LA, Edwards TJ, Graham B, Krieger K, Khadka S, Hopf-Jannasch A, LaCount DJ, Kuhn RJ, Belisle JT, and Perera R. A change in the cellular metabolic landscape provides a refractory environment for flavivirus replication (2022). (Reviewed and preparing for resubmission to PLoS Pathogens).

Abstract: Host-targeted therapeutics to control viral infection are gaining prominence given the vulnerability of viral replication at select host-interaction points and the limited possibility of developing drug resistant mutants. Nevertheless, the chemical and biological impact of many host-targeted therapeutics on both the cell and virus has not been elucidated and remains a key complication. Previously, it has been demonstrated that inhibition of fatty acid metabolism has significant antiviral potential. Here, we use a multidisciplinary approach to demonstrate how inhibition of fatty acid biosynthesis creates a metabolically refractory environment that drives viral dependence on alternate metabolic pathways for survival. By profiling the global metabolic landscape following inhibition of fatty acid biosynthesis, we identified additional biochemical pathways that, when inhibited in combination with fatty acid biosynthesis, displayed increased antiviral potential. Our studies also demonstrated that there was a direct link between changes in cellular chemical composition and the ultrastructural membrane architecture induced by viral gene products. Utilizing inhibitors to change these metabolic environments significantly impacted early

viral replication and disrupted the membrane architecture critical for the viral life cycle. Here, we have defined at a molecular level how shifting metabolic landscapes can be exploited to identify combinations of therapeutics that have a greater antiviral effect.

Project Contributions: Experimental design, data curation, formal analysis, manuscript editing. Data curation entailed generating dose-response curves for orlistat, C75 and 6TG; experimentation to validate the impact of each inhibitor on positive and negative strand DENV2 genome synthesis; and experimentation to determine additive effect of combined inhibitor treatment on DENV2 viral release.

B2.2 – SARS-CoV-2 Related Works

1. Burke JM, **St Clair LA**, Perera R, and Parker R. SARS-CoV-2 infection triggers widespread host mRNA decay leading to an mRNA export block. *RNA,* 27(11):1318-1329. doi: 10.1261/rna.078923.121

Abstract: The transcriptional induction of *interferon* (*IFN*) genes is a key feature of the mammalian antiviral response that limits viral replication and dissemination. A hallmark of severe COVID-19 disease caused by SARS-CoV-2 is the low presence of IFN proteins in patient serum despite elevated levels of *IFN*-encoding mRNAs, indicative of post-transcriptional inhibition of IFN protein production. Here, we performed single-molecule RNA visualization to examine the expression and localization of host mRNAs during SARS-CoV-2 infection. Our data show that the biogenesis of type I and type III *IFN* mRNAs is inhibited at multiple steps during SARS-CoV-2 infection. First, translocation of the interferon regulatory factor 3 (IRF3) transcription factor to the nucleus is limited in response to SARS-CoV-2, indicating that SARS-CoV-2 inhibits RLR-MAVS signaling and thus weakens transcriptional induction of *IFN* genes. Second, we observed that *IFN*

mRNAs primarily localize to the site of transcription in most SARS-CoV-2 infected cells, suggesting that SARS-CoV-2 either inhibits the release of *IFN* mRNAs from their sites of transcription and/or triggers decay of *IFN* mRNAs in the nucleus upon exiting the site of transcription. Lastly, nuclear-cytoplasmic transport of *IFN* mRNAs is inhibited during SARS-CoV-2 infection, which we propose is a consequence of widespread degradation of host cytoplasmic basal mRNAs in the early stages of SARS-CoV-2 replication by the SARS-CoV-2 Nsp1 protein, as well as the host antiviral endoribonuclease, RNase L. Importantly, *IFN* mRNAs can escape SARS-CoV-2-mediated degradation if they reach the cytoplasm, making rescue of mRNA export a viable means for promoting the immune response to SARS-CoV-2.

Project Contributions: Experimental design, data curation (all SARS-CoV-2 BSL3 work), formal analysis, manuscript editing.

2. Burke JM, Ripin N, **St Clair LA**, Worden-Sapper ER, Sawyer SL, Perera R, Parker R. RNase-L mediated RNA decay alters 3' end formation and splicing of host mRNAs (2022). (Submitted to *BioRχiv*, under review at *Review Commons*)

Abstract: The antiviral endoribonuclease, RNase L, is a vital component of the mammalian innate immune response that destroys host and viral RNA to reduce viral gene expression. Herein, we show that a consequence of RNase L-mediated decay of cytoplasmic host RNAs is the widespread re-localization of RNA-binding proteins (RBPs) from the cytoplasm to the nucleus, due to the presence of nuclear RNA. Concurrently, we observe global alterations to host RNA processing in the nucleus, including downstream of gene (DoG) transcriptional read-through and intron retention. While affecting many host mRNAs, these alterations are pronounced in mRNAs encoding type I and type III interferons and coincide with the retention of their mRNAs in the nucleus. Similar RNA processing defects also occur during infection with either dengue virus or

SARS-CoV-2 when RNase L is activated. These findings reveal that the distribution of RBPs between the nucleus and cytosol is fundamentally dictated by the availability of RNA in each compartment and thus viral infections that trigger cytoplasmic RNA degradation alter RNA processing due to the nuclear influx of RNA binding proteins.

Project Contributions: Experimental design, data curation (all SARS-CoV-2 BSL3 work), formal analysis, manuscript editing.

B2.3 – Patents Submitted

1. Spedding M[1], Perera R[1], St Clair LA[1]. Novel use of a modulator of glucosylceramide degradation. Demand International n°PCT/EP2021/006314, filed June 6, 2021. Patent pending.

[1]co-inventors

Patent Description: The present invention relates to a modulator of glucosylceramide degradation or a pharmaceutical acceptable salt thereof, as active ingredient, in an effective amount for treating or preventing viral infections and disorders associated to the viral infections.

The present invention also relates to a modulator of glucosylceramide degradation or a pharmaceutical acceptable salt thereof, as active ingredient, in an effective amount for its use for treating or preventing viral infections and disorders associated to the viral infections.

Surprisingly, the inventors have shown that the modulator of glucosylceramide degradation, and, in particular, ambroxol inhibits the replication of enveloped viruses, and in particular inhibits the replication of the SARS-CoV-2 virus and of the dengue virus. In particularly, the inventors have shown that sphingolipids (GSLs) are essential in the infection cycle of enveloped human RNA viruses, which are critically dependent on host cell lipid synthesis.

Furthermore, the inventors have shown that the modulator of glucosylceramide degradation is able to inhibit viral multiplication by inhibiting glucosylceramide degradation. The inventors have also shown that the modulator of glucosylceramide degradation has major effects in viral infections due to SARS-CoV-2, by blocking the access of the virus to the lungs, by blocking the access of the virus to ACE2/TMPRSS2 and lipid rafts and thus inhibiting the internalization of the virus. The inventors have also shown that the modulator of glucosylceramide degradation is able to protect the lungs and the cardiac function of the patient suffering from viral infection due to SARS-CoV-2, but also to protect the patient suffering from viral infection due to SARS-CoV-2 from muscle loss, and recovery from intensive care. The inventors have also shown that the modulator of glucosylceramide degradation is able to modulate the mitochondrial function.

Patent Contributions: Experimental design, data curation, formal analysis, and patent editing. The DENV2 analysis and work that contributed to the application for this patent is presented in Chapter 4 of this thesis. In parallel to the DENV2 work, additional parallel studies were carried out testing the efficacy of Ambroxol HCl against SARS-CoV-2 using Calu3 (lung adenocarcinoma) cells. Those studies are not presented here or elsewhere as they are ongoing.

B2.4 – Rocky Mountain Virology Association Meeting Reports

1. **St Clair LA**, Brehm AL, Cagle S, Dunham T, Faris J, Gendler P, Graham ME, Quackenbush SL, Rovnak J, Perera R (2021). The 21st Annual Meeting of the Rocky Mountain Virology Association. Viruses, 13(1): 2392.

2. Rovnak J, **St Clair LA**, McAlister C, Ogbu C, Perera R, and Cohrs RJ. (2020). The 20th Rocky Mountain Virology Association Meeting. Viruses, 13(1): 38.

3. Rovnak J, **St Clair LA**, Lian E, McAlister C, Perera R, and Cohrs RJ. (2020). The 19th Rocky Mountain Virology Association Meeting. Viruses, 12(1): 85.

4. Rovnak J, **St Clair LA**, Krieger K, Lian E, Perera R, and Cohrs RJ. (2019). The 18th Rocky Mountain Virology Association Meeting. Viruses, 11(1): 4.

Latest Abstract (2021): Nestled within the Rocky Mountain National Forest, 114 scientists and students gathered at Colorado State University's Mountain Campus for this year's 21st annual Rocky Mountain National Virology Association meeting. This 3-day retreat consisted of 31 talks and 30 poster presentations discussing advances in research pertaining to viral and prion diseases. The keynote address provided a timely discussion on zoonotic coronaviruses, lessons learned, and the path forward towards predicting, preparing, and preventing future viral disease outbreaks. Other invited speakers discussed advances in SARS-CoV-2 surveillance, molecular interactions involved in flavivirus genome assembly, evaluation of ethnomedicines for their efficacy against infectious diseases, multi-omic analyses to define risk factors associated with long COVID, the role that interferon lambda plays in control of viral pathogenesis, cell-fusion-dependent pathogenesis of varicella zoster virus, and advances in the development of a vaccine platform against prion diseases. On behalf of the Rocky Mountain Virology Association, this report summarizes select presentations.

Paper Contributions: 2018-2020, collaborated with Randy Cohrs and Joel Rovnak, et al. to organize and prepare meeting abstracts for publication. 2021: assembled conference abstracts; wrote paper abstract, introduction and figure legends; and managed final assembly of article for publication.

Appendix C: Copyright Information

Overview

This appendix contains copyright and publication licenses from published papers or images generated using Biorender.com.

Chapter 1 – Figure 1.1

49 Spadina Ave. Suite 200
Toronto ON M5V 2J1 Canada
www.biorender.com

Confirmation of Publication and Licensing Rights

March 3rd, 2022
Science Suite Inc.

Subscription:	*Student Plan Promo (Legacy)*
Agreement number:	*WI23MO03O3*
Journal name:	*Dissertation*

To whom this may concern,

This document is to confirm that Laura St Clair has been granted a license to use the BioRender content, including icons, templates and other original artwork, appearing in the attached completed graphic pursuant to BioRender's Academic License Terms. This license permits BioRender content to be sublicensed for use in journal publications.

All rights and ownership of BioRender content are reserved by BioRender. All completed graphics must be accompanied by the following citation: "Created with BioRender.com".

BioRender content included in the completed graphic is not licensed for any commercial uses beyond publication in a journal. For any commercial use of this figure, users may, if allowed, recreate it in BioRender under an Industry BioRender Plan.

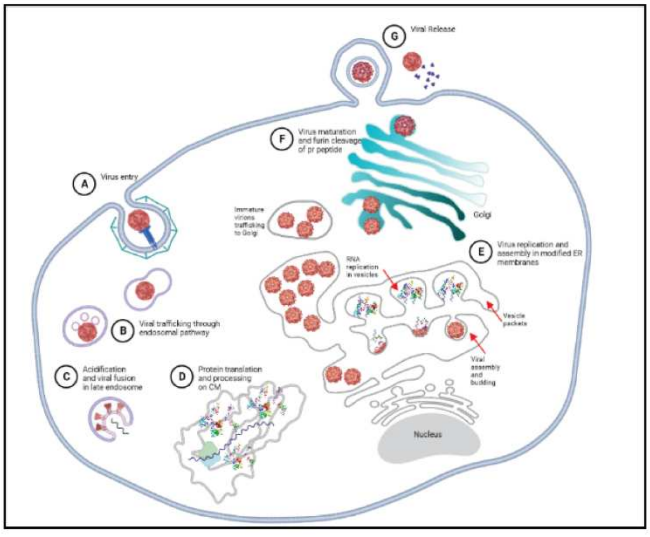

For any questions regarding this document, or other questions about publishing with BioRender refer to our BioRender Publication Guide, or contact BioRender Support at support@biorender.com.

Chapter 1 – Figure 1.2

49 Spadina Ave. Suite 200
Toronto ON M5V 2J1 Canada
www.biorender.com

Confirmation of Publication and Licensing Rights

March 4th, 2022
Science Suite Inc.

Subscription:	*Student Plan Promo (Legacy)*
Agreement number:	*NI23MTOX0A*
Journal name:	*Dissertation*

To whom this may concern,

This document is to confirm that Laura St Clair has been granted a license to use the BioRender content, including icons, templates and other original artwork, appearing in the attached completed graphic pursuant to BioRender's Academic License Terms. This license permits BioRender content to be sublicensed for use in journal publications.

All rights and ownership of BioRender content are reserved by BioRender. All completed graphics must be accompanied by the following citation: "Created with BioRender.com".

BioRender content included in the completed graphic is not licensed for any commercial uses beyond publication in a journal. For any commercial use of this figure, users may, if allowed, recreate it in BioRender under an Industry BioRender Plan.

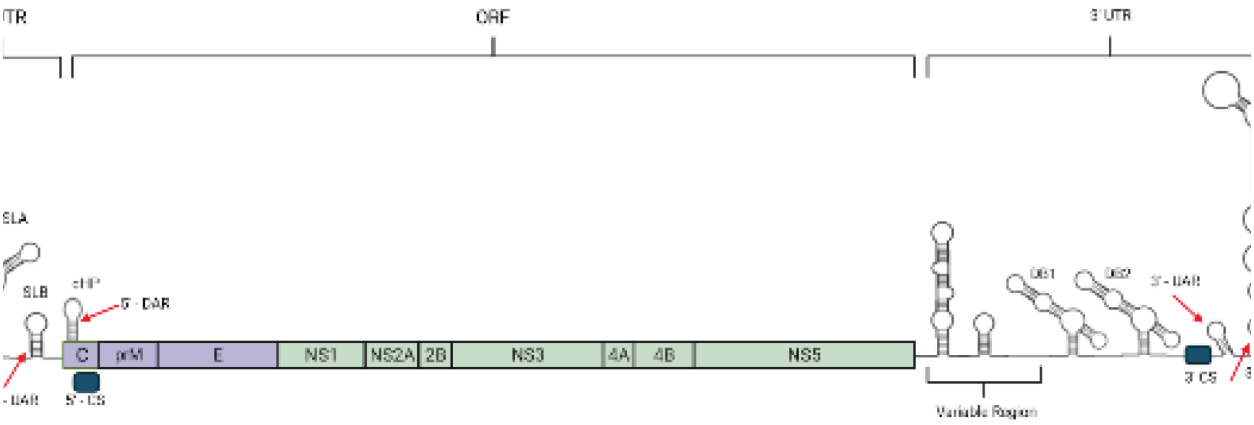

For any questions regarding this document, or other questions about publishing with BioRender refer to our BioRender Publication Guide, or contact BioRender Support at support@biorender.com.

Chapter 1 – Figure 1.3A

49 Spadina Ave. Suite 200
Toronto ON M5V 2J1 Canada
www.biorender.com

Confirmation of Publication and Licensing Rights

March 3rd, 2022
Science Suite Inc.

Subscription:	*Student Plan Promo (Legacy)*
Agreement number:	*IH23MSG9QV*
Journal name:	*Dissertation*

To whom this may concern,

This document is to confirm that Laura St Clair has been granted a license to use the BioRender content, including icons, templates and other original artwork, appearing in the attached completed graphic pursuant to BioRender's Academic License Terms. This license permits BioRender content to be sublicensed for use in journal publications.

All rights and ownership of BioRender content are reserved by BioRender. All completed graphics must be accompanied by the following citation: "Created with BioRender.com".

BioRender content included in the completed graphic is not licensed for any commercial uses beyond publication in a journal. For any commercial use of this figure, users may, if allowed, recreate it in BioRender under an Industry BioRender Plan.

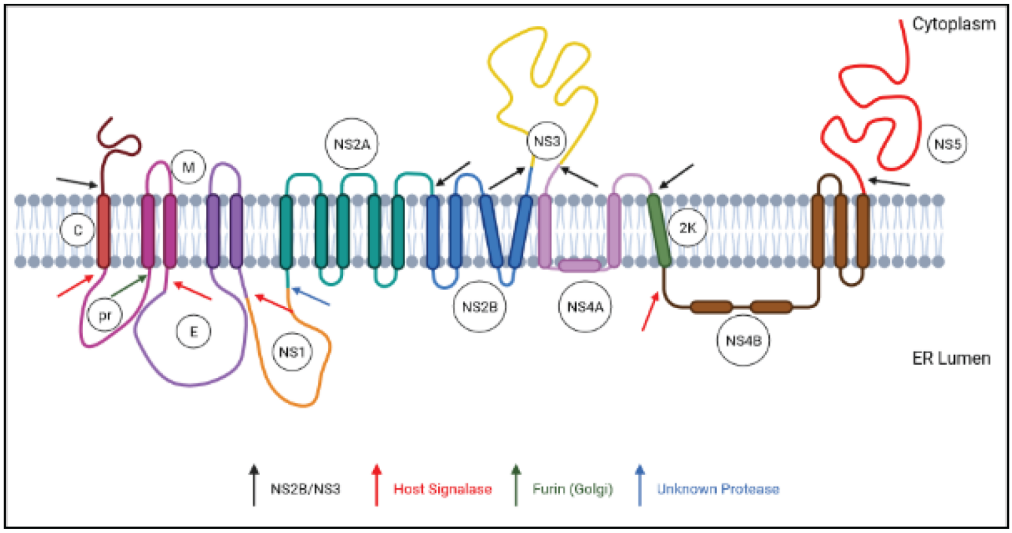

For any questions regarding this document, or other questions about publishing with BioRender refer to our BioRender Publication Guide, or contact BioRender Support at support@biorender.com.

Chapter 1 – Figure 1.3B

49 Spadina Ave. Suite 200
Toronto ON M5V 2J1 Canada
www.biorender.com

Confirmation of Publication and Licensing Rights

March 3rd, 2022
Science Suite Inc.

Subscription:	*Student Plan Promo (Legacy)*
Agreement number:	*UU23MSFBCC*
Journal name:	*Dissertation*

To whom this may concern,

This document is to confirm that Laura St Clair has been granted a license to use the BioRender content, including icons, templates and other original artwork, appearing in the attached completed graphic pursuant to BioRender's Academic License Terms. This license permits BioRender content to be sublicensed for use in journal publications.

All rights and ownership of BioRender content are reserved by BioRender. All completed graphics must be accompanied by the following citation: "Created with BioRender.com".

BioRender content included in the completed graphic is not licensed for any commercial uses beyond publication in a journal. For any commercial use of this figure, users may, if allowed, recreate it in BioRender under an Industry BioRender Plan.

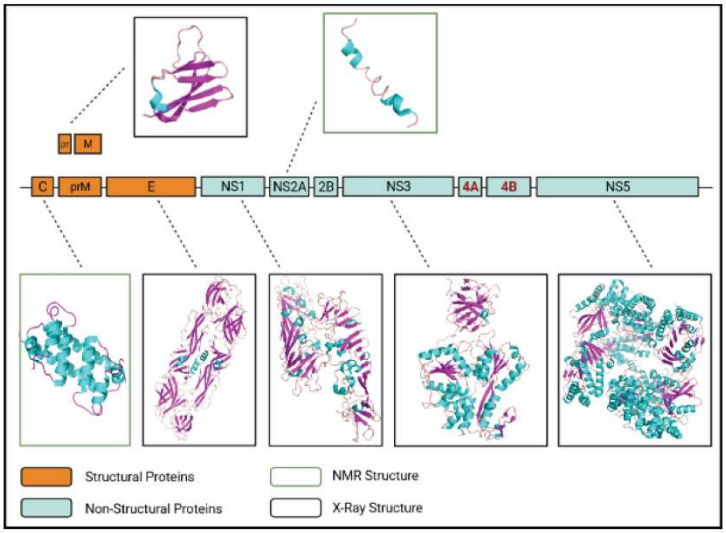

For any questions regarding this document, or other questions about publishing with BioRender refer to our BioRender Publication Guide, or contact BioRender Support at support@biorender.com.

Chapter 1 – Figure 1.4A-C

49 Spadina Ave. Suite 200
Toronto ON M5V 2J1 Canada
www.biorender.com

Confirmation of Publication and Licensing Rights

April 17th, 2022
Science Suite Inc.

Subscription:	*Student Plan Promo (Legacy)*
Agreement number:	*XP23T4RHWJ*
Journal name:	*Dissertation*

To whom this may concern,

This document is to confirm that Laura St Clair has been granted a license to use the BioRender content, including icons, templates and other original artwork, appearing in the attached completed graphic pursuant to BioRender's Academic License Terms. This license permits BioRender content to be sublicensed for use in journal publications.

All rights and ownership of BioRender content are reserved by BioRender. All completed graphics must be accompanied by the following citation: "Created with BioRender.com".

BioRender content included in the completed graphic is not licensed for any commercial uses beyond publication in a journal. For any commercial use of this figure, users may, if allowed, recreate it in BioRender under an Industry BioRender Plan.

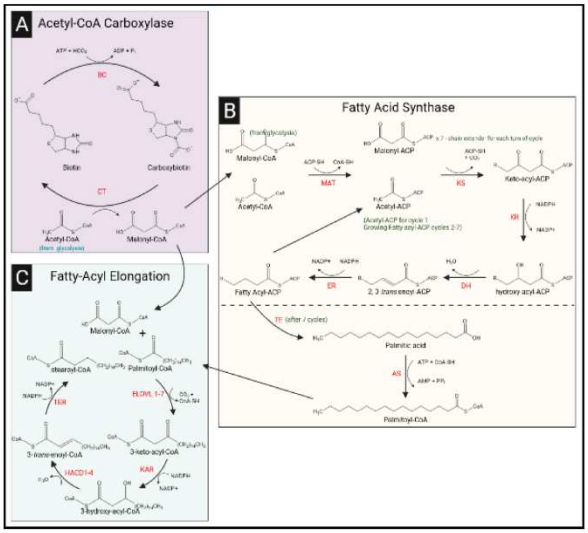

For any questions regarding this document, or other questions about publishing with BioRender refer to our BioRender Publication Guide, or contact BioRender Support at support@biorender.com.

Chapter 1 – Figure 1.4 D-F

49 Spadina Ave. Suite 200
Toronto ON M5V 2J1 Canada
www.biorender.com

Confirmation of Publication and Licensing Rights

April 17th, 2022
Science Suite Inc.

Subscription:	*Student Plan Promo (Legacy)*
Agreement number:	*RO23T4PKGE*
Journal name:	*Dissertation*

To whom this may concern,

This document is to confirm that Laura St Clair has been granted a license to use the BioRender content, including icons, templates and other original artwork, appearing in the attached completed graphic pursuant to BioRender's Academic License Terms. This license permits BioRender content to be sublicensed for use in journal publications.

All rights and ownership of BioRender content are reserved by BioRender. All completed graphics must be accompanied by the following citation: "Created with BioRender.com".

BioRender content included in the completed graphic is not licensed for any commercial uses beyond publication in a journal. For any commercial use of this figure, users may, if allowed, recreate it in BioRender under an Industry BioRender Plan.

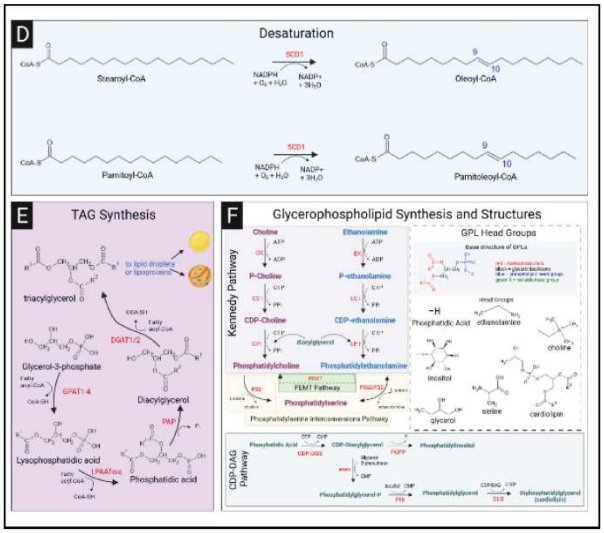

For any questions regarding this document, or other questions about publishing with BioRender refer to our BioRender Publication Guide, or contact BioRender Support at support@biorender.com.

Chapter 1 – Figure 1.5

49 Spadina Ave. Suite 200
Toronto ON M5V 2J1 Canada
www.biorender.com

Confirmation of Publication and Licensing Rights

March 19th, 2022
Science Suite Inc.

Subscription:	*Student Plan Promo (Legacy)*
Agreement number:	*MQ23OYM2D7*
Journal name:	*Dissertation*

To whom this may concern,

This document is to confirm that Laura St Clair has been granted a license to use the BioRender content, including icons, templates and other original artwork, appearing in the attached completed graphic pursuant to BioRender's Academic License Terms. This license permits BioRender content to be sublicensed for use in journal publications.

All rights and ownership of BioRender content are reserved by BioRender. All completed graphics must be accompanied by the following citation: "Created with BioRender.com".

BioRender content included in the completed graphic is not licensed for any commercial uses beyond publication in a journal. For any commercial use of this figure, users may, if allowed, recreate it in BioRender under an Industry BioRender Plan.

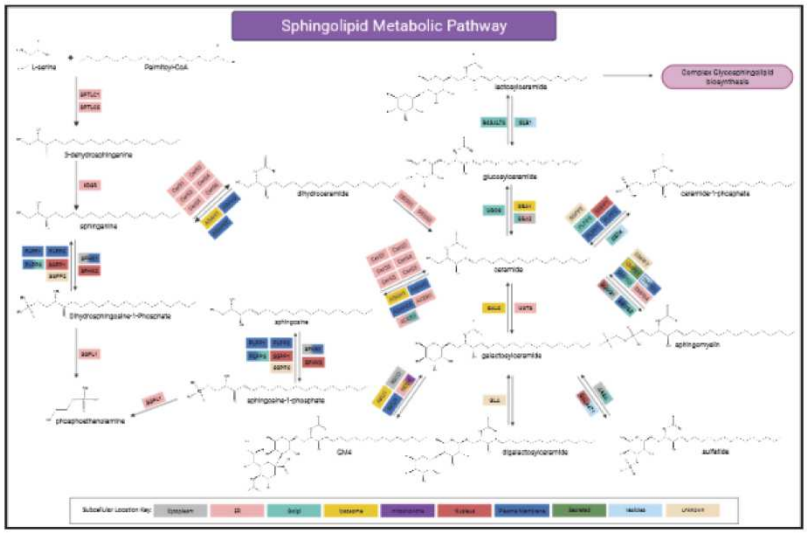

For any questions regarding this document, or other questions about publishing with BioRender refer to our BioRender Publication Guide, or contact BioRender Support at support@biorender.com.

Chapter 2 Manuscript

From: Laura Gasser
To: St Clair,Laura
Subject: Re: Fwd: Request for reprinting of manuscript
Date: Monday, February 28, 2022 8:21:02 AM

**** Caution: EXTERNAL Sender ****

Dear Laura St. Clair,

Thank you very much for your interest in said material.

All MDPI journals are Open Access and subject to the Creative Commons Attribution License (CC BY). The CC BY permits unrestricted use, distribution, and reproduction of the material in any medium, even commercially, ***provided the original work is properly cited***. You do not have to pay anything for permission.

For more information on the CC BY License, please see here:
https://creativecommons.org/licenses/by/4.0/legalcode

Best regards,
Laura Gasser

From: St Clair,Laura
Sent: Tuesday, February 22, 2022 11:38:52 AM
To: reprints@mdpi.com <reprints@mdpi.com>
Subject: Request for reprinting of manuscript

Dear MDPI Reprints Desk,

I am writing to request permission to reproduce the manuscript in the article entitled "Acyl-CoA Thioesterases: A Rheostat that Controls Activated Fatty Acids Modulates Dengue Virus Serotype 2 Replication," (https://www.mdpi.com/1999-4915/14/2/240) for my dissertation at Colorado State University.
I am requesting written permission. An e-mail letter of permission or acknowledgement will suffice. Please let me know if there are additional details I can provide or if additional steps are required.

Thank you,

Laura A. St. Clair
PhD Candidate
Pronouns: She, Her, Hers
Why Pronouns Matter

Chapter 3 – Figure 3.1A

49 Spadina Ave. Suite 200
Toronto ON M5V 2J1 Canada
www.biorender.com

Confirmation of Publication and Licensing Rights

January 21st, 2022
Science Suite Inc.

Subscription:	*Student Plan Promo (Legacy)*
Agreement number:	*XI23GXWV6T*
Journal name:	*Undetermined*

To whom this may concern,

This document is to confirm that Laura St Clair has been granted a license to use the BioRender content, including icons, templates and other original artwork, appearing in the attached completed graphic pursuant to BioRender's Academic License Terms. This license permits BioRender content to be sublicensed for use in journal publications.

All rights and ownership of BioRender content are reserved by BioRender. All completed graphics must be accompanied by the following citation: "Created with BioRender.com".

BioRender content included in the completed graphic is not licensed for any commercial uses beyond publication in a journal. For any commercial use of this figure, users may, if allowed, recreate it in BioRender under an Industry BioRender Plan.

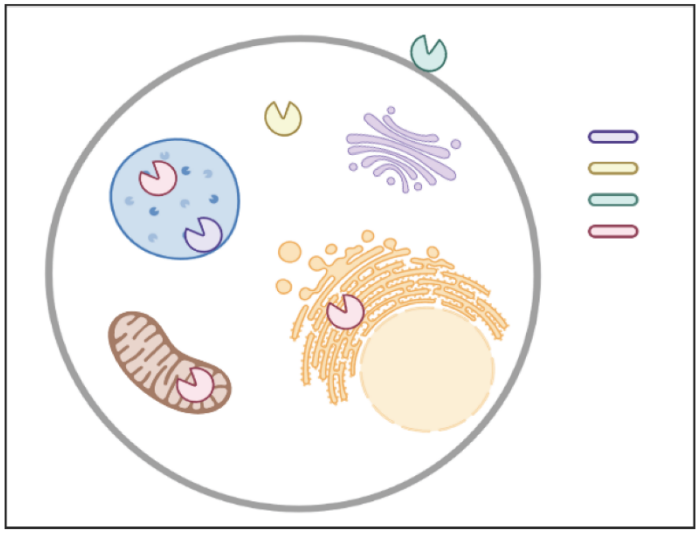

For any questions regarding this document, or other questions about publishing with BioRender refer to our BioRender Publication Guide, or contact BioRender Support at support@biorender.com.

Chapter 4 – Figure 4.2

49 Spadina Ave. Suite 200
Toronto ON M5V 2J1 Canada
www.biorender.com

Confirmation of Publication and Licensing Rights

April 11th, 2022
Science Suite Inc.

Subscription:	*Student Plan Promo (Legacy)*
Agreement number:	*UK23S97RSG*
Journal name:	*Dissertation*

To whom this may concern,

This document is to confirm that Laura St Clair has been granted a license to use the BioRender content, including icons, templates and other original artwork, appearing in the attached completed graphic pursuant to BioRender's Academic License Terms. This license permits BioRender content to be sublicensed for use in journal publications.

All rights and ownership of BioRender content are reserved by BioRender. All completed graphics must be accompanied by the following citation: "Created with BioRender.com".

BioRender content included in the completed graphic is not licensed for any commercial uses beyond publication in a journal. For any commercial use of this figure, users may, if allowed, recreate it in BioRender under an Industry BioRender Plan.

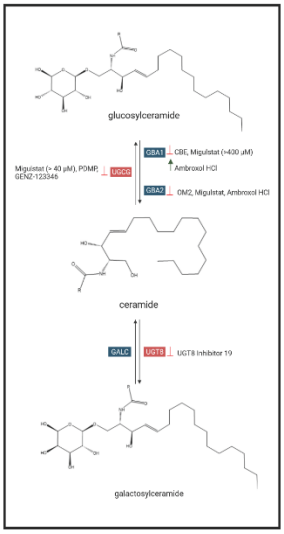

For any questions regarding this document, or other questions about publishing with BioRender refer to our BioRender Publication Guide, or contact BioRender Support at support@biorender.com.